

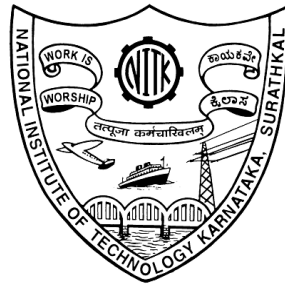
NEURAL NETWORK BASED NON-LINEAR CONTROL METHODS WITH OBSERVER DESIGN FOR ROBOTIC MANIPULATORS

Thesis

Submitted in partial fulfillment of the requirements for the degree of
DOCTOR OF PHILOSOPHY

by

M VIJAY



DEPARTMENT OF ELECTRICAL AND ELECTRONICS ENGINEERING

NATIONAL INSTITUTE OF TECHNOLOGY KARNATAKA,

SURATHKAL, MANGALORE - 575025

OCTOBER, 2018

TO MY FAMILY

DECLARATION

By the Ph.D. Research Scholar

I hereby declare that the Research Thesis entitled “**NEURAL NETWORK BASED NON-LINEAR CONTROL METHODS WITH OBSERVER DESIGN FOR ROBOTIC MANIPULATORS**” which is being submitted to the **National Institute of Technology Karnataka, Surathkal** in partial fulfillment of the requirements for the award of the Degree of **Doctor of Philosophy** in **Department of Electrical and Electronics Engineering** is a *bonafide report of the research work carried out by me*. The material contained in this Research Thesis has not been submitted to any University or Institution for the award of any degree.

M VIJAY

Reg. No: 121177EE12F02

Department of Electrical and Electronics Engineering

Place: NITK, Surathkal.

Date:

CERTIFICATE

This is to *certify* that the Research Thesis entitled **NEURAL NETWORK BASED NON-LINEAR CONTROL METHODS WITH OBSERVER DESIGN FOR ROBOTIC MANIPULATORS** submitted by **M VIJAY**, (Reg. No.: 121177 EE12F02) as the record of the research work carried out by him, is *accepted as the Research Thesis submission* in partial fulfillment of the requirements for the award of degree of **Doctor of Philosophy**.

Dr. DEBASHISHA JENA

(Research Guide)

(Name and Signature with Date and Seal)

Chairman - DRPC

(Signature with Date and Seal)

ACKNOWLEDGMENT

I wholeheartedly thank my dearest *Grand Parents* for enriching me with knowledge, strength, and confidence to complete this research work. I owe a broad sense of gratitude to my master *Dr. Debashisha Jena*, Department of Electrical and Electronics Engineering, National Institute of Technology Karnataka, Surathkal for consenting to be my guide, providing valuable suggestions, tirelessly going through my work, suggesting improvement at every step and offering rare insights and scholarly counseling. It is indeed a pleasant experience and bliss to work with him.

I would like to extend my sincere gratitude to *Dr. Ajay Kumar Yadav*, Department of Mechanical Engineering and *Dr. A. Karthikeyan*, Department of Electrical and Electronics Engineering, National Institute of Technology Karnataka, for their scholarly advice, continuous support and consistent encouragement as my RPAC members.

I wish to thank the National Institute of Technology Karnataka profusely, for giving me the opportunity and all the needed facilities to carry out my research work. In particular, I express my warm and sincere thanks to *Dr. B Venkatesa Perumal*, Head of the department. Also, express my heartfelt thanks to all the faculty members, research scholars of Department of Electrical and Electronics Engineering, National Institute of Technology Karnataka, for their kind co-operation, continuous support, and constant encouragement.

Place: NITK, Surathkal

M VIJAY

Date:

ABSTRACT

Robotic manipulators are often used in applications requiring high precision. It is inevitable to use a controller for the satisfactory operation of such manipulators. In general, an open-loop system subjected to torque disturbances and parameter uncertainties causes instability. Therefore, to ensure the global asymptotic stability, gravity compensation derived from either conventional or non-linear control methodologies with independent joint control is essential, resulting in a closed loop. As a result, several controllers have emerged during the last decades for improving the system stability with better disturbance rejection and small tracking error.

Since then, many derivatives and refinements to the classical controllers have been proposed. However, a fusion/hybridization of hard control (proportional integral derivative controller) and soft control (computational intelligence technique based) is an alternative choice for better performance. Therefore, an effort towards the designing of such fusion-based controllers is worth investigating. With this motivation, several hybrid controllers as applied to robotic manipulators are proposed.

First, the control strategy for robotic manipulator based on the coupling of artificial neuro-fuzzy inference system (ANFIS) with sliding mode control (SMC) is proposed. As a part, boundary sliding mode control (SMCB), boundary sliding mode control with PID sliding surface (PIDSMCB) and backstepping sliding mode control (BSMC) are developed for the best optimal criterion by using the genetic algorithm (GA) and particle swarm optimization (PSO). Further, they are applied for the control of 2-Degree of freedom (DOF) robot manipulator. The proposed neuro-fuzzy-based adaptive controller offers several advantages such as the consistent estimation and considerable robustness to parameter variation and external disturbance.

Second, control strategies for 3-DOF rigid robot manipulator based on the coupling of neural network (NN)-based adaptive observer with SMC are proposed. A radial basis function neural network (RBFNN)-based observer is used to estimate the tracking

position and velocity vectors of overhead transmission line de-icing robot manipulator (OTDIRM). To overcome local minima problem, the weights of both NN observer and NN approximator are adjusted off-line using PSO.

All the developed controllers are simulated extensively in MATLAB/SIMULINK. Numerical simulations using the dynamic model of a single-link rigid robot manipulator with two and three DOF in the presence of input torque disturbances are performed. Finally, the obtained simulation results considering various torque disturbances and uncertainties in terms of path tracking and disturbance rejection are validated through a set of experiments for a 2-DOF manipulator.

Keywords : Adaptive control, Disturbance rejection, Non-linear controllers, Optimal control, Robot manipulator, Sliding mode control.

Contents

List of Figures	vii
List of Tables	xv
List of abbreviations	xix
List of Nomenclature	xxiv
1 INTRODUCTION	1
1.1 INTRODUCTION	1
1.2 LITERATURE REVIEW	3
1.3 DYNAMIC MODELING OF ROBOT MANIPULATORS	5
1.3.1 Derivation of the Euler-Lagrange Formulation	6
1.4 DESIGN OF CONTROL SYSTEM FOR ROBOT MANIPULATOR	9
1.4.1 Control Schemes	9
1.4.2 Controller Design for Robot Manipulator	10
1.5 STABILITY OF NON-LINEAR SYSTEMS	10
1.5.1 Lyapunov's Method	11
1.6 MOTIVATION OF THE WORK	11
1.7 CONTRIBUTION OF THE THESIS	12
1.8 ORGANIZATION OF THE THESIS	13
2 CONVENTIONAL LINEAR AND NON-LINEAR CONTROL METHODS FOR A SINGLE-LINK ROBOT	17

2.1	INTRODUCTION	17
2.2	DESIGN OF CONVENTIONAL PID CONTROLLER	18
2.2.1	Optimal Control Systems	19
2.2.2	Local Search	20
2.2.3	Genetic Algorithm	21
2.2.4	Particle swarm optimization (PSO)	22
2.3	RESULTS AND DISCUSSIONS FOR TWO-MASS SINGLE-LINK ROBOT	24
2.4	DESIGN AND STABILITY OF SLIDING MODE CONTROLLER . . .	27
2.5	DESIGN AND STABILITY OF BACKSTEPPING SLIDING MODE CONTROLLER	32
2.6	ADAPTIVE BSMC	34
2.6.1	Stability of Adaptive BSMC	35
2.7	RESULTS AND DISCUSSIONS WITH BSMC FOR TWO-MASS SINGLE- LINK ROBOT	36
2.8	SUMMARY	42
3	PSO BASED NEURO-FUZZY SLIDING MODE CONTROL FOR A ROBOT MANIPULATOR	45
3.1	INTRODUCTION	45
3.2	CONTROLLER DESIGN AND STABILITY ANALYSIS FOR A 2- DOF ROBOT MANIPULATOR	46
3.2.1	SMCB with PID sliding surface and stability analysis	47
3.3	ADAPTIVE PIDSMCB DESIGN AND STABILITY ANALYSIS	49
3.3.1	Artificial Neural Network (ANN) Based PIDSMCB	49

3.3.2	Artificial Neuro Fuzzy Inference System (ANFIS) Based PIDSMCB	49
3.4	RESULTS AND DISCUSSIONS FOR THE 2-DOF ROBOT MANIP- ULATOR	51
3.5	RESULTS AND DISCUSSIONS FOR 3-DOF ROBOT MANIPULATOR	58
3.6	SUMMARY	65
4	NEURAL NETWORK BASED MODIFIED SLIDING MODE CONTROL TECHNIQUES WITH OBSERVER DESIGN FOR ROBOT MANIPU- LATORS	67
4.1	INTRODUCTION	67
4.2	OVERHEAD TRANSMISSION LINE DE-ICING ROBOT MANIPU- LATOR	69
4.3	NEURAL NETWORK-BASED MODIFIED SLIDING MODE CON- TROL (NNSMC)	71
4.4	NN BASED ADAPTIVE OBSERVER DESIGN AND CONTROL	73
4.4.1	Neural network-based adaptive observer (NNAO)	73
4.4.2	Neural Network-Based Adaptive Observer Sliding Mode Con- trol (NNAOSMC)	75
4.5	RESULTS AND DISCUSSIONS FOR SMC METHODOLOGIES	77
4.5.1	Dynamic Parameters of OTDIRM	77
4.6	NEURAL NETWORK-BASED MODIFIED BACKSTEPPING SLID- ING MODE CONTROL (NNBSMC)	82
4.7	AN ADAPTIVE OBSERVER BASED CONTROL OF OTDIRM	84
4.8	RESULTS AND DISCUSSIONS FOR BACKSTEPPING SMC METHOD- OLOGIES	87
4.8.1	Simulation studies	87

4.8.2	Experimental studies	91
4.9	DESIGN OF INTEGRAL BACKSTEPPING SLIDING MODE CONTROLLER (IBSMC)	95
4.10	DESIGN OF NEURAL NETWORK BASED INTEGRAL BACKSTEPPING SLIDING MODE CONTROL (NNIBSMC)	98
4.11	AN ADAPTIVE OBSERVER BASED CONTROL OF OTDIRM	100
4.11.1	Design of Neural Network Based Adaptive Observer Integral Backstepping Sliding Mode Control(NNAOIBSMC)	100
4.12	RESULTS AND DISCUSSIONS FOR INTEGRAL BACKSTEPPING SMC METHODOLOGIES	102
4.13	SUMMARY	106
5	NEURAL NETWORK BASED OBSERVER DESIGN AND MODIFIED TERMINAL SLIDING MODE CONTROL METHODOLOGIES FOR ROBOT MANIPULATOR	107
5.1	INTRODUCTION	107
5.2	DESIGN AND STABILITY OF TERMINAL SLIDING MODE CONTROL (TSMC)	108
5.3	DESIGN OF NEURAL NETWORK BASED TERMINAL SLIDING MODE CONTROL (NNTSMC)	111
5.4	AN ADAPTIVE OBSERVER BASED CONTROL OF ROBOT MANIPULATOR	113
5.5	RESULTS AND DISCUSSIONS FOR TSMC	115
5.6	DESIGN AND STABILITY OF BTSMC	119
5.7	DESIGN OF NNBTSMC	122
5.8	AN ADAPTIVE OBSERVER BASED CONTROL OF ROBOT MANIPULATOR	124

5.9	RESULTS AND DISCUSSIONS FOR BTSMC	126
5.10	DESIGN OF IBTSMC	130
5.11	DESIGN OF NEURAL NETWORK BASED INTEGRAL BACKSTEP- PING TERMINAL SLIDING MODE CONTROL (NNIBTSMC)	133
5.12	AN ADAPTIVE OBSERVER BASED CONTROL OF ROBOT MA- NIPULATOR	135
5.13	RESULTS AND DISCUSSIONS FOR IBTSMC	137
5.14	SUMMARY	141
6	CONCLUSION	143
6.1	CONCLUSION	143
6.2	FUTURE WORK	144
	Bibliography	145

List of Figures

1.1	: The mechanical structure of robot manipulator (Mittal and Nagrath, 2003).	2
1.2	: Two-mass rigid model of a single-link robot (Spong and Vidyasagar, 2008).	7
1.3	: Two-mass flexible model of a single-link robot (Spong and Vidyasagar, 2008).	8
2.1	: Block diagram of the PID controller for a single-link robot.	19
2.2	: Block diagram of PID controller with ISTE optimal criterion.	21
2.3	: Comparison of PID controller responses with ISTE for 0% step torque disturbance.	27
2.4	: Comparison of PID controller responses with ISTE for 10% step torque disturbance.	27
2.5	: Comparison of PID controller responses with ISTE for 20% step torque disturbance.	28
2.6	: Comparison of PID controller responses with ISTE for 30% step torque disturbance..	28
2.7	: Comparison of PID controller responses with ISTE for 40% step torque disturbance.	28
2.8	: Comparison of position tracking error for different percentage of torque disturbances with ISTE.	29
2.9	: Block diagram of the conventional SMC	29

2.10	: Block diagram of the BSMC.	35
2.11	: Block diagram of the adaptive BSMC.	35
2.12	: Tracking error with ISTE for 0% and 50% disturbances.	39
2.13	: Tracking Positions of end-effector with ISTE for various disturbances in input torque.	40
2.14	: Tracking Positions with ISTE for various disturbances.	41
2.15	: Control input and tracking positions of single-link with ISTE for 10% disturbances.	42
3.1	: Block diagram of the SMCB with PID sliding surface.	47
3.2	: Block diagram of the ANFIS adaptive SMCB with PID sliding surface.	50
3.3	: Rigid two link robot manipulator (Mittal and Nagrath, 2003).	52
3.4	: Tracking positions of Link 1 with PID, SMC and SMCB for 10% disturbance in input torque.	55
3.5	: Tracking positions of Link 2 with PID, SMC and SMCB for 10% disturbance in input torque.	56
3.6	: Tracking positions of Link 1 with PIDSMCB and APIDSMCB for 10% disturbance in input torque	56
3.7	Tracking positions of Link 2 with PIDSMCB and APIDSMCB for 10% disturbance in input torque	57
3.8	: Control input of Link 1 and Link 2 using SMC proposed controller for 10% disturbance in input torque.	57
3.9	: Control input of Link 1 and Link 2 using PIDSMCB proposed con- troller for 10% disturbance in input torque.	57
3.10	: Comparison of tracking error responses with APISMCB for 10% dis- turbance in input torque.	58
3.11	: A 3-DOF planar articulated robot manipulator (Lai et al., 2015).	59

3.12	Comparison of position tracking responses with different control schemes for 10% disturbance in input torque.	62
3.13	Control input of Link 1, Link 2 and Link 3 using different proposed controllers for 10% disturbance in input torque.	63
3.14	: Comparison of position tracking error responses with different control techniques for 10% disturbance in input torque.	64
3.15	: Side-by-side anova1 plots for PSO, NN, and ANFIS approaches. . . .	65
4.1	: A 3-DOF single-arm articulated OTDIRM	70
4.2	: A 3-DOF dual-arm articulated OTDIRM (Tran et al., 2015)	70
4.3	: Block diagram of the NNSMC scheme.	71
4.4	: Block diagram of the NNAOSMC scheme.	75
4.5	: Position tracking of link 1.	79
4.6	: Position tracking of link 2.	79
4.7	: Position tracking of link 3.	80
4.8	: Control torque for link 1.	80
4.9	: Control torque for link 2.	80
4.10	: Control torque for link 3.	81
4.11	: MSE of link 1 position tracking.	81
4.12	: MSE of link 2 position tracking.	81
4.13	: MSE of link 3 position tracking.	82
4.14	: Schematic arrangement of the NNBSMC.	83
4.15	: Block diagram of the NNAOBSMC scheme.	85
4.16	: Position tracking of link 1.	88
4.17	: Position tracking of link 2.	88
4.18	: Position tracking of link 3.	88

4.19 : Tracking error of link 1.	88
4.20 : Tracking error of link 2.	88
4.21 : Tracking error of link 3.	88
4.22 : Control input for link 1.	88
4.23 : Control input for link 2.	88
4.24 : Control input for link 3.	89
4.25 : MSE of link 1.	89
4.26 : MSE of link 2.	89
4.27 : MSE of link 3.	89
4.28 : Box plot representation of control torque for link 1.	91
4.29 : Box plot representation of control torque for link 2.	91
4.30 : Box plot representation of control torque for link 3.	91
4.31 : Microcontroller-based experimental setup for a two-link manipulator.	92
4.32 : Position tracking of link 1.	93
4.33 : Position tracking of link 2.	93
4.34 : Position tracking error of link 1 and link 2.	94
4.35 : Mean square error of link 1 and link 2 position tracking.	94
4.36 : Control torque for link 1 and link 2.	94
4.37 : Schematic arrangement of the NNIBSMC.	98
4.38 : Schematic arrangement of the NNAOIBSMC.	100
4.39 : Position tracking of link 1.	103
4.40 : Position tracking of link 2.	103
4.41 : Position tracking of link 3.	103
4.42 : Tracking error of link 1.	103
4.43 : Tracking error of link 2.	103

4.44	: Tracking error of link 3.	103
4.45	: Control input for link 1.	103
4.46	: Control input for link 2.	103
4.47	: Control input for link 3.	104
4.48	: MSE of link 1.	104
4.49	: MSE of link 2.	104
4.50	: MSE of link 3.	104
4.51	: Box plot representation of control torque for link 1.	105
4.52	: Box plot representation of control torque for link 2.	106
4.53	: Box plot representation of control torque for link 3.	106
5.1	: Block diagram of NNTSMC scheme.	111
5.2	: Block diagram of the NNAOTSMC scheme.	113
5.3	: Position tracking of link 1.	116
5.4	: Position tracking of link 2.	116
5.5	: Position tracking of link 3.	116
5.6	: Tracking error of link 1.	116
5.7	: Tracking error of link 2.	116
5.8	: Tracking error of link 3.	116
5.9	: Control input for link 1.	116
5.10	: Control input for link 2.	116
5.11	: Control input for link 3.	117
5.12	: MSE of link 1.	117
5.13	: MSE of link 2.	117
5.14	: MSE of link 3.	117

5.15	: Box plot representation of control torque for link 1.	119
5.16	: Box plot representation of control torque for link 2.	119
5.17	: Box plot representation of control torque for link 3.	119
5.18	: Block diagram of NNBTSMC scheme.	122
5.19	: Block diagram of the NNAOBTSMC scheme.	125
5.20	: Position tracking of link 1.	127
5.21	: Position tracking of link 2.	127
5.22	: Position tracking of link 3.	127
5.23	: Tracking error of link 1.	127
5.24	: Tracking error of link 2.	127
5.25	: Tracking error of link 3.	127
5.26	: Control input for link 1.	127
5.27	: Control input for link 2.	127
5.28	: Control input for link 3.	128
5.29	: MSE of link 1.	128
5.30	: MSE of link 2.	128
5.31	: MSE of link 3.	128
5.32	: Box plot representation of control torque for link 1.	129
5.33	: Box plot representation of control torque for link 2.	130
5.34	: Box plot representation of control torque for link 3.	130
5.35	: Block diagram of NNIBTSMC scheme.	134
5.36	: Block diagram of the NNAOIBTSMC scheme.	136
5.37	: Position tracking of link 1.	138
5.38	: Position tracking of link 2.	138
5.39	: Position tracking of link 3.	138

5.40	: Tracking error of link 1.	138
5.41	: Tracking error of link 2.	138
5.42	: Tracking error of link 3.	138
5.43	: Control input for link 1.	139
5.44	: Control input for link 2.	139
5.45	: Control input for link 3.	139
5.46	: MSE of link 1.	139
5.47	: MSE of link 2.	139
5.48	: MSE of link 3.	139
5.49	: Box plot representation of control torque for link 1.	140
5.50	: Box plot representation of control torque for link 2.	141
5.51	: Box plot representation of control torque for link 3.	141

List of Tables

2.3.1 : Fminsearch (PD Controller) for 10% torque disturbance.	24
2.3.2 : Fminsearch (PID Controller) for 10% torque disturbance.	24
2.3.3 : GA (PD controller) for 10% torque disturbance.	25
2.3.4 : GA (PID Controller) for 10% torque disturbance.	25
2.3.5 : GA (PID Controller) for 0% torque disturbance.	25
2.3.6 : GA (PID controller) for 20% torque disturbance.	26
2.3.7 : GA (PID controller) for 30% torque disturbance.	26
2.3.8 : GA (PID controller) for 40% torque disturbance	26
2.3.9 : GA (PID controller) for 50% torque disturbance.	26
2.6.1 : The obtained predicted results of the different membership functions. . .	37
2.7.1 : PD tuning parameters for 10% disturbance in torque.	37
2.7.2 : PID tuning parameters for 10% disturbance in torque.	37
2.7.3 : PID tuning parameters for various disturbances.	38
2.7.4 : BSMC tuning parameters for various disturbances.	39
3.3.1 : The predicted results of different membership function for various inputs.	51
3.4.1 : PID tuning parameters for 5% input torque disturbance.	53
3.4.2 : PID tuning parameters for 10% input torque disturbance.	53
3.4.3 : SMC parameters for 5%, 7.5%, and 10% input torque disturbances. . .	54

3.4.4 : SMCB parameters for 5%, 7.5%, and 10% input torque disturbances.	54
3.4.5 : PIDSMCB parameters for 5%, 7.5%, and 10% input torque disturbances.	54
3.4.6 : Comparison of control parameters from different approaches.	55
3.5.1 : PID Tuning Parameters for 10% disturbance in input torque	59
3.5.2 : SMC Parameters for 5%, 7.5%, and 10% input torque disturbances	60
3.5.3 : SMCB Parameters for 5%, 7.5%, and 10% input torque disturbances	61
3.5.4 : PIDSMCB parameters for 5%, 7.5% and 10% input torque disturbances	61
3.5.5 : Comparison of Control parameters from different approaches	61
4.5.1 : MSE comparison of CRLSMC (Tran et al., 2015), NNSMC and NNAOSMC.	82
4.8.1 : Physical parameters of the de-icing robot manipulator	87
4.8.2 : MSE examination of CRLSMC, NNBSMC and NNAOBSMC	89
4.8.3 : Total variance examination of CRLSMC, NNBSMC and NNAOBSMC	90
4.8.4 : 2-Norm of input examination of CRLSMC, NNBSMC and NNAOBSMC	90
4.12.1 MSE examination of CRLSMC, NNIBSMC and NNAOIBSMC	104
4.12.2 Total variance examination of CRLSMC (Tran et al., 2015), NNIB- SMC and NNAOIBSMC	105
4.12.3 2-Norm of input examination of CRLSMC (Tran et al., 2015), NNIB- SMC and NNAOIBSMC	105
5.5.1 : MSE examination of CRLSMC (Tran et al., 2015), NNTSMC and NNAOTSMC	117
5.5.2 : Total variance examination of CRLSMC (Tran et al., 2015), NNBTSMC and NNAOBTSMC	118
5.5.3 : 2-Norm of input examination of CRLSMC (Tran et al., 2015), NNTSMC and NNAOTSMC	118

5.9.1 : MSE examination of CRLSMC (Tran et al., 2015), NNBTSMC and NNAOBTSMC	128
5.9.2 : Total variance examination of CRLSMC (Tran et al., 2015), NNBTSMC and NNAOBTSMC	129
5.9.3 : 2-Norm of input examination of CRLSMC (Tran et al., 2015), NNBTSMC and NNAOBTSMC	129
5.13.1 MSE examination of CRLSMC (Tran et al., 2015), NNIBTSMC and NNAOIBTSMC	139
5.13.2 Total variance examination of CRLSMC (Tran et al., 2015), NNIBTSMC and NNAOIBTSMC	140
5.13.3 2-Norm of input examination of CRLSMC (Tran et al., 2015), NNIBTSMC and NNAOIBTSMC	140

Acronyms and Abbreviations

ABSMC	Adaptive Backstepping Sliding Mode Control
ANFIS	Artificial Neuro-Fuzzy Inference System
ANN	Artificial Neural Network
BSMC	Backstepping Sliding Mode Control
BTSMC	Backstepping Terminal Sliding Mode Control
CRLSMC	Sliding Mode Control Based on Chemical Reaction Optimization and Radial Basis Functional Link Net
CTC	Computed Torque Control
DIRM	De-Icing Robot Manipulator
DOF	Degrees Of Freedom
DSMC	Decoupled Terminal Sliding Mode Control
EC	Evolutionary Computation
FDSMC	Fuzzy Dynamic Sliding Mode Control
FDTSMC	Fast Decoupled Terminal Sliding Mode Control
GA	Genetic Algorithm
IATE	Integral Absolute Time Error
IBTSMC	Integral Backstepping Terminal Sliding Mode Control
ISE	Integral Square Error
ISTE	Integral Squared Time Squared-Weighted Error
LQR	Linear Quadratic Regulator

MIMO	Multi-Input And Multi-Output
MSE	Mean Square Error
NISMC	Non-Linear Integral Sliding Control
NAOBSMC	Neural Network Adaptive Observer Backstepping Sliding Mode Control
NNAOBTSMC	Neural Network Adaptive Observer based Backstepping Terminal Sliding Mode Control
NNAOIBSMC	Neural Network Adaptive Observer Integral Backstepping Sliding Mode Control
NNAOIBTSMC	Neural Network Adaptive Observer based Backstepping Terminal Sliding Mode Control
NNAOSMC	Neural Network Adaptive Observer Sliding Mode Control
NNAOTSMC	Neural Network Adaptive Observer based Terminal Sliding Mode Control
NNBSMC	Neural Network Based Backstepping Sliding Mode Control
NNBTSMC	Neural Network Backstepping Terminal Sliding Mode Control
NNIBSMC	Neural Network Based Integral Backstepping Sliding Mode Control
NNIBTSMC	Neural Network Integral Backstepping Terminal Sliding Mode Control
NNIBSMC	Neural Network Integral Backstepping Sliding Mode Control
NNSMC	Neural Network Sliding Mode Control
NNTSMC	Neural Network Terminal Sliding Mode control
OTDIRM	Overhead Transmission Line De-Icing Robot Manipulator
PD	Proportional Derivative

PI	Proportional Integral
PID	Proportional Integral Derivative
PSO	Particle Swarm Optimization
RBFNN	Radial Basis Function Neural Network
RNN	Recurrent Neural Network
SMC	Sliding Mode Control
SOTM	Second Order Terminal Sliding Mode
TSMC	Terminal Sliding Mode Control
TV	Total Variance
WNN	Wavelet Neural Network

List of Nomenclatures

Symbol	Explanation
ε	Approximation error
ε_{0N}	Approximation error with upper bound limit
λ	Positive constant
ϕ_a	Angle with respect to arm
ϕ_{ANF}	Thickness of the boundary layer of the ANFIS controller
ϕ_m	Angle with respect to the motor
σ	Gaussian RBF function
τ	Control torque
τ_d	External disturbance
τ_0	Equivalent control torque
b_i	Width of i^{th} neuron
C_i	Center of i^{th} neuron
g	gravity constant
G_{arm}	Transfer function of arm
G_{motor}	Transfer function of motor

Symbol	Explanation
J	Objective function
J_a	Arm inertia
J_m	Motor inertia
K_a	Spring constant
K_{ANF}	Switching gain constant of ANFIS controller
K_d	Derivative gain of the PID controller
K_i	Integral gain of PID controller
K_p	Proportional gain of PID controller
m	Number of neurons
p	Link velocity vector
q	Link position vector
q_r	Auxiliary signal
r	Ratio of gear box of the robot
s	sliding surface
t_r	rise time
V_c	Control stability function
V_o	Observer stability function
w	weight matrix
W^*	Ideal weight matrix

Chapter 1

INTRODUCTION

This chapter deals with the introduction to the thesis topic, which broadly refers to the control of robot manipulators. It also includes the related literature survey and the objectives so framed in addition to the organization of the thesis at the end.

1.1 INTRODUCTION

In the recent past, the development of robust control strategies for robotic manipulators has received considerable interest. By robust control strategies, we mean the approaches that are designed to allow dynamic behavior when confronted with modeling errors and unmodelled dynamics. Indeed, model uncertainties are frequently encountered in the robotics due to the unknown or changing payload, friction, backlash, flexible joints or robot components for which only simplified dynamical models are available. These model uncertainties may cause notable deviations between simulated and experimental results.

The mechanical structure of a robot manipulator consists of a series of rigid bodies (links) interconnected using articulations (joints). A robot manipulator is defined by an arm that guarantees the mobility, a wrist that confers dexterity, and an end-effector that accomplishes the task required for the robot as exhibited in Figure. 1.1. A robot manipulator is a type of robot which works similarly to a human arm. It is composed of set of joints separated in space by the arm links, and it looks like human wrist and elbow. As robots often do a better job than humans, they are used in replacing workers in dangerous, high precision, routine or repeated works.

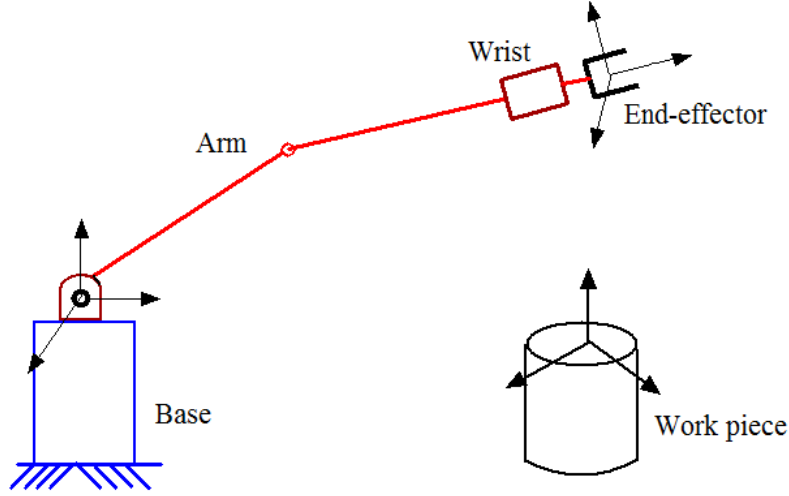


Figure 1.1 : The mechanical structure of robot manipulator (Mittal and Nagrath, 2003).

The dynamic equation of the robot manipulator with n -degrees of freedom (DOF) is characterized as:

$$D(q)\ddot{q} + C(q, \dot{q})\dot{q} + G(q) + F(q, \dot{q}) + \tau_d = \tau \quad (1.1)$$

where q , \dot{q} , and $\ddot{q} \in R^n$ are the joint/link position, velocity, and acceleration vectors, respectively, $D(q) \in R^{n \times n}$ is the symmetric positive definite inertia matrix, $C(q, \dot{q})\dot{q} \in R^{n \times n}$ is a matrix of Coriolis and centrifugal forces, $G(q) \in R^{n \times 1}$ consolidates the gravitational force, $F(q, \dot{q}) \in R^{n \times 1}$ incorporates the friction terms and τ_d represents external disturbances (Spong and Vidyasagar, 2008).

The dynamic equation (1.1) can be composed as:

$$\ddot{q} = D^{-1}(q)[\tau - (C(q, \dot{q})\dot{q} + G(q) + F(q, \dot{q}) + \tau_d)] \quad (1.2)$$

The exact dynamics of the industrial robot manipulator are not available to design a perfect controller. This includes the non-linearities, model uncertainties, elasticity, cross coupling and frictional effects that increases the system complexity. The primary objective of the generated control signal is to track the reference trajectory of the robot manipulator (Pradhan and Subudhi, 2012; Gracia et al., 2012; Piltan and Sulaiman, 2012). The modified linear or non-linear control techniques helps in enhancing the performance of the conventional control and to handle new control problems.

1.2 LITERATURE REVIEW

An overview of the robust control schemes for robot manipulators has been discussed in (Sage et al., 1999). In this paper, authors have explained the control strategies explicitly taking into account of robustness against modeling uncertainties and making the robot to track a time-varying reference trajectory. Most of the robust controllers are non-adaptive, i.e., they possess a time-invariant control law. Industrial robot manipulators are playing an essential role in growing industry (Caldwell, 2012). The lightweight and high-load to weight ratio constructions are required in present robots to fit the fast motion and high frequency operations (Spong and Vidyasagar, 2008).

The functioning of the robot manipulator depends on two types of approaches, i.e., contact type and non-contact type. In contact type approach, while functioning, the manipulator involves an environment, and in non-contact type approach it doesn't. Depending on the work, the robot manipulator can be classified into contact type manipulator and non-contact type manipulator. In general, the perfect robot is one which not only controls its movements but also controls the force that it applied to the environment (Mittal and Nagrath, 2003).

In general, actuators of the robot manipulator provide torque to drive the joints in maintaining required motion of links/arm to meet desired path or specified trajectory. In this process, the controller has to provide commands which can control the actuator to achieve specified trajectory of manipulator end-effector (Chaoui et al., 2009; Dong et al., 2013). In (Ang et al., 2005), authors have discussed the optimal controller which offers excellent stability, small tracking error, and better disturbance rejection. For improved performance, the controller has to be adaptive in nature, concerning linear/non-linear payload variations and uncertainties (De Filippis, 2012). An optimal adaptive-based controller has to be implemented to take responsibility for payload variations (Tan et al., 2012).

The conventional controllers with local optimization techniques for robot manipulators may not give the desirable results (Lewis et al., 1993). Traditional controllers with optimization techniques such as genetic algorithm (GA), neural and fuzzy based con-

trollers are used in the industry because of their reliability and ease of implementation (Naidu, 2002; Thomas et al., 2016). A robot problem solved by many algorithms provided better solutions to overcome the difficulties. The controllers with soft computing techniques (i.e., GA, neural and fuzzy) can provide an adaptive controller for variation in payloads and uncertainties (Craig, 1989; Chaudhary et al., 2014). Adaptive control schemes for robotics are playing a crucial role in recent research works. A GA based adaptive mode control schemes have been studied for many decades.

Design of a conventional controller is suitable only for the control of the system with complete knowledge of its dynamics. However, the precise dynamics of an industrial robot manipulator are not available, to design the perfect controller, due to nonlinearities, uncertainties, elasticity, cross coupling and frictional effects, which make the system highly complex. The primary objective of robot manipulator is to generate control signal that helps to track the reference trajectory (Santhakumar and Asokan, 2010; Pereira et al., 2014).

Non-linear control methods such as sliding mode control (SMC), artificial intelligence based adaptive control techniques helps in enhancing the performance of traditional control strategies. Many researchers have analyzed the SMC which is one of the best non-linear controllers that provide a fast response regarding trajectory tracking performance and disturbance rejection in the presence of uncertainties and external disturbances (Piltan and Sulaiman, 2012; Kohrt et al., 2013; Vijay and Jena, 2016; Amer et al., 2011; Song and Sun, 2014).

The terminal sliding mode control (TSMC) includes non-linear functions into the outline of the sliding hyperplane. In this work, a terminal sliding surface has designed where the trajectory tracking errors on the sliding surface approaches to zero in the constricted time. TSMC can provide robust tracking performance of the robot manipulator under uncertainties and different disturbance conditions. The essential prerequisite during the process of designing the SMC requires correct information of the system dynamics, i.e., non-linear frictions, the flexibility of links, backlash, etc (Chang, 2016).

The backstepping sliding mode control (BSMC) is developed to track the desired trajectory of the robot manipulator under various working conditions (Liu and Li, 2014).

The decoupled terminal sliding mode control (DSMC) has employed for a class of underactuated mechanical systems (Zhao et al., 2014). Authors in (Zheng et al., 2015), have discussed an integral sliding mode control (ISMC) and a non-linear ISMC (NISMC) for a second-order non-linear system. The combination of artificial intelligence with SMC techniques to control the non-linear systems are addressed in (Rossomando et al., 2014; Sun et al., 2011; Sharma et al., 2011). A new adaptive backstepping SMC (ABSMC) law with fuzzy monitoring technique is discussed for the desired trajectory tracking control of the non-linear system (Huang and Lewis, 2003).

A wavelet neural network is used (WNN) to approximate or estimate uncertainties and disturbances of the unknown model in (Wei et al., 2012). In (Tran et al., 2015), the authors discussed the conventional SMC based on the chemical reaction optimization and radial basis functional link net (CRLSMC) for the de-icing robot manipulator to achieve the desired trajectory tracking performance under various operating conditions. Authors in (Yang et al., 2013; Ginoya et al., 2014; Sun and Guo, 2017; Zhang et al., 2017; Noshadi et al., 2017), have developed control strategy based on output feedback to maintain the predefined control performance for a class of uncertain multi-input and multi-output (MIMO) non-linear systems.

In (Jafarnejadsani et al., 2013), an adaptive control based radial basis function neural network (RBFNN) is proposed for a variable-pitch and variable-speed wind turbine. In (Wen et al., 2017), a fuzzy dynamic SMC (FDSMC) technique is introduced to manage with uncertain active suspension system control, in which, the sliding surface function is concerted linearly with states and inputs. The propulsive positioning and online levitated balancing of a hybrid magnetic levitation are achieved by fuzzy neural based backstepping SMC scheme in (Wai et al., 2015).

1.3 DYNAMIC MODELING OF ROBOT MANIPULATORS

Robot manipulators can be described mathematically in different ways. The problem of kinematics is to describe the motion of the manipulator without consideration of

forces and torque which causes the movement. These equations determine the position and orientation of the end effector given the values for the joint variables (forward kinematics), and different values of the joint variables given the position and orientation of the end effector (inverse kinematics).

Dynamic modeling involves deriving the equations that explicitly describes the relationship between the forces and motion. These comparisons are necessary for the simulation of robot motion, and in the design of control algorithms. Computing the dynamics of the robot manipulators can be challenging. Researchers have discovered different approaches, where in general, there are two methods available; the Euler-Lagrange formulation, and the Newton-Euler formulation. In the standard Euler-Lagrange formulation the manipulator as a whole and the system is analyzed based on its kinematic and potential energy. The Newton-Euler formulation is quite distinctive because each link of the manipulator is treated in turn. The material in the section is partly collected from (Spong and Vidyasagar, 2008).

1.3.1 Derivation of the Euler-Lagrange Formulation

The motion of the robotic arm depends on the torque produced by the actuator. The arm and gearbox are stiff (i.e., no flexibilities). The movement of the end-effector is perpendicular to the generation, and therefore the potential is always zero. The two-mass rigid model of a single-link robot is given in Figure 1.2

For the considered model, the Lagrangian equation (L) becomes

$$K_{Rm} = \frac{1}{2}J_m\dot{\phi}_m^2 + \frac{1}{2}J_a\dot{\phi}_a^2 \quad (1.3)$$

$$V_{Rm} = 0 \quad (1.4)$$

$$L_{Rm} = K_{Rm} - V_{Rm} \quad (1.5)$$

The Euler-Lagrange equation gives

$$\frac{\partial}{\partial t} \frac{\partial L_{Rm}}{\partial \dot{\phi}_j} - \frac{\partial L_{Rm}}{\partial \phi_j} = \tau_j \quad (1.6)$$

$$(J_m + r^2 J_a)\ddot{\phi} - 0 = \tau \quad (1.7)$$

Where $\tau = u - f_m\dot{\phi}$ comes from the input torque u and the torque from the friction $f_m\dot{\phi}$.

The differential equation for the system can thus be written as:

$$(J_m + r^2 J_a)\ddot{\phi}_m + f_m\dot{\phi}_m = u \quad (1.8)$$

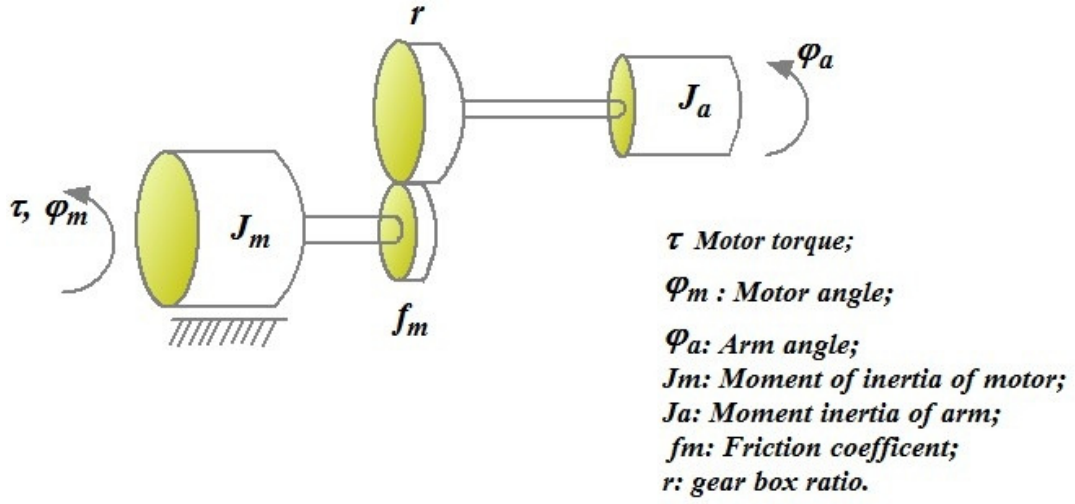


Figure 1.2 : Two-mass rigid model of a single-link robot (Spong and Vidyasagar, 2008).

In general, the resulting model can often be written as:

$$D(\varphi)\ddot{\varphi} + C(\varphi, \dot{\varphi})\dot{\varphi} + g(\varphi) = \tau \quad (1.9)$$

Where $D(\varphi)$ is the inertia matrix, $g(\varphi)$ is the gravity, τ is the motor torque, $C(\varphi, \dot{\varphi})\dot{\varphi}$ represents a matrix of Coriolis and centrifugal forces. This model denotes the rigid arm. They have stiff gear box connection which makes it possible to see them as only one mass.

$$(J_m + r^2 J_a)\ddot{\varphi}_m + f_m \dot{\varphi}_m = \tau \quad (1.10)$$

The inertia of the arm is multiplied, due to gear, with square of the gear ratio. The ratio of the gear box for robot is $r = \frac{1}{118}$. Sometimes, the modified arm inertia is used in the robot community instead of $\tilde{J}_a = r^2 J_a$.

The two-mass flexible model of a single-link robot indicating spring constant K_a and its damping coefficient d_a is illustrated in Figure 1.3. The equations for the two-mass flexible model are

$$J_m \ddot{\varphi}_m + f_m \dot{\varphi}_m + r d_a (r \dot{\varphi}_m - \dot{\varphi}_a) + r k_a (r \varphi_m - \varphi_a) = \tau \quad (1.11)$$

$$J_a \ddot{\varphi}_a - d_a (r \dot{\varphi}_m - \dot{\varphi}_a) - k_a (r \varphi_m - \varphi_a) = 0 \quad (1.12)$$

These equations can be transformed into state space form. It will be turn out practical

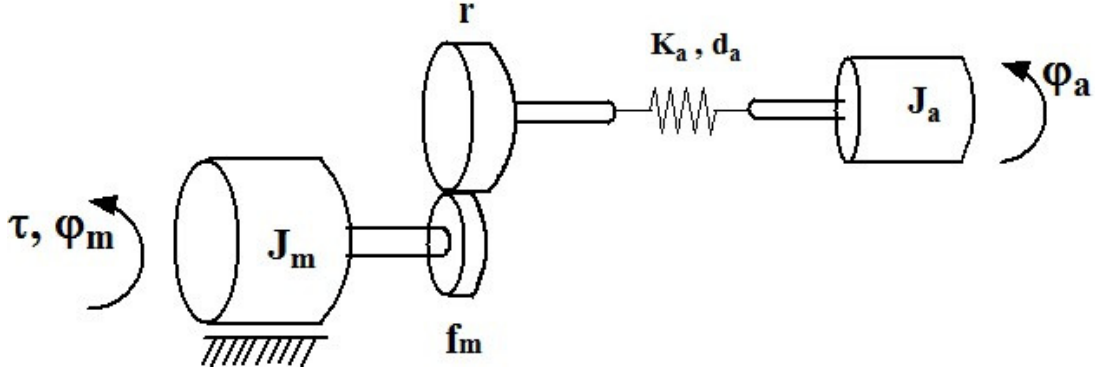


Figure 1.3 : Two-mass flexible model of a single-link robot (Spong and Vidyasagar, 2008).

to use $y = \dot{\phi}_m$

$$x(t) = \begin{bmatrix} r\phi_m(t) - \phi_a(t) \\ \dot{\phi}_m(t) \\ \dot{\phi}_a(t) \end{bmatrix} \quad (1.13)$$

$$\dot{x}(t) = Ax(t) + Bu(t) \quad (1.14)$$

$$y(t) = Cx(t) \quad (1.15)$$

$$A = \begin{bmatrix} 0 & r & -1 \\ -\frac{r.k_a}{J_m} & -\frac{f_m+r^2.d_a}{J_m} & \frac{r.d_a}{J_m} \\ \frac{k_a}{J_a} & \frac{r.d_a}{J_a} & -\frac{d_a}{J_a} \end{bmatrix} \quad (1.16)$$

$$B = \begin{bmatrix} 0 \\ \frac{1}{J_m} \\ 0 \end{bmatrix} \quad C = \begin{bmatrix} 0 & 1 & 0 \end{bmatrix} \quad (1.17)$$

Dynamic equation of the robot manipulator with n -DOF can be characterized as:

$$D(q)\ddot{q} + C(q, \dot{q})\dot{q} + G(q) + F(q, \dot{q}) + \tau_d = \tau \quad (1.18)$$

where q , \dot{q} and $\ddot{q} \in R^n$ are the link position, velocity, and acceleration vectors, respec-

tively, $D(q) \in R^{n \times n}$ is the symmetric positive definite inertia matrix, $C(q, \dot{q})\dot{q} \in R^{n \times n}$ is a matrix of Coriolis and centrifugal forces, $G(q) \in R^{n \times 1}$ consolidates the gravitational force, $F(q, \dot{q}) \in R^{n \times 1}$ incorporates the friction terms and τ_d represents external disturbances (Spong and Vidyasagar, 2008).

1.4 DESIGN OF CONTROL SYSTEM FOR ROBOT MANIPULATOR

Robot manipulators are compelling elements of today's industry. They are capable of performing many different tasks, and operations, are accurate and do not require standard safety and comfort elements which are necessary for humans. However, it needs much effort and many resources to make a robot function properly. Dynamic modeling means deriving equations that explicitly describes the relationship between force and motion in a system. In order to control a robot manipulator, as required by its operation, it is essential to consider the dynamic model in the design of the control algorithm and simulation of motion. The system is unstable in the open loop, and that achieves global asymptotic stability in the closed loop with gravity compensation and by building linear-nonlinear controllers or adaptive controllers with independent joint control schemes.

1.4.1 Control Schemes

The control schemes are organized in two approaches, some of them are listed below:

1. Linear Control Methods
 - PID Control Methods
 - Linear Quadratic Regulator (LQR)
 - H_∞ Control
 - State Feedback Control
2. Non-linear Control Methods

- Feedback Linearization Control Algorithm
- Sliding Mode Control
- Backstepping Control
- Adaptive fuzzy control
- PI, PD, PID like Fuzzy logic, Neural/ Artificial Neuro-Fuzzy Inference System (ANFIS) Controllers

1.4.2 Controller Design for Robot Manipulator

The objectives of the controller is to determine the characteristics of the controller so that the controlled output can be

1. Set to equal the reference; (i.e., Tracking).
2. Maintained at the reference values despite the unknown disturbances; (i.e., Disturbance rejection).
3. Conditions (1) and (2) are met despite the inherent uncertainties and changes in the plant dynamic characteristics; (i.e., Robustness)

1.5 STABILITY OF NON-LINEAR SYSTEMS

Unlike linear systems, the stability of nonlinear systems depends not only on physical properties of the system but also on the magnitude and nature of the input as well as the initial conditions as mentioned below

- A system is said to have local stability at an equilibrium state if, after a small perturbation, it eventually returns to that state.
- A system is said to have global stability at an equilibrium state if, for any perturbation (small or large), it eventually returns that state.

1.5.1 Lyapunov's Method

For any given state of equilibrium, it is common practice to transform coordinates in that state space so that the origin becomes the point of equilibrium. This is convenient for examining local stability and can be done for each point of equilibrium (Khalil, 2002; Branicky, 1998; Park et al., 2007).

1. $V(x)$ is a continuous and has first partial derivatives at origin.
2. $V(x) > 0$ for $x \neq 0$ and $V(0) = 0$
3. $\dot{V}(x) < 0$ for all $x \neq 0$

Note that these conditions are sufficient but not necessary for stability. $V(x)$ is often called a Lyapunov function. Now, Let us consider the stability analysis of the resulting closed-loop system from the following Lyapunov function candidate:

$$V = \frac{1}{2}z_1^T K_1 z_1 + \frac{1}{2}z_2^T D(q)z_2 + \frac{1}{2}\dot{\tilde{q}}^T D(q)\dot{\tilde{q}} \quad (1.19)$$

where $\dot{\tilde{q}} = \dot{q} - \hat{\dot{q}}$ is denoted as the velocity estimation error. Finally, Torque equation can be defined as:

$$\tau = D(q)\ddot{q}_d + C(q, \dot{\hat{q}}) + F(q) - K_d(\dot{\hat{q}} - \dot{q}_r) - K_1 z_1 \quad (1.20)$$

where the control gains K_d , K_I and L_d are positive definite diagonal matrices with $K_d = k_d I$, $K_I = k_I I$ and $L_d = l_d I$; where k_d , k_I and l_d are positive constants.

1.6 MOTIVATION OF THE WORK

In practice, it is strenuous to ascertain the system dynamics due to non-linearities, uncertainties, elasticity, cross coupling, and frictional effects, which make the system highly complex. Capturing of such dynamics are essential for reliable conventional controller design. Thus, emerged are the nonlinear control method based controllers. However, the nonlinear methods require prior information of the non-linear frictions, the flexibility of links, backlash, etc.

In case of a direct-drive robot, the problems of the backlash, friction, and compliance due to gears are excluded. The coupling among the links is important, and the

actuator dynamics add on to the system complexity. The critical issue involved in such an operation is suppression of disturbances at each robot joint due to all the modeled dynamics, such as nonlinearity, coupling effects and payload uncertainties.

Among the wide-ranging available controllers (hard and soft), it is apparent that no specific solution seems to stand out from the others remarkably. On this line, the research work in this thesis aims to investigate the fusion/hybridization of hard and soft controllers for enhancing the operational behavior of the dynamic system. As an outcome, adaptive SMC, neuro-fuzzy for 2-DOF robot manipulator and NN based adaptive observer control with SMC for 3-DOF manipulator is developed.

1.7 CONTRIBUTION OF THE THESIS

The control of robotic systems is vital, and these systems are in general MIMO and non-linear. The primary objective of the proposed control system is to follow the desired trajectory, which postulates the generation of a control signal to reduce the tracking error between the robot manipulator actual position and desired position to zero.

This thesis describes a new adaptive SMC for 2-DOF and 3-DOF robot manipulators with a proportional integral derivative (PID) sliding surface methodologies. The adaptive SMC algorithm can estimate the value of adaptive gain constant (K_{WANF}) and adaptive boundary layer thickness (ϕ_{ANF}) in real time. An adaptive PIDSMC that can handle different levels of input torque disturbances is derived, and the stability of the closed-loop system has been established. Two adaptive controllers, i.e., neuro and neuro-fuzzy controllers are proposed, and their performances are also compared. The numerical simulation is presented to verify the effectiveness of the proposed control scheme. It is further shown that the proposed neuro-fuzzy based adaptive PIDSMC (APIDSMC) scheme offers several advantages such as consistent estimation of K_{WANF} and ϕ_{ANF} and considerable robustness to parameter variation and external disturbance.

Different type of control approaches for 3-DOF overhead transmission line de-icing robot manipulator (OTDIRM) is proposed to eliminate the effect of disturbances and uncertainties associated with the direct measurement. The control laws for tracking of

the OTDIRM are developed by combining different types of modified SMC techniques and NN-based approximations. For a precise trajectory tracking performance and enhanced disturbance rejection under various operating conditions, NN-based adaptive observer non-linear SMC methodologies have been developed. The parameters of the proposed SMC methodologies and neural network (NN) adaption weights are derived using the minimization of the quadratic performance indices, wherein the minimization is achieved with particle swarm optimization (PSO).

Further, RBFNN-based observer estimates the position and velocity vectors of the link of the overhead transmission line de-icing robot manipulator (OTDIRM) without any measurements feedback. The Chattering effect is mitigated by applying boundary layer phenomenon, and the controller stability is proved by using Lyapunov stability analysis. Both simulation and experiment results are provided to demonstrate the validity and effectiveness of the proposed control methods.

1.8 ORGANIZATION OF THE THESIS

The thesis is organized as follows:

Chapter 1 deals with the introduction to the topics covered in the thesis namely linear and non-linear control methods of robot manipulators. It also includes literature survey on these issues and the framed objectives, in addition to the organization of the thesis at the end.

In chapter 2, different types of controllers are developed for the two-mass model of a single link robot to acquire dynamic properties and improve the global stability. The primary objectives of these controllers are to provide stability, good disturbance rejection and small tracking error. The proportional derivative (PD) and proportional integral derivative (PID) conventional controllers are developed for three different control strategies, i.e., Integral absolute time error (IATE), Integral square error (ISE) and Integral square time-weighted error (ISTE) using “Fminsearch” and GA. The performances of these controllers are compared with various torque disturbances regarding path tracking and disturbance rejection.

Another control strategy for the robotic manipulator based on the coupling of the ANFIS with BSMC is presented. Initially, the PID controllers have been developed for the three different control strategies (IATE, ISE, and ISTE) using PSO. The coefficients of sliding surface and switching gains of SMC are designed for the best optimal criterion using PSO. Finally, an ANFIS network is trained, which can generate the adaptive control signal for the robot manipulator. The stability of the system is validated by the checking the Lyapunov stability theorem. The simulation results of this controller are compared with various torque disturbances regarding path tracking and disturbance rejection.

In chapter 3, different combinations of linear and non-linear control methodologies are developed for the 2-DOF robot manipulator to acquire dynamic properties and improve the global stability. These control strategies for robot manipulator are based on the coupling of the ANFIS and SMC techniques. Initially, SMC with PID sliding surface is adapted to control the robot manipulator. The parameters of the sliding surface are obtained by minimizing quadratic performance indices using PSO. Finally, an ANFIS adaptive controller is proposed to generate the adaptive control signal.

Chapter 4 examines the structure of an observer-based several typical sliding mode controllers design (i.e., SMC, BSMC, and IBSMC) for 3-DOF OTDIRM. Primarily, the control laws for tracking of the OTDIRM are formulated by a combination of SMC, BSMC, and IBSMC with NN approximation techniques (i.e., NNSMC, NNBSMC, and NNIBSMC). RBFNN observer-based adaptive controllers (i.e., NNAOSMC, NNAOBSMC, and NNAOIBSMC) are designed for the robust control of the OTDIRM, which are the combinations of SMC, BSMC, IBSMC, NN estimation and adjustment laws. In all these methodologies, the weights of both NN observer and NN approximator are tuned off-line utilizing PSO. The RBFNN-based adaptive observers are intended to estimate the tracking position and velocity vectors of the OTDIRM. The stability of the developed control schemes is checked by using detailed Lyapunov stability analysis. Finally, the abilities of the proposed NN-based adaptive observer sliding mode controllers are tested against input disturbances and uncertainties.

Chapter 5 discusses the composition of an observer-based different terminal sliding

mode controllers (i.e., Terminal sliding mode control (TSMC), Backstepping terminal sliding mode control (BTSMC) and Integral backstepping terminal sliding mode control (IBTSMC)) for 3-DOF OTDIRM. Primarily, the control laws for tracking of the OTDIRM are formulated by the combination of TSMC, BTSMC, and IBTSMC with NN approximation techniques (i.e., NNTSMC, NNBTSMC, and NNIBTSMC). For the precise trajectory tracking performance and enhanced disturbance rejection under various disturbance conditions, NN-based adaptive observer different types of terminal sliding mode controller are developed (i.e., NNAOTSMC, NNAOBTSMC, and NNAOIBTSMC). The weights of both NN observer and NN approximator are adjusted off-line utilizing PSO to obviate the local minima problems. The RBFNN-based observers are intended to estimate the tracking position and velocity vectors of the OTDIRM. The Lyapunov stability functions are used to verify the stability of the proposed control methods. Finally, the robustness of the proposed methods are checked against input disturbances and uncertainties.

Chapter 6 gives the overall summary of the results described in the previous chapters. Further, the scope for future research work in this area is also discussed.

Chapter 2

CONVENTIONAL LINEAR AND NON-LINEAR CONTROL METHODS FOR A SINGLE-LINK ROBOT

This chapter discusses the different types of conventional linear and non-linear controllers which are developed for a two-mass model of a single-link robot.

2.1 INTRODUCTION

Industrial robot manipulators are playing an essential role in the growing industry. Adaptive control schemes are playing a crucial role in recent robotics research work (Mittal and Nagrath, 2003; Pradhan, 2013). In general, the actuator of the robotic manipulator provides necessary torque to drive the joints and to maintain the required motion of links. In order to meet the prescribed trajectory, the controller has to provide commands, which in turn control the actuator (Benosman and Le Vey, 2004). In (Lewis et al., 1993), authors have explained the conventional controllers with local search optimization techniques for robot manipulators, which may not give the desirable results. But controllers with optimization techniques such as GA, neural and fuzzy provide reliable results and are simple to implement. In (Merchán-Cruz and Morris, 2006), authors have discussed the role of computed torque controller (CTC), which is used to control the robot manipulator. To provide the required torque, CTC uses feedback linearization and non-linear feedback control law (Houpis and Sheldon, 2013).

An optimal controller provides excellent stability, better disturbance rejection, and

small tracking error. To improve the system performance, the controller has to sense the information from linear or non-linear functions concerning the payload variations and uncertainties. The payload variations and uncertainties should be considered while developing an optimal adaptive controller. Controller with soft computing techniques (i.e., GA, neural and fuzzy based algorithms) will be able to provide such an adaptive controller for variation in the payloads and uncertainties.

2.2 DESIGN OF CONVENTIONAL PID CONTROLLER

The computed PID control torque required to control a robot system is defined as

$$\tau = D(q)(\ddot{q}_d + u) + C(q, \dot{q})\dot{q} + G(q) + F(q, \dot{q}) + \tau_d \quad (2.1)$$

The PID controller law can be described as

$$u = K_p e + K_i \int e dt + K_d \frac{d}{dt} e \quad (2.2)$$

where, error e (desired path(q_d) – actual Path(q)), K_p is $n \times n$ positive proportional gain matrix, K_i is $n \times n$ positive integral matrix, and K_d is $n \times n$ positive derivative gain matrix parameters.

The resulting linear error dynamics are

$$\ddot{q}_d + K_p e + K_i \int e dt + K_d \frac{d}{dt} e = 0 \quad (2.3)$$

The equivalent control (τ_0) is defined from Eq.(2.1) as

$$\tau_0 = D(q)(\ddot{q}_d) + C(q, \dot{q})\dot{q} + G(q) + F(q, \dot{q}) + \tau_d \quad (2.4)$$

The PID controller should be providing a sufficient degree of stability for disturbance in the input torque and the step change in the end effector load. The integral of the position error should be minimized with different optimum control strategies. According to the linear system theory, convergence of the tracking error to zero is guaranteed (Siciliano and Khatib, 2016). The block diagram of the PID controller for a single-link robot is given in Figure 2.1.

A complete review of the existing PD control schemes with gravity compensation can be found in (Kelly, 1997) with robustness analysis. Integral action is added (PID control) to reject the constant perturbations at the cost of reduced bandwidth in the closed-loop system. There is an considerable increase in use of PID control in in-

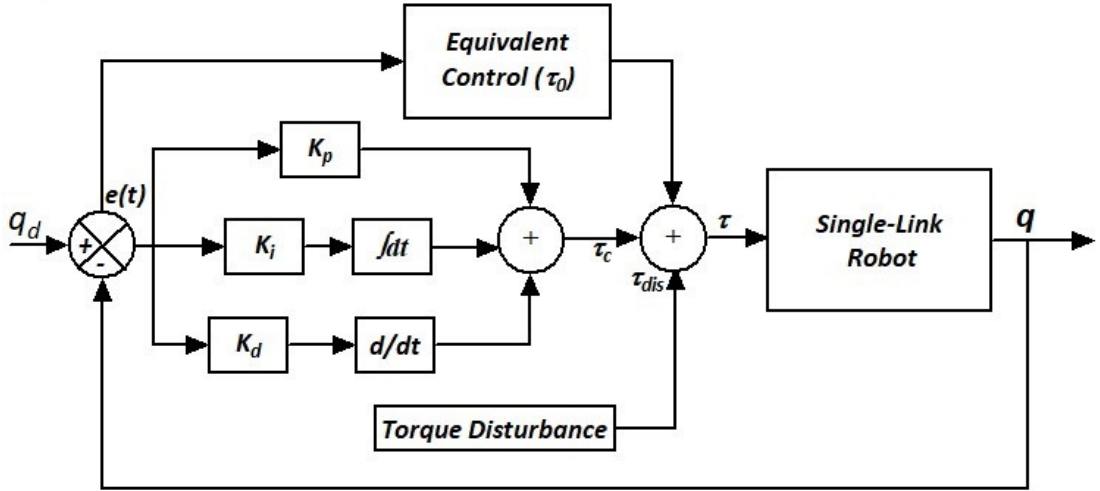


Figure 2.1 : Block diagram of the PID controller for a single-link robot.

dustrial manipulators; however, only the local asymptotic stability can be guaranteed (Arimoto, 1996). In (Hu et al., 2011), authors have discussed the role of tuning techniques for PID controller and address the iterative tuning method of PID control for robot manipulator based on the response of the closed-loop system. Implementation of PID controllers and tuning techniques were also discussed by (Ang et al., 2005). In (Gopinathan et al., 2012), authors have proposed a class of stabilizing decentralized PID controllers for a n-link robot manipulator system. The range of decentralized PID control parameters for a n-link robot manipulator is obtained using Kharitonov theorem and stability boundary equations.

2.2.1 Optimal Control Systems

The optimal control system parameters depend on the definition of optimality. Mostly, it involves zero steady state step error systems; the primary function of a feedback control system is to minimize the error. The integral of position error should be minimized for different performance indices (Tarokh and Zhang, 2014). The system optimum parameters depend on the definition of optimality i.e., to minimize objective function J given in equation (2.5).

$$J = \int_0^{\infty} t^b [e]^m dt \quad (2.5)$$

where J is the objective function value, e is the error of position signal. Normally $m=2$; $b=0, 1$ and 2 represent three different optimum criterion: ISE, ISTE and Integral Squared Time Squared-Weighted Error (IST²E) respectively. The same equation (2.5) can be used to derive IATE by taking $m=1$ and $b=1$. In optimal control design, the controller parameters are obtained by minimizing certain predefined performance indices. These performance indices can be ISE, ISTE, IATE, IST²E or any user-defined function as taken in case of the LQR. Usually, conventional local search algorithms such as gradient descent, conjugate gradient descent, etc., are used to minimize the performance indices. However, the convergence of these gradient-based algorithms are highly dependent on initial search point and there are possibilities for the solution to reach local minimum, especially for a multi-modal performance index. These limitations of the conventional local search algorithms can be addressed by using global search algorithms such as evolutionary computation (EC), GA, PSO or any other derivative-free algorithm.

The block diagram given in Figure 2.2 indicates the optimum control strategies (i.e., *ISTE*) to find the better solution and finally converges for the solution with optimum tuning parameters and minimum objective function value.

2.2.2 Local Search

Local search algorithm (i.e., $F_{minsearch}$) provides the minimum solution from a random variable as an initial value. The command function is $x = fminsearch(fun, x_0)$, and it starts at the point x_0 and returns a value x which is local minimization of the function. Initial state can be a scalar, vector, or matrix.

The $F_{minsearch}$ uses the simplex search method, and it is a direct search method that does not use numerical or analytical gradients. If n_{min} is the length of x , a simplex in n_{min} -dimensional space is characterized by the $n_{min} + 1$ distinct vectors. In two-space, a simplex is a triangle; in three-space, it is a pyramid. At each step of the search, a new point in or near the current simplex is generated. The function value at the new simplex and, usually one of the vertices is replaced by the new point, giving a new simplex. This step is repeated until the diameter of the simplex is less than the specified

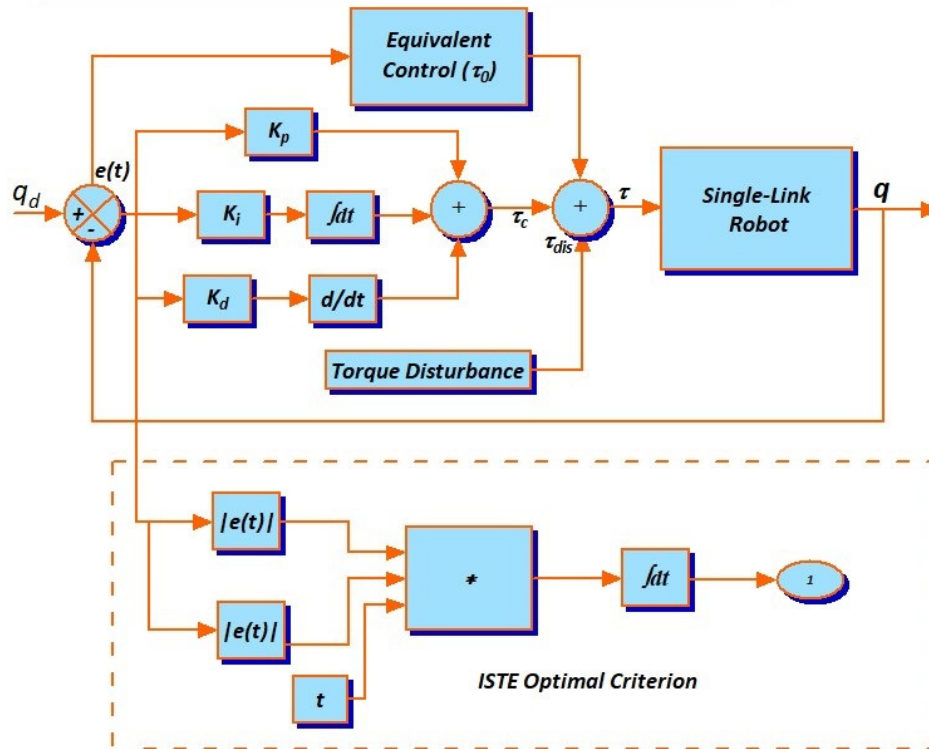


Figure 2.2 : Block diagram of PID controller with ISTE optimal criterion.

tolerance (Lagarias et al., 1998).

2.2.3 Genetic Algorithm

The genetic algorithm (GA) is a computational model of biological evolution based on random search. It searches from population to population but not individual to individual. It does not involve any derivatives to get solutions. Hence, it is called a derivative-free optimization technique (Lin and Brandt, 1998; Kim and Kang, 2003).

It begins with the initial population of binary strings called chromosomes. Each chromosome representing a possible solution to the given problem and finally converged with an optimum criterion. Reproduction, crossover, and mutation are the primary operations of GA. The overall steps involved in implementing a GA are:

1. Generate an initial, random population of individuals for a fixed size.
2. Evaluate their fitness function.

3. Select the fittest members of the population.
4. Reproduce using a probabilistic method (e.g., Roulette Wheel).
5. Implement crossover operation on the reproduced chromosomes.
6. Execute mutation operation with low probability.
7. Repeat step 2 until a predefined convergence criterion is met.

2.2.4 Particle swarm optimization (PSO)

PSO (Chen et al., 2009; Agrawal et al., 2008) is a stochastic global optimization method which is based on simulation of social behavior. As in GA and EC, PSO exploits a population of potential solutions to probe the search space. In PSO, no operators inspired by natural evolution are applied to extract a new generation of candidate solutions. Instead of mutation, PSO relies on the exchange of information between individuals, called particles, of the population, called a swarm. In effect, each particle adjusts its trajectory towards its own previous best position, and towards the best former position attained by any member of its neighborhood. In the global variant of PSO, the whole swarm is considered as the neighborhood. Thus, global sharing of information takes place and particles profit from the discoveries and previous experience of all other companions during the search for promising regions of the landscape. Several variants of PSO have been proposed up to date, following Eberhart and Kennedy who were the first to introduce this method (Ge et al., 2007).

Initially, assuming the search space is d -dimensional, so the i^{th} particle of the swarm is represented by a d -dimensional vector $X_i = [X_{i1}, X_{i2}, \dots, X_{id}]$ and best particle of the swarm, i.e., the particle with the lowest function value, is denoted by index g_α . The best previous position of the i^{th} particle is recorded and represented as $P_i = [P_{i1}, P_{i2}, \dots, P_{id}]$ and the position change (velocity) of the i^{th} particle is $V_i = [V_{i1}, V_{i2}, \dots, V_{id}]$. The particles are manipulated according to the equation 2.6

$$V_i^{k+1} = \chi(w_\alpha V_i^k + c_1 r_{r1}^k (P_i^k - X_i^k) + c_2 r_{r2}^k (P_{g_\alpha}^k - X_i^k)) \quad (2.6)$$

$$X_i^{k+1} = X_i^k + V_i^{k+1} \quad (2.7)$$

where $i = 1, 2, \dots, N$ and N is the size of the population which is used to control and constrict velocities; w_α is the inertia weight, c_1 and c_2 are two positive constants, called the cognitive and social parameter respectively; r_{i1} and r_{i2} are random numbers uniformly distributed within the range $[0, 1]$. Equation 2.6 is used to determine the i^{th} particle's new velocity, at each iteration, as well as a new position of the i^{th} particle, adding its new velocity, to its current position. The performance of each particle is measured according to a fitness function. In optimization problems, the fitness function is usually identical with the objective function under consideration. The role of the inertia weight w_α is considered important for the PSO's convergence behavior. The inertia weight is employed to control the impact of the previous history of velocities on the current velocity. A large inertia weight facilitates exploration while a small one tends to facilitate exploitation of current search area. A proper value for the inertia weight w_α provides the balance between the global and local exploration ability of the swarm, and, thus results in better solutions. The following steps describe the algorithm for PSO.

- Step 1: Initialize a population of particles with random positions and velocities on d -dimensions in the problem space.
- Step 2: For each particle, evaluate the desired optimization fitness function in d variables.
- Step 3: Compare particle's fitness evaluation with its $pbest$. If current value is better than $pbest$, then set $pbest$ equal to the current value, and p_i equals to the current location x_i in d -dimensional space.
- Step 4: Identify the particle in the neighborhood with the best success so far, and assign its index to the variable.
- Step 5: Change the velocity and position of the particle according to equation (2.6).
- Step 6: Move to step (2) until a criterion is met, usually a sufficiently good fitness or a maximum number of iterations.

2.3 RESULTS AND DISCUSSIONS FOR TWO-MASS SINGLE-LINK ROBOT

Simulation is carried out for the two-mass single-link model shown in Figure 1.3. The robot controller is designed for IATE, ISE and ISTE control strategies for different torque disturbance conditions. Results are obtained by tuning conventional controllers with the local Fminsearch algorithm and global controller with GA under various disturbance conditions. The parameters of two-mass flexible single-link robot are considered as: $J_m = 9 \times 10^{-4} \text{ Kg.m}^2$, $J_a = 10.9 \text{ Kg.m}^2$, $f_m = 6.3 \times 10^{-2} \text{ N}$, $K_a = 1.5 \times 10^5$, $d_a = 70$ and $r = \frac{1}{118}$.

Table 2.3.1 : Fminsearch (PD Controller) for 10% torque disturbance.

Sl. No	Controlling Parameters	IATE	ISE	ISTE
1	K_p	-15.433	-9.066	-12.504
2	K_d	10.719	8.361	10.612
Objective Function Value (J)		0.014	0.0039	7.7×10^{-4}

Table 2.3.2 : Fminsearch (PID Controller) for 10% torque disturbance.

Sl. No	Controlling Parameters	IATE	ISE	ISTE
1	K_p	-11.025	-13.088	-17.22
2	K_i	-11.619	11.221	12.642
3	K_d	10.587	8.476	10.736
Objective Function Value (J)		0.01408	0.0039	7.769×10^{-4}

Table 2.3.1 shows the PD tuning parameters from Fminsearch for the controller of the two-mass flexible single-link robot with IATE, ISE, and ISTE control strategies for 10% torque disturbance. Table 2.3.2 shows PID tuning parameters from Fminsearch method for the controller of robot model with IATE, ISE, and ISTE control strategies for 10% torque disturbance. Table 2.3.3 shows PD Tuning parameters from GA Method with

Table 2.3.3 : GA (PD controller) for 10% torque disturbance.

Sl. No	Controlling Parameters	IATE	ISE	ISTE
1	K_p	0.013	0.003	0.005
2	K_d	10.771	10.838	10.826
Objective Function Value (J)		0.0144	0.0033	8.01×10^{-5}

Table 2.3.4 : GA (PID Controller) for 10% torque disturbance.

S.No	Controlling Parameters	IATE	ISE	ISTE
1	K_p	0.005	0.009	0.06
2	K_i	0.05	0.146	0.24
3	K_d	10.737	8.371	10.806
Objective Function Value (J)		0.0144	0.00394	8.01×10^{-5}

IATE, ISE and ISTE control strategies for 10% torque disturbance. Table 2.3.4 shows the PID tuning parameters of single-link robot for different control strategies with 10% torque disturbances. From these results, it is inferred that the GA (PID controller) gives better performance for the considered three optimal strategies. Hence, further analysis are carried out with GA (PID controller) for various operating conditions.

Table 2.3.5 : GA (PID Controller) for 0% torque disturbance.

Sl. No	Controlling Parameters	IATE	ISE	ISTE
1	K_p	0.006	0.003	0.008
2	K_i	0.053	0	0
3	K_d	10.722	8.281	10.657
Objective Function Value (J)		0.0144	0.00394	8.01×10^{-5}

Tables 2.3.6, 2.3.7, 2.3.8 and 2.3.9 are showing the PID parameters of GA based controller for 0 %, 20%, 30%, 40%, and 50% torque disturbances, respectively. Objective values of all controllers with ISTE are minimum in comparison with other optimum criteria. Hence, by observing these values for various disturbances, PID controller with ISTE optimum criterion provides better tracking performance.

Table 2.3.6 : GA (PID controller) for 20% torque disturbance.

Sl. No	Controlling Parameters	IATE	ISE	ISTE
1	K_p	0.028	0.002	0.011
2	K_i	0.027	0.378	0.438
3	K_d	10.794	8.353	10.836
Objective Function Value (J)		0.0144	0.00394	8.01×10^{-5}

Table 2.3.7 : GA (PID controller) for 30% torque disturbance.

Sl. No	Controlling Parameters	IATE	ISE	ISTE
1	K_p	0.007	0.001	0.031
2	K_i	0.026	0.001	2.707
3	K_d	10.763	8.325	10.985
Objective Function Value (J)		0.0144	0.00394	8.03×10^{-5}

Table 2.3.8 : GA (PID controller) for 40% torque disturbance

Sl. No	Controlling Parameters	IATE	ISE	ISTE
1	K_p	0.021	0.015	0.013
2	K_i	0.144	0.002	0.021
3	K_d	10.814	8.316	10.777
Objective Function Value (J)		0.01443	0.00394	8.05×10^{-5}

Table 2.3.9 : GA (PID controller) for 50% torque disturbance.

Sl. No	Controlling Parameters	IATE	ISE	ISTE
1	K_p	0.062	0.025	0.039
2	K_i	0.07	0.025	0.062
3	K_d	10.797	8.313	10.859
Objective Function Value (J)		0.01443	0.0039	8.1×10^{-5}

Figure 2.3 to Figure 2.7 show the responses of a single-link robot model for various torque disturbances with ISTE optimum criterion. In these responses, it is observed that GA PID controller can able to provide optimal tuning parameters to meet the robust de-

sired trajectory. Figure 2.8 shows the error response plot for 0% and 40% disturbances. From this figure, it is inferred that with the increase in the disturbance levels, the disturbance rejection capacity is decreasing.

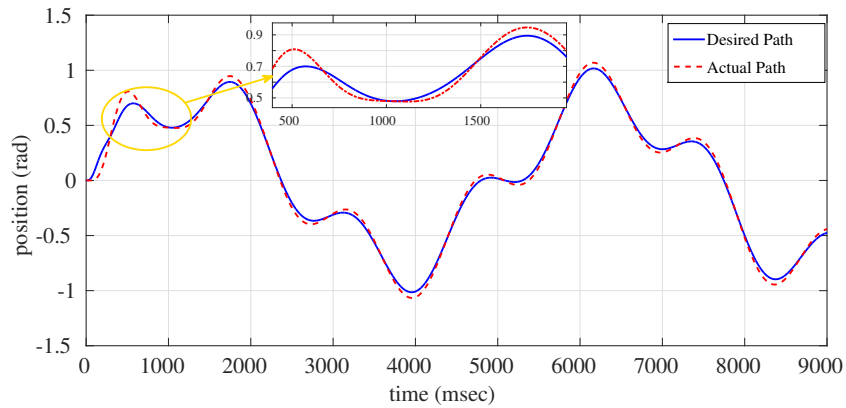


Figure 2.3 : Comparison of PID controller responses with ISTE for 0% step torque disturbance.

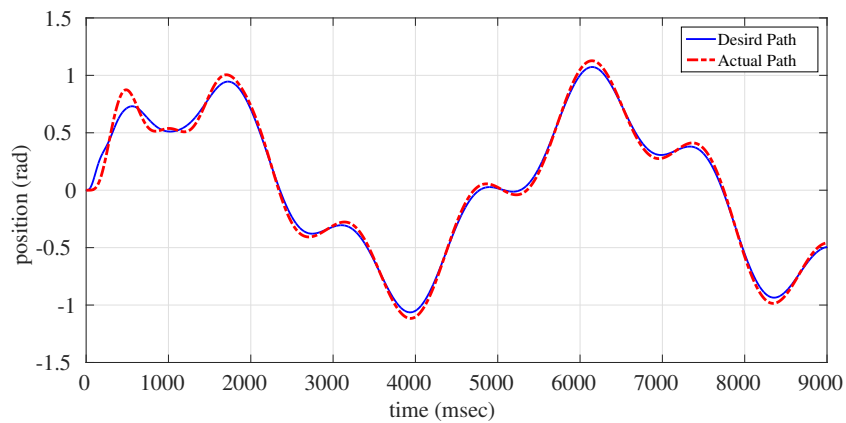


Figure 2.4 : Comparison of PID controller responses with ISTE for 10% step torque disturbance.

2.4 DESIGN AND STABILITY OF SLIDING MODE CONTROLLER

SMC is one of the influential non-linear controllers for linear and non-linear systems. It provides a systematic solution for two primary essential control challenges, i.e., stability

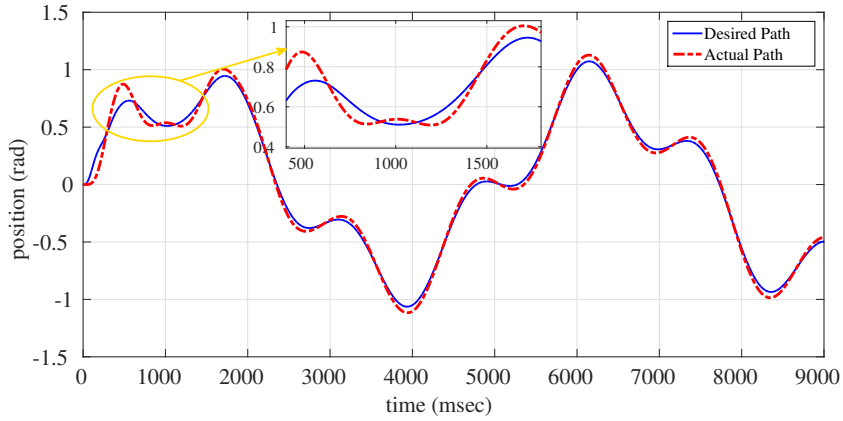


Figure 2.5 : Comparison of PID controller responses with ISTE for 20% step torque disturbance.

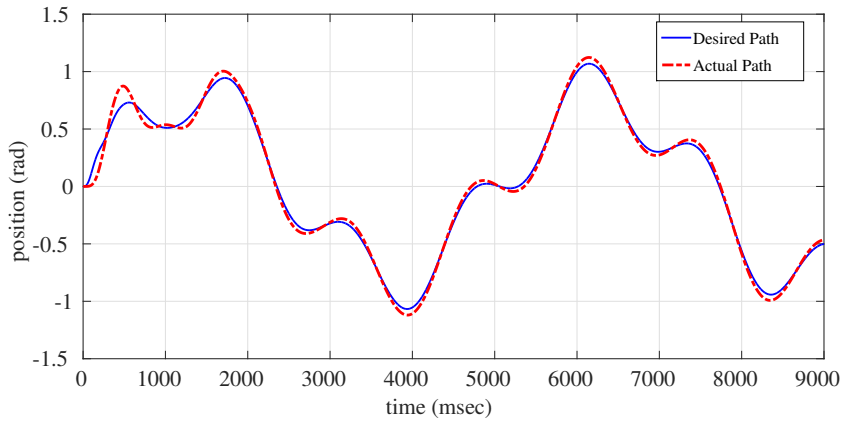


Figure 2.6 : Comparison of PID controller responses with ISTE for 30% step torque disturbance..

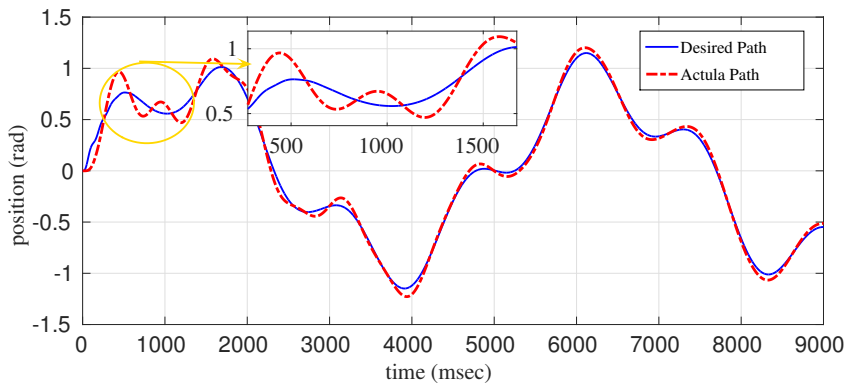


Figure 2.7 : Comparison of PID controller responses with ISTE for 40% step torque disturbance.

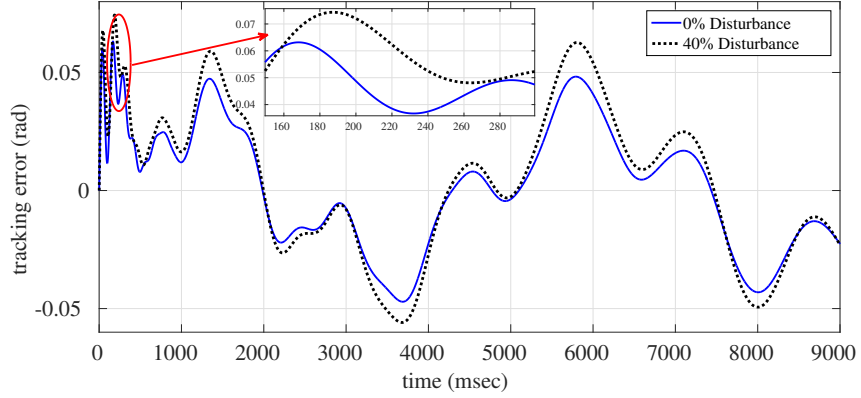


Figure 2.8 : Comparison of position tracking error for different percentage of torque disturbances with ISTE.

and robustness (Amer et al., 2011). The block diagram of the conventional SMC is shown in Figure 2.9.

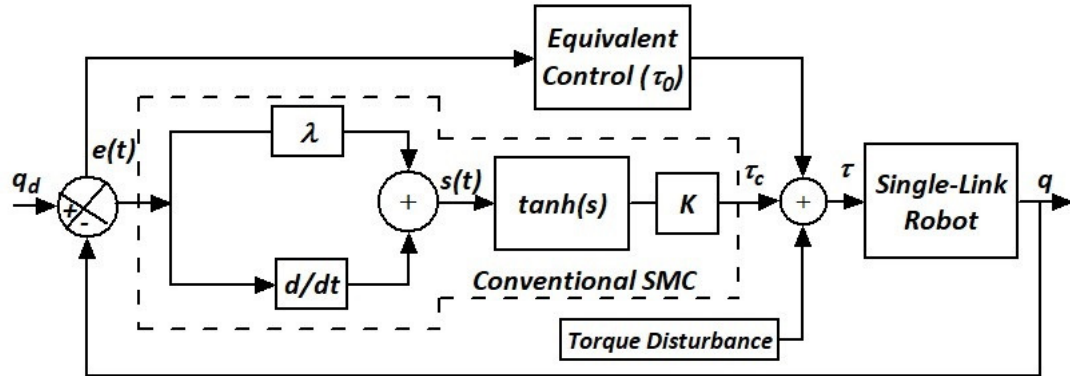


Figure 2.9 : Block diagram of the conventional SMC

Total input control torque to the robot is defined as:

$$\tau = \tau_0 + \tau_c \quad (2.8)$$

where ' τ_0 ' is the equivalent control torque, ' τ_c ' is the sliding mode control torque. A time varying sliding surface ' s ' is given by the following equation

$$s = \dot{e} + \lambda e \quad (2.9)$$

where ' λ ' is positive constant. The main aim of this method is to keep ' s ' near to zero. The purpose of SMC is to force tracking error ' e ' to approach the sliding surface and then move along the sliding surface to the origin. Therefore, the sliding surface should

be stable, which means the error dies out asymptotically and this implies that the system dynamics tracks the desired trajectory. The derivative of sliding surface concerning time can be expressed as follows:

$$\dot{s} = \ddot{e} + \lambda \dot{e} \quad (2.10)$$

$$\dot{s} = \ddot{q}_d - \ddot{q} + \lambda \dot{e} \quad (2.11)$$

where $\ddot{e} = \ddot{q}_d - \ddot{q}$, substituting the value of \ddot{q} from equation (1.2) in equation (2.11) gives

$$\dot{s} = \ddot{q}_d + \lambda \dot{e} - D^{-1}(q)[\tau - (C(q, \dot{q})\dot{q} + G(q) + F(q, \dot{q}) + \tau_d)] \quad (2.12)$$

The control effort is derived from the solution of $\dot{s} = 0$. This control effort is known as equivalent control effort represented by τ_0 , which is required to achieve the desired performance without uncertainties (i.e., $\tau_d = 0$).

$$\dot{s} = \ddot{q}_d + \lambda \dot{e} - D^{-1}(q)[\tau - (C(q, \dot{q})\dot{q} + G(q) + F(q, \dot{q}))] = 0 \quad (2.13)$$

$$\tau_0 = D(q)[\ddot{q}_d + \lambda \dot{e}] + (C(q, \dot{q})\dot{q} + G(q) + F(q, \dot{q})) \quad (2.14)$$

However, if unpredictable disturbances or uncertainties occur, the equivalent control effort cannot ensure the favorable control performance. Therefore, auxiliary control effort is designed to eliminate the effect of the unpredictable disturbances. To prove the stability of the control system, Lyapunov like Lemma is used. For this purpose, the Lyapunov function is chosen as:

$$V = \frac{1}{2} s^T s \quad (2.15)$$

A sufficient condition to guarantee that the trajectory of the tracking position error will translate from reaching phase to sliding phase is to select proper control strategy, also known as the reaching condition.

$$\dot{V} = s^T \dot{s} < 0, s \neq 0 \quad (2.16)$$

To obtain the reaching control signal τ_c , equation (2.16) can be defined as:

$$\dot{V} = s^T [\ddot{q}_d + \lambda \dot{e} - D^{-1}(q)[(\tau_0 + \tau_c)] - D^{-1}(q)(C(q, \dot{q})\dot{q} + G(q) + F(q, \dot{q}))] \quad (2.17)$$

Substituting equation (2.14) into equation (2.17), we get

$$\dot{V} = s^T \dot{s} = -s^T D^{-1}(q) \tau_c \quad (2.18)$$

To ensure $s^T \dot{s} < 0$, the reaching control law is selected as:

$$\tau_c = D(q) K_w \text{sign}(s) \quad (2.19)$$

Substituting equation (2.19) in equation (2.18), the Lyapunov stability condition becomes

$$\dot{V} < -s^T D^{-1}(q)D(q)K_w \text{sign}(s) \quad (2.20)$$

$$\dot{V} < -K_w s^T \text{sign}(s)$$

$$\dot{V} < -K_w |s| \quad (2.21)$$

where $|s| = s^T \text{sign}(s)$.

In equation (2.19) the sign function is used. This function creates more chattering on the control torque. To avoid this chattering effect, sign function is replaced by the tanh (hyperbolic tangent) function.

$$\dot{V} < -K_w s^T \tanh(s) \quad (2.22)$$

In above equation, $s^T \tanh(s)$ is always positive so that entire equation becomes negative provided that s satisfies the following conditions.

1. if s is positive and $\tanh(s)$ is also positive then $s^T \tanh(s)$ is always positive
2. if s is negative and $\tanh(s)$ is also negative then $s^T \tanh(s)$ is always positive

Finally, the reaching control signal τ_c is given as follows

$$\tau_c = K_w D(q) \tanh\left(\frac{d}{dt}e + \lambda e\right) \quad (2.23)$$

Where, $K_w = \text{diag}\{K_{w1}, K_{w2} \dots K_{wn}\}$ represents reaching control gain matrix with the upper bound of uncertainties. Tuning positive time constant K_w given equation in (2.23) is one of the most important challenges in conventional SMC. Based on the discontinuous part, the chattering phenomenon can lead to oscillations in output (Ho et al., 2009). The boundary layer concept is used to reduce the chattering on the control signal. In boundary layer (ϕ) method, the basic idea is to replace the discontinuous function by a smooth saturation function near to small neighborhood of the switching surface. This replacement causes an increase in performance error. Therefore, to compensate the error performance an updated control law is needed. In this work, the saturation function is considered as given in equation (2.24).

$$\text{sat}\left(\frac{s}{\phi}\right) = \begin{cases} \tanh\left(\frac{s}{\phi}\right), & \text{for } \left|\frac{s}{\phi}\right| \geq 1; \\ \frac{s}{\phi}, & \text{for } \left|\frac{s}{\phi}\right| < 1. \end{cases} \quad (2.24)$$

Finally, the SMC control law with boundary layer becomes

$$\tau_c = K \tanh\left(\frac{\frac{d}{dt}e + \lambda e}{\phi}\right) \quad (2.25)$$

where K is positive gain matrix and it is defined as $K = K_w D(q)$.

2.5 DESIGN AND STABILITY OF BACKSTEPPING SLIDING MODE CONTROLLER

The backstepping methodology is a nonlinear scheme generally utilized as a part of controller design. The mathematical model of robot is expressed in (2.26), (2.27) and (2.28) as:

$$\dot{x}_1 = x_2 \quad (2.26)$$

$$\dot{x}_2 = \ddot{q} = D^{-1}(q)[\tau - (C(q, \dot{q})\dot{q} + G(q) + F(q, \dot{q}) + \tau_d)] \quad (2.27)$$

$$y = x_1 \quad (2.28)$$

where x_1 and x_2 are the position and velocity vectors of the robot.

The position tracking error of the system is given as:

$$e_1 = q_d - q \quad (2.29)$$

The stabilizing function is characterized as

$$\alpha_1 = \lambda_1 e_1 \quad (2.30)$$

where α_1 and λ_1 are steady term and positive constant, respectively. The upgraded tracking error of velocity of the robot is characterized in (2.31) and appeared as:

$$e_2 = \dot{e}_1 + \alpha_1 \quad (2.31)$$

The primary Lyapunov stability function is characterized as:

$$V_1 = \frac{1}{2}e_1^2 \quad (2.32)$$

Equations (2.33) and (2.34) are derived from (2.31) and (2.32) that expressed as:

$$e_2 = \dot{q}_d - \dot{q} + \alpha_1 \quad (2.33)$$

$$\dot{V}_1 = e_1(e_2 - \alpha_1) = e_1 e_2 - \lambda_1 e_1^2 \quad (2.34)$$

From (2.33), we get

$$\dot{e}_2 = \ddot{q}_d - D^{-1}(q)[\tau - (C(q, \dot{q})\dot{q} + G(q) + F(q, \dot{q}) + \tau_d)] + \dot{\alpha}_1 \quad (2.35)$$

The second Lyapunov stability function is described as:

$$V = V_1 + \frac{1}{2}s^T s \quad (2.36)$$

The satisfactory condition, which gives the affirmation that the tracking error will make an elucidation from achieving stage to sliding stage, is called the achieving condition and given in (2.37).

$$\dot{V} < 0, s \neq 0 \quad (2.37)$$

Where ‘ s ’ is the sliding surface. It is characterized as:

$$s = e_1 + e_2 \quad (2.38)$$

The derivative of the second Lyapunov stability function is given in (2.39).

$$\dot{V} = e_1 e_2 - \lambda_1 e_1^2 + s^T (\dot{e}_1 + \dot{e}_2) \quad (2.39)$$

By substituting \dot{e}_1 and \dot{e}_2 in (2.39), yields:

$$\begin{aligned} \dot{V} = & e_1 e_2 - \lambda_1 e_1^2 + s^T [(1 + \lambda_1)\dot{e}_1 + \ddot{q}_d - D^{-1}(q)[\tau - (C(q, \dot{q})\dot{q} \\ & + G(q) + F(q, \dot{q}) + \tau_d)]] \end{aligned} \quad (2.40)$$

The total input control torque (τ) to the robot is characterized as:

$$\tau = \tau_0 + \tau_c \quad (2.41)$$

By substituting (2.41) in (2.40), we get

$$\begin{aligned} \dot{V} = & e_1 e_2 - \lambda_1 e_1^2 + s^T [(1 + \lambda_1)\dot{e}_1 + \ddot{q}_d - D^{-1}(q)[\tau_0 + \tau_c - (C(q, \dot{q})\dot{q} \\ & + G(q) + F(q, \dot{q}) + \tau_d)]] \end{aligned} \quad (2.42)$$

The arrangement of $\dot{s} = 0$ gives the control signal, which is known as equivalent control law and it is denoted by ‘ τ_0 ’. This equivalent control law is essential to fulfill the execution of favored trajectory tracking without considering the disturbances and uncertainties (i.e., $\tau_d = 0$).

$$\tau_0 = D(q)((1 + \lambda_1)\dot{e}_1 + \ddot{q}_d) + C(q, \dot{q})\dot{q} + G(q) + F(q, \dot{q}) \quad (2.43)$$

An extra control exertion is needed to wipe out the unpredictable disturbances and uncertainties as equivalent control torque (τ_0) is lacking to provide the favored tracking performance. Ultimately, the tracking error dies out asymptotically, which means the sliding surface becomes stable. To exhibit the stability of the created control framework for robot, the Lyapunov-like Lemma is utilized.

From (2.42) and (2.43) we arrive at an expression for \dot{V} as follows:

$$\dot{V} = e_1 e_2 - \lambda_1 e_1^2 + s^T (-D^{-1}(q) \tau_c) \quad (2.44)$$

To meet the Lyapunov stability condition, the corrective control law (τ_c) is defined as $\tau_c = D(q)(e_2 + K_w \text{sign}(s))$. It is substituted in (2.44) which yields:

$$\dot{V} = -\lambda_1 e_1^2 - e_2^2 - K_w s^T \text{sign}(s) \quad (2.45)$$

where K_w is the sliding gain.

$$\dot{V} \leq -\lambda_1 e_1^2 - e_2^2 - K_w |s| \quad (2.46)$$

where $|s| = s^T \text{sign}(s)$.

The chattering effect on the control input signal is introduced by the signum function ('sign'), which is utilized as a part of (2.45), so as to diminish or dispense with this impact, the signum function ('sign') is replaced by the hyperbolic tangent function ('tanh') as given in (2.47).

$$\dot{V} \leq -\lambda_1 e_1^2 - e_2^2 - K_w s^T \tanh(s) \quad (2.47)$$

The term ' $s^T \tanh(s)$ ' in (2.47) is constantly positive so that whole condition gets to be negative (i.e., $s^T \tanh(s) > 0$ if either $s > 0$ or $s < 0$).

The achieving control signal (τ_c) is given as:

$$\tau_c = D(q) \left[e_2 + K_w \tanh \left((1 + \lambda_1) e_1 + \frac{d}{dt} e_1 \right) \right] \quad (2.48)$$

Where $K_w = \text{diag}\{K_{w1}, K_{w2}, \dots, K_{wn}\}$ is control gain matrix.

The BSMC control law is defined as:

$$\tau_c = D(q) e_2 + K \tanh \left(\frac{(1 + \lambda_1) e_1 + \frac{d}{dt} e_1}{\phi} \right) \quad (2.49)$$

where $K = D(q) K_w$.

Figure 2.10 illustrates the frame work of the BSMC for single-link robot model. Where, ϕ is the boundary layer thickness of the BSMC controller and K is the sliding gain constant.

2.6 ADAPTIVE BSMC

In the adaptive neuro-fuzzy inference system (ANFIS), for a given input and output data set, the toolbox function makes a fuzzy inference system (FIS) whose membership functions are tuned using either a back propagation algorithm alone or in a compounding

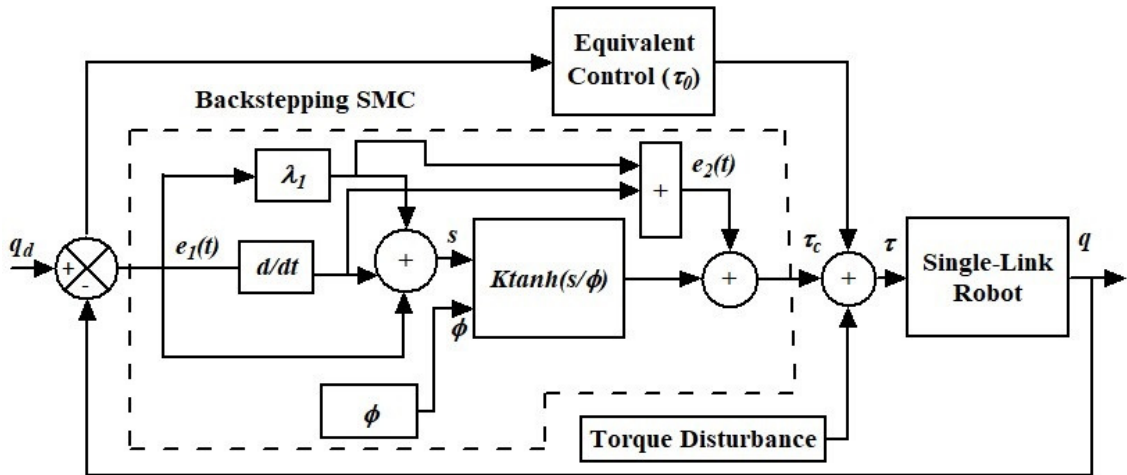


Figure 2.10 : Block diagram of the BSMC.

with the least method. Both artificial neural network (ANN) and fuzzy logic are used in ANFIS architecture. In the process of developing the ANFIS adaptive controller, the training was performed on MATLAB environment under various input membership functions for different operating conditions.

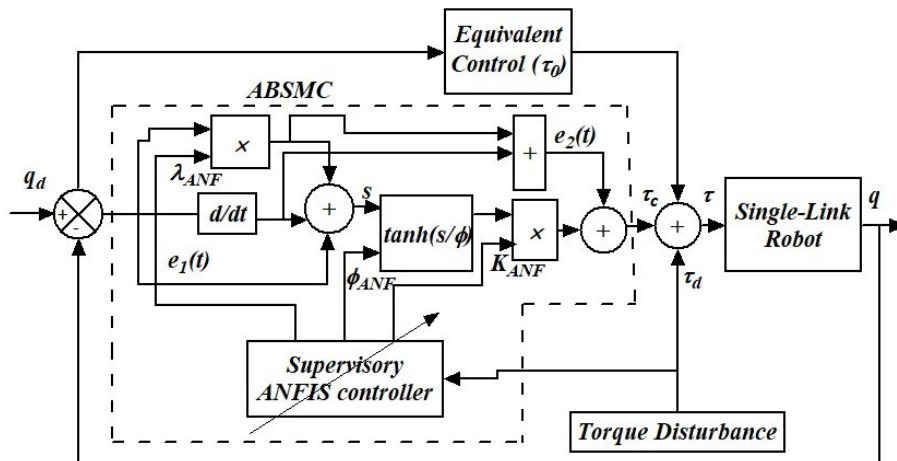


Figure 2.11 : Block diagram of the adaptive BSMC.

2.6.1 Stability of Adaptive BSMC

Similar to equation 2.38, the sliding surface for adaptive BSMC can be defined as:

$$s = e_1 + e_2 \quad (2.50)$$

From equation (2.39), we can define Lyapunov stability equation for ABSMC is

$$\dot{V} = \dot{V}_1 + s^T \dot{s} \quad (2.51)$$

$$= e_1 e_2 - \lambda_{ANF} e_1^2 + s^T \dot{s} \quad (2.52)$$

$$= e_1 e_2 - \lambda_{ANF} e_1^2 + s^T (\dot{e}_1 + \dot{e}_2) \quad (2.53)$$

A sufficient condition for stability is defined as:

$$\dot{V} \leq 0, \quad s \neq 0 \quad (2.54)$$

$$\dot{V} \leq -\lambda_{ANF} e_1^2 - e_2^2 - K_{ANF} s^T \tanh(s) \quad (2.55)$$

where λ_{ANF} is an ANFIS/adaptive positive coefficient and K_{ANF} is ANFIS/adaptive reaching control coefficient of ABSMC. Equation (2.55) can be written as:

$$\dot{V} \leq -e^T Q e - K_{ANF} s^T \tanh(s) \quad (2.56)$$

In above equation $s^T \tanh(s)$ is always positive so that entire equation becomes negative provided that s satisfies the following conditions.

- if s is positive and $\tanh(s)$ is also positive then $s^T \tanh(s)$ is always positive
- if s is negative and $\tanh(s)$ is also negative then $s^T \tanh(s)$ is always positive

Finally, the reaching control signal τ_c is given as follows

$$\tau_c = e_2 + (K_{ANF}) \tanh\left(\frac{(1 + \lambda_{ANF})e_1 + \frac{d}{dt}e_1}{\phi_{ANF}}\right) \quad (2.57)$$

where ϕ_{ANF} is the thickness of boundary layer provided by ANFIS. Table 2.6.1 gives the training error values for switching gain constant (K_{ANF}), boundary layer thickness (ϕ_{ANF}) and positive constant (λ_{ANF}) of ANFIS adaptive BSMC under various membership functions.

From Table 2.6.1, it is observed that the ‘gauss2mf’ membership function provides minimum training error for all three cases. Finally, ‘gauss2mf’ membership function is used for designing of ANFIS network for adaptive BSMC.

2.7 RESULTS AND DISCUSSIONS WITH BSMC FOR TWO-MASS SINGLE-LINK ROBOT

Simulation is carried out for the two-mass flexible single-link robot in MATLAB. Initially, the optimum PID controller is designed for IATE, ISE, and ISTE control strate-

Table 2.6.1 : The obtained predicted results of the different membership functions.

Sl. No	Membership Function	Training Error for K_{ANF}	Training Error for ϕ_{ANF}	Training Error for λ_{ANF}
1	gaussmf	0.001068	2.16×10^{-7}	3.23×10^{-4}
2	gauss2mf	0.001053	1.09×10^{-7}	1.02×10^{-4}
3	primf	0.001072	3.29×10^{-7}	4.34×10^{-4}
4	dsimf	0.001133	2.37×10^{-7}	3.48×10^{-4}
5	psigmf	0.001123	2.37×10^{-7}	3.57×10^{-4}
6	gbellmf	0.097216	1.36×10^{-7}	3.18×10^{-4}
7	trimf	0.001202	2.07×10^{-7}	3.51×10^{-4}
8	trapmf	0.001089	2.40×10^{-7}	2.47×10^{-4}

gies for various torque disturbance conditions and with uncertainty in parameters. Results are accomplished by tuning the parameters through global search algorithm, i.e., PSO under various operating conditions.

Table 2.7.1 : PD tuning parameters for 10% disturbance in torque.

Sl. No	Controlling Parameters	IATE	ISE	ISTE
1	K_p	0.021	0.002	0.015
2	K_d	13.17	24.83	15.82
Objective Function Value (J)		0.0267	0.00457	0.062

Table 2.7.2 : PID tuning parameters for 10% disturbance in torque.

Sl. No	Controlling Parameters	IATE	ISE	ISTE
1	K_p	0.023	0.042	0.634
2	K_i	0.023	0.123	0.434
3	K_d	11.24	19.27	16.30
Objective Function Value (J)		0.0104	0.00294	8.106×10^{-5}

Tables 2.7.1 and 2.7.2 shows the performance index values and tuning parameters for

different optimal control strategies with 10% torque disturbance and 10% uncertainty in parameters by PSO. From these tables, it is noticed that PID controller gives minimum objective function value than the PD controller. And also, it is observed that the model with ISTE control strategy gives minimum objective function values compared to IATE and ISE optimal control strategies. In view of these results, PID controller with ISTE control strategy has been selected for further simulation works.

Table 2.7.3 : PID tuning parameters for various disturbances.

Sl. No	Torque Disturbance (%)	K_p	K_i	K_d	J
1	0	0.102	0.314	12.432	8.102×10^{-5}
2	10	0.634	0.434	16.30	8.106×10^{-5}
3	20	0.021	0.323	11.638	8.10×10^{-5}
4	30	0.024	3.808	11.096	8.4×10^{-5}
5	40	0.043	0.102	11.88	8.52×10^{-5}
6	50	0.048	0.072	10.829	8.56×10^{-5}

Table 2.7.3 shows the PID tuning parameters from PSO for controller of two-mass single-link robot model with ISTE control strategies for 0%, 20%, 30%, 40%, and 50% disturbances in input torque. Table 2.7.4 provides the tuning parameters of BSMC. The objective values which are provided by BSMC are very less in comparison with PID controller objective values.

The complete controller arrangement (shown in Figure 2.11) can provide good tracking trajectory for a single-link robot model even in the presence of disturbances in input torque and with 10% uncertainty in system parameters. Figure 2.12 shows the error response plot for various disturbance conditions and it is inferred that the disturbance rejection capacity has improved with increase in disturbance levels. Figures 2.13b to 2.14c illustrates the responses of robot model for various torque disturbances with ISTE as optimum criterion.

Totally 50 iterations have been taken into consideration to create a dataset of parameters (% of disturbance, K , λ_1 and ϕ) for the ANFIS controller. Here K_{ANF} , λ_{ANF} , and ϕ_{ANF} are tuned adaptively for input disturbances ranging from 0% to 50%. Fi-

Table 2.7.4 : BSMC tuning parameters for various disturbances.

Sl. No	Torque Disturbance (%)	λ_1	ϕ	K	J
1	0	9.325	0.214	963.02	3.14×10^{-7}
2	10	4.32	0.033	257.25	3.246×10^{-7}
3	20	8.612	0.147	372.02	4.565×10^{-7}
4	30	8.324	0.333	452.13	7.10×10^{-7}
5	40	7.0165	0.408	918.662	2.34×10^{-6}
6	50	9.847	0.637	762.348	3.626×10^{-6}

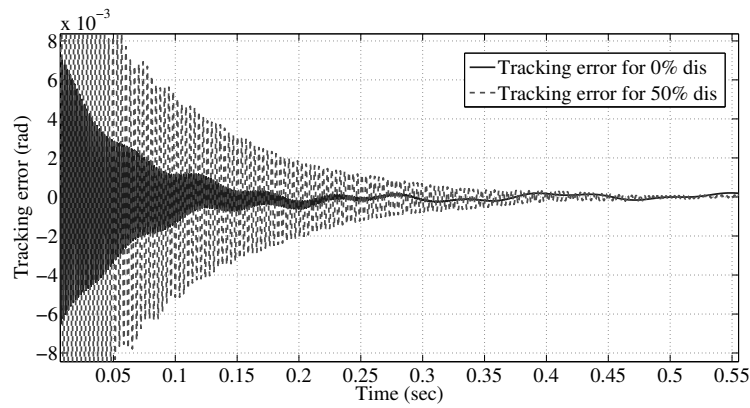
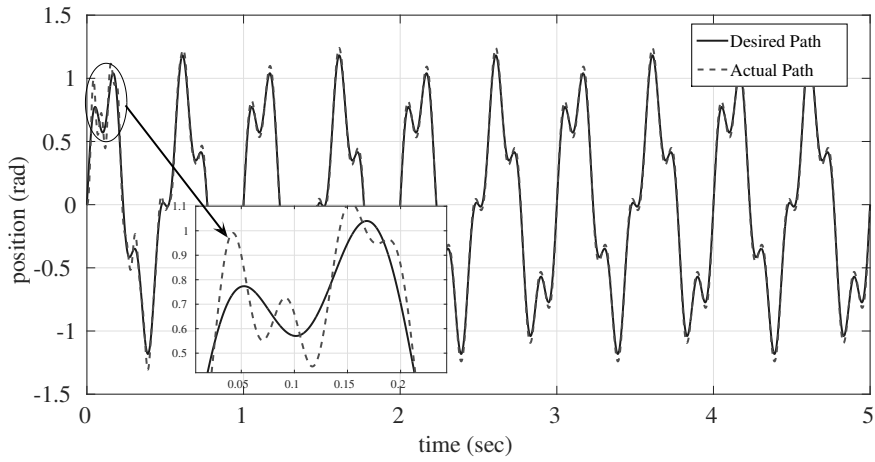
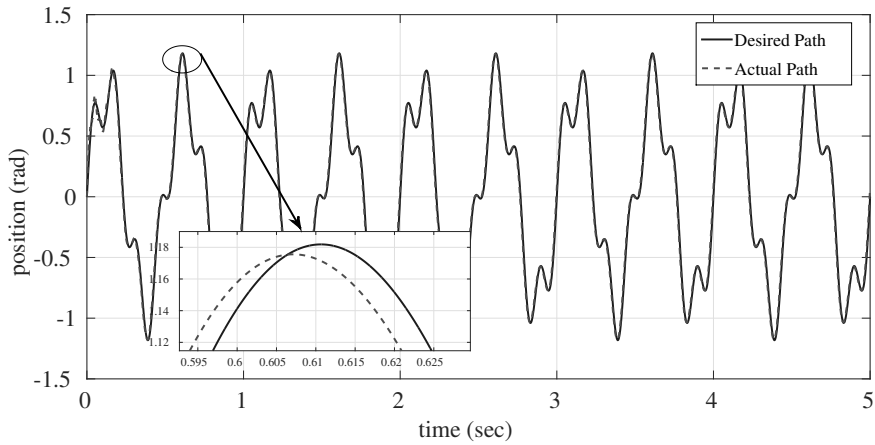


Figure 2.12 : Tracking error with ISTE for 0% and 50% disturbances.

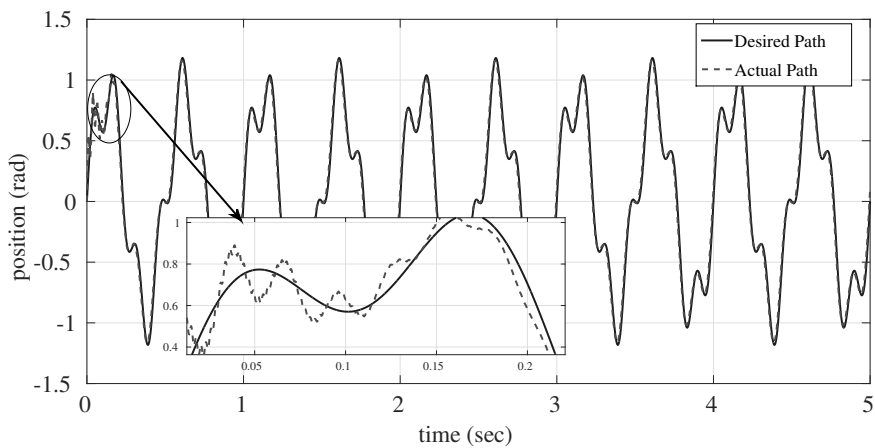
nally, an ANFIS controller has been developed to generate the adaptive control signal for the robot manipulator. Figure 2.15a shows the control input to the arm link of the robot. The results of optimized adaptive BSMC controller is compared with BSMC controller for 10% disturbance and shown in Figure 2.15b. The adaptive BSMC results are satisfactory.



(a) : Position tracking of single-link robot model for 0% disturbance.

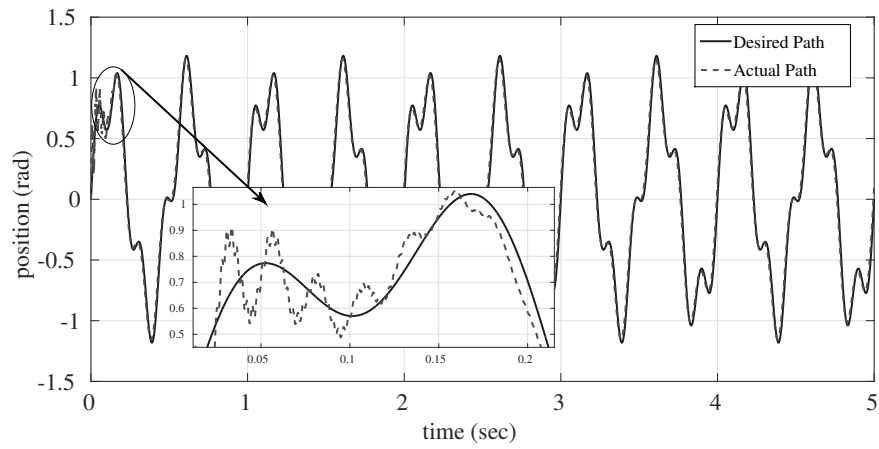


(b) : Position tracking of single-link robot model for 10% disturbance.

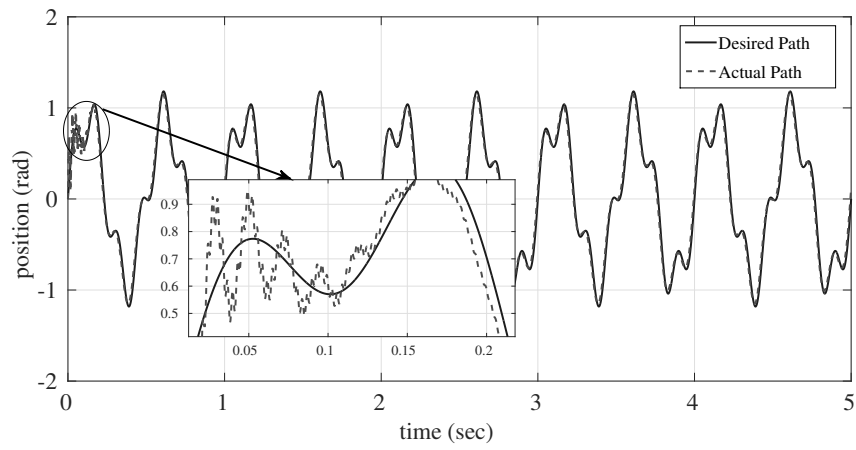


(c) : Position tracking of single-link robot model for 20% disturbance.

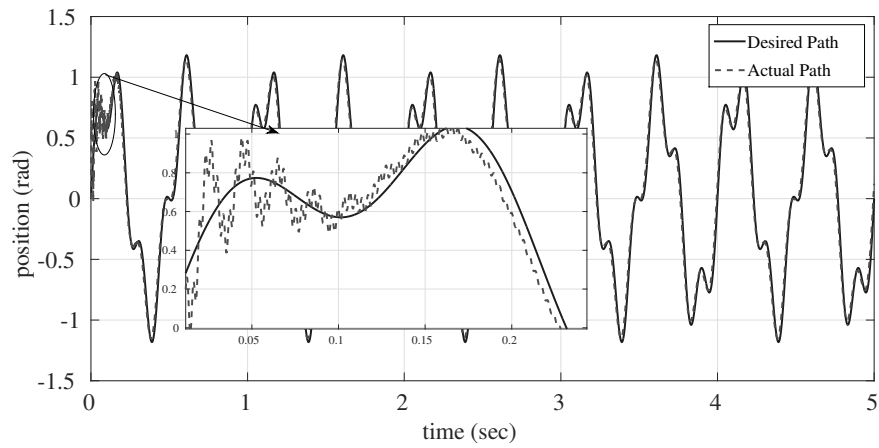
Figure 2.13 : Tracking Positions of end-effector with ISTE for various disturbances in input torque.



(a) : Position tracking of single-link robot model for 30% disturbance.

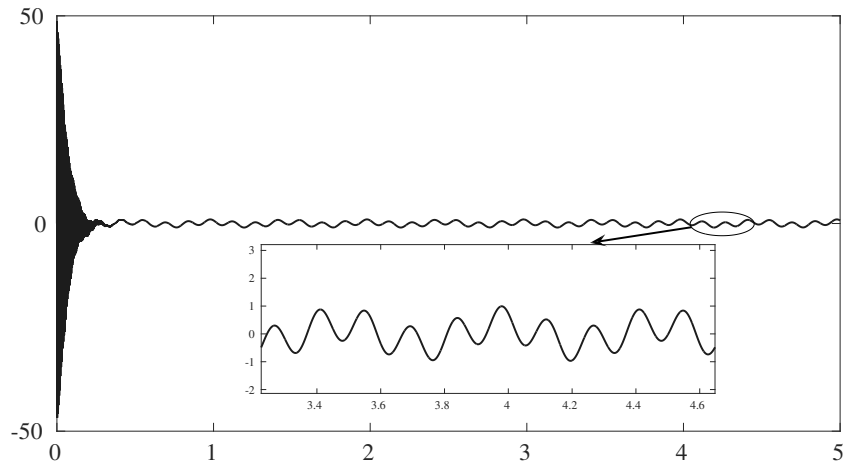


(b) : Position tracking of single-link robot model for 40% disturbance.

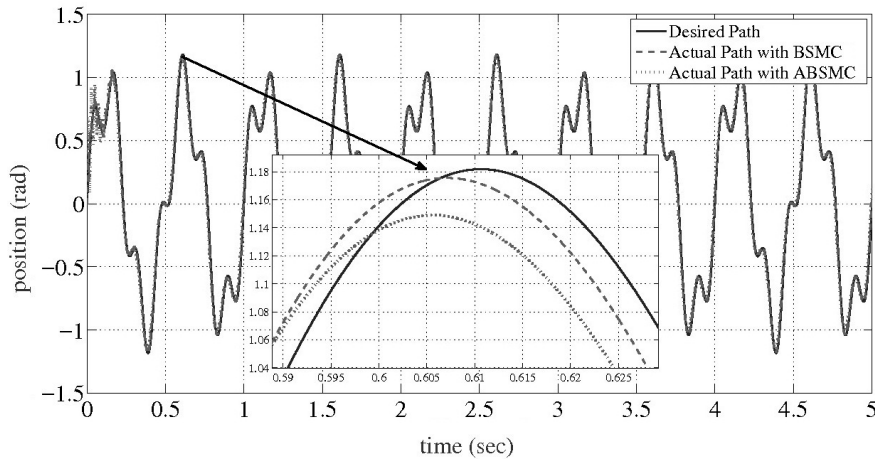


(c) : Position tracking of single link robot model for 50% disturbance.

Figure 2.14 : Tracking Positions with ISTE for various disturbances.



(a) : Control input of actuator using ABSMC proposed controller.



(b) : Tracking Positions of single-link robot using ABSMC proposed controller.

Figure 2.15 : Control input and tracking positions of single-link with ISTE for 10% disturbances.

2.8 SUMMARY

The two-mass flexible single-link robot with the gearbox is developed, and the control parameters are tuned using Fminsearch and GA for different torque disturbances and uncertainties. The following inferences are observed from the simulation results,

- GA tuning algorithm provides better stability, minimum tracking error and good disturbance rejection over Fminsearch tuning algorithm.
- The tracking of robot manipulator by considering ISTE control strategy provides

minimum objective function value in comparison with IATE and ISE.

- PID tuning with GA for ISTE gives minimum tracking error and good disturbance rejection compared to other algorithms.

Hence, the PID controller with GA tuning algorithm and ISTE optimum criterion is considered as an adaptive controller for the single-link robot.

The control parameters of the two-mass single-link robot are also tuned using PSO. The following inferences are observed from the simulation results,

- PSO based PID tuning parameters gives minimum tracking error and good disturbance rejection.
- The tracking of the robot model while considering the ISTE control strategy provides minimum objective function value in comparison with IATE and ISE.
- ANFIS adaptive BSMC controller is robust while considering the uncertainties in the system parameters and disturbances in the input torque.

Chapter 3

PSO BASED NEURO-FUZZY SLIDING MODE CONTROL FOR A ROBOT MANIPULATOR

This chapter discusses the variations of SMC controller in which PID sliding surface is taken into consideration for the control of 2-DOF and 3-DOF robot manipulators.

3.1 INTRODUCTION

This non-linear controller provides acceptable control performance with stability and robustness for non-linear systems (Iordanou and Surgenor, 1997). However, conventional SMC which are used extensively has certain disadvantages. Firstly, chattering problem can cause high-frequency oscillations in the controller output, secondly sensitivity to input disturbances and parameter uncertainties. Chattering phenomenon can cause issues such as saturation and heat in mechanical parts of the robot manipulators. To overcome the chattering problem, various solutions have been reported in the literature which can be classified into two categories: boundary layer saturation method and estimated uncertain method (Khalil, 2002; Curk and Jezernik, 2001).

In recent years, Neural Networks (NNs), Fuzzy logic, and Neuro-fuzzy are combined with SMC. These combinations are used in non-linear, time variant, and uncertain plant. Some researchers applied the fuzzy logic methodology in SMC to reduce the chattering (Barrero et al., 2002), and other researchers have used sliding mode methodology in a fuzzy logic controller (FLC) to improve the stability of the system (Aloui et al., 2011). The utilization of the adaptive neural networks to a robot manipu-

lator is presented in (Perez et al., 2012) which explains recurrent neural networks and Lyapunov function methodology. An adaptive type-2 FLC for flexible-joint manipulators with structured and unstructured dynamical uncertainties have been introduced in (Chaoui et al., 2013). In (Abdel et al., 2011), the authors have proposed fuzzy partition to the state variables based on the Lyapunov synthesis. Authors in (Zeinali and Notash, 2010) have presented a methodology that enables the designer to derive the rule base of the control method systematically.

This chapter presents a new adaptive SMC methodologies for 2-DOF and 3-DOF robot manipulators. The adaptive SMC algorithm can estimate the value of the switching gain constant (K_w) and boundary layer thickness (ϕ) in real time. A PID sliding surface method is adopted instead of a conventional sliding surface method. An adaptive PID sliding mode control with boundary layer (APIDSMCB) that can handle different level of input torque disturbances is derived, and the stability of the closed-loop system is established. The numerical simulation is presented to verify the effectiveness of the proposed control scheme. It is inferred that the proposed APIDSMCB scheme offers several advantages such as substantial robustness to parameter variation and external disturbance.

3.2 CONTROLLER DESIGN AND STABILITY ANALYSIS FOR A 2-DOF ROBOT MANIPULATOR

In this work, PSO is used to minimize the objective functions. Simulations are carried out to estimate the following design control parameters

1. Finding the optimal sliding surface parameters K_p , K_i and K_d of conventional PID controller.
2. Calculating the optimal parameters λ , K_w and ϕ of SMC and SMC with boundary layer (i.e., SMCB) controllers.
3. Calculating the optimal parameters K_p , K_i , K_d , K_w , and ϕ of PIDSMCB controller.

3.2.1 SMCB with PID sliding surface and stability analysis

In SMC, it is very important to implement the sliding surface 's' which is expected to provide desired control specifications and performance. The trajectories are enforced to lie on the sliding surface. The block diagram of SMCB with PID sliding surface is given in Figure 3.1

The sliding PID surface in the space of tracking error can be defined as

$$s = K_p e + K_i \int e dt + K_d \frac{d}{dt} e \quad (3.1)$$

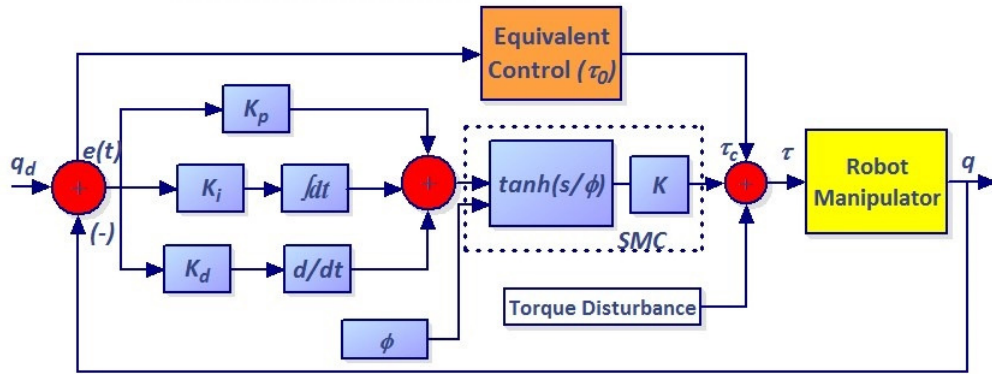


Figure 3.1 : Block diagram of the SMCB with PID sliding surface.

The derivative of sliding surface with respect to time is expressed as

$$\dot{s} = K_p \dot{e} + K_i e + K_d [\ddot{q}_d - \ddot{q}] \quad (3.2)$$

Substituting equation (1.2) into above equation (3.2), we get

$$\dot{s} = K_p \dot{e} + K_i e + K_d [\ddot{q}_d - D^{-1}(q)(\tau - (C(q, \dot{q})\dot{q} + G(q) + F(q, \dot{q}) + \tau_d))] \quad (3.3)$$

The control effort is derived as the solution of $\dot{s} = 0$, without uncertainties (i.e., $\tau_d = 0$) to achieve the desired performance under nominal model is referred as equivalent control effort, represented by τ_0 .

$$\dot{s} = K_p \dot{e} + K_i e + K_d [\ddot{q}_d - D^{-1}(q)(\tau - (C(q, \dot{q})\dot{q} + G(q) + F(q, \dot{q}))) = 0 \quad (3.4)$$

$$\tau_0 = K_d^{-1} K_p D(q) \dot{e} + K_d^{-1} K_i D(q) e + D(q) \ddot{q}_d + [C(q, \dot{q})\dot{q} + G(q) + F(q, \dot{q})] \quad (3.5)$$

However, in case of unpredictable disturbances or uncertainties, the equivalent control effort cannot ensure the favorable control performance. Therefore, auxiliary control effort should be designed to eliminate the effect of the unpredictable disturbances. For

this purpose, the Lyapunov function can be chosen as:

$$V = \frac{1}{2}s^T s \quad (3.6)$$

The reaching condition can be defined as:

$$\dot{V} = s^T \dot{s} < 0, s \neq 0 \quad (3.7)$$

To obtain the reaching control signal τ_c , equation (3.7) is defined as:

$$\begin{aligned} \dot{V} = & s^T [K_p \dot{e} + K_i e + K_d \ddot{q}_d] - s^T K_d D^{-1}(q) [\tau_0 + \tau_c] + s^T K_d D^{-1}(q) [C(q, \dot{q}) \dot{q} \\ & + G(q) + F(q, \dot{q})] \end{aligned} \quad (3.8)$$

Substituting equation (3.5) into equation (3.8), we get

$$\dot{V} = s^T [0] - s^T K_d D^{-1}(q) \tau_c \quad (3.9)$$

To ensure $s^T \dot{s} < 0$, the reaching control law should be selected as:

$$\tau_c = K_d^{-1} D(q) K_w \text{sign}(s) \quad (3.10)$$

$$\tau_c = K \text{sign}(s) \quad (3.11)$$

where $K = K_d^{-1} K_w D(q)$ is a positive gain matrix. Obviously, substituting equation (3.10) into equation (3.9) we get

$$\dot{V} < -s^T K_d D(q)^{-1} (K_d^{-1} D(q) K_w \text{sign}(s)) \quad (3.12)$$

$$\dot{V} < -K_w s^T \text{sign}(s)$$

$$\dot{V} < -K_w |s| \quad (3.13)$$

In order to avoid chattering effect, the sign function in equation (3.11) is replaced by the tanh (hyperbolic tangent) function.

$$\dot{V} < -K_w s^T \tanh(s) \quad (3.14)$$

Similar to equation (2.22), we can prove stability condition for above equation. Finally, the reaching control signal τ_c is given as follows

$$\tau_c = K \tanh \left(\frac{K_p e + K_i \int e dt + K_d \frac{d}{dt} e}{\phi} \right) \quad (3.15)$$

3.3 ADAPTIVE PIDSMCB DESIGN AND STABILITY ANALYSIS

3.3.1 Artificial Neural Network (ANN) Based PIDSMCB

In ANN, two-layer feed-forward networks with sigmoid hidden neurons and linear output neurons can fit well in the multi-dimensional mapping problems, given consistent data and enough neurons in its hidden layer. The network will be trained with Levenberg-Marquardt backpropagation algorithm. Backpropagation is a specific technique for implementing descent in weight space for a multilayer feedforward network. In hidden layer, the network is trained with 10 number of neurons.

Similar to equation (3.1), the sliding surface for adaptive PIDSMCB can be defined as

$$s = K_p e + K_i \int e dt + K_d \frac{d}{dt} e \quad (3.16)$$

From equation (3.7), we can define the necessary conditions for Lyapunov stability

$$\dot{V} = s^T \dot{s} < 0, \quad s \neq 0 \quad (3.17)$$

Similarly, the stability of this controller can be proved from equation (3.14)

$$\dot{V} < -s^T \tanh(s) \quad (3.18)$$

Finally, we can define the final control law developed by Neuro based adaptive PIDSMCB is

$$\tau_c = K_{NN} \tanh \left(\frac{K_p e + K_i \int e dt + K_d \frac{d}{dt} e}{\phi_{NN}} \right) \quad (3.19)$$

Where $K_{NN} = (K_{WNN})K_d^{-1}D(q)$ and $K_{WNN} = \text{diag}\{K_{WNN1}, K_{WNN2} \dots K_{WNNn}\}$ is adaptive switching gain matrix and ϕ_{NN} is adaptive boundary layer thickness of NN-based APIDSMCB.

3.3.2 Artificial Neuro Fuzzy Inference System (ANFIS) Based PIDSMCB

In ANFIS, for a given input/output data set, the toolbox function constructs a FIS whose membership functions are tuned (adjusted) using either a backpropagation algorithm alone or in combination with the least square method. Both ANN and fuzzy logic are used in architecture (Jang, 1993). In the process of developing the ANFIS adaptive controller, the training was performed on MATLAB environment by using various input

membership functions with multiple training datasets under different disturbance conditions. Figure 3.2 illustrates the framework of the ANFIS adaptive SMCB with PID sliding surface. Here, ANFIS model provides adaptive K_{ANF} and ϕ_{ANF} to the SMCB for different torque disturbance conditions.

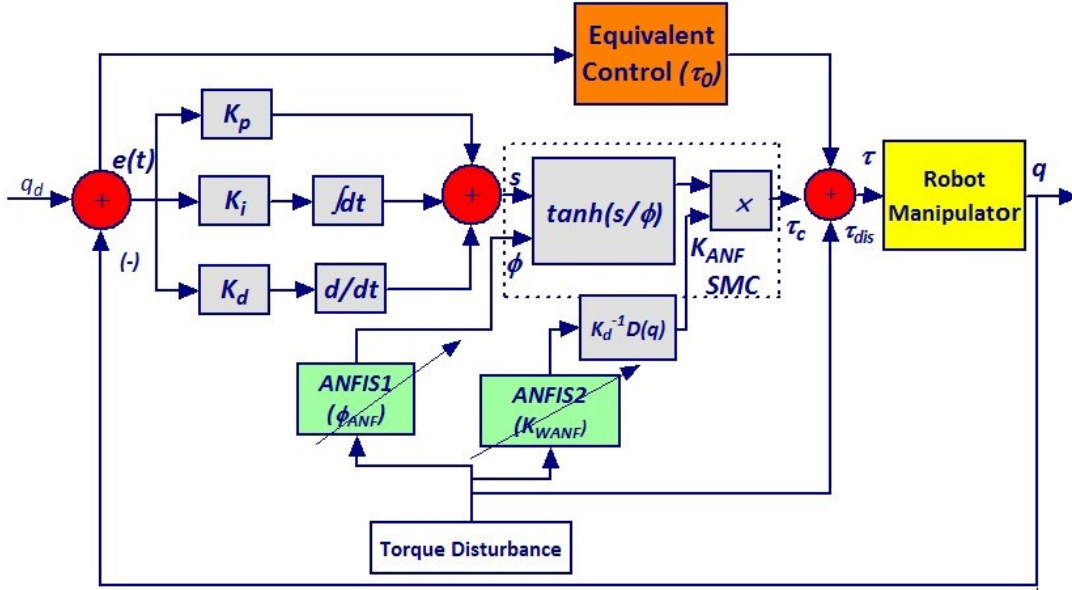


Figure 3.2 : Block diagram of the ANFIS adaptive SMCB with PID sliding surface.

Similar to equation (3.1), the sliding surface for adaptive PIDSMCB can be defined as

$$s = K_p e + K_i \int e dt + K_d \frac{d}{dt} e \quad (3.20)$$

From equation (3.7), we can define the necessary conditions for Lyapunov stability

$$\dot{V} = s^T \dot{s} < 0, \quad s \neq 0 \quad (3.21)$$

The stability of of this controller can be proved from equation (3.14), then

$$\dot{V} < -s^T \tanh(s) \quad (3.22)$$

Finally, we can define the final control law developed by APIDSMCB is

$$\tau_c = (K_{ANF}) \tanh \left(\frac{K_p e + K_i \int e dt + K_d \frac{d}{dt} e}{\phi_{ANF}} \right) \quad (3.23)$$

Where $K_{ANF} = (K_{WANF})K_d^{-1}D(q)$ and $K_{WANF} = \text{diag}\{K_{WANF1}, K_{WANF2} \dots K_{WANFn}\}$ is adaptive switching gain matrix. Table 3.3.1 gives the training error values for adaptive switching gain constant (K_{WANF}) and adaptive boundary layer thickness (ϕ_{ANF}) of SMC under various membership functions. Totally 8 membership functions and 300

Epochs are considered for training of each ANFIS network. From Table 3.3.1 , it is ob-

Table 3.3.1 : The predicted results of different membership function for various inputs.

Sl. No	Used Membership Function (MF)	No. of Membership Functions	Epochs	Training Error Values for K_{WANF}	Training Error Values for ϕ_{ANF}
1	gaussmf	10	300	0.001068	2.16×10^{-7}
2	gauss2mf	10	300	0.001053	1.09×10^{-7}
3	primf	10	300	0.001072	3.29×10^{-7}
4	dsimf	10	300	0.001133	2.37×10^{-7}
5	psigmf	10	300	0.001123	2.37×10^{-7}
6	gbellmf	10	300	0.097216	1.36×10^{-7}
7	trimf	10	300	0.001202	2.07×10^{-7}
8	trapmf	10	300	0.001089	2.40×10^{-7}

served that the ‘gauss2mf ’ provides minimum training error for the both cases. Finally, gauss2mf membership function is used in designing of the ANFIS network for SMC.

3.4 RESULTS AND DISCUSSIONS FOR THE 2-DOF ROBOT MANIPULATOR

Simulation is carried out for the 2-DOF robot manipulator in MATLAB. Initially, the optimum robot manipulator controller is designed for IATE, ISE, and ISTE control strategies for different torque disturbances. Results are obtained by tuning the parameters through global search algorithm, i.e., PSO under various input torque disturbance conditions.

The dynamic equation of the robot manipulator model (shown in Figure 3.3) is given by

$$\begin{bmatrix} D_{11} & D_{12} \\ D_{21} & D_{22} \end{bmatrix} \begin{bmatrix} \ddot{q}_1 \\ \ddot{q}_2 \end{bmatrix} + \begin{bmatrix} C_1(q_1, q_2) \dot{q}_2 \\ C_2(q_1, q_2) \dot{q}_1 \end{bmatrix} + \begin{bmatrix} G_1(q_1) \\ G_2(q_2) \end{bmatrix} = \begin{bmatrix} \tau_1 \\ \tau_2 \end{bmatrix} + \begin{bmatrix} \tau_{d1} \\ \tau_{d2} \end{bmatrix}$$

where

$$\begin{aligned} D_{11} &= \left[\left(\frac{1}{3} m_1 + m_2 \right) L_1^2 \right] + \frac{1}{3} m_2 L_2^2 + m_2 L_1 L_2 \cos(q_2) \\ D_{12} = D_{21} &= m_2 \left[\frac{1}{3} L_2^2 + \frac{1}{2} L_1 L_2 \cos(q_2) \right] \\ D_{22} &= \frac{1}{3} m_2 L_2^2 \end{aligned}$$

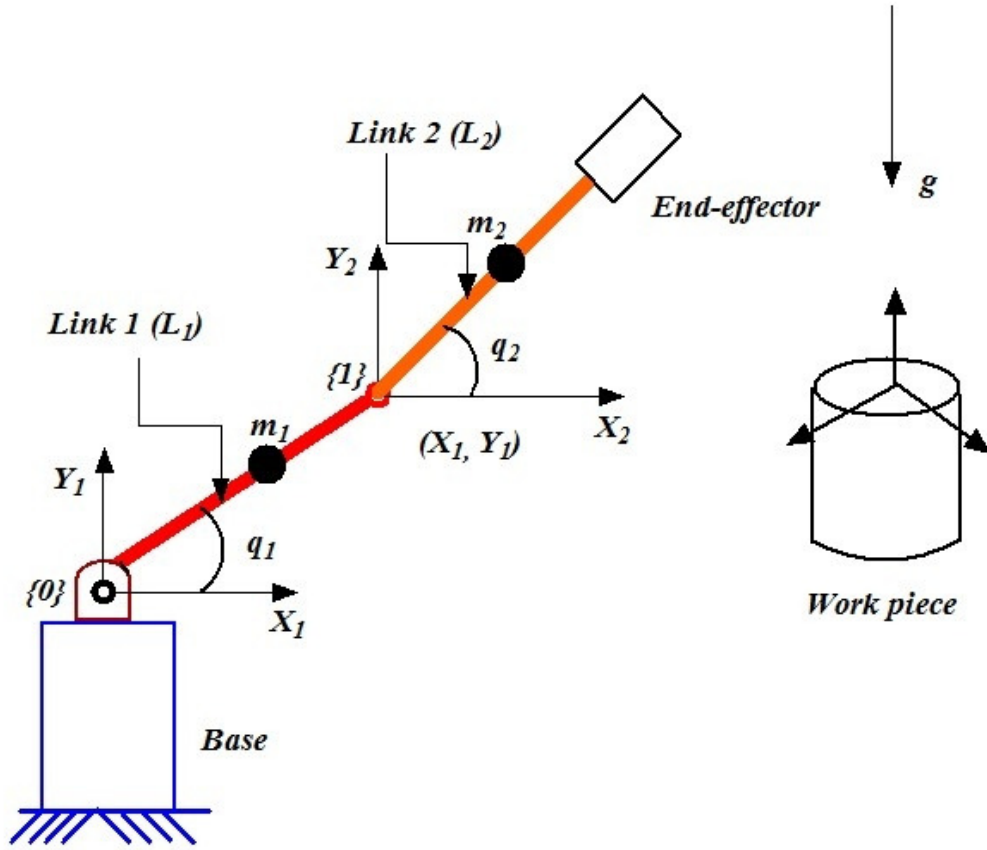


Figure 3.3 : Rigid two link robot manipulator (Mittal and Nagrath, 2003).

$$\begin{aligned}
 C_1(q_1, q_2) &= -m_2 L_1 L_2 \sin(q_2) \dot{q}_1 - \frac{1}{2} m_2 L_1 L_2 \sin(q_2) \dot{q}_2 \\
 C_2(q_1, q_2) &= \frac{1}{2} m_2 L_1 L_2 \sin(q_2) \dot{q}_1 \\
 G_1(q_1) &= \left[\left(\frac{1}{2} m_1 + m_2 \right) L_1 \cos(q_1) + \frac{1}{2} m_2 L_2 \cos(q_1 + q_2) \right] g \\
 G_2(q_2) &= \frac{1}{2} m_2 L_2 \cos(q_1 + q_2) g
 \end{aligned} \tag{3.24}$$

The physical parameters under consideration are listed as follows: $m_1=10$ kg, $m_2=10$ kg, $L_1=0.5$ m, $L_2=0.5$ m and $g = 9.8m/s^2$. m_1 and m_2 are the two joint masses, L_1 and L_2 are the arm lengths, τ_1 , τ_2 are input torque and τ_{d1} , τ_{d2} are disturbance torques of robot manipulator.

Table 3.4.1 and 3.4.2 show the conventional PID control tuning parameters resulted from PSO with IATE, ISE, and ISTE control strategies for 5% and 10% torque dis-

Table 3.4.1 : PID tuning parameters for 5% input torque disturbance.

Sl. No	Controlling Parameters	IATE	ISE	ISTE
1	K_{p1}	514.5	819.5	532.8
2	K_{i1}	156.6	574.8	217.8
3	K_{d1}	42.55	459.9	168.7
4	K_{p2}	204.7	119.73	686.7
5	K_{i2}	318.8	257.6	329.4
6	K_{d2}	901.3	40.21	164.8
Objective function value (J)		0.5147	0.0180	0.0168

Table 3.4.2 : PID tuning parameters for 10% input torque disturbance.

Sl.No	Controlling Parameters	IATE	ISE	ISTE
1	K_{p1}	814.9	665.6	814.9
2	K_{i1}	631.5	799.5	631.5
3	K_{d1}	745.1	122.1	745.1
4	K_{p2}	380.2	416.7	380.2
5	K_{i2}	427.6	716.5	427.6
6	K_{d2}	169.7	777.6	169.7
Objective Function value (J)		0.5506	0.09713	0.0313

turbances. From the above tables, it is observed that the model with ISTE control strategy gives minimum objective function values (i.e., 0.0168 and 0.0313 for 5% and 10% disturbances in input torque, respectively) compared to IATE and ISE optimal control strategies. Finally, ISTE control strategy has been selected for further simulation works of robot manipulator. Table 3.4.3 shows the SMC parameters and objective function values for 5%, 7.5%, and 10% torque disturbances resulting from PSO. Table 3.4.4 shows the SMCB parameters and objective function values for 5%, 7.5%, and 10% torque disturbances resulting from PSO. The maximum operating torque (τ) under 10% input torque disturbance is 0.8×10^4 Nm. For a 10% disturbance of input torque (i.e. 800 Nm) the PID parameters obtained from PSO tuning of PIDSMCB are found

Table 3.4.3 : SMC parameters for 5%, 7.5%, and 10% input torque disturbances.

Sl.No	Parameters of SMC	5%dis	7.5%dis	10%dis
1	K	297.1	178.3932	315.7
2	λ	57.42	550.8505	9.25
Objective Function Value (J)		0.0009	0.00058	0.0073

Table 3.4.4 : SMCB parameters for 5%, 7.5%, and 10% input torque disturbances.

Sl.No	Parameters of SMCB	5%dis	7.5%dis	10%dis
1	K	454.25	634.8768	589.03
2	λ	934.49	816.5764	870.44
3	ϕ	0.3858	0.5959	0.0842
Objective Function Value (J)		3.386×10^{-6}	5.5×10^{-6}	6.742×10^{-7}

Table 3.4.5 : PIDSMCB parameters for 5%, 7.5%, and 10% input torque disturbances.

Sl.No	Controlling Parameters	5%dis	7.5%dis	10%dis
1	K_{p1}	870.5	439.8	734.5
2	K_{i1}	265.6	217.5	780.2
3	K_{d1}	573.7	533.1	461.3
4	K_{p2}	411.9	831.4	747.2
5	K_{i2}	36.9	450.4	786.4
6	K_{d2}	490.4	600.9	106.1
7	K	662.6	766.2	992.9
8	ϕ	0.5215	0.4978	0.1709
Objective Function Value (J)		1.498×10^{-5}	3.437×10^{-6}	6.168×10^{-7}

to be, $K_{p1} = 734.5$, $K_{i1} = 780.2$, $K_{d1} = 461.3$, $K_{p2} = 742.2$, $K_{i2} = 786.4$ and $K_{d2} = 106.1$ as given in Table 3.4.5. These tuned PID parameters are kept fixed for all iterations but the sliding control parameters (K and ϕ) are calculated using PSO. For data generation, K and ϕ are obtained for various input disturbances ranging from 0% to 11% with a step size of almost 0.1% disturbance. Total 115 number of data sets (% of disturbance,

K and ϕ) are collected by PSO tuned PIDSMCB. Among those data sets, 110 number of data sets are used for training and the rest 5 data sets are used for testing the ANFIS controller. Finally, results of the APIDSMCB are compared with the PSO tuned PIDSMCB controller in Table 3.4.6.

Table 3.4.6 : Comparison of control parameters from different approaches.

Sl. No	Disturbance in input Torque (%)	Parameters from PSO		Objective Function Value (J)	Parameters from ANFIS		Objective Function Value (J_{ANF})
		K_w	ϕ		K_{WANF}	ϕ_{ANF}	
1	1.75	913.5	0.381	2.45×10^{-6}	722.1	0.048	4.61×10^{-4}
2	2.85	962.8	0.755	6.01×10^{-6}	924	0.022	4.25×10^{-5}
3	7.55	367.8	0.766	3.5×10^{-5}	1026	0.175	2.88×10^{-5}
4	9.35	699.7	0.763	3.49×10^{-5}	994.5	0.016	4.03×10^{-6}
5	10.82	602.8	0.487	4.09×10^{-6}	964.4	0.065	8.08×10^{-6}

Figures 3.4 and 3.5 show the response of robot manipulator link positions for 10% disturbance in input torque with ISTE optimum criterion under PID, SMC, and SMCB methods. Figures 3.6 and 3.4 show the response of robot manipulator link positions for 10% disturbance in input torque with ISTE optimum criterion under PIDSMCB and APIDSMCB methods. From the Figures 3.4 and 3.7, it is clear that the tracking error is minimum for PIDSMCB compared to conventional PID, SMC, and SMCB. Figures 3.8 and 3.9 show control torque input by using SMC and APISMCB proposed controllers, respectively. Figure 3.10 shows the tracking error responses for 10% disturbance in input torque under PIDSMCB.

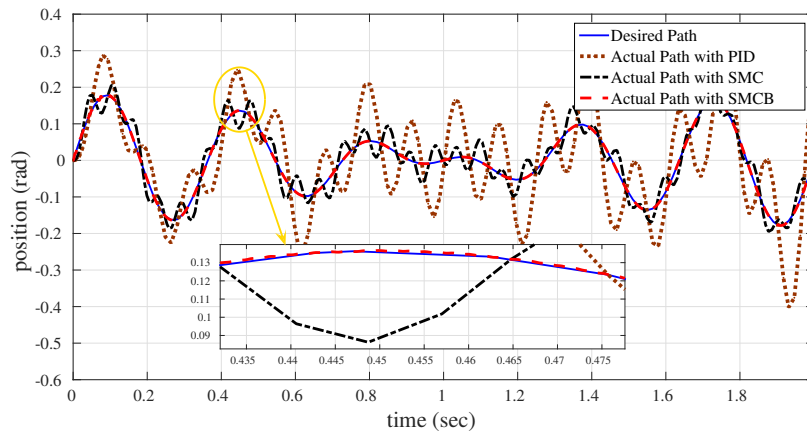


Figure 3.4 : Tracking positions of Link 1 with PID, SMC and SMCB for 10% disturbance in input torque.

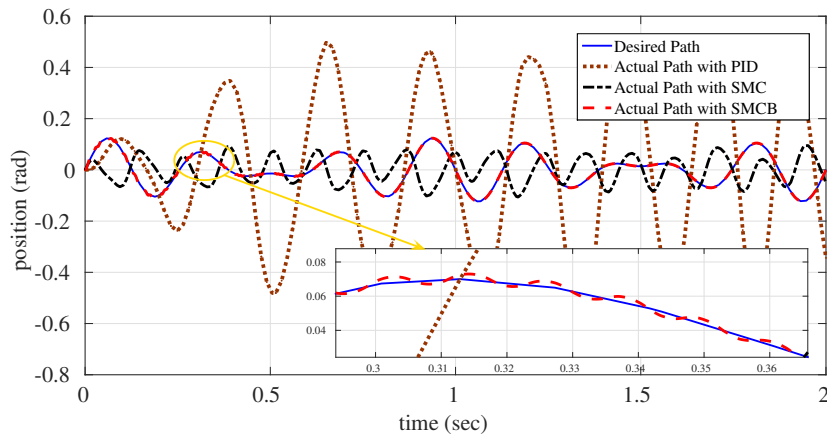


Figure 3.5 : Tracking positions of Link 2 with PID, SMC and SMCB for 10% disturbance in input torque.

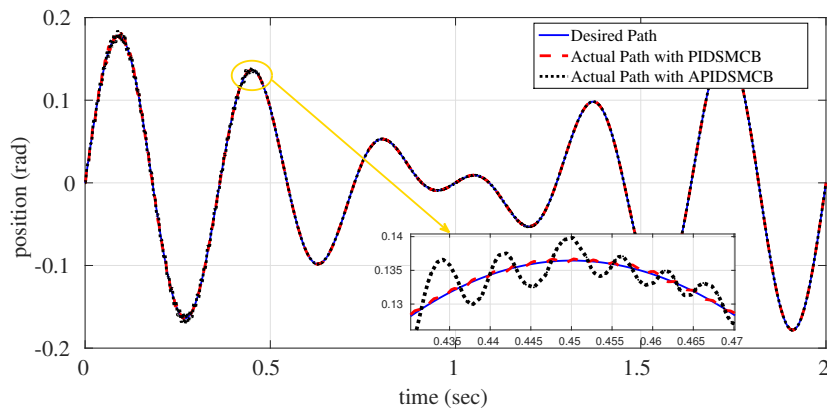


Figure 3.6 : Tracking positions of Link 1 with PIDSMCB and APIDSMCB for 10% disturbance in input torque

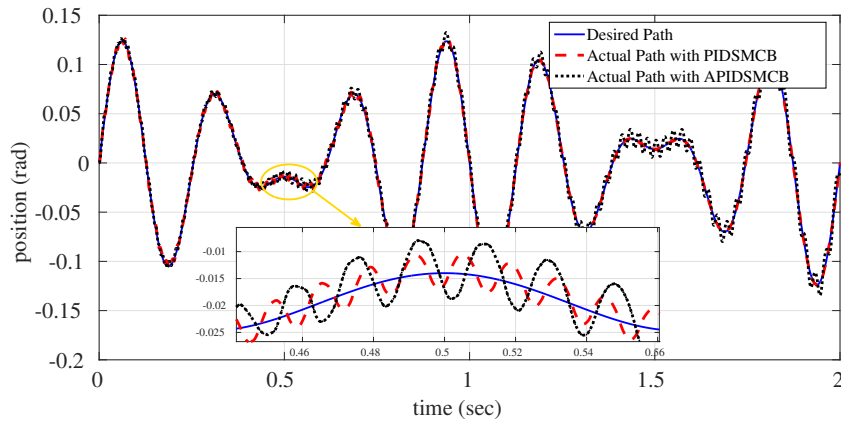


Figure 3.7 Tracking positions of Link 2 with PIDSMCB and APIDSMCB for 10% disturbance in input torque

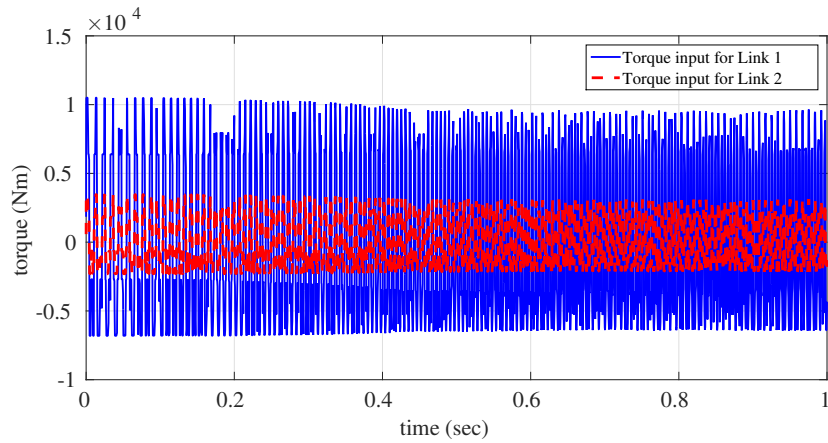


Figure 3.8 : Control input of Link 1 and Link 2 using SMC proposed controller for 10% disturbance in input torque.

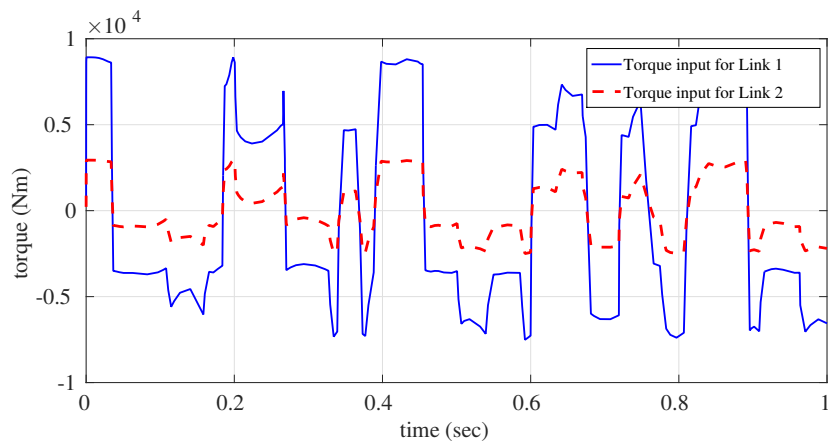


Figure 3.9 : Control input of Link 1 and Link 2 using PIDSMCB proposed controller for 10% disturbance in input torque.

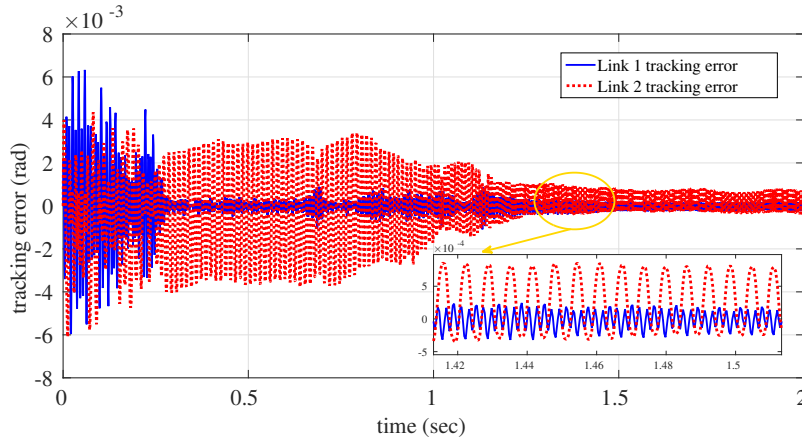


Figure 3.10 : Comparison of tracking error responses with APISMCB for 10% disturbance in input torque.

3.5 RESULTS AND DISCUSSIONS FOR 3-DOF ROBOT MANIPULATOR

Numerical simulations are performed for the 3-DOF rigid robot manipulator in MATLAB and SIMULINK. Figure 3.11 shows three-link rigid robot manipulator, where $q_1(t)$, $q_2(t)$ and $q_3(t)$ are angular positions, m_1 , m_2 and m_3 are link masses, L_1 , L_2 and L_3 are the link lengths, $\tau_1(t)$, $\tau_2(t)$ and $\tau_3(t)$ are the input torque of robot manipulator. The physical parameters under consideration are listed as follows: $m_1=5.4$ kg, $m_2=29.5$ kg, $m_3=18.5$ kg, $L_1=0.58$ m, $L_2=0.5$ m, $L_3=0.79$ m and $g = 9.8m/s^2$. Initial conditions are $q(0) = [q_1(0), q_2(0), q_3(0)]^T = 0$ and $\dot{q}(0) = [\dot{q}_1(0), \dot{q}_2(0), \dot{q}_3(0)]^T = 0$. The reference tracking signals are $q_{d1}(t) = 0.09 \sin(\pi t) + 0.03 \sin(14\pi t)$, $q_{d2}(t) = 0.07 \sin(17\pi t) + 0.056 \sin(9\pi t)$ and $q_{d3}(t) = 0.12 \sin(5\pi t) + 0.09 \sin(2\pi t)$. The most essential parameters that affect the control performance of the robot manipulator are frictional terms (i.e. $F(q(t), \dot{q}(t))$) and external disturbances (τ_d). Considered friction terms are $F(q_1, \dot{q}_1) = 5\dot{q}_1 + 5\text{sign}(\dot{q}_1)$, $F(q_2, \dot{q}_2) = 10\dot{q}_2 + 10\text{sign}(\dot{q}_2)$ and $F(q_3, \dot{q}_3) = 15\dot{q}_3 + 15\text{sign}(\dot{q}_3)$.

Table 3.5.1 shows the conventional PID control tuning parameters resulted from PSO with IATE, ISE, and ISTE control strategies for 10% torque disturbance. From the Table 3.5.1, it is observed that the model with ISTE control strategy gives minimum objective function value compared to IATE and ISE optimal control strategies. Finally, ISTE control strategy has been taken as the performance index for further simulation

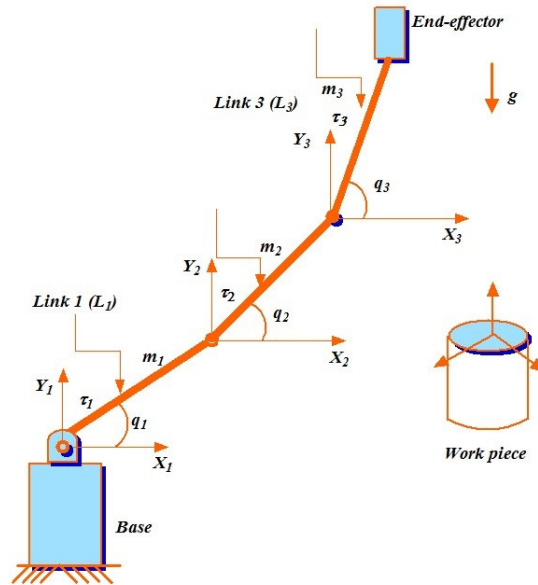


Figure 3.11 : A 3-DOF planar articulated robot manipulator (Lai et al., 2015).

Table 3.5.1 : PID Tuning Parameters for 10% disturbance in input torque

Sl. No	Controlling Parameters	IATE	ISE	ISTE
1	K_{p1}	814.9	665.6	627.3
2	K_{i1}	631.5	799.5	631.5
3	K_{d1}	745.1	122.1	745.1
4	K_{p2}	380.2	416.7	380.2
5	K_{i2}	427.6	716.5	427.6
6	K_{d2}	169.7	777.6	169.7
7	K_{p3}	703.8	554.5	516.2
8	K_{i3}	520.4	688.4	520.4
9	K_{d3}	117.5	127.5	871.2
Objective Function Value (J)		0.5506	0.09713	0.0113

works of the robot manipulator.

Table 3.5.2 shows the SMC parameters and objective function values for 5%, 7.5%, and 10% torque disturbances resulting from PSO. Table 3.5.3 shows the SMCB parameters and objective function values for 5%, 7.5%, and 10% torque disturbances resulting from PSO. Figures 3.12a to 3.12c shows the responses of robot manipulator link po-

Table 3.5.2 : SMC Parameters for 5%, 7.5%, and 10% input torque disturbances

Sl. No	Parameters of SMC	5%dis	7.5%dis	10%dis
1	K_w	297.1	178.3932	315.7
2	λ	57.42	550.8505	9.25
Objective Function Value (J)		0.009	0.0058	0.073

sitions for 10% disturbance in input torque with ISTE optimum criterion under PID, SMC, SMCB and PIDSMCB methods. From these figures, it is clear that the tracking error is minimum for SMCB compared to conventional PID and SMC.

For a 10% disturbance of input torque, the PID parameters obtained from PSO tuning of PIDSMCB are found to be, $K_{p1} = 734.5$, $K_{i1} = 780.2$, $K_{d1} = 461.3$, $K_{p2} = 742.2$, $K_{i2} = 786.4$ and $K_{d2} = 106.1$, $K_{p3}=814.9$, $K_{i3}=631.5$ and $K_{d3}=745.1$ as given in Table 3.5.4. These tuned PID parameters given are kept fixed for all iterations but the sliding control parameters (K_w and ϕ) are calculated by using PSO. For data generation K_w and ϕ are obtained for various input disturbances ranging from 0 to 11% with a step size of almost 0.1% disturbance. Total 115 number of data (% of disturbance, K_w and ϕ) are collected by PIDSMCB tuned by PSO. Among those data 110 has been used for training and rest 5 data are used for testing adaptive controllers. Finally, testing results of the neuro and neuro-fuzzy based APIDSMCB are compared using the statistical analysis ANOVA (Analysis of variance) as shown in Figure 3.15. In descriptive statistics, ‘anova1’ performs a one-way ANOVA for comparing the means of two or more groups of data.

Figures 3.13a, 3.13b and 3.13c show control torque input by using PID, SMC, and PIDSMCB respectively. From the figures, it is clear that conventional SMC creates more chattering in control torque compared PIDSMCB method. Figures 3.14a, 3.14b and 3.14c show the Tracking error response under 10% torque disturbance in input torque under PID, SMC, and PIDSMCB methods.

Table 3.5.3 : SMCB Parameters for 5%, 7.5%, and 10% input torque disturbances

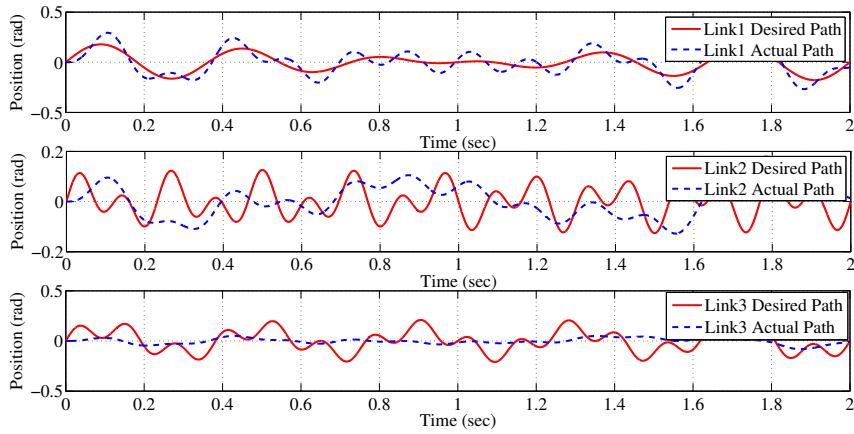
Sl. No	Parameters of SMCB	5%dis	7.5%dis	10%dis
1	K_w	454.25	634.8768	589.03
2	λ	934.49	816.5764	870.44
3	ϕ	0.3858	0.5959	0.0842
Objective Function Value (J)		3.386×10^{-4}	5.5×10^{-4}	6.742×10^{-4}

Table 3.5.4 : PIDSMCB parameters for 5%, 7.5% and 10% input torque disturbances

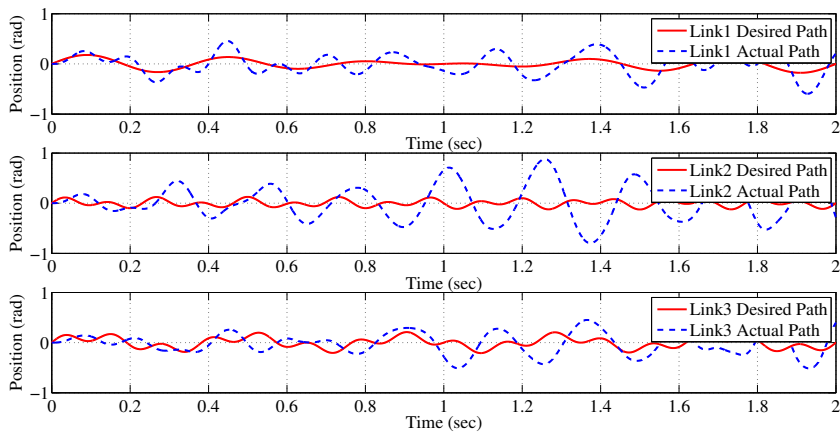
Sl.No	Controlling Parameters	5%dis	7.5%dis	10%dis
1	K_{p1}	870.5	439.8	734.5
2	K_{i1}	265.6	217.5	780.2
3	K_{d1}	573.7	533.1	461.3
4	K_{p2}	411.9	831.4	747.2
5	K_{i2}	36.9	450.4	786.4
6	K_{d2}	490.4	600.9	106.1
7	K_{p3}	814.9	665.6	814.9
8	K_{i3}	631.5	799.5	631.5
9	K_{d3}	745.1	122.1	745.1
10	K_w	662.6	766.2	992.9
11	ϕ	0.5215	0.4978	0.1709
Objective Function Value (J)		1.498×10^{-5}	3.437×10^{-5}	6.168×10^{-5}

Table 3.5.5 : Comparison of Control parameters from different approaches

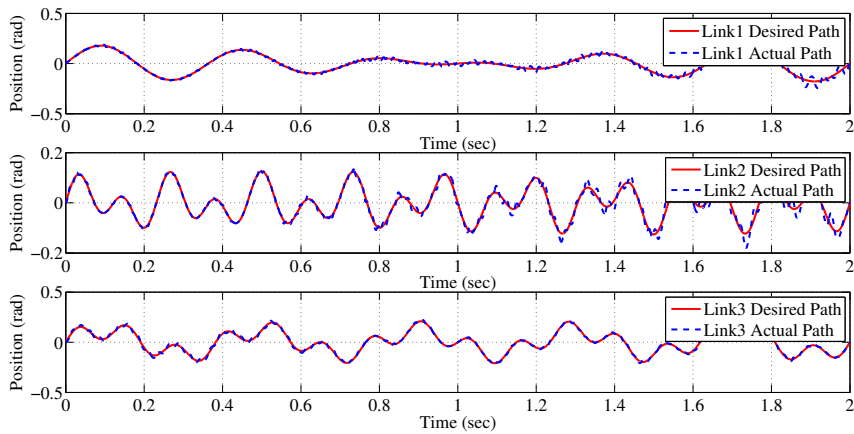
Disturbance (%)	Parameters from PSO		J	Parameters from NN		J_{NN}	Parameters from ANFIS		J_{ANF}
	K_w	ϕ		K_{WNN}	ϕ_{NN}		K_{WANF}	ϕ_{ANF}	
1.75	913.5	0.381	2.45×10^{-6}	140	0.048	7.91×10^{-5}	722.1	0.048	4.61×10^{-4}
2.85	962.8	0.755	6.01×10^{-6}	228	0.022	1.11×10^{-4}	924	0.022	4.25×10^{-5}
7.55	367.8	0.766	3.5×10^{-5}	604	0.8354	6.36×10^{-4}	1026	0.175	2.88×10^{-5}
9.35	699.7	0.763	3.49×10^{-5}	700	0.108	5.21×10^{-4}	994.5	0.016	4.03×10^{-6}
10.82	602.8	0.487	4.09×10^{-6}	865.6	0.03427	2.81×10^{-4}	964.4	0.065	8.08×10^{-6}



(a) : Position tracking of Link 1, Link 2 and Link 3 with PID controller.

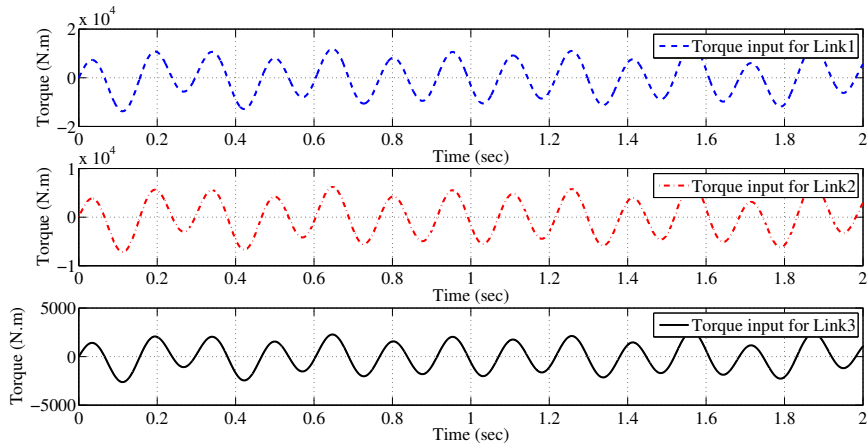


(b) : Position tracking of Link 1, Link 2 and Link 3 with SMC.

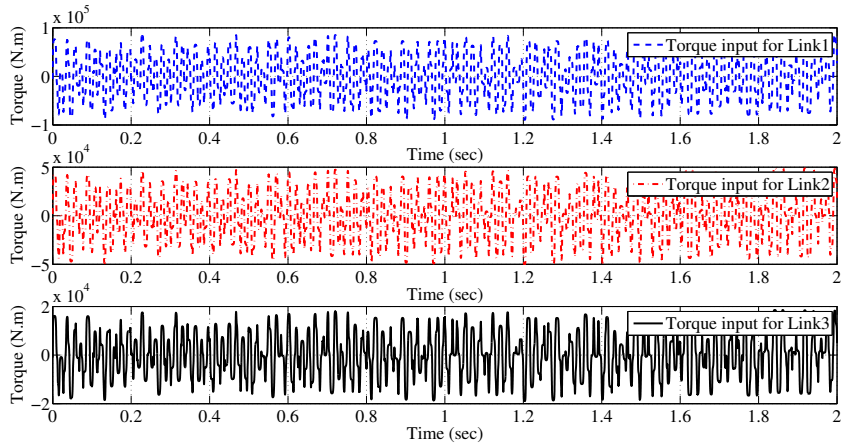


(c) : Position Tracking of Link 1, Link 2 and Link 3 with PIDSMCB.

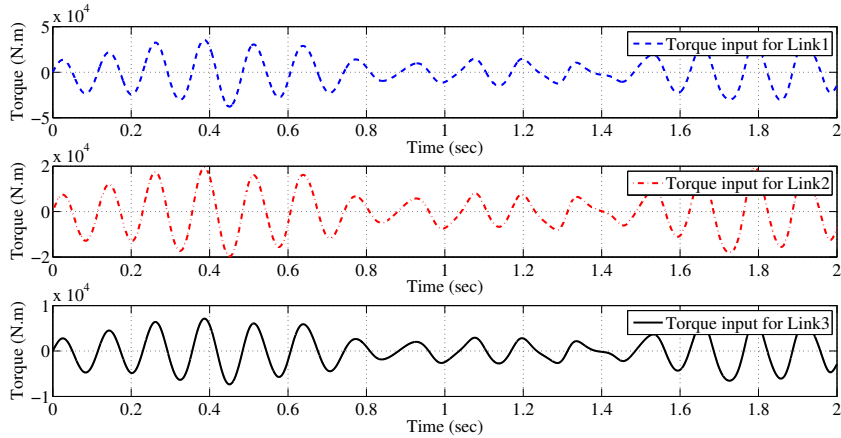
Figure 3.12 Comparison of position tracking responses with different control schemes for 10% disturbance in input torque.



(a) : Control input for Link 1, Link 2 and Link 3 with PID controller.

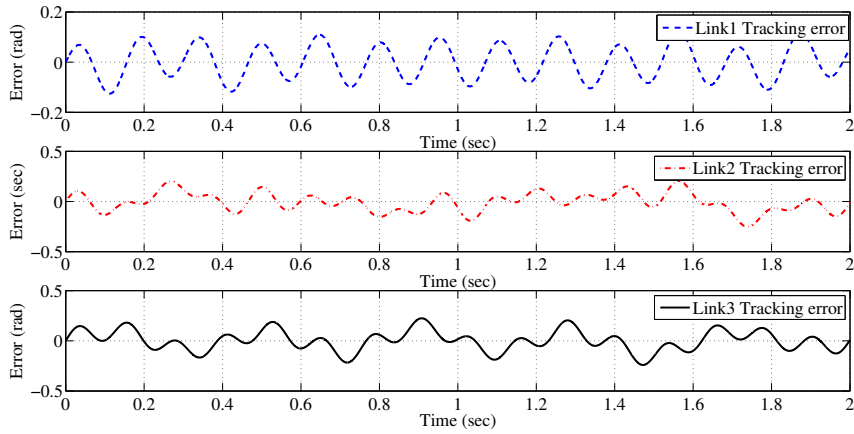


(b) : Control input for Link 1, Link 2 and Link 3 with SMC.

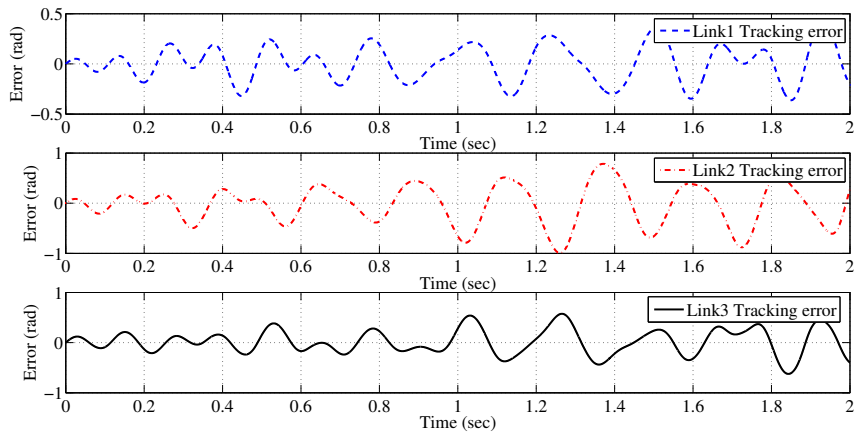


(c) Control input for Link 1, Link 2 and Link 3 with PIDSMCB controller.

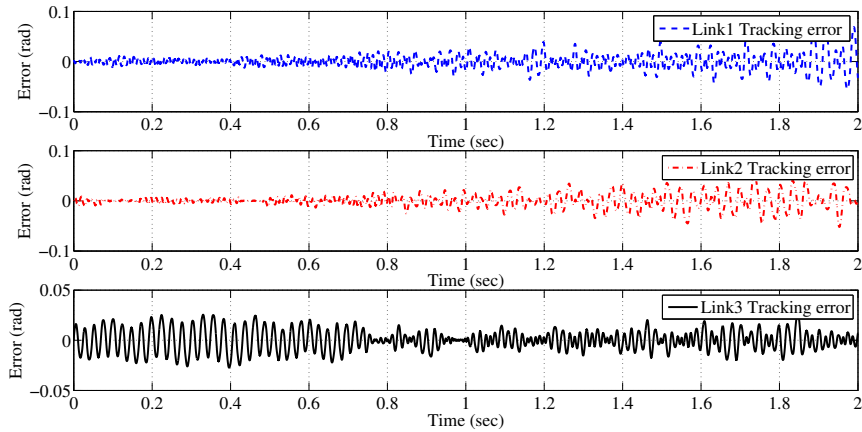
Figure 3.13 Control input of Link 1, Link 2 and Link 3 using different proposed controllers for 10% disturbance in input torque.



(a) : Tracking error for Link 1, Link 2 and Link 3 with PID controller.



(b) : Tracking error for Link 1, Link 2 and Link 3 with SMC.



(c) : Tracking error for Link 1, Link 2 and Link 3 with PIDSMCB controller.

Figure 3.14 : Comparison of position tracking error responses with different control techniques for 10% disturbance in input torque.

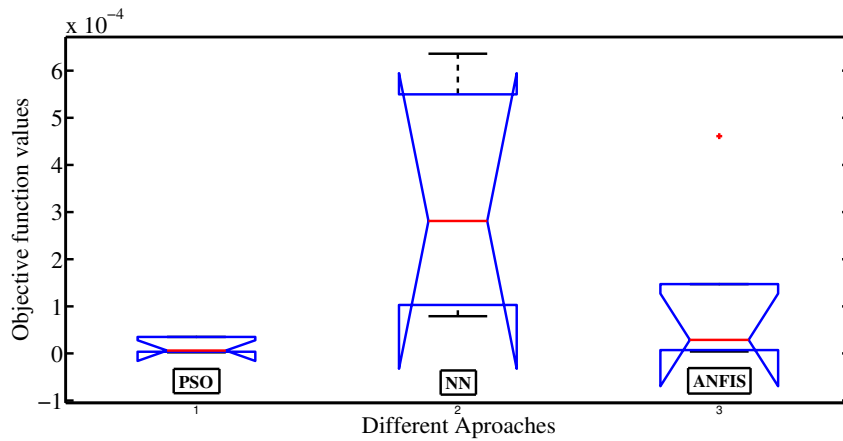


Figure 3.15 : Side-by-side anova1 plots for PSO, NN, and ANFIS approaches.

3.6 SUMMARY

This chapter discusses variations of SMC controller in which PID sliding surface is taken into consideration. The PSO is used to obtain the optimal sliding surface parameters and sliding control parameters with objective functions as IATE, ISE, and ISTE. Simulation results show that the ISTE control strategy provides minimum objective function value compared to ISE and IATE. Control performance of SMCB and PIDSMCB are analysed in terms of tracking error, disturbance rejection, and elimination of chattering. For a real-time control, neuro and neuro-fuzzy based APIDSMCB are recommended. It is found that the neuro-fuzzy based APIDSMCB gives better performance compared to neuro APIDSMCB. A neuro-fuzzy based APIDSMCB can be used for real-time control of robot manipulator where the sliding control parameters are changed adaptively. Lyapunov stability theorem rigorously guarantees the stability of the proposed control system.

Chapter 4

NEURAL NETWORK BASED MODIFIED SLIDING MODE CONTROL TECHNIQUES WITH OBSERVER DESIGN FOR ROBOT MANIPULATORS

This chapter discusses different types of observer-based sliding mode controllers (i.e., SMC, BSMC and Integral BSMC (IBSMC)) for 3-DOF OTDIRM. The results are compared using different performance methods.

4.1 INTRODUCTION

Control of the robotic systems that are non-linear and MIMO is vital due to their wide range of applications. The main aim of the robot control is to track the reference trajectory (Gracia et al., 2012). In general, nonlinear controllers can handle different problems with more robustness in the presence of system uncertainties and external disturbances. Most common nonlinear control strategies such as feedback linearization control, SMC and adaptive or artificial intelligence based control methodologies have been proposed to solve MIMO control system problems (Piltan and Sulaiman, 2012; Kohrt et al., 2013). SMC is one of the influential robust controllers to control robot manipulators, which have been analyzed by many researchers.

The performance of the robot manipulator using SMC can provide robust trajectory tracking under uncertainties and different disturbance conditions. Design of this controller can be carried out by considering system parameters without including the

dynamic effects, such as backlash, elasticity of joints or links and non-linear friction, etc. A chattering free adaptive second order terminal sliding mode (SOTM) control is proposed for trajectory tracking of the robot manipulator (Mondal and Mahanta, 2014). Hybrid learning sliding surfaces, a new fast decoupled terminal sliding mode control (FDTSMC) scheme is presented in (Liu and Li, 2014; Zhao et al., 2014) which describes the elimination of the singularity problem in control law. NISMIC for uncertain nonlinear systems is addressed in (Zheng et al., 2015). Icing formation on overhead transmission line is hazardous and it may result in damage to power systems during fault conditions (Xie and Li, 2006). In (Tran et al., 2015), authors discussed SMC methodology based on CRLSMC to the 3-link de-icing robot manipulator (DIRM) for achieving the robust tracking without strict conditions and system dynamics. The dynamic neural network (DNN) based robust control method for uncertain nonlinear systems is addressed in (Dinh, 2012).

(Sun et al., 2011) have designed a neural network based adaptive observer and controller for a two-link robot manipulator. In (Rossomando et al., 2014), authors have developed a neuroadaptive sliding mode control for a mobile robot manipulator for compensating the time delay. (Huang and Lewis, 2003), have proposed a recurrent neural network (RNN) based predictive control for a nonlinear dynamic system. In those papers, the authors have not considered OTDIRM as a system which has high dynamical complexity. This chapter mainly differs from (Sun et al., 2011; Rossomando et al., 2014; Sharma et al., 2011; Huang and Lewis, 2003) by considering a different complex dynamic system. However, the authors in (Wei et al., 2012) have taken the OTDIRM system but they have directly used the wavelet NN controller instead of taking the observer-based controller.

OTDIRM is a highly complex dynamic system. Without considering dynamic complexities, it is difficult to meet the desired trajectory. In view of this, (Tran et al., 2015) has developed a control techniques for a 3-link de-icing robot considering the dynamic conditions. In the present work, an alternate control strategy is developed with better input and output performance.

Electrical overhead transmission lines are affected during cold weather due to wet

snow or ice accretion which increases wind load effects, thereby increasing the transmission line tension. The increase in line tension causes undesirable effects on the power systems. Therefore, de-icing of electrical transmission lines have to be carried out. The use of robot manipulators is a good solution for de-icing. In this chapter different control approaches of 3-DOF OTDIRM are discussed to eliminate the effect of noises or disturbances and uncertainties associated with the direct measurement. The control laws for tracking of the OTDIRM are developed by combining different types of modified SMC techniques and NN-based approximations. For the precise trajectory tracking performance and enhanced disturbance rejection under various operating conditions, NN-based adaptive observer non-linear SMC methodologies are developed in this work. The parameters of different SMC methodologies and NN adaption weights are obtained by minimizing the quadratic performance indices, wherein, the minimization is dealt with PSO.

The primary goal of the anticipated controller is to maintain the steadiness and robustness of overall approach in the presence of uncertainties and disturbances under various operative conditions. RBFNN-based observer estimates the position and velocity vectors of the link of the OTDIRM without any measurements. The predicted positions and velocities from one RBFNN are fed as a contribution to another RBFNN identifier whose output is the auxiliary control signal (τ_{NN}). However, on the downside, many computations are required to design the parameters of the proposed methods. Chattering effect is mitigated by applying boundary layer phenomenon, and the controller stability is proved by using Lyapunov stability analysis. Both simulation and experiment results demonstrate the validity and effectiveness of the proposed control methods.

4.2 OVERHEAD TRANSMISSION LINE DE-ICING ROBOT MANIPULATOR

Transmission line icing is one of the most significant factors affecting the safety and reliability of a power system. The adverse impact of icing on transmission lines can result

in tower collapse, unnecessary tripping, and power outages. This inevitably poses severe challenges to power utilities. Robot manipulator de-icing technology can mitigate icing problems without interrupting power supply on transmission lines.

Figure 4.1 and 4.2 shows the architecture of a 3-DOF single-arm and dual-arm articulated OTDIRM respectively. The joint velocity vector is $\dot{q} = [\dot{q}_1, \dot{q}_2, \dot{q}_3]^T$ and the joint position vector is $q = [q_1, q_2, q_3]^T$.

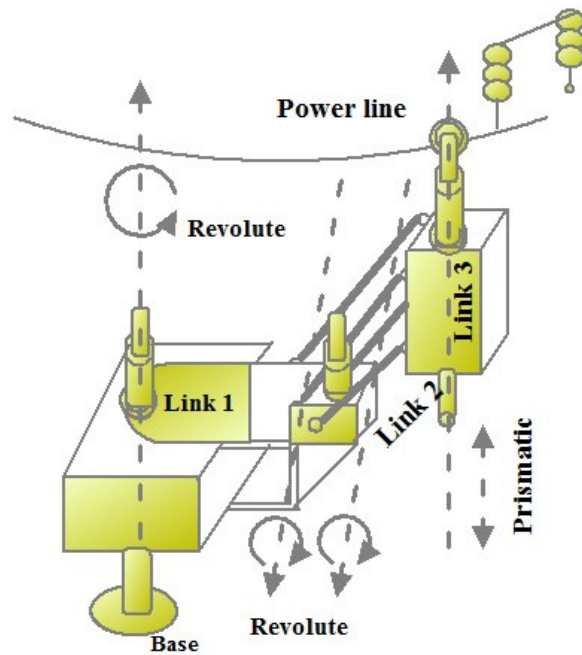


Figure 4.1 : A 3-DOF single-arm articulated OTDIRM

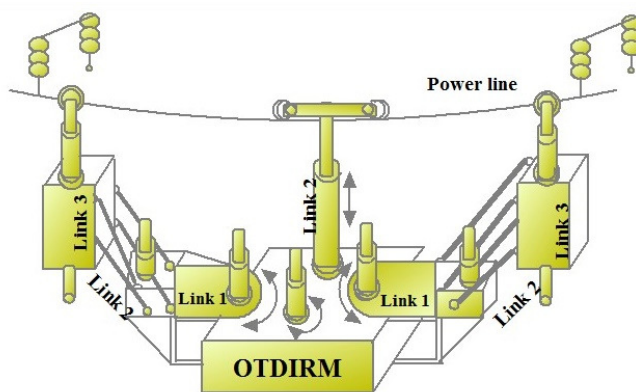


Figure 4.2 : A 3-DOF dual-arm articulated OTDIRM (Tran et al., 2015)

4.3 NEURAL NETWORK-BASED MODIFIED SLIDING MODE CONTROL (NNSMC)

Neural network (NN) based adaptive control systems are used to approximate the unknown non-linearities, due to their inherent approximation capabilities. In this design, the radial basis activation function (RBF) is considered to approximate the unknown non-linearities of the OTDIRM. The approximation function is $f(X) : R^q \rightarrow R^3$ and defined as:

$$f(X) = W^T \sigma(X) + \varepsilon(X) \quad (4.1)$$

where ‘ X ’ is input vector, $W \in R^{m \times 3}$ is the weight matrix, ‘ m ’ is the number of neurons ($m > 1$), and ‘ ε ’ is the approximation error and $\sigma(X) = [\sigma_1(X), \sigma_2(X), \sigma_3(X) \dots \sigma_m(X)]^T$ is the Gaussian RBF function. This Gaussian RBF function is defined as:

$$\sigma_i(X) = \exp\left(-\frac{\|X - C_i\|^2}{2b_i^2}\right), \quad i = 1, 2, \dots, m \quad (4.2)$$

where ‘ C_i ’ and ‘ b_i ’ are the center and widths of the i^{th} neuron respectively. The schematic representation of NNSMC is shown in Figure 4.3. The combined SMC and RBFNN identifier is designed for the OTDIRM to provide better trajectory tracking performance and disturbance rejection under unknown non-linearities.

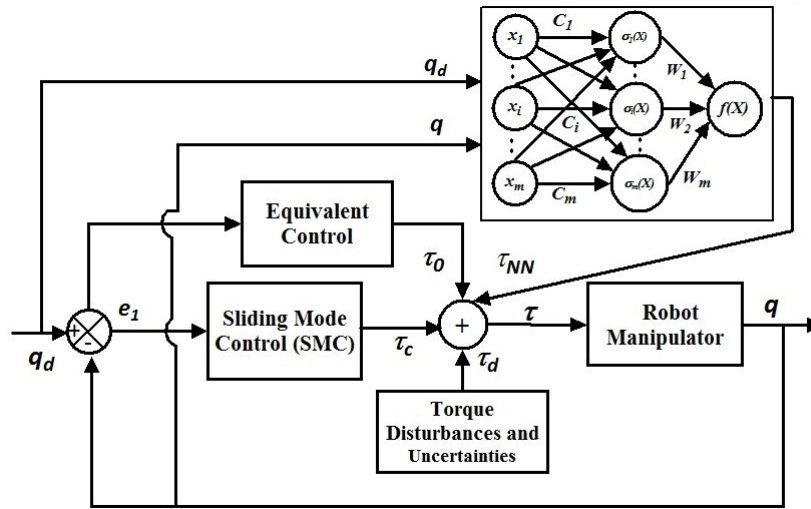


Figure 4.3 : Block diagram of the NNSMC scheme.

The tracking error of position (e) is defined as

$$e = q_d - q \quad (4.3)$$

$$\dot{q}_r = \dot{q}_d + \lambda_1 e \quad (4.4)$$

where ‘ \dot{q}_r ’ and ‘ λ_1 ’ are auxiliary signal and positive definite constant matrix respectively. Then sliding surface is redefined as:

$$s = \dot{q}_r - \dot{q} = \dot{e} + \lambda_1 e \quad (4.5)$$

By substituting Eqs. (4.4) and (4.5) in Eq. (1.18), we get

$$D(q)\dot{s} = -C(q, \dot{q})s + f(X) + \tau_d - \tau \quad (4.6)$$

$$f(X) = D(q)\ddot{q}_r + C(q, \dot{q})\dot{q}_r + F(q, \dot{q}) + G(q) \quad (4.7)$$

where ‘ X ’ is a state vector, $X = [\ddot{q}_d^T, \dot{q}_d^T, q_d^T, \dot{q}^T, q^T]^T$ and ‘ τ_d ’ represents torque disturbances and uncertainties. The estimation of $f(X)$ is defined as:

$$\hat{f}(X) = \hat{W}^T \sigma(X) \quad (4.8)$$

Using Eqs. (4.1), (4.6) and (4.8) yields

$$D(q)\dot{s} = -C(q, \dot{q})s + \tilde{W}^T \sigma(X) + \hat{W}^T \sigma(X) + \varepsilon^* + \tau_d - \tau \quad (4.9)$$

where $\tilde{W} = W^* - \hat{W}$, W^* is ideal weights matrix.

Theorem 4.3.1. Consider the robot manipulator is demonstrated by (1.18), if the total control torque is defined as $\tau = \tau_0 + \tau_c + \tau_{NN}$, in which modified SMC law is defined as $\tau_c = k_1 s + K \tanh(\frac{s}{\phi})$, τ_0 is equivalent control torque and the NN identifier is expressed as $\tau_{NN} = \hat{W}^T \sigma(X)$ with estimated adaptation law. The estimated adaptation law for NN identifier is defined as:

$$\dot{\hat{W}} = -\dot{\tilde{W}} = B\sigma(X)s^T \quad (4.10)$$

where ‘ B ’ is a positive definite matrix, the tracking errors of position and velocity (i.e., e and \dot{e}) of the system asymptotically converge to zero as $t \rightarrow \infty$.

Proof. The Lyapunov stability function is defined as:

$$V = \frac{1}{2}s^T D(q)s + \frac{1}{2}\text{tr}(\tilde{W}^T B^{-1}\tilde{W}) \quad (4.11)$$

$$\dot{V} = \frac{1}{2}s^T \dot{D}(q)s + s^T D(q)\dot{s} + \text{tr}(\tilde{W}^T B^{-1}\dot{\tilde{W}}) \quad (4.12)$$

By substituting Eq (4.9) in Eq (4.12), we get

$$\dot{V} = \frac{1}{2}s^T \{\dot{D}(q) - 2C(q, \dot{q})\}s + s^T \{\tilde{W}^T \sigma(X) + \varepsilon^* + \tau_d - k_1 s \quad (4.13)$$

$$-K \tanh\left(\frac{s}{\phi}\right)\} + \text{tr}(\tilde{W}^T B^{-1}\dot{\tilde{W}})$$

$$= \frac{1}{2}s^T \{\dot{D}(q) - 2C(q, \dot{q})\}s + s^T \{\varepsilon^* + \tau_d - k_1 s - K \tanh\left(\frac{s}{\phi}\right)\} \quad (4.14)$$

$$+ \text{tr}\{\tilde{W}^T (B^{-1}\dot{\tilde{W}} + \sigma(X)s^T)\}$$

Since, $\dot{D}(q) - 2C(q, \dot{q})$ is skew symmetric (i.e., $\frac{1}{2}s^T [\dot{D}(q) - 2C(q, \dot{q})]s = 0$), from Eqs. (2.22) and (4.10), \dot{V} can be rewritten as:

$$\dot{V} \leq -k_1 s^T s + \|s\| \delta_0 \quad (4.15)$$

where ‘ δ_0 ’ is upper bound of $\|\varepsilon^* + \tau_d\|$. The term $\|s\|\delta_0$ is bounded by $\|s\|\delta_0 \leq \frac{1}{2}(\|s\|^2 + \rho\delta_0^2)$, where $\rho > 0$ is chosen such that $\int_0^\infty \rho dt < \infty$ and then substituted in Eq. (4.15) to get stability criteria with finite boundedness.

$$\dot{V} \leq -k_1\|s\|^2 + \frac{1}{2}(\|s\|^2 + \rho\delta_0^2) \quad (4.16)$$

Integrating both sides of Eq. (4.16) from $t = 0$ to T , yields

$$V(T) - V(0) \leq -(k_1 - \frac{1}{2}) \int_0^T \|s\|^2 dt + \frac{1}{2}\delta_0^2 \int_0^T \rho dt, \quad (\forall k_1 > 2) \quad (4.17)$$

Since, $V(T) \geq 0$ and $\int_0^\infty \rho dt < \infty$ holds,

$$\limsup_{T \rightarrow \infty} \frac{1}{T} \int_0^T \|s\|^2 dt \leq \frac{1}{(k_1 - \frac{1}{2})} [V(0) + \frac{1}{2}\delta_0^2 \int_0^\infty \rho dt] \limsup_{T \rightarrow \infty} \frac{1}{T} = 0 \quad (4.18)$$

From the Eqs. (4.17) and (4.18), we can obtain $s \rightarrow 0$ as $t \rightarrow \infty$. Therefore, we can conclude, from the Eq.(4.5), the trajectory tracking errors e and \dot{e} asymptotically converge to zero as $t \rightarrow \infty$. Therefore, proposed NNSMC satisfies the stability criteria. \square

4.4 NN BASED ADAPTIVE OBSERVER DESIGN AND CONTROL

4.4.1 Neural network-based adaptive observer (NNAO)

The NN based adaptive observer is developed to estimate link or joint positions and velocities of the OTDIRM.

Let us define the following variables

$$\dot{q} = p \quad (4.19)$$

where ‘ q ’ and ‘ p ’ are link position and velocity vectors of OTDIRM. Eq. (1.18) is redefined as:

$$\dot{p} = H(q, p) - D^{-1}(q)\tau_d + D^{-1}(q)\tau \quad (4.20)$$

where $H(q, p) = -D^{-1}(q)[C(q, p)p + G(q) + F(q, p)]$. According to the approximation property of NN, the estimation function of $H(q, p)$ is defined as:

$$H(q, p) = W_o^{*T} \sigma_o(q, p) + \varepsilon_o^*(q, p), \quad \|\varepsilon_o^*(q, p)\| \leq \varepsilon_{oN} \quad (4.21)$$

where ‘ W_o^{*T} ’ is an optimal weight matrix, ‘ $\varepsilon_o^*(q, p)$ ’ and ‘ ε_{oN} ’ are approximation error, and it’s upper bound limit respectively. The NN based adaptive observer estimates q and p as \hat{q} and \hat{p} respectively, and the observer estimation errors are $\tilde{q} = q - \hat{q}$ and $\tilde{p} = p - \hat{p}$. Then, the functional estimate of Eq. (4.21) in terms of \hat{q} and \hat{p} can be given by Eq. (4.22) and is shown as:

$$H(q, p) = \hat{W}_o^T \sigma_o(\hat{q}, \hat{p}) \quad (4.22)$$

Let us define the proposed NN based adaptive observer as

$$\dot{\hat{q}} = \hat{p} + \Lambda_1 \tilde{q} \quad (4.23)$$

$$\dot{\hat{p}} = \hat{W}_o^T \sigma_o(\hat{q}, \hat{p}) + D^{-1}(q) \tau + \Lambda_2 \tilde{q} + \Lambda_3 \dot{\tilde{q}} \quad (4.24)$$

where Λ_1, Λ_2 and Λ_3 are positive design constants.

$$\dot{\tilde{q}} = \tilde{p} - \Lambda_1 \tilde{q} \quad (4.25)$$

$$\dot{\tilde{p}} = \dot{p} - \dot{\hat{p}} \quad (4.26)$$

$$\dot{\tilde{p}} = W_o^{*T} \sigma_o(q, p) - W_o^{*T} \sigma_o(\hat{q}, \hat{p}) + W_o^{*T} \sigma_o(\hat{q}, \hat{p}) - \hat{W}_o^T \sigma_o(\hat{q}, \hat{p}) \quad (4.27)$$

$$-D^{-1}(q) \tau_d - \Lambda_2 \tilde{q} - \Lambda_3 \dot{\tilde{q}}$$

$$\dot{\tilde{p}} = W_o^{*T} \tilde{\sigma}_o(q, p) + \tilde{W}_o^T \sigma_o(\hat{q}, \hat{p}) - D^{-1}(q) \tau_d + \varepsilon_o^* - \Lambda_2 \tilde{q} - \Lambda_3 \dot{\tilde{q}} \quad (4.28)$$

By substituting Eq. (4.25) in Eq. (4.28), we get

$$\dot{\tilde{p}} = W_o^{*T} \tilde{\sigma}_o(q, p) + \tilde{W}_o^T \sigma_o(\hat{q}, \hat{p}) - D^{-1}(q) \tau_d + \varepsilon_o^* - \Lambda_3 \tilde{p} \quad (4.29)$$

where $\tilde{\sigma}_o(q, p) = \sigma_o(q, p) - \sigma_o(\hat{q}, \hat{p})$, $\tilde{W}_o = W_o^* - \hat{W}_o$ and $\Lambda_2 = \Lambda_1 \Lambda_3$, $\tilde{p} = \dot{\tilde{q}}$.

Theorem 4.4.1. *Let NN observer is characterized by (4.23) and (4.24) respectively and the evaluated adaptation law for the observer is designed as*

$$\dot{\hat{W}}_o = -\dot{\tilde{W}}_o = B_o \sigma_o(\hat{q}, \hat{p}) \tilde{p}^T \quad (4.30)$$

where ‘ B_o ’ denotes a positive definite matrix, then the estimated errors of observer \tilde{q} and \tilde{p} are asymptotically converge to zero.

Proof. Lyapunov stability function of observer is defined as:

$$V = \frac{1}{2} \tilde{p}^T \tilde{p} + \frac{1}{2} \text{tr}(\tilde{W}_o^T B_o^{-1} \tilde{W}_o) \quad (4.31)$$

$$\dot{V} = \tilde{p}^T \{W_o^{*T} \tilde{\sigma}_o(q, p) + \tilde{W}_o^T \sigma_o(\hat{q}, \hat{p}) - D^{-1}(q) \tau_d + \varepsilon_o^* - \Lambda_3 \tilde{p}\} \quad (4.32)$$

$$+ \text{tr}(\tilde{W}_o^T B_o^{-1} \dot{\tilde{W}}_o)$$

$$\dot{V} = \tilde{p}^T \{W_o^{*T} \tilde{\sigma}_o(q, p) - D^{-1}(q) \tau_d + \varepsilon_o^*\} - \Lambda_3 \tilde{p}^T \tilde{p} + \text{tr}\{\tilde{W}_o^T (B_o^{-1} \dot{\tilde{W}}_o) \quad (4.33)$$

$$+ \sigma_o(\hat{q}, \hat{p}) \tilde{p}^T)$$

$$\dot{V} \leq -\Lambda_3 \tilde{p}^T \tilde{p} + \|\tilde{p}\| \beta_0 \quad (4.34)$$

where ‘ β_0 ’ is an upper bound of $\|W_o^{*T} \tilde{\sigma}_o(q, p) - D^{-1}(q) \tau_d + \varepsilon_o^*\|$. The term $\|\tilde{p}\| \beta_0$ is bounded by $\|\tilde{p}\| \beta_0 \leq \frac{1}{2} (\|\tilde{p}\|^2 + \rho \beta_0^2)$ and then substituted in Eq. (4.34) to get a stability criteria with finite boundedness.

$$\dot{V} \leq -\Lambda_3 \tilde{p}^T \tilde{p} + \frac{1}{2} (\|\tilde{p}\|^2 + \rho \beta_0^2) \quad (4.35)$$

Integrating both sides of Eq. (4.35) from $t = 0$ to T , yields

$$V(T) - V(0) \leq -(\Lambda_3 - \frac{1}{2}) \int_0^T \|\tilde{p}\|^2 dt + \beta_0^2 \int_0^T \rho dt, \quad (\forall \Lambda_3 > 2) \quad (4.36)$$

Since, $V(T) \geq 0$ and $\int_0^\infty \rho dt < \infty$ holds,

$$\limsup_{T \rightarrow \infty} \frac{1}{T} \int_0^T \|\tilde{p}\|^2 dt \leq \frac{1}{(\Lambda_3 - \frac{1}{2})} [V(0) + \frac{1}{2} \beta_0^2 \int_0^\infty \rho dt] \limsup_{T \rightarrow \infty} \frac{1}{T} = 0 \quad (4.37)$$

From Eqs. (4.36) and (4.37), we can obtain $\tilde{p} \rightarrow 0$ as $t \rightarrow \infty$. Therefore, we can conclude $\tilde{q} \rightarrow 0$ and $\tilde{p} \rightarrow 0$, i.e., the proposed NNAO satisfies the stability criteria. \square

4.4.2 Neural Network-Based Adaptive Observer Sliding Mode Control (NNAOSMC)

In this section, design of NNAO is used to develop the NNAOSMC for trajectory tracking of OTDIRM. Figure. 4.4 shows the schematic diagram of NNAOSMC.

The estimation errors of link position and velocity are defined as:

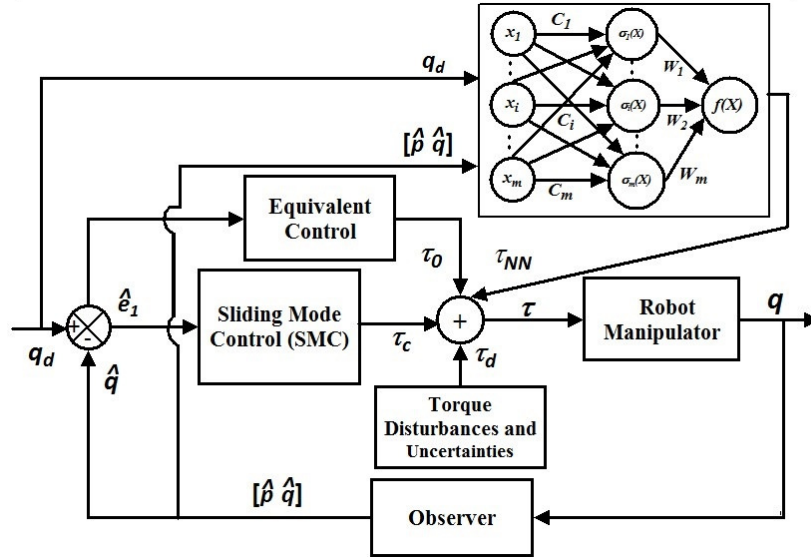


Figure 4.4 : Block diagram of the NNAOSMC scheme.

$$\hat{e} = q_d - \hat{q} \quad (4.38)$$

$$\dot{\hat{e}} = \dot{q}_d - \dot{\hat{q}} \quad (4.39)$$

We can define estimated sliding surface as:

$$\hat{s} = \frac{\dot{\hat{e}} + \lambda_2 \hat{e}}{\phi} \quad (4.40)$$

Theorem 4.4.2. Consider robot manipulator described by (1.18). Let the NN observer estimates q and p as \hat{q} and \hat{p} , respectively and the observer estimation errors are $\tilde{q} = q - \hat{q}$ and $\tilde{p} = p - \hat{p}$. Based on the estimation of q and p , the estimation of $f(X)$ defined in Eq. (4.7) is expressed as:

$$\hat{f}(\hat{X}) = \hat{W}_c^T \sigma(\hat{X}), \quad \hat{X} = [\ddot{q}_d^T, \dot{q}_d^T, q_d^T, \hat{p}^T, \hat{q}^T]^T \quad (4.41)$$

where ' \hat{W}_c ' is adaptation law of NN approximation in the NNAOSMC scheme. The adaptation law is defined as:

$$\dot{\hat{W}}_c = -\dot{\tilde{W}}_c = B_c \sigma(\hat{X}) \hat{s}^T \quad (4.42)$$

where ' B_c ' is a positive definite constant matrix. The control law of the NNAOSMC is defined as:

$$\tau = \Lambda_3 \hat{s} + K \tanh\left(\frac{\hat{s}}{\phi}\right) + \hat{W}_c^T \sigma(\hat{X}) \quad (4.43)$$

where ' $\Lambda_3 \hat{s} + K \tanh(\frac{\hat{s}}{\phi})$ ' is the boundary sliding mode control law and ' $\hat{W}_c^T \sigma(\hat{X})$ ' is the NN approximation to robot manipulator, then the estimation errors \tilde{q} and \tilde{p} are asymptotically converges to zero.

Proof. Consider the Lyapunov stability function for NNAOSMC as

$$V = V_o + V_c \quad (4.44)$$

where ' V_o ' and ' V_c ' are observer and controller stability candidate functions respectively.

$$V_o = \tilde{p}^T \tilde{p} + \frac{1}{2} \text{tr}(\tilde{W}_o^T B_o^{-1} \tilde{W}_o) \quad (4.45)$$

$$V_c = \frac{1}{2} s^T D(q) s + \frac{1}{2} \text{tr}(\tilde{W}_c^T B_c^{-1} \tilde{W}_c) \quad (4.46)$$

The derivative of Eq. (4.46) becomes

$$\dot{V}_c = \frac{1}{2} s^T \dot{D}(q) s + s^T D(q) \dot{s} + \text{tr}(\tilde{W}_c^T B_c^{-1} \dot{\tilde{W}}_c) \quad (4.47)$$

$$= \frac{1}{2} s^T \{\dot{D}(q) - 2C(q, p)\} s + s^T \{\tilde{W}_c^T \sigma(X) + \hat{W}_c^T \tilde{\sigma}(X) + \varepsilon^* + \tau_d \quad (4.48)$$

$$- \Lambda_3 \hat{s} - K \tanh\left(\frac{\hat{s}}{\phi}\right)\} + \text{tr}(\tilde{W}_c^T B_c^{-1} \dot{\tilde{W}}_c)$$

Since, $\dot{D}(q) - 2C(q, p)$ is skew symmetric and $s = \hat{s} + \dot{\tilde{q}} + \Lambda_1 \tilde{q} = \hat{s} + \tilde{p}$, we get

$$\dot{V}_c = \hat{s}^T \{\tilde{W}_c^T \tilde{\sigma}(\hat{X}) + \varepsilon^* + \tau_d\} + \tilde{p}^T \{\tilde{W}_c^T \sigma(\hat{X}) + \hat{W}_c^T \tilde{\sigma}(\hat{X}) + \varepsilon^* + \tau_d\} \quad (4.49)$$

$$- \Lambda_3 \hat{s}^T \hat{s} - \Lambda_3 \tilde{p}^T \hat{s} - K \hat{s}^T \tanh\left(\frac{\hat{s}}{\phi}\right) + \text{tr}\{\tilde{W}_c^T (B_c^{-1} \dot{\tilde{W}}_c + \sigma(\hat{X}) \hat{s}^T)\}$$

We can denote ' γ_0 ' is an upper bound of $\|\hat{W}_c^T \tilde{\sigma}(\hat{X}) + \varepsilon^* + \tau_d\|$ and $\zeta = \{\tilde{W}_c^T \sigma(\hat{X}) + \hat{W}_c^T \tilde{\sigma}(\hat{X}) + \varepsilon^* + \tau_d\}$, then there exists positive constant ' ζ_0 ' such that $\|\zeta\| \leq \zeta_0$.

$$\dot{V}_c \leq \|\hat{s}\| \gamma_0 + \|\tilde{p}\| \zeta_0 - \Lambda_3 \hat{s}^T \hat{s} - \Lambda_3 \tilde{p}^T \hat{s} \quad (4.50)$$

The terms $\|\hat{s}\| \gamma_0$, $\|\tilde{p}\| \zeta_0$ and $-\Lambda_3 \tilde{p}^T \hat{s}$ are bounded by $\|\hat{s}\| \gamma_0 \leq \frac{1}{2} (\|\hat{s}\|^2 + \rho \gamma_0^2)$, $\|\tilde{p}\| \zeta_0 \leq \frac{1}{2} (\|\tilde{p}\|^2 + \rho \zeta_0^2)$ and $-\Lambda_3 \tilde{p}^T \hat{s} \leq \frac{\Lambda_3}{2} (\|\tilde{p}\|^2 + \|\hat{s}\|^2)$ respectively. The bounded terms are substituted in Eq. (4.50) to get a stability criteria with finite boundedness.

Finally, we get:

$$\dot{V}_c \leq -\left(\frac{\Lambda_3}{2} - \frac{1}{2}\right) \|\hat{s}\|^2 + \left(\frac{\Lambda_3}{2} + \frac{1}{2}\right) \|\tilde{p}\|^2 + \frac{1}{2} \rho \left(\gamma_0^2 + \zeta_0^2\right), \quad \forall (\Lambda_3 > 2) \quad (4.51)$$

The derivative of Eq. (4.45) and from Eq. (4.33), we get

$$\dot{V}_o = \tilde{p}^T \{W_o^{*T} \tilde{\sigma}_o(q, p) - D^{-1}(q) \tau_d + \varepsilon_o^*\} - \Lambda_3 \tilde{p}^T \tilde{p} + \text{tr}\{\tilde{W}_o^T (B_o^{-1} \dot{\tilde{W}}_o \quad (4.52)$$

$$+ \sigma_o(\hat{q}, \hat{p}) \tilde{p}^T)$$

Since, $\|W_o^{*T} \tilde{\sigma}_o(q, p) - D^{-1}(q) \tau_d + \varepsilon_o^*\| \leq \beta_0$ and $\|\tilde{p}\| \beta_0$ is bounded by $\|\tilde{p}\| \beta_0 \leq \frac{1}{2} (\|\tilde{p}\|^2 +$

$\rho\beta_0^2$), then

$$\dot{V}_o \leq -\Lambda_3 \tilde{p}^T \tilde{p} + \frac{1}{2}(\|\tilde{p}\|^2 + \rho\beta_0^2) \quad (4.53)$$

$$\dot{V} = \dot{V}_o + \dot{V}_c \quad (4.54)$$

$$\dot{V} \leq -\frac{1}{2}(\Lambda_3 - 2)\|\tilde{p}\|^2 - \frac{1}{2}(\Lambda_3 - 1)\|\hat{s}\|^2 + \frac{1}{2}\rho(\gamma_0^2 + \zeta_0^2 + \beta_0^2), \quad \forall (\Lambda_3 > 2) \quad (4.55)$$

Integrating both sides from $t = 0$ to T , yields

$$V(T) - V(0) \leq -\frac{1}{2}(\Lambda_3 - 1) \int_0^T \|\hat{s}\|^2 dt - \frac{1}{2}(\Lambda_3 - 2) \int_0^T \|\tilde{p}\|^2 dt \quad (4.56)$$

$$+ \frac{1}{2}(\gamma_0^2 + \zeta_0^2 + \beta_0^2) \int_0^T \rho dt$$

Since, $V(T) \geq 0$ and $\int_0^\infty \rho dt < \infty$ holds,

$$\limsup_{T \rightarrow \infty} \sup \frac{1}{T} \left\{ (\Lambda_3 - 1) \int_0^T \|\hat{s}\|^2 dt + (\Lambda_3 - 2) \int_0^T \|\tilde{p}\|^2 dt \right\} \quad (4.57)$$

$$\leq 2[V(0) + \frac{1}{2}(\gamma_0^2 + \zeta_0^2 + \beta_0^2) \int_0^\infty \rho dt] \limsup_{T \rightarrow \infty} \frac{1}{T} = 0$$

From Eqs. (4.56) and (4.57), it is clear that $\tilde{p} \rightarrow 0$, $\hat{s} \rightarrow 0$ as $t \rightarrow \infty$. That concludes $\tilde{q} \rightarrow 0$ and $\tilde{p} \rightarrow 0$. Therefore, the proposed NNAOSMC satisfies the stability criteria. \square

4.5 RESULTS AND DISCUSSIONS FOR SMC METHODOLOGIES

Simulation was carried out for the 3-DOF OTDIRM in MATLAB and SIMULINK. Figure 4.1(b) shows three-link OTDIRM, where q_1, q_2 are angular positions (*rad*) and q_3 is displacement position (*m*) and m_1, m_2 and m_3 are link masses (*kg*), L_1, L_2 and L_3 are the link lengths (*m*), τ_1, τ_2 and τ_3 are the input torques of the robot manipulator (*Nm*).

4.5.1 Dynamic Parameters of OTDIRM

Using the dynamic equation of over head de-icing robot manipulator, from Eq. (1.18), the system parameters are defined as follows:

$$D(q) = \begin{bmatrix} D_{11} & D_{12} & D_{13} \\ D_{21} & D_{22} & D_{23} \\ D_{31} & D_{32} & D_{33} \end{bmatrix}$$

$$\begin{aligned}
D_{11} &= \frac{9}{4}m_1L_1 + m_2 \left(\frac{1}{4}c_2L_2 + L_1^2 + L_1L_2[c_1^2 - s_1^2] \right) + m_3(c_2L - L_2^2 + L_2^2 + 2c_2L_1L_2) \\
D_{22} &= \frac{1}{4}m_2L_2^2 + m_3L_2^2 + \frac{4}{3}m_1L_1^2 \\
D_{23} &= D_{32} = m_3c_2L_2 \\
D_{33} &= m_3 \\
D_{13} &= D_{31} = D_{12} = D_{21} = 0 \\
C(q, \dot{q}) &= \begin{bmatrix} C_{11} & C_{12} & C_{13} \\ C_{21} & C_{22} & C_{23} \\ C_{31} & C_{32} & C_{33} \end{bmatrix} \\
C_{11} &= -8m_2L_1L_2c_1s_1\dot{q}_1 - \left(\frac{1}{2}m_2L_2^2c_2s_2 + 2m_3[L_1L_2s_2 + L_2^2c_2s_2] \right) \dot{q}_2 \\
C_{22} &= -m_3L_2s_2\dot{q}_3 \\
C_{23} &= -2m_3L_2s_2\dot{q}_2 \\
C_{32} &= -m_3L_2s_2\dot{q}_2 \\
C_{33} &= C_{12} = C_{13} = C_{31} = 0 \\
G(q) &= \begin{bmatrix} \left(\frac{1}{2}c_1c_2L_2 + c_1L_1 \right) m_2g \\ \left(-\frac{1}{2}s_1s_2L_2m_2 + c_2L_2m_3 \right) g \\ m_3g \end{bmatrix} \tag{4.58}
\end{aligned}$$

where $c_1 = \cos(q_1)$, $c_2 = \cos(q_2)$, $s_1 = \sin(q_1)$ and $s_2 = \sin(q_2)$. The physical parameters of the system, the desired reference trajectories and important parameters that affect the control performance of the robotic systems (i.e. uncertainties and external disturbances) are considered according to literature (Tran et al., 2015). All the simulated responses of the proposed method are compared with those presented in (Tran et al., 2015) and are positively verified. The physical parameters under consideration are listed as follows: $m_1 = 3 \text{ kg}$, $m_2 = 2 \text{ kg}$, $m_3 = 2.5 \text{ kg}$, $L_1 = 0.14 \text{ m}$, $L_2 = 0.32 \text{ m}$ and $g = 9.8 \text{ m/s}^2$. Initial conditions are $q(0) = [q_1(0), q_2(0), q_3(0)]^T = [0, 1, 1]^T$ and $\dot{q}(0) = [\dot{q}_1(0), \dot{q}_2(0), \dot{q}_3(0)]^T = [1, 0, 0]^T$. The reference tracking signals are $q_{d1}(t) = \sin(t)$, $q_{d2}(t) = \cos(t)$ and $q_{d3}(t) = \cos(t)$.

The most important parameters that affect the control performance of the robot ma-

nipulator are friction terms $F(q, \dot{q})$ and external disturbances (τ_d). Considered friction terms are $F(q_1, \dot{q}_1) = 20\dot{q}_1 + 0.8\text{sign}(\dot{q}_1)$, $F(q_2, \dot{q}_2) = 4\dot{q}_2 + 0.16\text{sign}(\dot{q}_2)$ and $F(q_3, \dot{q}_3) = 4\dot{q}_3 + 0.16\text{sign}(\dot{q}_3)$. The external disturbances are $\tau_{d1} = 5 \sin(5t)$, $\tau_{d2} = 0.5 \sin(5t)$ and $\tau_{d3} = 0.5 \sin(5t)$. SMC parameters are $K_{w1} = 931.51$, $K_{w2} = 931.51$ and $K_{w3} = 931.51$, $\lambda = 156$ and $\phi = 0.1$. The simulated responses of overhead transmission line deicing robot manipulator, which includes position tracking, tracking error, control torque and means square error (MSE) are depicted in Figure 4.5 to Figure 4.13.

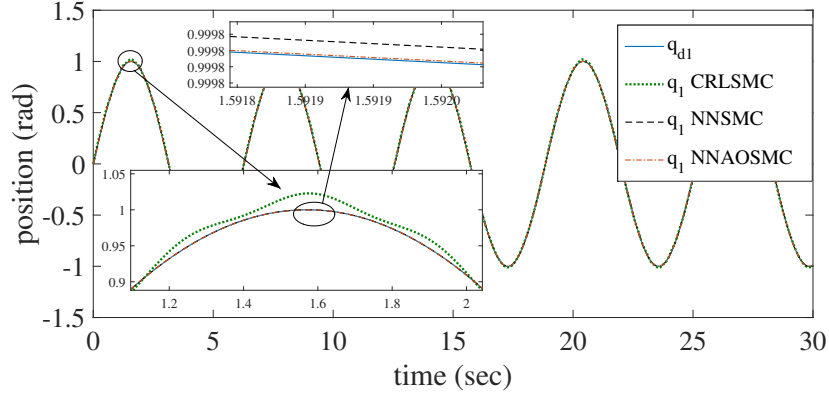


Figure 4.5 : Position tracking of link 1.

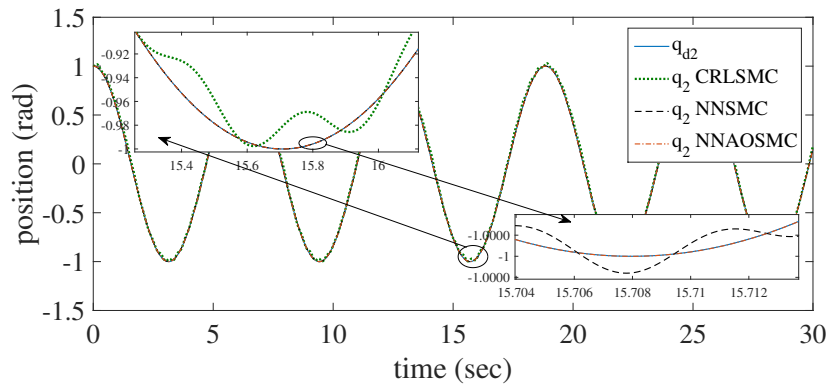


Figure 4.6 : Position tracking of link 2.

The MSE of the position tracking responses is expressed as:

$$MSE_i = \frac{1}{T} \sum_{t=1}^T (q_{di} - \hat{q}_i)^2, \quad i = 1, 2, 3 \quad (4.59)$$

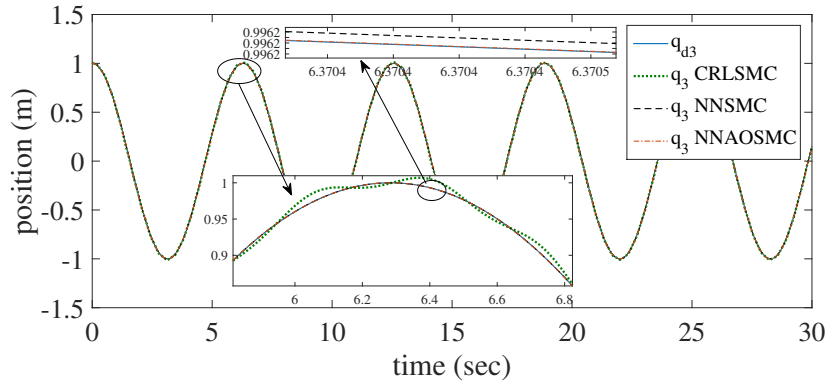


Figure 4.7 : Position tracking of link 3.

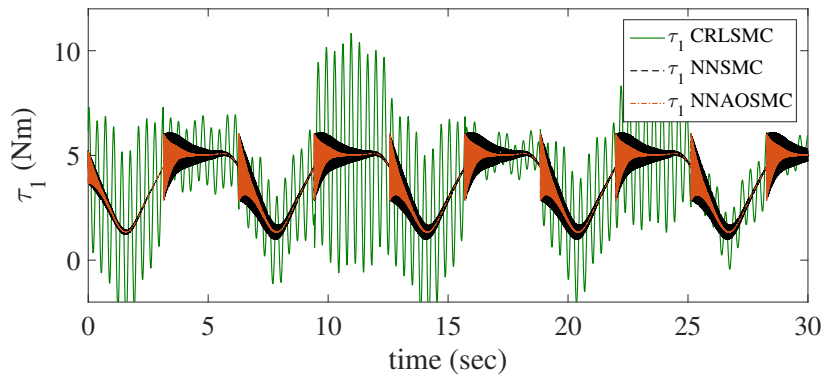


Figure 4.8 : Control torque for link 1.

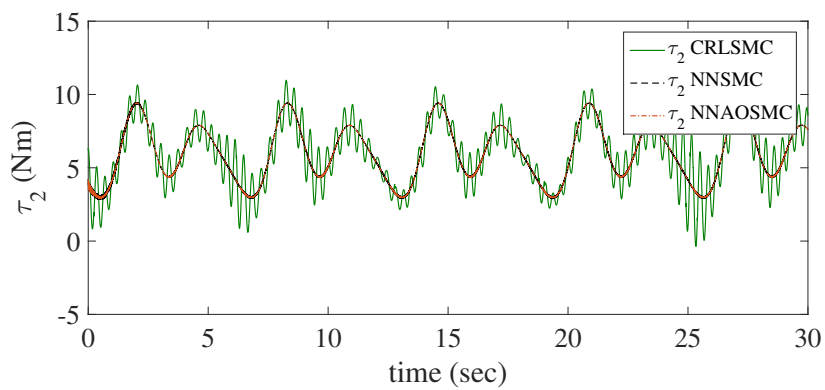


Figure 4.9 : Control torque for link 2.

where q_{di} and \hat{q}_i are the desired and estimated positions of i^{th} link respectively, T is the total sampling time. Table 4.5.1 explains the MSE values of link 1, link 2, and link 3 tracking positions of overhead transmission line deicing robot manipulator. From the ta-

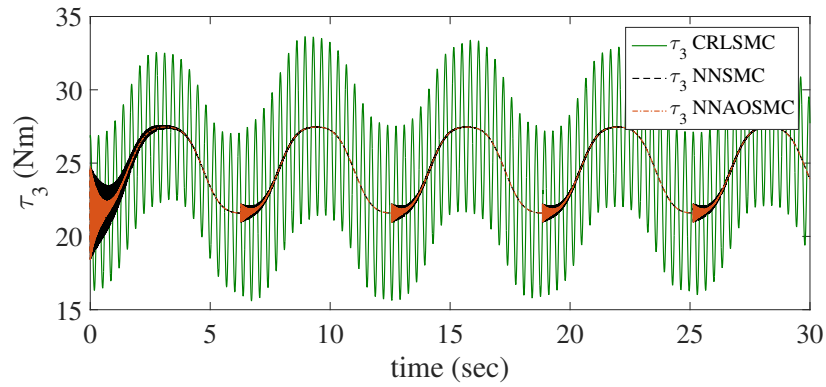


Figure 4.10 : Control torque for link 3.

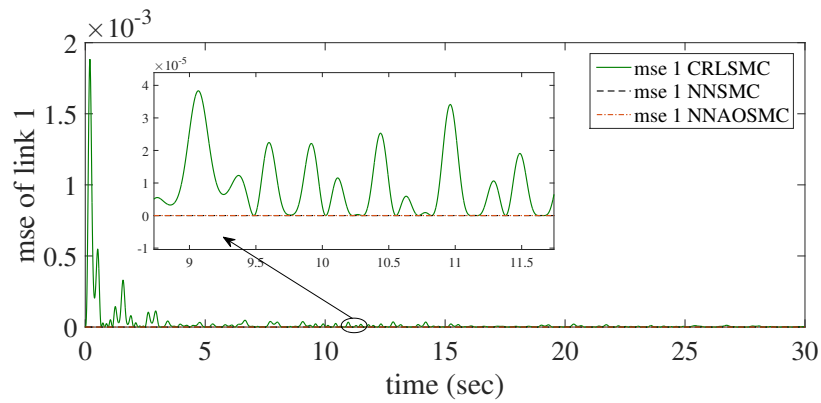


Figure 4.11 : MSE of link 1 position tracking.

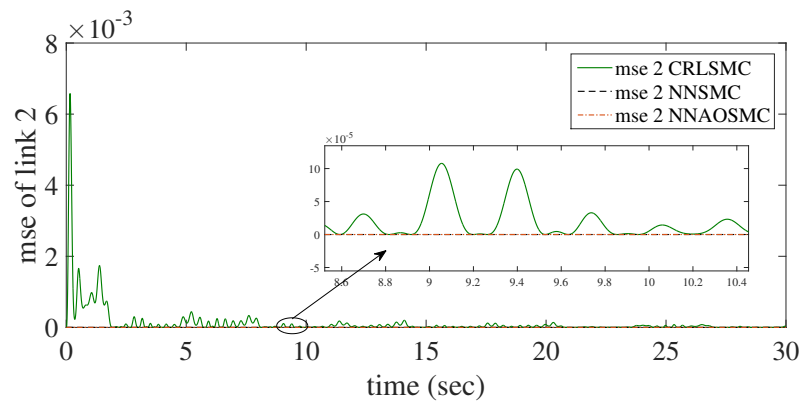


Figure 4.12 : MSE of link 2 position tracking.

ble, it is clear that the proposed NNAOSMC has better trajectory tracking performance and MSE values are lower than the CRLSMC (Tran et al., 2015) and NNSMC. Figure 4.5 to Figure 4.7 illustrate tracking positions, Figure 4.8 to Figure 4.10 show control

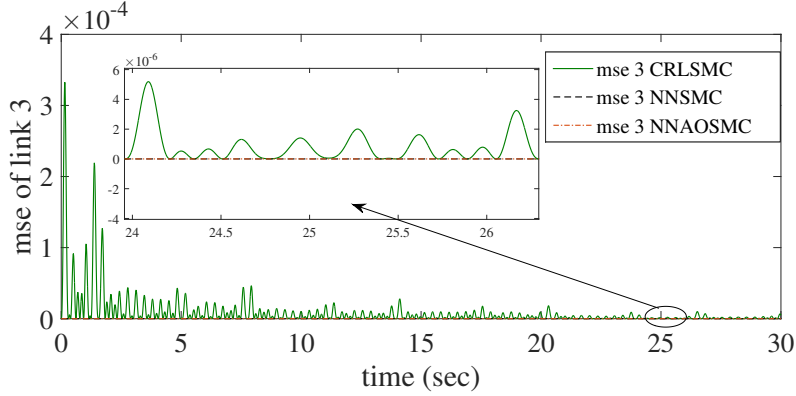


Figure 4.13 : MSE of link 3 position tracking.

Table 4.5.1 : MSE comparison of CRLSMC (Tran et al., 2015), NNSMC and NNAOSMC.

Sl.No	MSE	CRLSMC	NNSMC	NNAOSMC
1	MSE_1	2.732×10^{-6}	4.203×10^{-13}	5.616×10^{-15}
2	MSE_2	3.526×10^{-5}	2.425×10^{-14}	4.847×10^{-18}
3	MSE_3	4.864×10^{-6}	2.061×10^{-15}	2.115×10^{-18}

input torque and Figure 4.11 to Figure 4.13 illustrate mean square error of tracking positions of link 1, link 2, and link 3 of overhead transmission line deicing robot manipulator.

4.6 NEURAL NETWORK-BASED MODIFIED BACK-STEPPING SLIDING MODE CONTROL (NNB-SMC)

In this section, the RBFNN is utilized to build up the control plans for the OTDIRM to track the desired trajectories under unknown dynamics of the system. Figure 4.14 demonstrates the schematic representation of NNBSMC.

Tracking error of position is defined as:

$$e_1 = q_d - q \quad (4.60)$$

$$\dot{q}_r = \dot{q}_d + (1 + \lambda_1)e_1 \quad (4.61)$$

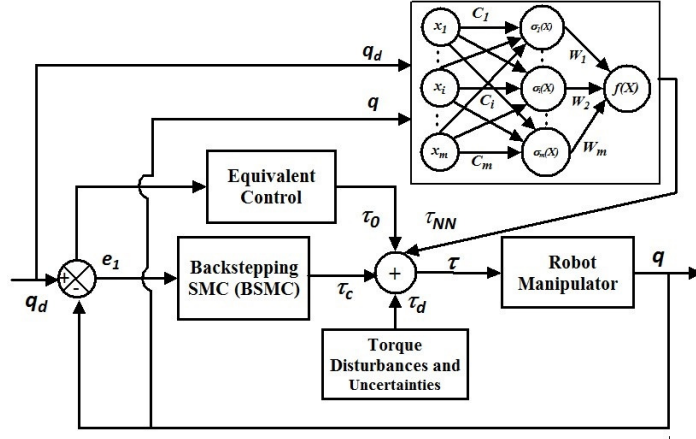


Figure 4.14 : Schematic arrangement of the NNBSMC.

where ‘ \dot{q}_r ’ is auxiliary signal.

The modified sliding surface (s) is characterized as:

$$s = \dot{q}_r - \dot{q} = \dot{e}_1 + (1 + \lambda_1)e_1 \quad (4.62)$$

From (1.18), (4.61) and (4.62), we get

$$D(q)\dot{s} = -C(q, \dot{q})s + f(X) + \tau_d - \tau \quad (4.63)$$

where ‘ τ_d ’ represents external torque disturbances.

$$f(X) = D(q)\ddot{q}_r + C(q, \dot{q})\dot{q}_r + F(q, \dot{q}) + G(q) \quad (4.64)$$

where $X = [\ddot{q}_d^T, \dot{q}_d^T, q_d^T, \dot{q}^T, q^T]^T$.

The approximation of $f(X)$ is defined in (4.65).

$$f(X) = \hat{W}^T \sigma(X) \quad (4.65)$$

where ‘ \hat{W} ’ is the NN adjustment law, $\sigma(X)$ is the basis function. Now (4.63) can be revised as:

$$D(q)\dot{s} = -C(q, \dot{q})s + \tilde{W}^T \sigma(X) + \hat{W}^T \sigma(X) + \varepsilon^* + \tau_d - \tau \quad (4.66)$$

where $\tilde{W} = W^* - \hat{W}$, W^* and ε^* are ideal weights matrix and approximation error respectively.

Theorem 4.6.1. Consider the robot manipulator is demonstrated by (1.18), if the total control torque is expressed as $\tau = \tau_0 + \tau_c + \tau_{NN}$, in which control law of BSMC is defined as $\tau_c = k_1 s + K \tanh\left(\frac{(1+\lambda_1)e_1 + \frac{d}{dt}e_1}{\phi}\right)$ and $\tau_{NN} = \hat{W}^T \sigma(X)$. The evaluated adaptive law for the NN identifier is characterized as:

$$\dot{\hat{W}}^T = -\dot{\tilde{W}}^T = B\sigma(X)s^T \quad (4.67)$$

where ‘ B ’ is a positive definite matrix, the tracking errors of position and velocity (i.e., e and \dot{e}) of the system asymptotically converge to zero as $t \rightarrow \infty$.

Proof. NNBSMC stability function is given in (4.68).

$$V = \frac{1}{2}s^T D(q)s + \frac{1}{2}tr(\tilde{W}^T B^{-1}\tilde{W}) \quad (4.68)$$

$$\dot{V} = \frac{1}{2}s^T \dot{D}(q)s + s^T D(q)\dot{s} + tr(\tilde{W}^T B^{-1}\dot{\tilde{W}}) \quad (4.69)$$

By substituting (4.66) in (4.69), we get

$$\begin{aligned} \dot{V} = & \frac{1}{2}s^T [\dot{D}(q) - 2C(q, \dot{q})]s + s^T [\tilde{W}^T \sigma(X) + \varepsilon^* + \tau_d - k_1 s \\ & - K \tanh\left(\frac{s}{\phi}\right)] + tr(\tilde{W}^T B^{-1}\dot{\tilde{W}}) \end{aligned} \quad (4.70)$$

Since, $\dot{D}(q) - 2C(q, \dot{q})$ is a skew symmetric matrix, the first term in (4.70) becomes zero (i.e., $\frac{1}{2}s^T [\dot{D}(q) - 2C(q, \dot{q})]s = 0$), from (2.47) and (4.67), \dot{V} can be rewritten as:

$$\dot{V} \leq -k_1 s^T s + \|s\| \delta_0 \quad (4.71)$$

where ' δ_0 ' is the upper bound of $\|\varepsilon^* + \tau_d\|$. The term $\|s\| \delta_0$ is bounded by $\|s\| \delta_0 \leq \frac{1}{2}(\|s\|^2 + \rho \delta_0^2)$, where $\rho > 0$ is picked to such an extent that $\int_0^\infty \rho dt < \infty$ and further substituted in (4.71) to get stability criteria with finite boundedness.

$$\dot{V} \leq -k_1 \|s\|^2 + \frac{1}{2}(\|s\|^2 + \rho \delta_0^2) \quad (4.72)$$

Integrating both sides of (4.72) from $t = 0$ to T , yields

$$V(T) - V(0) \leq -(k_1 - \frac{1}{2}) \int_0^T \|s\|^2 dt + \frac{1}{2} \delta_0^2 \int_0^T \rho dt, \quad (\forall k_1 > 2) \quad (4.73)$$

Since, $V(T) \geq 0$ and $\int_0^\infty \rho dt < \infty$ holds,

$$\begin{aligned} \limsup_{T \rightarrow \infty} \frac{1}{T} \int_0^T \|s\|^2 dt \leq & \frac{1}{(k_1 - \frac{1}{2})} \left[V(0) \right. \\ & \left. + \frac{1}{2} \delta_0^2 \int_0^\infty \rho dt \right] \limsup_{T \rightarrow \infty} \frac{1}{T} = 0 \end{aligned} \quad (4.74)$$

From (4.73) and (4.74), we can get $s \rightarrow 0$ as $t \rightarrow \infty$. Subsequently, we can conclude, from (4.62), the tracking errors of position and velocity (i.e., e and \dot{e}) asymptotically converges to zero as $t \rightarrow \infty$. Therefore, the stability criteria is fulfilled by the proposed NNBSMC scheme. \square

4.7 AN ADAPTIVE OBSERVER BASED CONTROL OF OTDIRM

The neural network based adaptive observer backstepping sliding mode control (NNAOBSMC) is developed with the help of NNAO for precise desired trajectory tracking and improve the disturbance rejection under different working conditions (i.e., external disturbances and uncertainties) of OTDIRM. Figure 4.15 demonstrates the structure of the NNAOBSMC. The evaluated error of the link position is characterized as:

$$\hat{e}_1 = q_d - \hat{q} \quad (4.75)$$

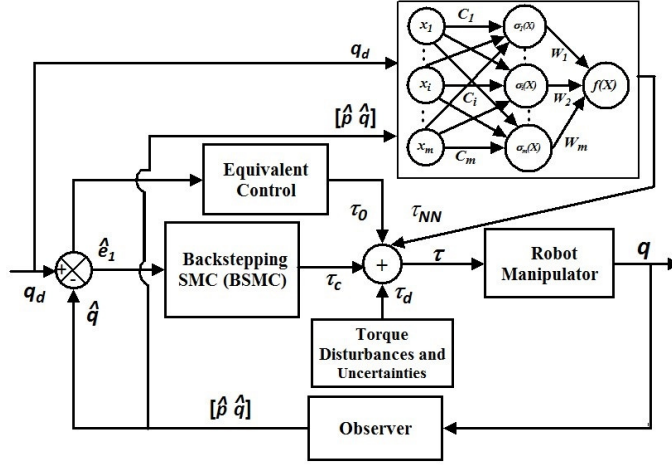


Figure 4.15 : Block diagram of the NNAOBSMC scheme.

$$\hat{e}_1 = \dot{q}_d - \dot{\hat{q}} \quad (4.76)$$

The estimated sliding surface ‘ \hat{s} ’ is designed as:

$$\hat{s} = \frac{\hat{e}_1 + (\lambda_1 + 1)\hat{e}_1}{\phi} \quad (4.77)$$

Theorem 4.7.1. Let the NNAO estimates q and p as \hat{q} and \hat{p} , estimation errors are $\tilde{q} = q - \hat{q}$ and $\tilde{p} = p - \hat{p}$. Then, the approximation function of $f(X)$ described in (4.64) is conveyed as:

$$\hat{f}(\hat{X}) = \hat{W}_c^T \sigma(\hat{X}), \quad \hat{X} = [\dot{q}_d^T, \dot{q}_d^T, \dot{q}_d^T, \hat{p}^T, \hat{q}^T]^T \quad (4.78)$$

where ‘ \hat{W}_c ’ is estimated adaptation matrix.

The adaptation law is defined as:

$$\dot{\hat{W}}_c = -\dot{\tilde{W}}_c = B_c \sigma(\hat{X}) \hat{s}^T \quad (4.79)$$

The NNAOBSMC law is characterized as:

$$\tau = \Lambda_3 \hat{s} + K \tanh\left(\frac{\hat{s}}{\phi}\right) + \hat{W}_c^T \sigma(\hat{X}) \quad (4.80)$$

where ‘ $\Lambda_3 \hat{s} + K \tanh(\frac{\hat{s}}{\phi})$ ’ is the boundary sliding mode control law and ‘ $\hat{W}_c^T \sigma(\hat{X})$ ’ is the approximation function to robot manipulator, then the estimation errors \tilde{q} and \tilde{p} are asymptotically converge to zero.

Proof. The Lyapunov stability candidate function for NNAOBSMC is characterized as:

$$V = V_o + V_c \quad (4.81)$$

where ‘ V_o ’ and ‘ V_c ’ are the observer stability and controller stability candidate functions respectively.

$$V_o = \tilde{p}^T \tilde{p} + \frac{1}{2} \text{tr}(\tilde{W}_o^T B_o^{-1} \tilde{W}_o) \quad (4.82)$$

$$V_c = \frac{1}{2} s^T D(q) s + \frac{1}{2} \text{tr}(\tilde{W}_c^T B_c^{-1} \tilde{W}_c) \quad (4.83)$$

The derivative of (4.83) becomes

$$\dot{V}_c = \frac{1}{2} s^T \dot{D}(q) s + s^T D(q) \dot{s} + \text{tr}(\tilde{W}_c^T B_c^{-1} \dot{\tilde{W}}_c) \quad (4.84)$$

Since, $\dot{D}(q) - 2C(q, p)$ is a skew symmetric matrix and $s = \hat{s} + \dot{\tilde{q}} + \Lambda_1 \tilde{q} = \hat{s} + \tilde{p}$, we get

$$\begin{aligned} \dot{V}_c = & \hat{s}^T \{ \hat{W}_c^T \tilde{\sigma}(\hat{X}) + \varepsilon^* + \tau_d \} + \tilde{p}^T \{ \tilde{W}_c^T \sigma(\hat{X}) + \hat{W}_c^T \tilde{\sigma}(\hat{X}) + \varepsilon^* + \tau_d \} \quad (4.85) \\ & - \Lambda_3 \hat{s}^T \hat{s} - \Lambda_3 \tilde{p}^T \hat{s} - K \hat{s}^T \tanh\left(\frac{\hat{s}}{\phi}\right) + \text{tr}\{ \tilde{W}_c^T (B_c^{-1} \dot{\tilde{W}}_c + \sigma(\hat{X}) \hat{s}^T) \} \end{aligned}$$

where ‘ γ_0 ’ is maximum limit of $\| \hat{W}_c^T \tilde{\sigma}(\hat{X}) + \varepsilon^* + \tau_d \|$ and $\zeta = \{ \tilde{W}_c^T \sigma(\hat{X}) + \hat{W}_c^T \tilde{\sigma}(\hat{X}) + \varepsilon^* + \tau_d \}$, corresponding to this ‘ ζ ’, there exists a positive constant ‘ ζ_0 ’ such that $\| \zeta \| \leq \zeta_0$.

$$\dot{V}_c \leq \| \hat{s} \| \gamma_0 + \| \tilde{p} \| \zeta_0 - \Lambda_3 \hat{s}^T \hat{s} - \Lambda_3 \tilde{p}^T \hat{s} \quad (4.86)$$

The terms $\| \hat{s} \| \gamma_0$, $\| \tilde{p} \| \zeta_0$ and $-\Lambda_3 \tilde{p}^T \hat{s}$ are bounded by $\| \hat{s} \| \gamma_0 \leq \frac{1}{2} (\| \hat{s} \|^2 + \rho \gamma_0^2)$, $\| \tilde{p} \| \zeta_0 \leq \frac{1}{2} (\| \tilde{p} \|^2 + \rho \zeta_0^2)$ and $-\Lambda_3 \tilde{p}^T \hat{s} \leq \frac{\Lambda_3}{2} (\| \tilde{p} \|^2 + \| \hat{s} \|^2)$ respectively. To induce stability criteria with finite boundedness, the constrained terms are substituted in (4.86). The expression for \dot{V}_c gets to be:

$$\dot{V}_c \leq -\left(\frac{\Lambda_3}{2} - \frac{1}{2}\right) \| \hat{s} \|^2 + \left(\frac{\Lambda_3}{2} + \frac{1}{2}\right) \| \tilde{p} \|^2 + \frac{1}{2} \rho (\gamma_0^2 + \zeta_0^2), \quad \forall (\Lambda_3 > 2) \quad (4.87)$$

The derivative of (4.82) and from (4.33), we will get

$$\begin{aligned} \dot{V}_o = & \tilde{p}^T \{ W_o^{*T} \tilde{\sigma}_o(q, p) - D^{-1}(q) \tau_d + \varepsilon_o^* \} - \Lambda_3 \tilde{p}^T \tilde{p} + \text{tr}\{ \tilde{W}_o^T (B_o^{-1} \dot{\tilde{W}}_o \\ & + \sigma_o(\hat{q}, \hat{p}) \tilde{p}^T) \} \end{aligned} \quad (4.88)$$

Since, $\| W_o^{*T} \tilde{\sigma}_o(q, p) - D^{-1}(q) \tau_d + \varepsilon_o^* \| \leq \beta_0$ and $\| \tilde{p} \| \beta_0$ is bounded by $\| \tilde{p} \| \beta_0 \leq \frac{1}{2} (\| \tilde{p} \|^2 + \rho \beta_0^2)$, then

$$\dot{V}_o \leq -\Lambda_3 \tilde{p}^T \tilde{p} + \frac{1}{2} (\| \tilde{p} \|^2 + \rho \beta_0^2) \quad (4.89)$$

$$\dot{V} = \dot{V}_o + \dot{V}_c \quad (4.90)$$

$$\begin{aligned} \dot{V} \leq & -\frac{1}{2} (\Lambda_3 - 2) \| \tilde{p} \|^2 - \frac{1}{2} (\Lambda_3 - 1) \| \hat{s} \|^2 + \frac{1}{2} \rho (\gamma_0^2 + \zeta_0^2 \\ & + \beta_0^2), \quad \forall (\Lambda_3 > 2) \end{aligned} \quad (4.91)$$

Integrating both sides from $t = 0$ to T , yields

$$V(T) - V(0) \leq -\frac{1}{2} (\Lambda_3 - 1) \int_0^T \| \hat{s} \|^2 dt - \frac{1}{2} (\Lambda_3 - 2) \int_0^T \| \tilde{p} \|^2 dt \quad (4.92)$$

$$+ \frac{1}{2} (\gamma_0^2 + \zeta_0^2 + \beta_0^2) \int_0^T \rho dt$$

Since, $V(T) \geq 0$ and $\int_0^\infty \rho dt < \infty$ holds,

$$\limsup_{T \rightarrow \infty} \frac{1}{T} \left[(\Lambda_3 - 1) \int_0^T \| \hat{s} \|^2 dt + (\Lambda_3 - 2) \int_0^T \| \tilde{p} \|^2 dt \right] \leq 2 \left[V(0) \right. \quad (4.93)$$

$$\left. + \frac{1}{2} (\gamma_0^2 + \zeta_0^2 + \beta_0^2) \int_0^\infty \rho dt \right] \limsup_{T \rightarrow \infty} \frac{1}{T} = 0$$

From (4.92) and (4.93), it is clear that $\tilde{p} \rightarrow 0$, $\hat{s} \rightarrow 0$ as $t \rightarrow \infty$. That concludes $\tilde{q} \rightarrow 0$ and $\tilde{p} \rightarrow 0$. Thus, the proposed NNAOBSMC fulfills the stability criteria. \square

4.8 RESULTS AND DISCUSSIONS FOR BACKSTEPPING SMC METHODOLOGIES

4.8.1 Simulation studies

In this section, MATLAB/SIMULINK tool has been used to carry out simulations for the 3-DOF OTDIRM. Figure 4.1 demonstrates the architecture of a de-icing robot manipulator. The link position and velocity vectors are $q = [q_1, q_2, q_3]^T$ and $\dot{q} = [\dot{q}_1, \dot{q}_2, \dot{q}_3]^T$ respectively. The desired reference trajectories for de-icing robot manipulator and essential parameters that influence the control activity of the robotic systems (i.e., uncertainties and external disturbances) are considered according to literature (Tran et al., 2015). The physical parameters of the OTDIRM are listed in Table 4.8.1.

Table 4.8.1 : Physical parameters of the de-icing robot manipulator

Sl. No	Symbol	Definition	Value
1	m_1	Mass of the link 1	3(kg)
2	m_2	Mass of the link 2	2(kg)
3	m_3	Mass of the link 3	2.5(kg)
4	L_1	Length of the link 1	0.14(m)
5	L_2	Length of the link 2	0.32(m)
6	g	Gravitational constant	9.81(m/s ²)

Initial conditions are $q(0) = [0.9, 0.1, 0.1]^T$ and $\dot{q}(0) = [0, 0, 0]^T$. The reference tracking signals are $q_{d1}(t) = \sin(t)$, $q_{d2}(t) = \cos(t)$ and $q_{d3}(t) = \cos(t)$. Considered friction terms are $F(q_1, \dot{q}_1) = 20\dot{q}_1 + 0.8\text{sign}(\dot{q}_1)$, $F(q_2, \dot{q}_2) = 4\dot{q}_2 + 0.16\text{sign}(\dot{q}_2)$ and $F(q_3, \dot{q}_3) = 4\dot{q}_3 + 0.16\text{sign}(\dot{q}_3)$. The external disturbances are $\tau_{d1} = 5 \sin(5t)$, $\tau_{d2} = 0.5 \sin(5t)$ and $\tau_{d3} = 0.5 \sin(5t)$. BSMC parameters are $\lambda_1 = 60$, $K_{w1} = 540$, $K_{w2} = 540$, $K_{w3} = 540$ and $\phi = 0.004$. The simulated responses of the OTDIRM are compared with those presented in (Tran et al., 2015) are shown in figures from 4.16 to 4.27.

Output performance: To evaluate output performance, the MSE of tracking positions are computed. The total sampling time is ‘ T ’, desired trajectory is ‘ q_{di} ’ and estimated trajectory is ‘ \hat{q}_i ’ of the i^{th} link, tracking position mean square error (MSE) is

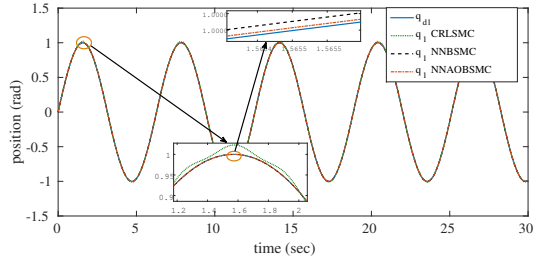


Figure 4.16 : Position tracking of link 1.

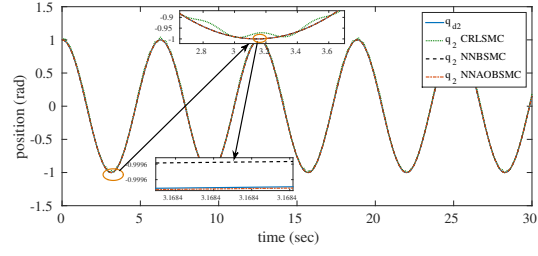


Figure 4.17 : Position tracking of link 2.

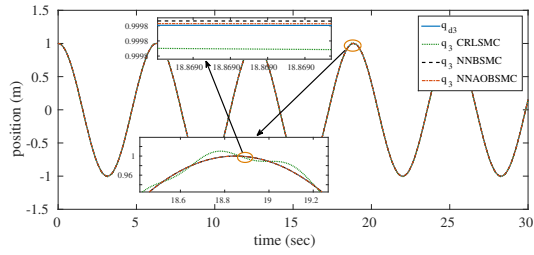


Figure 4.18 : Position tracking of link 3.

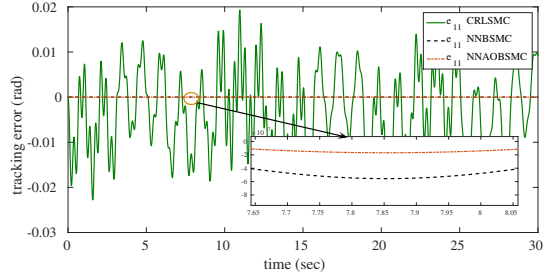


Figure 4.19 : Tracking error of link 1.

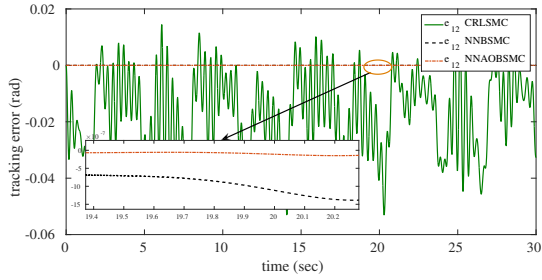


Figure 4.20 : Tracking error of link 2.

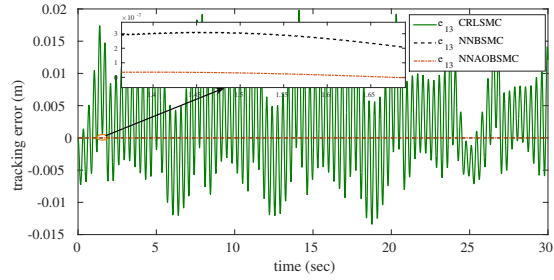


Figure 4.21 : Tracking error of link 3.

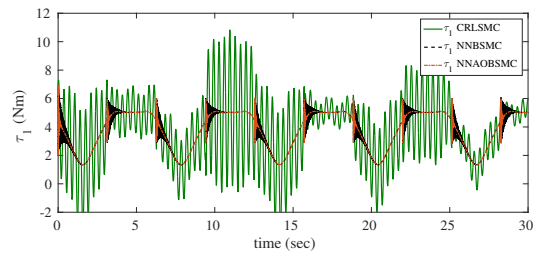


Figure 4.22 : Control input for link 1.

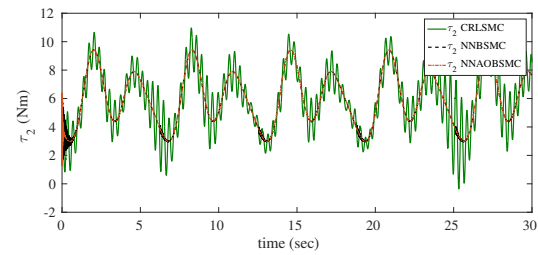


Figure 4.23 : Control input for link 2.

given in (4.94).

$$MSE_i = \frac{1}{T} \sum_{t=1}^T [q_{di} - \hat{q}_i]^2, \quad i = 1, 2, 3 \quad (4.94)$$

The MSE values of the 3-DOF OTDIRM trajectories under different control method-

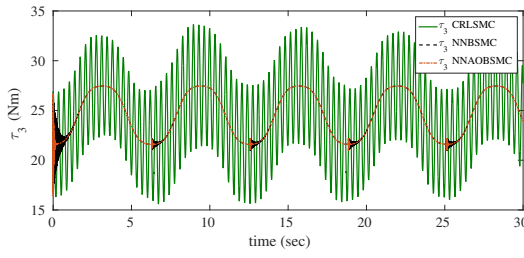


Figure 4.24 : Control input for link 3.

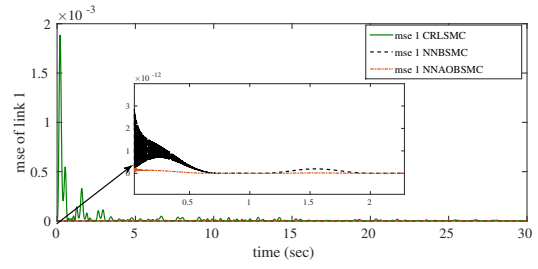


Figure 4.25 : MSE of link 1.

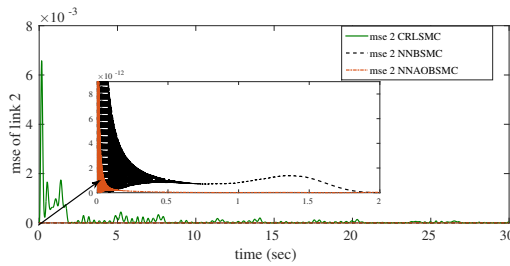


Figure 4.26 : MSE of link 2.

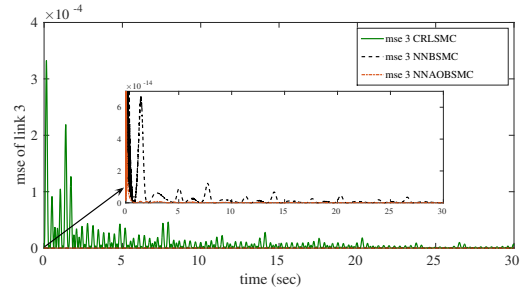


Figure 4.27 : MSE of link 3.

Table 4.8.2 : MSE examination of CRLSMC, NNBSMC and NNAOBSMC

Sl. No	MSE	CRLSMC	NNBSMC	NNAOBSMC
1	link 1	2.732×10^{-6}	2.642×10^{-15}	6.285×10^{-16}
2	link 2	3.526×10^{-5}	2.171×10^{-14}	5.589×10^{-19}
3	link 3	4.864×10^{-6}	1.007×10^{-15}	2.385×10^{-15}

ologies, such as CRLSMC, NNBSMC and NNAOBSMC are presented in Table 4.8.2. From the table, it is ascertained that NNAOBSMC provides least MSE values in comparison with other methods (i.e., NNAOBSMC system has better tracking trajectory performance). Figure 4.16 to Figure 4.18 indicate tracking positions, Figure 4.19 to Figure 4.21 indicate tracking errors and Figure 4.22 to Figure 4.24 show control torque. From the Figure 4.22 to Figure 4.24, it is clear that the control torque is smoother for NNAOBSMC compared with existing CRLSMC. This indicates that the proposed method requires less control effort for same trajectory tracking. The MSE response plots of the OTDIRM link trajectories exhibited from Figure 4.25 to Figure 4.27.

Input performance: In order to evaluate the manipulated input usage, total variation

(TV) (Mondal and Mahanta, 2014) of the input $u(t)$ is calculated as

$$TV = \sum_{j=1}^{\infty} \|u_{j+1} - u_j\| \quad (4.95)$$

This should be as small as possible. The TV is a good measure of the signal "smoothness". A large value of TV means more excessive input usage or more complex controllers (Mondal and Mahanta, 2014).

Energy of the input signal is calculated by using the 2-Norm method. The control energy is expected to be as small as possible. The output and input performance are calculated for the period from 0 to 30 sec with a sampling time of 0.0001 sec.

From Table 4.8.3 and 4.8.4, it clear that the values of TV and 2-Norm of input for proposed methods are very small as compared to existing method CRLSMC in (Tran et al., 2015).

Table 4.8.3 : Total variance examination of CRLSMC, NNBSMC and NNAOBSMC

Sl. No	Total Variance (TV)	CRLSMC	NNBSMC	NNAOBSMC
1	link 1	6.1354	1.8393	1.7750
2	link 2	4.8902	3.5519	3.5407
3	link 3	20.8775	5.1932	5.1339

Table 4.8.4 : 2-Norm of input examination of CRLSMC, NNBSMC and NNAOBSMC

Sl. No	2-Norm of Input	CRLSMC	NNBSMC	NNAOBSMC
1	link 1	2.4778×10^3	2.2123×10^3	2.207×10^3
2	link 2	3.4905×10^3	3.4535×10^3	3.4530×10^3
3	link 3	1.3727×10^4	1.3550×10^4	1.3549×10^4

Figure 4.28, Figure 4.29 and Figure 4.30 show the box plot of control torque for link 1, link 2, and link 3, respectively, with the mean, median, $\pm 25\%$ quartiles (notch boundaries), $\pm 75\%$ quartiles (box ends), $\pm 95\%$ bounds and the outliers. From the size of the boxes shown, it is clear that the NNAOBSMC control strategy experiences minimum variation than others. Comparing the box plot of NNBSMC and NNAOBSMC, it observed that NNAOBSMC has less variation in control input torque for link 1, link 2, and link 3 of the OTDIRM.

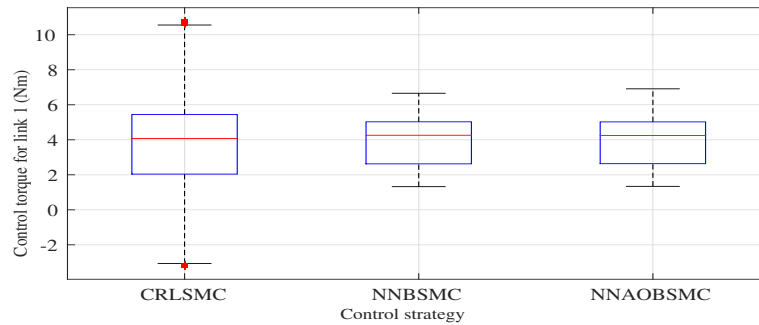


Figure 4.28 : Box plot representation of control torque for link 1.

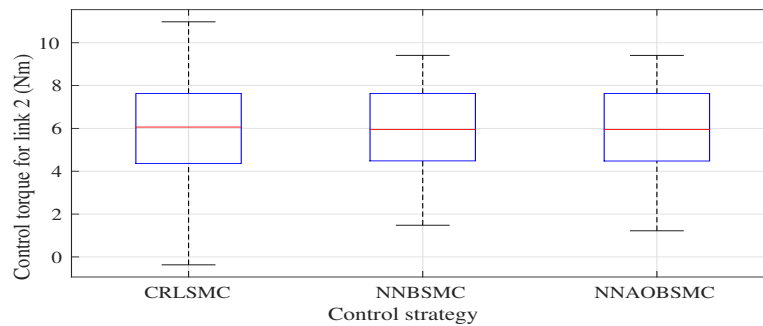


Figure 4.29 : Box plot representation of control torque for link 2.

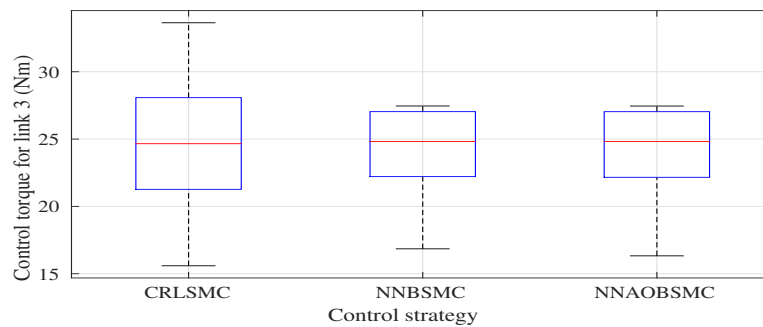


Figure 4.30 : Box plot representation of control torque for link 3.

4.8.2 Experimental studies

A two-link manipulator is designed to demonstrate the effectiveness of the proposed NNAOBSMC method. Considering the trade-off between the cost and performance, a microcontroller-based DC servo motor drivers have been used for the implementation of a two-link manipulator as shown in Fig. 4.31. The control board used in this

work is a 32-bit Arduino DUE, which offers a two-fold simplification on the hardware and software development process. On the hardware front, the microcontroller (Atmel®SAM3X8E) has an operating frequency of 84MHz with a flash memory of 512 KB and SRAM of 100 KB on the ARM® Cortex™-M3 processor.

On the software front, writing, modeling and deploying the code to the Arduino DUE board is made easy because of the open-source Arduino Software Development Environment, which has numerous libraries. RMCS-220X high-torque encoder dc

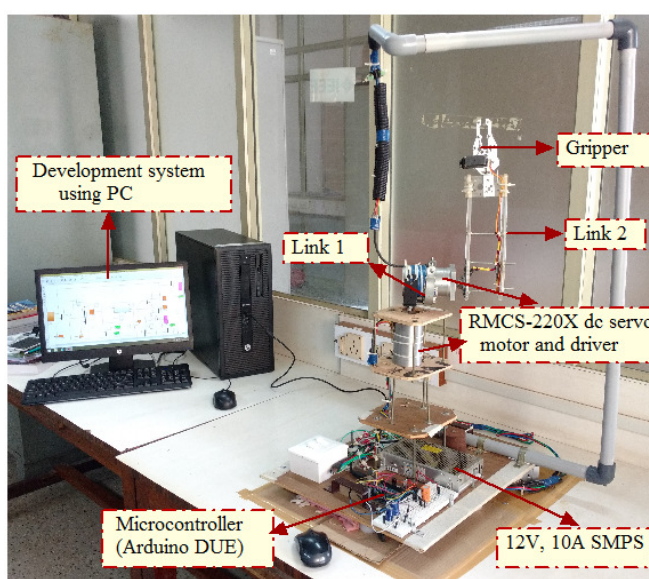


Figure 4.31 : Microcontroller-based experimental setup for a two-link manipulator.

servo motor and drivers are used as actuators for the two-link manipulator. RMCS-220X is designed for easy installation and operation with multiple interfaces. It integrates a high-torque dc motor with 18000 RPM base motor and metal gearbox and gears for 10RPM. It houses a 0.2 deg resolution quadrature optical encoder on its output shaft that allows the superior position and speed control with zero backlash at the output. It offers speed and position control via UART, I2C, PPM input signal and simple analog voltage input.

The physical parameters of the two-link manipulator are listed as follows: $m_1 = 0.484$ kg, $m_2 = 0.310$ kg, $L_1 = 0.22$ m, $L_2 = 0.328$ m and $g = 9.8$ m/s². Initial conditions are $q(0) = [0, 1]^T$ and $\dot{q}(0) = [1, 0]^T$. The reference tracking signals are $q_{d1}(t) = \sin(t)$ and $q_{d2}(t) = \cos(t)$. Considered friction terms are $F(q_1, \dot{q}_1) = 0.2\dot{q}_1 + 0.12\text{sign}(\dot{q}_1)$,

$F(q_2, \dot{q}_2) = 0.4\dot{q}_2 + 0.16\text{sign}(\dot{q}_2)$. The external disturbances are $\tau_{d1} = 0.5 \sin(5t)$ and $\tau_{d2} = 0.55 \sin(5t)$. The external disturbances are applied in off-line mode. It is to mention here that the control variable and other sensed parameter values through sensors are taken into MATLAB and are plotted then after. BSMC parameters are $\lambda_1 = 6.5042$, $K_{w1} = 1$, $K_{w2} = 1$ and $\phi = 0.322$. Simulated MSE values of link 1 and link 2 are $MSE_1 = 1.5968 \times 10^{-8}$ and $MSE_2 = 6.894 \times 10^{-9}$. Experimental MSE values of link 1 and link 2 are $MSE_1 = 1.2 \times 10^{-4}$ and $MSE_2 = 1.4 \times 10^{-3}$.

Figures 4.32 and 4.33 present the tracking performance of desired trajectories by pro-

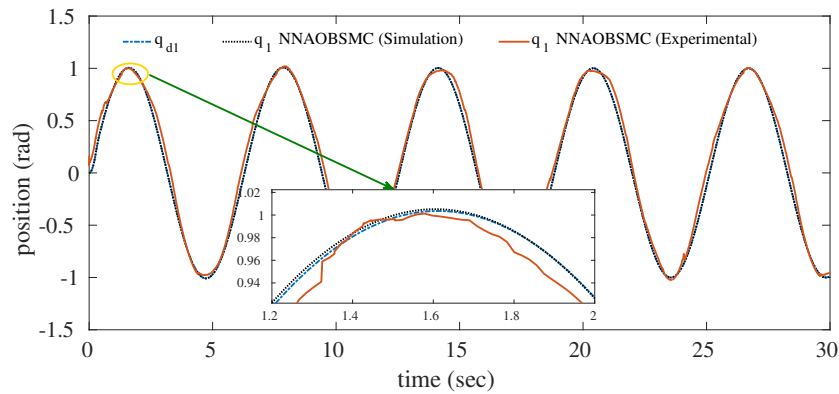


Figure 4.32 : Position tracking of link 1.

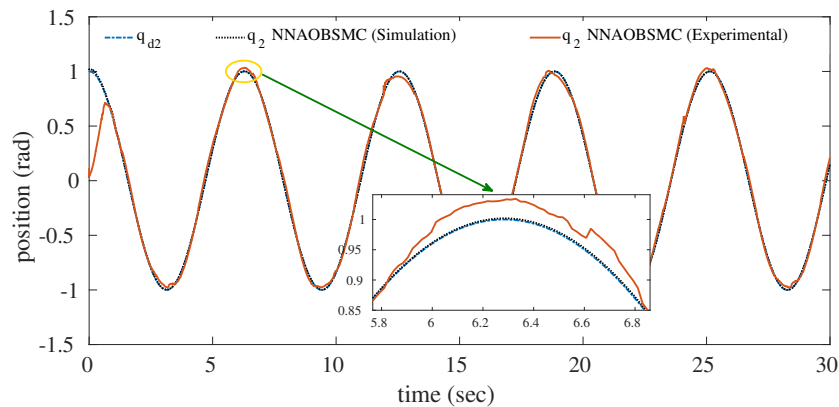


Figure 4.33 : Position tracking of link 2.

posed method (i.e., NNAOBSMC). Figure 4.35 represents MSE response and Figure 4.36 shows the control torque for link 1 and link 2 of the two-link manipulator. The experimental results in Figures 4.32 and 4.33 show that, in the interval from beginning to 2 sec, a favorable tracking response cannot be obtained due to the sudden impact

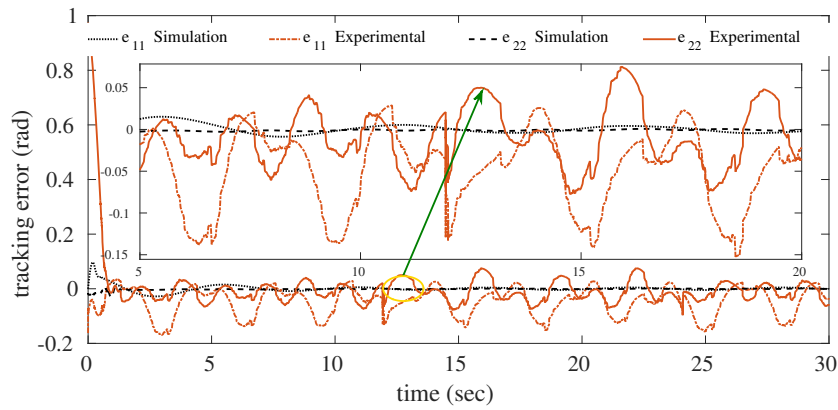


Figure 4.34 : Position tracking error of link 1 and link 2.

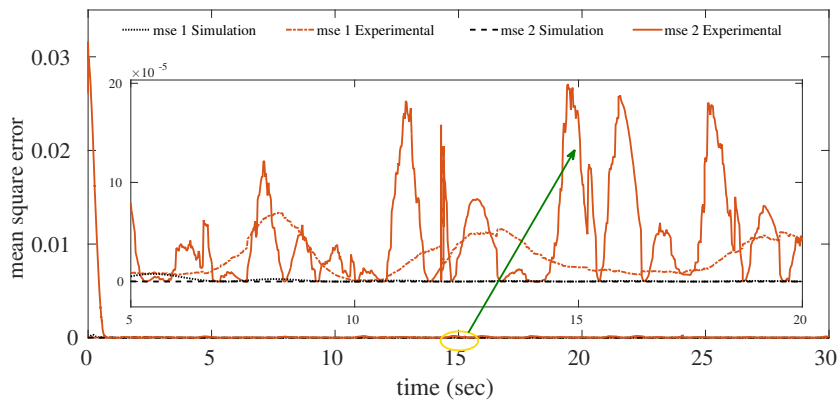


Figure 4.35 : Mean square error of link 1 and link 2 position tracking.

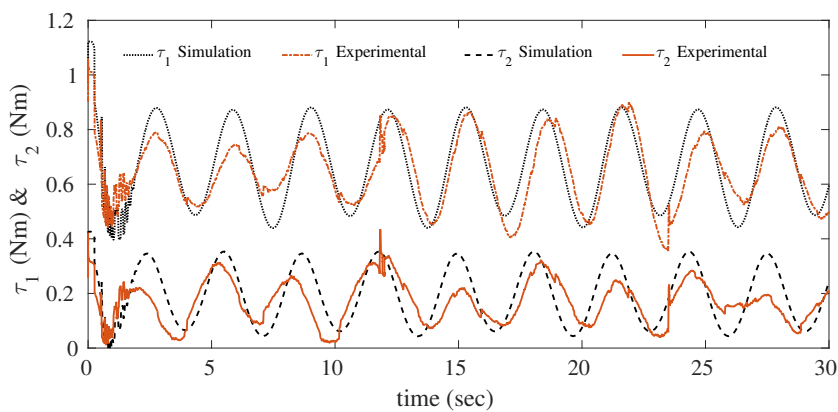


Figure 4.36 : Control torque for link 1 and link 2.

of nonlinearities, external disturbances, and uncertainties. From Figure 4.35, it is clear that the trajectory errors of two-link manipulator asymptotically converges to zero and the theoretical analysis of the proposed method (i.e., NNAOBSMC) is verified.

4.9 DESIGN OF INTEGRAL BACKSTEPPING SLIDING MODE CONTROLLER (IBSMC)

The backstepping methodology is a nonlinear scheme utilized as a part of controller design. The various points of interest in this approach incorporate its expansive arrangement of all around and asymptotically settling control laws and its ability to enhance robustness and take care of versatile issues. Backstepping sliding mode control includes non-linear frameworks into numerous subsystems. The mathematical model of OTDIRM is expressed in Eqs. (4.96), (4.97) and 4.98 are given as:

$$\dot{x}_1 = x_2 \quad (4.96)$$

$$\dot{x}_2 = \ddot{q} = D^{-1}(q)[\tau - (C(q, \dot{q})\dot{q} + G(q) + F(q, \dot{q}) + \tau_d)] \quad (4.97)$$

$$y = x_1 \quad (4.98)$$

where x_1 and x_2 are the position and velocity vectors of the OTDIRM. The position tracking error of the system is given as:

$$e_1 = q_d - q \quad (4.99)$$

The stabilizing function is characterized as:

$$\alpha_1 = \lambda_1 e_1 \quad (4.100)$$

The integral action of the tracking error of position is characterized as:

$$\alpha_2 = \lambda_2 \int_0^t e_1 dt \quad (4.101)$$

where λ_1 and λ_2 are positive constants. The tracking error of the velocity has upgraded with stability function and integral action of tracking error of the position of the OTDIRM. It is characterized in Eq. (4.102) and appeared as:

$$e_2 = \dot{e}_1 + \alpha_1 + \alpha_2 \quad (4.102)$$

The primary Lyapunov stability function is characterized as:

$$V_1 = \frac{1}{2} e_1^2 \quad (4.103)$$

By taking the derivative of the Eq. (4.103), we get:

$$\dot{V}_1 = e_1 \dot{e}_1 \quad (4.104)$$

From Eq. (4.102), can be changed as:

$$e_2 = \dot{q}_d - \dot{q} + \alpha_1 + \alpha_2 \quad (4.105)$$

$$\dot{V}_1 = e_1(e_2 - \alpha_1 - \alpha_2) = e_1 e_2 - \lambda_1 e_1^2 - \lambda_2 e_1 \int_0^t e_1 dt \quad (4.106)$$

By taking the derivative of e_2 , it becomes:

$$\dot{e}_2 = \ddot{q}_d - \ddot{q} + \lambda_1 \dot{e}_1 + \lambda_2 e_1 \quad (4.107)$$

From Eq. (1.2) and Eq. (4.107), we get:

$$\begin{aligned} \dot{e}_2 = & \ddot{q}_d - D^{-1}(q)[\tau - (C(q, \dot{q})\dot{q} + G(q) + F(q, \dot{q}) + \tau_d)] + \lambda_1 \dot{e}_1 \\ & + \lambda_2 e_1 \end{aligned} \quad (4.108)$$

The second Lyapunov stability function is characterized as:

$$V = V_1 + \frac{1}{2}s^T s \quad (4.109)$$

The satisfactory condition, which gives the affirmation that the tracking error will make an elucidation from achieving stage to sliding stage, is called the achieving condition and given in Eq. (4.110) is imparted as:

$$\dot{V} < 0, s \neq 0 \quad (4.110)$$

The sliding surface ('s') is characterized as:

$$s = e_1 + e_2 \quad (4.111)$$

The derivative of the second Lyapunov stability function is characterized as:

$$\dot{V} = \dot{V}_1 + s^T \dot{s} \quad (4.112)$$

$$= e_1 e_2 - \lambda_1 e_1^2 - \lambda_2 e_1 \int_0^t e_1 dt + s^T (\dot{e}_1 + \dot{e}_2) \quad (4.113)$$

By substituting \dot{e}_1 and \dot{e}_2 in above Eq. (4.113), yields

$$= e_1 e_2 - \lambda_1 e_1^2 - \lambda_2 e_1 \int_0^t e_1 dt + s^T ((1 + \lambda_1)\dot{e}_1 + \lambda_2 e_1 + \ddot{q}_d - \ddot{q}) \quad (4.114)$$

$$\dot{V} = e_1 e_2 - \lambda_1 e_1^2 - \lambda_2 e_1 \int_0^t e_1 dt + s^T [(1 + \lambda_1)\dot{e}_1 + \lambda_2 e_1 + \ddot{q}_d$$

$$- D^{-1}(q)(\tau - (C(q, \dot{q})\dot{q} + G(q) + F(q, \dot{q}) + \tau_d))] \quad (4.115)$$

The total input control torque (τ) to the OTDIRM is characterized as:

$$\tau = \tau_0 + \tau_c \quad (4.116)$$

By substituting Eq. (4.116) in Eq.(4.115), we get

$$\dot{V} = e_1 e_2 - \lambda_1 e_1^2 - \lambda_2 e_1 \int_0^t e_1 dt + s^T [(1 + \lambda_1)\dot{e}_1 + \lambda_2 e_1 + \ddot{q}_d$$

$$- D^{-1}(q)((\tau_0 + \tau_c) - (C(q, \dot{q})\dot{q} + G(q) + F(q, \dot{q}) + \tau_d))] \quad (4.117)$$

The arrangement of $\dot{s} = 0$ gives the control signal, which is known as equivalent control law and it is denoted by ' τ_0 '. This equivalent control law is essential to fulfilling the execution of favored trajectory tracking without considering disturbances and uncertainties

(i.e., $\tau_d = 0$).

$$\dot{s} = (1 + \lambda_1)\dot{e}_1 + \lambda_2 e_1 + \ddot{q}_d - D^{-1}(q)[\tau_0 - (C(q, \dot{q})\dot{q} + G(q) + F(q, \dot{q}))] = 0 \quad (4.118)$$

$$\tau_0 = D(q)((1 + \lambda_1)\dot{e}_1 + \lambda_2 e_1 + \ddot{q}_d) + C(q, \dot{q})\dot{q} + G(q) + F(q, \dot{q}) \quad (4.119)$$

An extra control exertion is needed to wipe out the unpredictable disturbances and uncertainties as equivalent control torque (τ_0) is lacking to provide the favored tracking performance. Ultimately, the tracking error dies out asymptotically, which means the sliding surface becomes stable. To exhibit the stability of the created control framework for OTDIRM, the Lyapunov-like Lemma is utilized. From Eqs. (4.117) and (4.119).

We arrive at an expression for \dot{V} as follows:

$$\dot{V} = e_1 e_2 - \lambda_1 e_1^2 - \lambda_2 e_1 \int_0^t e_1 dt + s^T (-D^{-1}(q) \tau_c) \quad (4.120)$$

The corrective control law (τ_c) is defined as:

$$\tau_c = D(q) \left(\frac{1}{s^T} (e_1 e_2 - \lambda_2 e_1 \int_0^t e_1 dt) + K_w \text{sign}(s) \right) \quad (4.121)$$

$$\dot{V} = e_1 e_2 - \lambda_1 e_1^2 - \lambda_2 e_1 \int_0^t e_1 dt - s^T \left(\frac{1}{s^T} (e_1 e_2 - \lambda_2 e_1 \int_0^t e_1 dt) + K_w \text{sign}(s) \right) \quad (4.122)$$

$$\dot{V} = -\lambda_1 e_1^2 - K_w s^T \text{sign}(s) \quad (4.123)$$

where K_w is the sliding gain.

$$\dot{V} \leq -\lambda_1 |e_1|^2 - K_w |s| \quad (4.124)$$

where $|s| = s^T \text{sign}(s)$. The chattering effect on the control input signal is introduced by the signum function ('sign'), which is utilized as a part of Eq. (4.123), to diminish or dispense with this impact, the signum function ('sign') is substituted by the hyperbolic tangent function ('tanh') and communicated in Eq. (4.125).

$$\dot{V} \leq -\lambda_1 e_1^2 - K_w s^T \tanh(s) \quad (4.125)$$

The term ' $s^T \tanh(s)$ ' in Eq. (4.125) is constantly positive so that whole condition gets to be negative (i.e., $s^T \tanh(s) > 0$ if either $s > 0$ or $s < 0$). The achieving control signal (τ_c) is modified as:

$$\tau_c = D(q) \left[\frac{1}{s^T} (e_1 e_2 - \lambda_2 e_1 \int_0^t e_1 dt) + K_w \tanh \left((1 + \lambda_1) e_1 + \lambda_2 \int_0^t e_1 dt + \frac{d}{dt} e_1 \right) \right] \quad (4.126)$$

Where $K_w = \text{diag}\{K_{w1}, K_{w2}, \dots, K_{wn}\}$ is positive gains matrix.

The IBSMC control law is defined as:

$$\tau_c = D(q) \left(\frac{1}{sT} (e_1 e_2 - \lambda_2 e_1 \int_0^t e_1 dt) \right) + K \tanh \left(\frac{(1 + \lambda_1) e_1 + \lambda_2 \int_0^t e_1 dt + \frac{d}{dt} e_1}{\phi} \right) \quad (4.127)$$

where $K = D(q)K_w$.

4.10 DESIGN OF NEURAL NETWORK BASED INTEGRAL BACKSTEPPING SLIDING MODE CONTROL (NNIBSMC)

In this section, the RBFNN is utilized to build up the control plans for the OTDIRM to track the desired trajectories under unknown dynamics of the system. Figure 4.37 demonstrates the schematic representation of NNIBSMC.

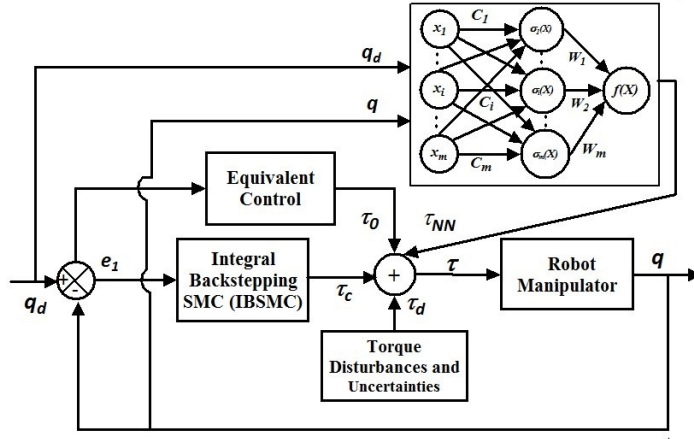


Figure 4.37 : Schematic arrangement of the NNIBSMC.

Tracking error of position is defined as:

$$e_1 = q_d - q \quad (4.128)$$

$$\dot{q}_r = \dot{q}_d + (1 + \lambda_1) e_1 + \lambda_2 \int_0^t e_1 dt \quad (4.129)$$

where ' \dot{q}_r ' is auxiliary signal. The modified sliding surface (s) is characterized as:

$$s = \dot{q}_r - \dot{q} = \dot{e}_1 + (1 + \lambda_1) e_1 + \lambda_2 \int_0^t e_1 dt \quad (4.130)$$

From (1.18), (4.129) and (4.130), we get

$$D(q)\dot{s} = -C(q, \dot{q})s + f(X) + \tau_d - \tau \quad (4.131)$$

$$f(X) = D(q)\ddot{q}_r + C(q, \dot{q})\dot{q}_r + F(q, \dot{q}) + G(q) \quad (4.132)$$

where $X = [\ddot{q}_d^T, \dot{q}_d^T, q_d^T, \dot{q}^T, q^T]^T$. The approximation of $f(X)$ is defined in Eq. (4.133) as:

$$\hat{f}(X) = \hat{W}^T \sigma(X) \quad (4.133)$$

where ‘ \hat{W} ’ is the NN adjustment law, $\sigma(X)$ is the basis function. The Eq. (4.131) can be revised as:

$$D(q)\dot{s} = -C(q, \dot{q})s + \tilde{W}^T \sigma(X) + \hat{W}^T \sigma(X) + \tau_d - \tau \quad (4.134)$$

where $\tilde{W} = W^* - \hat{W}$, W^* is ideal weights matrix.

Theorem 4.10.1. *Consider the robot manipulator is demonstrated by (1.18), if the total control torque is expressed as $\tau = \tau_0 + \tau_c + \tau_{NN}$, in which control law of IBSMC is defined as $\tau_c = k_1 s + K \tanh\left(\frac{(1+\lambda_1)e_1 + \lambda_2 \int_0^t e_1 dt + \frac{d}{dt} e_1}{\phi}\right)$, $\tau_0 = D(q)\left(\dot{e}_1(1+\lambda_1) + \lambda_2 e_1 + \ddot{q}_d\right) + C(q, \dot{q})\dot{q} + G(q) + F(q, \dot{q})$ and $\tau_{NN} = \hat{W}^T \sigma(X)$. The evaluated adaptive law for the NN identifier is characterized as:*

$$\dot{\hat{W}}^T = -\dot{\tilde{W}}^T = B \sigma(X) s^T \quad (4.135)$$

where ‘ B ’ is denoted as a positive definite matrix, the tracking errors of position and velocity (i.e., e and \dot{e}) of the system asymptotically converge to zero as $t \rightarrow \infty$.

Proof. NNIBSMC stability function is given in Eq. (4.136) and characterized as:

$$V = \frac{1}{2} s^T D(q) s + \frac{1}{2} \text{tr}(\tilde{W}^T B^{-1} \tilde{W}) \quad (4.136)$$

$$\dot{V} = \frac{1}{2} s^T \dot{D}(q) s + s^T D(q) \dot{s} + \text{tr}(\tilde{W}^T B^{-1} \dot{\tilde{W}}) \quad (4.137)$$

By substituting Eq. (4.134) in Eq. (4.137), we get

$$\dot{V} = \frac{1}{2} s^T \{\dot{D}(q) - 2C(q, \dot{q})\} s + s^T \{\tilde{W}^T \sigma(X) + \varepsilon^* + \tau_d - k_1 s \quad (4.138)$$

$$- K \tanh\left(\frac{s}{\phi}\right)\} + \text{tr}(\tilde{W}^T B^{-1} \dot{\tilde{W}})$$

$$= \frac{1}{2} s^T \{\dot{D}(q) - 2C(q, \dot{q})\} s + s^T \{\varepsilon^* + \tau_d - k_1 s - K \tanh\left(\frac{s}{\phi}\right)\} \quad (4.139)$$

$$+ \text{tr}\{\tilde{W}^T (B^{-1} \dot{\tilde{W}} + \sigma(X) s^T)\}$$

Since, $\dot{D}(q) - 2C(q, \dot{q})$ is skew symmetric (i.e., $\frac{1}{2} s^T [\dot{D}(q) - 2C(q, \dot{q})] s = 0$), from Eqs. (4.125) and (4.135), \dot{V} can be rewritten as:

$$\dot{V} \leq -k_1 s^T s + \|s\| \delta_0 \quad (4.140)$$

where ‘ δ_0 ’ is an upper bound of $\|\varepsilon^* + \tau_d\|$. The term $\|s\| \delta_0$ is bounded by $\|s\| \delta_0 \leq \frac{1}{2} (\|s\|^2 + \rho \delta_0^2)$, where $\rho > 0$ is picked to such an extent that $\int_0^\infty \rho dt < \infty$ and further

substituted in Eq. (4.140) to get stability criteria with finite boundedness.

$$\dot{V} \leq -k_1 \|s\|^2 + \frac{1}{2} (\|s\|^2 + \rho \delta_0^2) \quad (4.141)$$

Integrating both sides of Eq. (4.141) from $t = 0$ to T , yields

$$V(T) - V(0) \leq -(k_1 - \frac{1}{2}) \int_0^T \|s\|^2 dt + \frac{1}{2} \delta_0^2 \int_0^T \rho dt, \quad (\forall k_1 > 2) \quad (4.142)$$

Since, $V(T) \geq 0$ and $\int_0^\infty \rho dt < \infty$ holds,

$$\limsup_{T \rightarrow \infty} \frac{1}{T} \int_0^T \|s\|^2 dt \leq \frac{1}{(k_1 - \frac{1}{2})} \left[V(0) + \frac{1}{2} \delta_0^2 \int_0^\infty \rho dt \right] \limsup_{T \rightarrow \infty} \frac{1}{T} = 0 \quad (4.143)$$

From the Eqs. (4.142) and (4.143), we can get $s \rightarrow 0$ as $t \rightarrow \infty$. Subsequently, from the Eq. (4.130), the tracking errors of position and velocity (i.e., e and \dot{e}) are asymptotically converge to zero as $t \rightarrow \infty$. Therefore, the stability criteria is fulfilled by the proposed NNIBSMC scheme. \square

4.11 AN ADAPTIVE OBSERVER BASED CONTROL OF OTDIRM

4.11.1 Design of Neural Network Based Adaptive Observer Integral Backstepping Sliding Mode Control(NNAOIBSMC)

The NNAOIBSMC is developed with the help of NNAO for precise desired trajectory tracking and improve the disturbance rejection under different working conditions (i.e., external disturbances and uncertainties) of OTDIRM. Figure. 4.38 demonstrates the structure of the NNAOIBSMC.

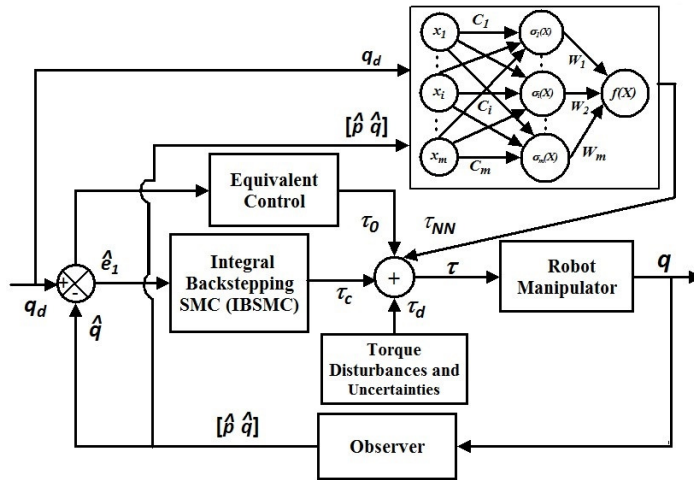


Figure 4.38 : Schematic arrangement of the NNAOIBSMC.

The evaluated error of the link position is characterized as:

$$\hat{e}_1 = q_d - \hat{q} \quad (4.144)$$

$$\dot{\hat{e}}_1 = \dot{q}_d - \dot{\hat{q}} \quad (4.145)$$

The estimated sliding surface ‘ \hat{s} ’ is designed as:

$$\hat{s} = \frac{(1 + \lambda_1)\hat{e}_1 + \lambda_2 \int_0^t \hat{e}_1 dt + \frac{d}{dt} \hat{e}_1}{\phi} \quad (4.146)$$

Theorem 4.11.1. *The NNAO estimates q and p as \hat{q} and \hat{p} , estimation errors are $\tilde{q} = q - \hat{q}$ and $\tilde{p} = p - \hat{p}$. Then, the perspective of \hat{q} and \hat{p} , the approximation function of $f(X)$ described in Eq. (4.132) is conveyed as:*

$$\hat{f}(\hat{X}) = \hat{W}_c^T \sigma(\hat{X}), \quad \hat{X} = [\ddot{q}_d^T, \dot{q}_d^T, \dot{q}_d^T, \hat{p}^T, \hat{q}^T]^T \quad (4.147)$$

where ‘ \hat{W}_c ’ is estimated adaptation matrix. The adaptation law is defined as:

$$\dot{\hat{W}}_c = -\dot{\tilde{W}}_c = B_c \sigma(\hat{X}) \hat{s}^T \quad (4.148)$$

The NNAOIBSMC law is characterized as:

$$\tau = \Lambda_3 \hat{s} + K \tanh\left(\frac{\hat{s}}{\phi}\right) + \hat{W}_c^T \sigma(\hat{X}) \quad (4.149)$$

where ‘ $\Lambda_3 \hat{s} + K \tanh(\frac{\hat{s}}{\phi})$ ’ is the boundary sliding mode control law and ‘ $\hat{W}_c^T \sigma(\hat{X})$ ’ is the NN estimation to robot manipulator, then the estimation errors \tilde{q} and \tilde{p} are asymptotically converges to zero.

Proof. The Lyapunov stability candidate function for NNAOIBSMC is characterized as:

$$V = V_o + V_c \quad (4.150)$$

where ‘ V_o ’ is observer stability function and ‘ V_c ’ is controller stability candidate function.

$$V_o = \tilde{p}^T \tilde{p} + \frac{1}{2} \text{tr}(\tilde{W}_o^T B_o^{-1} \tilde{W}_o) \quad (4.151)$$

$$V_c = \frac{1}{2} s^T D(q) s + \frac{1}{2} \text{tr}(\tilde{W}_c^T B_c^{-1} \tilde{W}_c) \quad (4.152)$$

The derivative of Eq. (4.152) becomes

$$\dot{V}_c = \frac{1}{2} s^T \dot{D}(q) s + s^T D(q) \dot{s} + \text{tr}(\tilde{W}_c^T B_c^{-1} \dot{\tilde{W}}_c) \quad (4.153)$$

$$= \frac{1}{2} s^T \{\dot{D}(q) - 2C(q, p)\} s + s^T \{\tilde{W}_c^T \sigma(X) + \hat{W}_c^T \tilde{\sigma}(X) + \varepsilon^* + \tau_d \quad (4.154)$$

$$- \Lambda_3 \hat{s} - K \tanh\left(\frac{\hat{s}}{\phi}\right)\} + \text{tr}(\tilde{W}_c^T B_c^{-1} \dot{\tilde{W}}_c)$$

Since, $\dot{D}(q) - 2C(q, p)$ is skew symmetric (i.e., $\frac{1}{2} s^T [\dot{D}(q) - 2C(q, \dot{q})] s = 0$) and $s = \hat{s} + \dot{\hat{q}} + \Lambda_1 \tilde{q} = \hat{s} + \tilde{p}$, we get

$$\dot{V}_c = \hat{s}^T \{\hat{W}_c^T \tilde{\sigma}(\hat{X}) + \varepsilon^* + \tau_d\} + \tilde{p}^T \{\tilde{W}_c^T \sigma(\hat{X}) + \hat{W}_c^T \tilde{\sigma}(\hat{X}) + \varepsilon^* \quad (4.155)$$

$$+ \tau_d\} - \Lambda_3 \hat{s}^T \hat{s} - \Lambda_3 \tilde{p}^T \hat{s} - K \hat{s}^T \tanh\left(\frac{\hat{s}}{\phi}\right) + \text{tr}\{\tilde{W}_c^T (B_c^{-1} \dot{\tilde{W}}_c + \sigma(\hat{X}) \hat{s}^T)\}$$

where ‘ γ_0 ’ is maximum limit of $\|\hat{W}_c^T \tilde{\sigma}(\hat{X}) + \varepsilon^* + \tau_d\|$ and $\zeta = \{\tilde{W}_c^T \sigma(\hat{X}) + \hat{W}_c^T \tilde{\sigma}(\hat{X}) + \varepsilon^* + \tau_d\}$, at that point there exists a positive constant ‘ ζ_0 ’ such that $\|\zeta\| \leq \zeta_0$.

$$\dot{V}_c \leq \|\hat{s}\| \gamma_0 + \|\tilde{p}\| \zeta_0 - \Lambda_3 \hat{s}^T \hat{s} - \Lambda_3 \tilde{p}^T \hat{s} \quad (4.156)$$

The terms $\|\hat{s}\|\gamma_0$, $\|\tilde{p}\|\zeta_0$ and $-\Lambda_3\tilde{p}^T\hat{s}$ are bounded by $\|\hat{s}\|\gamma_0 \leq \frac{1}{2}(\|\hat{s}\|^2 + \rho\gamma_0^2)$, $\|\tilde{p}\|\zeta_0 \leq \frac{1}{2}(\|\tilde{p}\|^2 + \rho\zeta_0^2)$ and $-\Lambda_3\tilde{p}^T\hat{s} \leq \frac{\Lambda_3}{2}(\|\tilde{p}\|^2 + \|\hat{s}\|^2)$ respectively. To induce stability criteria with finite boundedness, the constrained terms are substituted in Eq. (4.156). The expression for \dot{V}_c gets to be:

$$\dot{V}_c \leq -\left(\frac{\Lambda_3}{2} - \frac{1}{2}\right)\|\hat{s}\|^2 + \left(\frac{\Lambda_3}{2} + \frac{1}{2}\right)\|\tilde{p}\|^2 + \frac{1}{2}\rho\left(\gamma_0^2 + \zeta_0^2\right), \quad \forall (\Lambda_3 > 2) \quad (4.157)$$

The derivative of Eq. (4.151) and from Eq. (4.33), we get

$$\dot{V}_o = \tilde{p}^T \{W_o^{*T} \tilde{\sigma}_o(q, p) - D^{-1}(q)\tau_d + \varepsilon_o^*\} - \Lambda_3\tilde{p}^T\tilde{p} + tr\{\tilde{W}_o^T (B_o^{-1}\dot{\tilde{W}}_o + \sigma_o(\hat{q}, \hat{p})\tilde{p}^T)\} \quad (4.158)$$

Since, $\|W_o^{*T} \tilde{\sigma}_o(q, p) - D^{-1}(q)\tau_d + \varepsilon_o^*\| \leq \beta_0$ and $\|\tilde{p}\|\beta_0$ is bounded by $\|\tilde{p}\|\beta_0 \leq \frac{1}{2}(\|\tilde{p}\|^2 + \rho\beta_0^2)$, then

$$\dot{V}_o \leq -\Lambda_3\tilde{p}^T\tilde{p} + \frac{1}{2}(\|\tilde{p}\|^2 + \rho\beta_0^2) \quad (4.159)$$

$$\dot{V} = \dot{V}_o + \dot{V}_c \quad (4.160)$$

$$\dot{V} \leq -\frac{1}{2}\left(\Lambda_3 - 2\right)\|\tilde{p}\|^2 - \frac{1}{2}\left(\Lambda_3 - 1\right)\|\hat{s}\|^2 + \frac{1}{2}\rho\left(\gamma_0^2 + \zeta_0^2 + \beta_0^2\right), \quad \forall (\Lambda_3 > 2) \quad (4.161)$$

Integrating both sides from $t = 0$ to T , yields

$$V(T) - V(0) \leq -\frac{1}{2}\left(\Lambda_3 - 1\right)\int_0^T \|\hat{s}\|^2 dt - \frac{1}{2}\left(\Lambda_3 - 2\right)\int_0^T \|\tilde{p}\|^2 dt \quad (4.162)$$

$$+ \frac{1}{2}\left(\gamma_0^2 + \zeta_0^2 + \beta_0^2\right)\int_0^T \rho dt$$

Since, $V(T) \geq 0$ and $\int_0^\infty \rho dt < \infty$ holds,

$$\limsup_{T \rightarrow \infty} \frac{1}{T} \left\{ \left(\Lambda_3 - 1\right)\int_0^T \|\hat{s}\|^2 dt + \left(\Lambda_3 - 2\right)\int_0^T \|\tilde{p}\|^2 dt \right\} \leq \quad (4.163)$$

$$2 \left[V(0) + \frac{1}{2}(\gamma_0^2 + \zeta_0^2 + \beta_0^2)\int_0^\infty \rho dt \right] \limsup_{T \rightarrow \infty} \frac{1}{T} = 0$$

From Eqs. (4.163) and (4.163), it is clear that $\tilde{p} \rightarrow 0$, $\hat{s} \rightarrow 0$ as $t \rightarrow \infty$. That concludes $\tilde{q} \rightarrow 0$ and $\tilde{p} \rightarrow 0$. Thusly, the proposed NNAOIBSMC fulfills the stability criteria. \square

4.12 RESULTS AND DISCUSSIONS FOR INTEGRAL BACKSTEPPING SMC METHODOLOGIES

MATLAB/SIMULINK tool has been used to carry out simulations for the 3-DOF OTDIRM. The link position and velocity vectors are $q = [q_1, q_2, q_3]^T$ and $\dot{q} = [\dot{q}_1, \dot{q}_2, \dot{q}_3]^T$ respectively. The desired reference trajectories for de-icing robot manipulator and essential parameters that influence the control activity of the robotic systems (i.e., uncertainties and external disturbances) are considered according to literature (Tran et al., 2015). IBSMC parameters are $\lambda_1 = 100$, $\lambda_2 = 20$, $K_{w1} = 970$, $K_{w2} = 970$, $K_{w3} = 970$

and $\phi = 0.004$. The simulated responses of the OTDIRM are compared with those presented in (Tran et al., 2015) are shown in figures from 4.39 to 4.50.

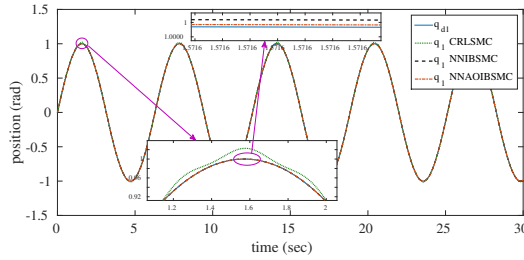


Figure 4.39 : Position tracking of link 1.

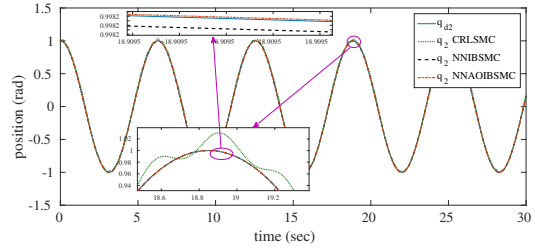


Figure 4.40 : Position tracking of link 2.

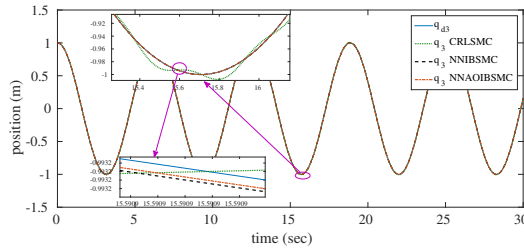


Figure 4.41 : Position tracking of link 3.

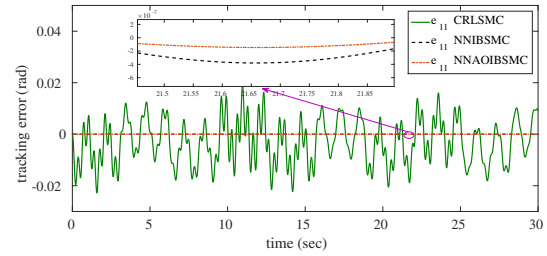


Figure 4.42 : Tracking error of link 1.

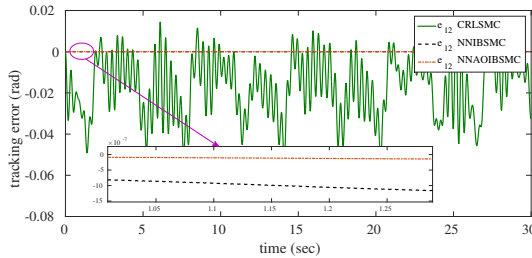


Figure 4.43 : Tracking error of link 2.

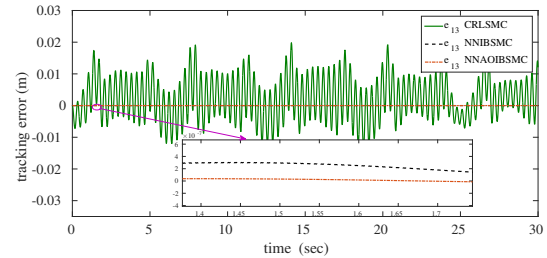


Figure 4.44 : Tracking error of link 3.

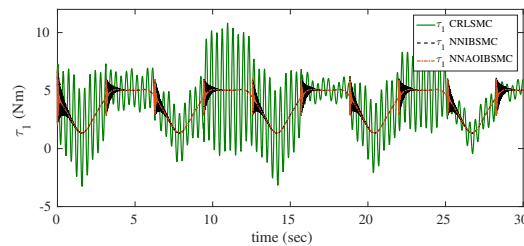


Figure 4.45 : Control input for link 1.

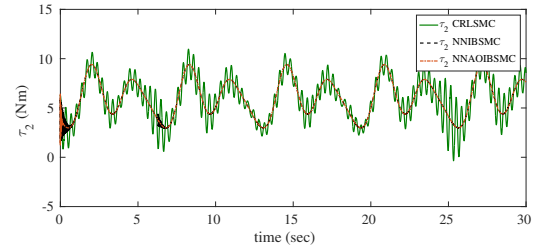


Figure 4.46 : Control input for link 2.

The MSE values of the 3-DOF OTDIRM trajectories under different control methodologies, such as CRLSMC in (Tran et al., 2015), NNIBSMC and NNAOIBSMC are

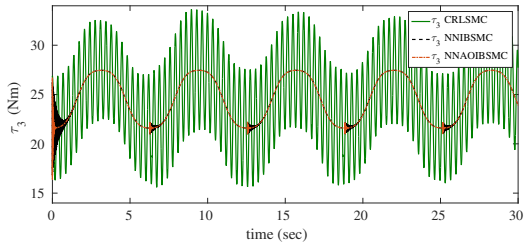


Figure 4.47 : Control input for link 3.

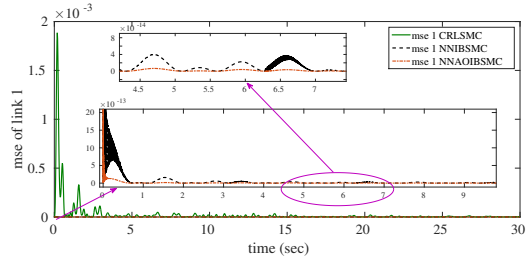


Figure 4.48 : MSE of link 1.

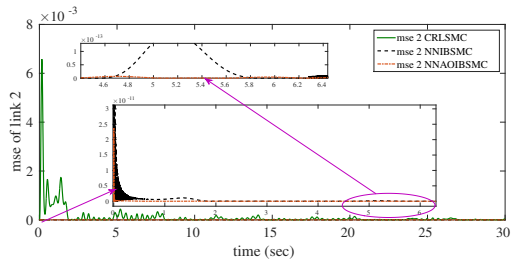


Figure 4.49 : MSE of link 2.

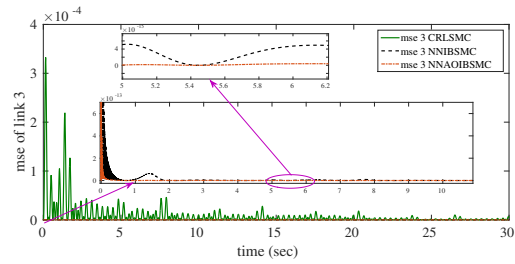


Figure 4.50 : MSE of link 3.

Table 4.12.1 : MSE examination of CRLSMC, NNIBSMC and NNAOIBSMC

Sl. No	MSE	CRLSMC	NNIBSMC	NNAOIBSMC
1	MSE_1	2.732×10^{-6}	4.202×10^{-15}	6.054×10^{-16}
2	MSE_2	3.526×10^{-5}	3.939×10^{-15}	3.299×10^{-17}
3	MSE_3	4.864×10^{-6}	3.14×10^{-16}	5.287×10^{-20}

presented in Table 4.12.1. From the table, it is ascertained that NNAOIBSMC provides least MSE values in comparison with other methods (i.e., NNAOIBSMC system has better tracking trajectory performance). Figure 4.39 to Figure 4.41 indicate tracking positions, Figure 4.42 to Figure 4.44 indicate tracking errors and Figure 4.45 to Figure 4.47 show control torque. From the Figure 4.45 to Figure 4.47, it is clear that the control torque is smoother for NNAOIBSMC compared with existing CRLSMC (Tran et al., 2015). This indicates that the proposed method requires less control effort for same trajectory tracking. The MSE response plots of the OTDIRM link trajectories exhibited from Figure 4.48 to Figure 4.50. From Table 4.12.2 and 4.12.3, it clear that the values of TV and 2-Norm of input for proposed methods are very small as compared to existing method CRLSMC (Tran et al., 2015). The energy of the input signal is calculated by using the 2-Norm method. The control energy is expected to be as small as

Table 4.12.2 : Total variance examination of CRLSMC (Tran et al., 2015), NNIBSMC and NNAOIBSMC

Sl. No	Total Variance (TV)	CRLSMC	NNIBSMC	NNAOIBSMC
1	link 1	6.1354	1.8414	1.7751
2	link 2	4.8902	3.5523	3.5407
3	link 3	20.8775	5.1943	5.1339

possible. The output and input performances are calculated for the period from 0 to 30 sec with a sampling time of 0.0001 sec.

Table 4.12.3 : 2-Norm of input examination of CRLSMC (Tran et al., 2015), NNIBSMC and NNAOIBSMC

Sl. No	2-Norm of Input	CRLSMC	NNIBSMC	NNAOIBSMC
1	link 1	2.4778×10^3	2.2124×10^3	2.2079×10^3
2	link 2	3.4905×10^3	3.4535×10^3	3.4530×10^3
3	link 3	1.3727×10^4	1.3555×10^4	1.3549×10^4

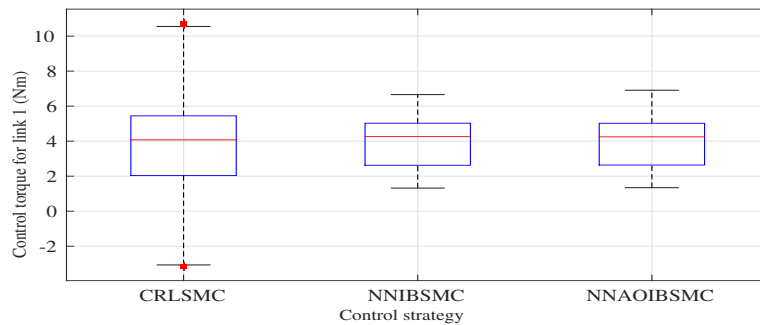


Figure 4.51 : Box plot representation of control torque for link 1.

Figure 4.51, Figure 4.52 and Figure 4.53 show the box plot of control torque for link 1, link 2 and link 3 with the mean, median, $\pm 25\%$ quartiles (notch boundaries), $\pm 75\%$ quartiles (box ends), $\pm 95\%$ bounds and the outliers. From the size of the boxes shown, it is clear that the NNAOIBSMC control strategy experiences minimum variation than others. Comparing the box plot of NNIBSMC and NNAOIBSMC, it observed that NNAOIBSMC has less variation in control input torque for link 1, link 2 and link 3 of

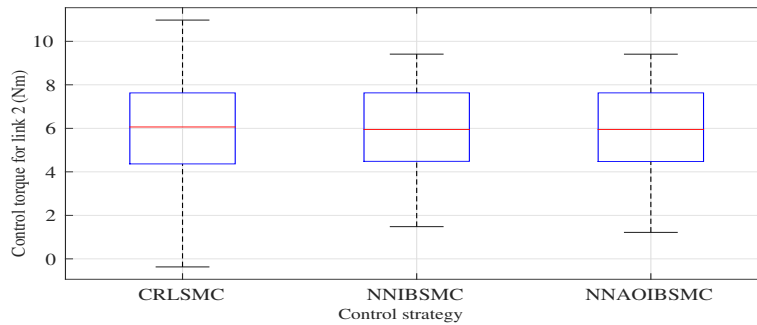


Figure 4.52 : Box plot representation of control torque for link 2.

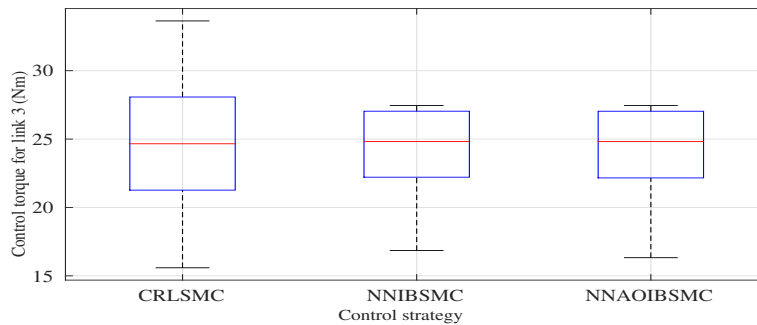


Figure 4.53 : Box plot representation of control torque for link 3.

the OTDIRM.

4.13 SUMMARY

In this chapter, different control methodologies are proposed for the 3-DOF OTDRIM. The proposed control approaches are based on the modified sliding mode control techniques; neural network based approximators and observers to provide robustness to external disturbances and parameter uncertainties. In general, the results illustrate that the proposed observer-based controller offers a superior tracking performance and smoother control input compared to other existing methods. The derivation of the control law guarantees the convergence of the tracking error. Several performance methods are examined to support the strength of the proposed and existing control approaches. The box plots of control torques show that the observer-based control scheme has less variation in control input compared to other methods.

Chapter 5

NEURAL NETWORK BASED OBSERVER DESIGN AND MODIFIED TERMINAL SLIDING MODE CONTROL METHODOLOGIES FOR ROBOT MANIPULATOR

This chapter discusses different types of the observer-based terminal sliding mode control methodologies, i.e., TSMC, BTSMC and IBTSMC for a 3-DOF OTDIRM. Finally, the results are verified by comparing the input and output performances.

5.1 INTRODUCTION

In this chapter, discussion is carried out on different control methods of 3-DOF OTDIRM to eliminate the effects of disturbance and uncertainty associated with the direct measurements. The designing of a new controller considers the combination of different types of modified TSMC schemes with NN identifier and NN observer. The optimal weights of the NN observer, NN identifier, and the various TSMC parameters are obtained with the help of PSO. Estimated position and velocity vectors of the RBFNN based observer are fed to another RBFNN based identifier to approximate the auxiliary control input torque to the de-icing robot manipulator. The chattering effect is mitigated by utilizing the boundary layer phenomenon while the Lyapunov stability test ensures the stability of the anticipated control strategy.

In (Tran et al., 2015), authors discussed the CRLSMC for the de-icing robot manip-

ulator to achieve the desired trajectory tracking performance under various operating conditions. In (Rossomando et al., 2014), authors have designed a conventional SMC scheme based on NN for better trajectory tracking of the mobile robot manipulator. The position control of the 2-link robot manipulator is designed by considering the combination of conventional SMC and NN based observer (Sun et al., 2011). In (Wei et al., 2012), the WNN based controller is designed for the de-icing robot manipulator without consideration of an observer-based control structure. This chapter mainly differs from (Tran et al., 2015), (Rossomando et al., 2014), (Sun et al., 2011) and (Wei et al., 2012), by replacing conventional SMC with the modified backstepping TSMC scheme in combination with PSO based observer and identifier. Several performance methods are examined to show the effectiveness of the proposed control technique.

5.2 DESIGN AND STABILITY OF TERMINAL SLIDING MODE CONTROL (TSMC)

In the conventional SMC, the convergence of the state is usually asymptotic due to the linearity of the switching plane. However, this convergence can only be achieved in infinite time, although the SMC parameters can be adjusted to make convergence faster. For high-precision control systems, faster convergence is the priority and can only be achieved at large control inputs. These large control inputs can lead to the saturation of the actuator. The TSMC includes nonlinear function in the outline of the sliding hyperplane. By using a nonlinear sliding surface, TSMC enables the rapid convergence of the state without the need for an extensive control action. A non-singular terminal sliding mode manifold is used to design a chattering free adaptive control scheme for the robot manipulator.

The input control torque (τ) to the OTDIRM is defined as:

$$\tau = \tau_0 + \tau_c \quad (5.1)$$

Where ' τ_0 ' and ' τ_c ' are the equivalent and the sliding mode control torques respectively. A time varying sliding surface vector ' s ' is given by the following Equation (5.2) and

defined as:

$$s = \dot{e} + \frac{1}{\lambda} e^{\frac{\Omega_1}{\Omega_2}} \quad (5.2)$$

where λ , Ω_1 , and Ω_2 ($1 < \frac{\Omega_1}{\Omega_2} < 2$) are positive odd numbers. The purpose of terminal sliding mode control law is to force tracking error (' e ') to approach the sliding surface and then move along the sliding surface (' s ') to the origin. The derivative of sliding surface with respect to time is expressed in Equation (5.3) and (5.4) as follows:

$$\dot{s} = \ddot{e} + \frac{\Omega_1}{\lambda \Omega_2} e^{\frac{\Omega_1 - \Omega_2}{\Omega_2}} \dot{e} \quad (5.3)$$

$$\dot{s} = \ddot{q}_d - \ddot{q} + \frac{\Omega_1}{\lambda \Omega_2} e^{\frac{\Omega_1 - \Omega_2}{\Omega_2}} \dot{e} \quad (5.4)$$

where $\ddot{e} = \ddot{q}_d - \ddot{q}$ and substituting the value of \ddot{q} from Equation (1.2) in Equation (5.4) gives

$$\dot{s} = \ddot{q}_d + \frac{\Omega_1}{\lambda \Omega_2} e^{\frac{\Omega_1 - \Omega_2}{\Omega_2}} \dot{e} - D^{-1}(q)[\tau - (C(q, \dot{q})\dot{q} + G(q) + F(q, \dot{q}) + \tau_d)] \quad (5.5)$$

The control effort is derived from the solution of $\dot{s} = 0$. This control effort is known as equivalent control effort represented by ' τ_0 ', which is required to achieve the desired trajectory tracking without considering disturbances and uncertainties (i.e., $\tau_d = 0$).

$$\dot{s} = \ddot{q}_d + \frac{\Omega_1}{\lambda \Omega_2} e^{\frac{\Omega_1 - \Omega_2}{\Omega_2}} \dot{e} - D^{-1}(q)[\tau_0 - (C(q, \dot{q})\dot{q} + G(q) + F(q, \dot{q}))] = 0 \quad (5.6)$$

$$\tau_0 = D(q)\left(\ddot{q}_d + \frac{\Omega_1}{\lambda \Omega_2} e^{\frac{\Omega_1 - \Omega_2}{\Omega_2}} \dot{e}\right) + C(q, \dot{q})\dot{q} + G(q) + F(q, \dot{q}) \quad (5.7)$$

However, if unpredictable disturbances or uncertainties occur, the equivalent control effort (τ_0) cannot ensure the desired trajectory tracking performance. Therefore, an auxiliary control effort is required to eliminate the effect of the unpredictable disturbances. Finally, the sliding surface should be stable, which means the error dies out asymptotically. The Lyapunov like Lemma is used to prove the stability of the designed control system. The Lyapunov stability function is defined as:

$$V = \frac{1}{2} s^T s \quad (5.8)$$

A sufficient condition, which guarantees that the tracking position error will translate from reaching phase to sliding phase is also known as the reaching condition and expressed in Eq. (5.9).

$$\dot{V} = s^T \dot{s} < 0, s \neq 0 \quad (5.9)$$

To get the control torque (' τ_c '), the Eq. (5.9) can be defined as:

$$\dot{V} = s^T \left[\ddot{q}_d + \frac{\Omega_1}{\lambda \Omega_2} e^{\frac{\Omega_1 - \Omega_2}{\Omega_2} \dot{e}} - D^{-1}(q)(\tau_0 + \tau_c) - D^{-1}(q)(C(q, \dot{q})\dot{q} + G(q) + F(q, \dot{q})) \right] \quad (5.10)$$

Substituting Eq. (5.7) into Eq. (5.10), we get

$$\dot{V} = s^T \dot{s} = -s^T D^{-1}(q) \tau_c \quad (5.11)$$

To ensure $s^T \dot{s} < 0$, the control torque is chosen as:

$$\tau_c = D(q) K_w \text{sign}(s) \quad (5.12)$$

Substituting Eq. (5.12) into Eq. (5.11), then the Lyapunov stability condition becomes

$$\dot{V} < -s^T D^{-1}(q) D(q) K_w \text{sign}(s) \quad (5.13)$$

$$\dot{V} < -K_w s^T \text{sign}(s)$$

$$\dot{V} < -K_w |s| \quad (5.14)$$

where $|s| = s^T \cdot \text{sign}(s)$. The 'sign' function, which is used in Eq. (5.12) creates more chattering effect on the control torque. In order to avoid this chattering effect, the 'sign' function is replaced by the 'tanh' (hyperbolic tangent) function and expressed in Eq. (5.15).

$$\dot{V} < -K_w s^T \tanh(s) \quad (5.15)$$

The term ' $s^T \tanh(s)$ ' in Eq. (5.15) is always positive so that entire equation becomes negative provided that ' s ' satisfies the following conditions.

1. if ' s ' is negative and $\tanh(s)$ is also negative then $s^T \tanh(s)$ is always positive
2. if ' s ' is positive and $\tanh(s)$ is also positive then $s^T \tanh(s)$ is always positive

Finally, the reaching control torque (τ_c) is given in Eq. (5.16) and follows as:

$$\tau_c = K_w D(q) \tanh \left(\dot{e} + \frac{1}{\lambda} e^{\frac{\Omega_1}{\Omega_2}} \right) \quad (5.16)$$

where $K_w = \text{diag}\{K_{w1}, K_{w2}, \dots, K_{wn}\}$ is control gain matrix with the upper bound of uncertainties. Tuning positive time constant K_w given in Eq. (5.16) is one of the most important challenges in conventional sliding mode control.

Finally, the SMC control law with boundary layer becomes

$$\tau_c = K \tanh \left(\frac{\frac{d}{dt} e + \frac{1}{\lambda} e^{\frac{\Omega_1}{\Omega_2}}}{\phi} \right) \quad (5.17)$$

where ‘ K ’ is positive gain matrix and it is defined as $K = K_w D(q)$. When $s = 0$ is reached at $t = t_r$, $e = 0$ becomes terminal surface. The effect of terminal surface will take the state of e from $e(t_r) \neq 0$ to $e(t_r + t_s) = 0$ with finite time t_s given by

$$t_s = \frac{\lambda \Omega_2}{\Omega_1 - \Omega_2} \left(e^{1 - \frac{\Omega_1}{\Omega_2}} \right) \quad (5.18)$$

5.3 DESIGN OF NEURAL NETWORK BASED TERMINAL SLIDING MODE CONTROL (NNTSMC)

In this section, the RBFNN is utilized to build up the control plans for the robot manipulator to track the desired trajectories under unknown dynamics of the system. Figure 5.1 demonstrates the schematic representation of NNBTSMC.

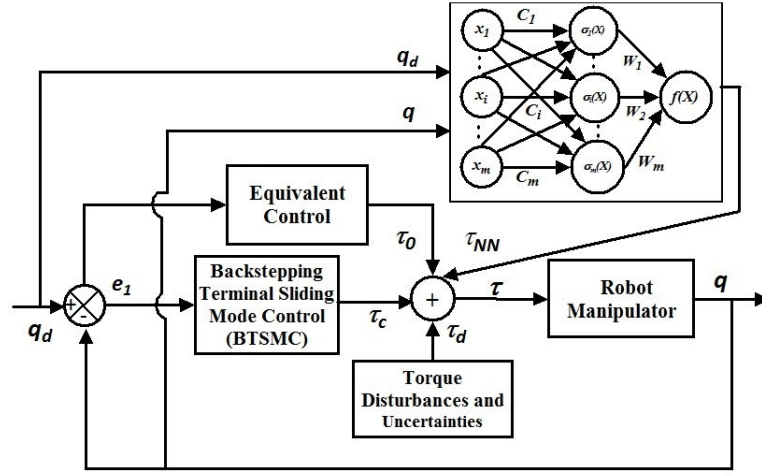


Figure 5.1 : Block diagram of NNTSMC scheme.

Tracking error of position is defined as:

$$e = q_d - q \quad (5.19)$$

$$\dot{q}_r = \dot{q}_d + \frac{1}{\lambda} e^{\frac{\Omega_1}{\Omega_2}} \quad (5.20)$$

where ‘ \dot{q}_r ’ is auxiliary signal. The modified sliding surface (s) is characterized as:

$$s = \dot{q}_r - \dot{q} = \frac{d}{dt} e + \frac{1}{\lambda} e^{\frac{\Omega_1}{\Omega_2}} \quad (5.21)$$

From (1.18), (5.20) and (5.21), we get

$$D(q)\dot{s} = -C(q, \dot{q})s + f(X) + \tau_d - \tau \quad (5.22)$$

where ‘ τ_d ’ represents external torque disturbances.

$$f(X) = D(q)\ddot{q}_r + C(q, \dot{q})\dot{q}_r + F(q, \dot{q}) + G(q) \quad (5.23)$$

where $X = [\ddot{q}_d^T, \dot{q}_d^T, q_d^T, \dot{q}^T, q^T]^T$.

The approximation of $f(X)$ is defined in (5.24).

$$f(X) = \hat{W}^T \sigma(X) \quad (5.24)$$

where ‘ $\sigma(X)$ ’ is the basis function and ‘ \hat{W} ’ is the NN adjustment law. Now (5.22) can be revised as:

$$D(q)\dot{s} = -C(q, \dot{q})s + \tilde{W}^T \sigma(X) + \hat{W}^T \sigma(X) + \varepsilon^* + \tau_d - \tau \quad (5.25)$$

where $\tilde{W} = W^* - \hat{W}$, W^* and ε^* are ideal weights matrix and approximation error respectively.

Theorem 5.3.1. *Consider the robot manipulator is demonstrated by (1.18), if the total control torque is expressed as $\tau = \tau_0 + \tau_c + \tau_{NN}$, in which control law of TSMC is characterized as $\tau_c = k_1 s + K \tanh(\frac{s}{\phi})$ and $\tau_{NN} = \hat{W}^T \sigma(X)$. The evaluated adaptive law for the NN identifier is characterized as:*

$$\dot{\hat{W}}^T = -\dot{\tilde{W}}^T = B \sigma(X) s^T \quad (5.26)$$

where ‘ B ’ is a positive definite matrix and the tracking errors of position and velocity (i.e. e and \dot{e}) of the system asymptotically converge to zero as $t \rightarrow \infty$.

Proof. NNTSMC stability function is given in (5.27).

$$V = \frac{1}{2} s^T D(q) s + \frac{1}{2} \text{tr}(\tilde{W}^T B^{-1} \tilde{W}) \quad (5.27)$$

$$\dot{V} = \frac{1}{2} s^T \dot{D}(q) s + s^T D(q) \dot{s} + \text{tr}(\tilde{W}^T B^{-1} \dot{\tilde{W}}) \quad (5.28)$$

By substituting (5.25) in (5.28), we get

$$\begin{aligned} \dot{V} = & \frac{1}{2} s^T [\dot{D}(q) - 2C(q, \dot{q})] s + s^T [\tilde{W}^T \sigma(X) + \varepsilon^* + \tau_d - k_1 s \\ & - K \tanh(\frac{s}{\phi})] + \text{tr}(\tilde{W}^T B^{-1} \dot{\tilde{W}}) \end{aligned} \quad (5.29)$$

Since, $\dot{D}(q) - 2C(q, \dot{q})$ is a skew symmetric matrix, the first term in (5.29) becomes zero (i.e. $\frac{1}{2} s^T [\dot{D}(q) - 2C(q, \dot{q})] s = 0$), from (5.15) and (5.26), \dot{V} can be rewritten as:

$$\dot{V} \leq -k_1 s^T s + \|s\| \delta_0 \quad (5.30)$$

where ‘ δ_0 ’ is the upper bound of $\|\varepsilon^* + \tau_d\|$. The term $\|s\| \delta_0$ is bounded by $\|s\| \delta_0 \leq \frac{1}{2} (\|s\|^2 + \rho \delta_0^2)$, where $\rho > 0$ is picked to such an extent that $\int_0^\infty \rho dt < \infty$ and further substituted in (5.30) to get stability criteria with finite boundedness.

$$\dot{V} \leq -k_1 \|s\|^2 + \frac{1}{2} (\|s\|^2 + \rho \delta_0^2) \quad (5.31)$$

Integrating both sides of (5.31) from $t = 0$ to T , yields

$$V(T) - V(0) \leq -(k_1 - \frac{1}{2}) \int_0^T \|s\|^2 dt + \frac{1}{2} \delta_0^2 \int_0^T \rho dt, \quad (\forall k_1 > 2) \quad (5.32)$$

Since, $V(T) \geq 0$ and $\int_0^\infty \rho dt < \infty$ holds,

$$\limsup_{T \rightarrow \infty} \frac{1}{T} \int_0^T \|s\|^2 dt \leq \frac{1}{(k_1 - \frac{1}{2})} \left[V(0) + \frac{1}{2} \delta_0^2 \int_0^\infty \rho dt \right] \limsup_{T \rightarrow \infty} \frac{1}{T} = 0 \quad (5.33)$$

From (5.32) and (5.33), we get $s \rightarrow 0$ as $t \rightarrow \infty$. Subsequently, we can conclude, from (5.21), the tracking errors of position and velocity (i.e. e and \dot{e}) asymptotically converge to zero as $t \rightarrow \infty$. Therefore, the stability criteria is fulfilled by the proposed NNTSMC scheme. \square

Remark 5.3.2. *The addition of TSMC and NN identifier provides the robust controller; and such errors caused by extrinsic disturbances and uncertainties. The NN identifier can be remunerated to give better trajectory tracking and intensify the disturbance rejection under different disturbance conditions.*

5.4 AN ADAPTIVE OBSERVER BASED CONTROL OF ROBOT MANIPULATOR

The neural network based adaptive observer terminal sliding mode control (NNAOTSMC) is developed with the help of NNAO for the precise desired trajectory tracking and to improve the disturbance rejection under different working conditions (i.e., external disturbances and uncertainties) of the robot manipulator. Figure 5.2 demonstrates the structure of the NNAOTSMC.

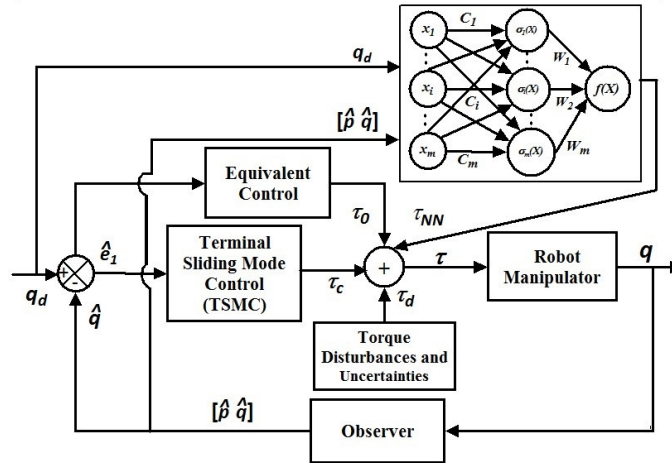


Figure 5.2 : Block diagram of the NNAOTSMC scheme.

The evaluated error of the link position is characterized as:

$$\hat{e} = q_d - \hat{q} \quad (5.34)$$

The estimated sliding surface ‘ \hat{s} ’ is designed as:

$$\hat{s} = \frac{\frac{d}{dt}\hat{e} + \frac{1}{\lambda}\hat{e}^{\Omega_1}}{\phi} \quad (5.35)$$

Theorem 5.4.1. *Considered robot manipulator described by (1.18). Let the NNAO estimates q and p as \hat{q} and \hat{p} , estimation errors are $\tilde{q} = q - \hat{q}$ and $\tilde{p} = p - \hat{p}$. Then, the approximation function of $f(X)$ described in (5.23) is conveyed as:*

$$\hat{f}(\hat{X}) = \hat{W}_c^T \sigma(\hat{X}), \quad \hat{X} = [\ddot{q}_d^T, \dot{q}_d^T, \dot{q}_d^T, \hat{p}^T, \hat{q}^T]^T \quad (5.36)$$

where ‘ \hat{W}_c ’ is estimated adaptation matrix.

The adaptation law is defined as:

$$\dot{\hat{W}}_c = -\dot{\tilde{W}}_c = B_c \sigma(\hat{X}) \hat{s}^T \quad (5.37)$$

The updated control law of NNAOTSMC is characterized as:

$$\tau = \Lambda_3 \hat{s} + K \tanh\left(\frac{\hat{s}}{\phi}\right) + \hat{W}_c^T \sigma(\hat{X}) \quad (5.38)$$

where ‘ $\Lambda_3 \hat{s} + K \tanh(\frac{\hat{s}}{\phi})$ ’ is the boundary sliding mode control law and ‘ $\hat{W}_c^T \sigma(\hat{X})$ ’ is the approximation function to robot manipulator, then the estimation errors \tilde{q} and \tilde{p} are asymptotically converge to zero.

Proof. The Lyapunov stability candidate function for NNAOTSMC is characterized as:

$$V = V_o + V_c \quad (5.39)$$

where ‘ V_o ’ and ‘ V_c ’ are the observer stability and controller stability candidate functions respectively.

$$V_o = \tilde{p}^T \tilde{p} + \frac{1}{2} \text{tr}(\tilde{W}_o^T B_o^{-1} \tilde{W}_o) \quad (5.40)$$

$$V_c = \frac{1}{2} s^T D(q) s + \frac{1}{2} \text{tr}(\tilde{W}_c^T B_c^{-1} \tilde{W}_c) \quad (5.41)$$

The derivative of (5.41) becomes

$$\dot{V}_c = \frac{1}{2} s^T \dot{D}(q) s + s^T D(q) \dot{s} + \text{tr}(\tilde{W}_c^T B_c^{-1} \dot{\tilde{W}}_c) \quad (5.42)$$

Since, $\dot{D}(q) - 2C(q, p)$ is a skew symmetric matrix and $s = \hat{s} + \dot{\tilde{q}} + \Lambda_1 \tilde{q} = \hat{s} + \tilde{p}$, then we get

$$\begin{aligned} \dot{V}_c &= \hat{s}^T \{ \hat{W}_c^T \tilde{\sigma}(\hat{X}) + \varepsilon^* + \tau_d \} + \tilde{p}^T \{ \tilde{W}_c^T \sigma(\hat{X}) + \hat{W}_c^T \tilde{\sigma}(\hat{X}) + \varepsilon^* + \tau_d \} \\ &\quad - \Lambda_3 \hat{s}^T \hat{s} - \Lambda_3 \tilde{p}^T \hat{s} - K \hat{s}^T \tanh\left(\frac{\hat{s}}{\phi}\right) + \text{tr}\{ \tilde{W}_c^T (B_c^{-1} \dot{\tilde{W}}_c + \sigma(\hat{X}) \hat{s}^T) \} \end{aligned} \quad (5.43)$$

where ‘ γ_0 ’ is maximum limit of $\| \hat{W}_c^T \tilde{\sigma}(\hat{X}) + \varepsilon^* + \tau_d \|$ and $\zeta = \{ \tilde{W}_c^T \sigma(\hat{X}) + \hat{W}_c^T \tilde{\sigma}(\hat{X}) + \varepsilon^* + \tau_d \}$, corresponding to this ‘ ζ ’, there exists a positive constant ‘ ζ_0 ’ such that $\| \zeta \| \leq \zeta_0$.

$$\dot{V}_c \leq \| \hat{s} \| \gamma_0 + \| \tilde{p} \| \zeta_0 - \Lambda_3 \hat{s}^T \hat{s} - \Lambda_3 \tilde{p}^T \hat{s} \quad (5.44)$$

The terms $\| \hat{s} \| \gamma_0$, $\| \tilde{p} \| \zeta_0$ and $-\Lambda_3 \tilde{p}^T \hat{s}$ are bounded by $\| \hat{s} \| \gamma_0 \leq \frac{1}{2} (\| \hat{s} \|^2 + \rho \gamma_0^2)$, $\| \tilde{p} \| \zeta_0 \leq \frac{1}{2} (\| \tilde{p} \|^2 + \rho \zeta_0^2)$ and $-\Lambda_3 \tilde{p}^T \hat{s} \leq \frac{\Lambda_3}{2} (\| \tilde{p} \|^2 + \| \hat{s} \|^2)$ respectively. To induce stability criteria with finite boundedness, the constrained terms are substituted in (5.44). The expression for \dot{V}_c gets to be:

$$\dot{V}_c \leq -\left(\frac{\Lambda_3}{2} - \frac{1}{2}\right) \| \hat{s} \|^2 + \left(\frac{\Lambda_3}{2} + \frac{1}{2}\right) \| \tilde{p} \|^2 + \frac{1}{2} \rho (\gamma_0^2 + \zeta_0^2), \quad \forall (\Lambda_3 > 2) \quad (5.45)$$

The derivative of (5.40) and from (4.33), we will get

$$\begin{aligned} \dot{V}_o = & \tilde{p}^T \{W_o^{*T} \tilde{\sigma}_o(q, p) - D^{-1}(q) \tau_d + \varepsilon_o^*\} - \Lambda_3 \tilde{p}^T \tilde{p} + tr\{\tilde{W}_o^T (B_o^{-1} \dot{W}_o \\ & + \sigma_o(\hat{q}, \hat{p}) \tilde{p}^T)\} \end{aligned} \quad (5.46)$$

Since, $\|W_o^{*T} \tilde{\sigma}_o(q, p) - D^{-1}(q) \tau_d + \varepsilon_o^*\| \leq \beta_0$ and $\|\tilde{p}\| \beta_0$ is bounded by $\|\tilde{p}\| \beta_0 \leq \frac{1}{2}(\|\tilde{p}\|^2 + \rho \beta_0^2)$, then

$$\dot{V}_o \leq -\Lambda_3 \tilde{p}^T \tilde{p} + \frac{1}{2}(\|\tilde{p}\|^2 + \rho \beta_0^2) \quad (5.47)$$

$$\dot{V} = \dot{V}_o + \dot{V}_c \quad (5.48)$$

$$\begin{aligned} \dot{V} \leq & -\frac{1}{2}(\Lambda_3 - 2)\|\tilde{p}\|^2 - \frac{1}{2}(\Lambda_3 - 1)\|\hat{s}\|^2 + \frac{1}{2}\rho(\gamma_0^2 + \zeta_0^2 \\ & + \beta_0^2), \quad \forall (\Lambda_3 > 2) \end{aligned} \quad (5.49)$$

Integrating both sides from $t = 0$ to T , yields

$$\begin{aligned} V(T) - V(0) \leq & -\frac{1}{2}(\Lambda_3 - 1) \int_0^T \|\hat{s}\|^2 dt - \frac{1}{2}(\Lambda_3 - 2) \int_0^T \|\tilde{p}\|^2 dt \\ & + \frac{1}{2}(\gamma_0^2 + \zeta_0^2 + \beta_0^2) \int_0^T \rho dt \end{aligned} \quad (5.50)$$

Since, $V(T) \geq 0$ and $\int_0^\infty \rho dt < \infty$ holds,

$$\begin{aligned} \limsup_{T \rightarrow \infty} \frac{1}{T} \left[(\Lambda_3 - 1) \int_0^T \|\hat{s}\|^2 dt + (\Lambda_3 - 2) \int_0^T \|\tilde{p}\|^2 dt \right] & \leq 2 \left[V(0) \right. \\ & \left. + \frac{1}{2}(\gamma_0^2 + \zeta_0^2 + \beta_0^2) \int_0^\infty \rho dt \right] \limsup_{T \rightarrow \infty} \frac{1}{T} = 0 \end{aligned} \quad (5.51)$$

From (5.50) and (5.51), it is clear that $\tilde{p} \rightarrow 0$, $\hat{s} \rightarrow 0$ as $t \rightarrow \infty$. That concludes $\tilde{q} \rightarrow 0$ and $\tilde{p} \rightarrow 0$. Thus, the proposed NNAOTSMC fulfills the stability criteria. \square

5.5 RESULTS AND DISCUSSIONS FOR TSMC

The desired reference trajectories for de-icing robot manipulator and essential parameters that influence the control activity of the robotic systems (i.e., uncertainties and external disturbances) are considered according to literature (Tran et al., 2015). The physical parameters of the OTDIRM are listed in Table 4.8.1. TSMC parameters are $\lambda = 200$, $\Omega_1=5$, $\Omega_2=3$, $K_{w1} = 440$, $K_{w2} = 440$, $K_{w3} = 440$ and $\phi = 0.1$. The finite times for proposed method (i.e., NNAOTSMC) are calculated as 0.0621 sec, 0.0642 sec and 0.0639 sec for link 1, link 2, and link 3 respectively. The simulated responses of the OTDIRM are compared with those presented in (Tran et al., 2015) are shown in Figures from 5.3 to 5.14.

Output performance : To evaluate output performance, the MSE of tracking positions

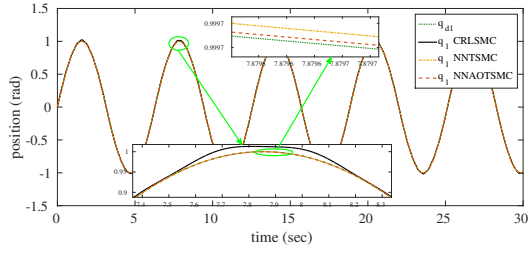


Figure 5.3 : Position tracking of link 1.

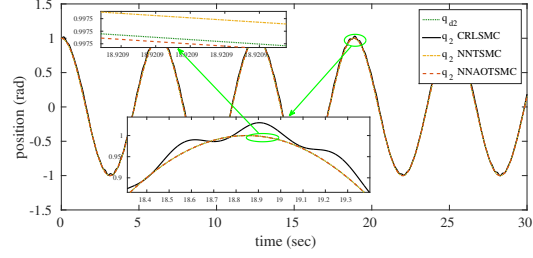


Figure 5.4 : Position tracking of link 2.

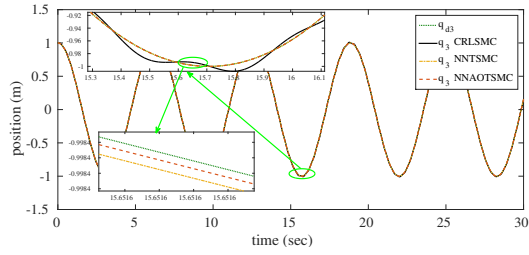


Figure 5.5 : Position tracking of link 3.

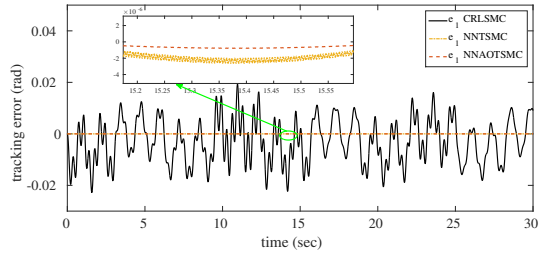


Figure 5.6 : Tracking error of link 1.

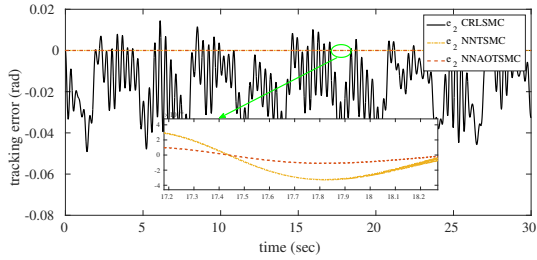


Figure 5.7 : Tracking error of link 2.

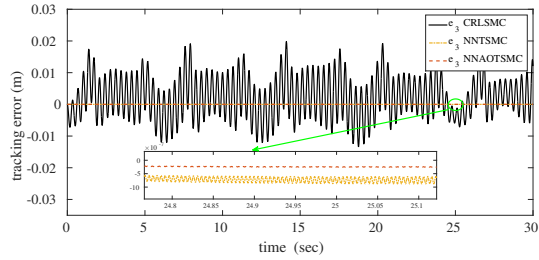


Figure 5.8 : Tracking error of link 3.

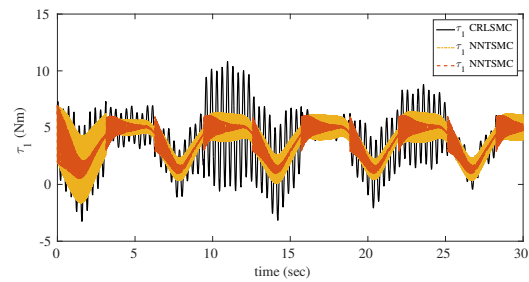


Figure 5.9 : Control input for link 1.

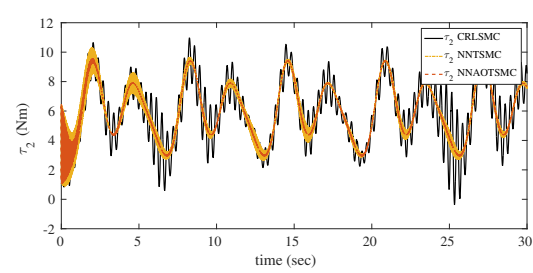


Figure 5.10 : Control input for link 2.

are computed. The total sampling time is ' T ', desired trajectory is ' q_{di} ' and estimated trajectory is ' \hat{q}_i ' of the i^{th} link, tracking position mean square error (MSE) is given in (5.52).

$$MSE_i = \frac{1}{T} \sum_{t=1}^T [q_{di} - \hat{q}_i]^2, \quad i = 1, 2, 3 \quad (5.52)$$

The MSE values of the 3-DOF OTDIRM trajectories under different control method-

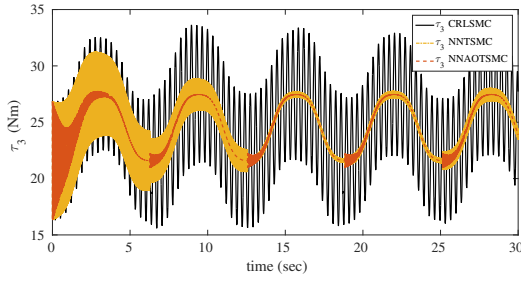


Figure 5.11 : Control input for link 3.

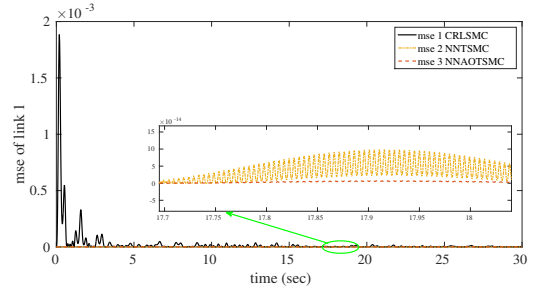


Figure 5.12 : MSE of link 1.

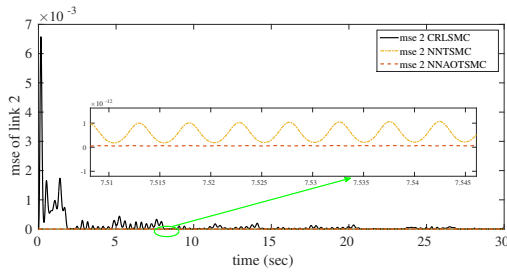


Figure 5.13 : MSE of link 2.

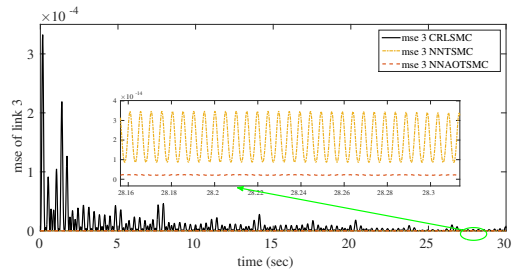


Figure 5.14 : MSE of link 3.

Table 5.5.1 : MSE examination of CRLSMC (Tran et al., 2015), NNTSMC and NNAOTSMC

Sl. No	MSE	CRLSMC	NNTSMC	NNAOTSMC
1	link 1	2.732×10^{-6}	9.465×10^{-15}	1.723×10^{-14}
2	link 2	3.526×10^{-5}	4.649×10^{-18}	1.526×10^{-18}
3	link 3	4.864×10^{-6}	2.136×10^{-16}	2.924×10^{-18}

ologies, such as CRLSMC in (Tran et al., 2015), NNTSMC and NNAOTSMC are presented in Table 5.5.1. From the table, it is ascertained that NNAOTSMC provides least MSE values in comparison with other methods (i.e., NNAOTSMC system has better tracking trajectory performance). Figure 5.3 to Figure 5.5 indicate tracking positions, Figure 5.6 to Figure 5.8 indicate tracking errors and Figure 5.9 to Figure 5.11 show control torque. From the Figure 5.9 to Figure 5.11, it is clear that the control torque is smoother for NNAOTSMC compared with existing CRLSMC (Tran et al., 2015). This indicates that the proposed method requires less control effort for same trajectory tracking. The MSE response plots of the OTDIRM link trajectories exhibited from Figure 5.12 to Figure 5.14.

Input performance : In order to evaluate the manipulated input usage, we calculated

TV (Mondal and Mahanta, 2014) of the input $u(t)$ is calculated as

$$TV = \sum_{j=1}^{\infty} \|u_{j+1} - u_j\| \quad (5.53)$$

This should be as small as possible. The total variation is a good measure of the signal "smoothness". A large value of TV means excessive input usage or more complex controllers (Mondal and Mahanta, 2014). The energy of the input signal is calculated

Table 5.5.2 : Total variance examination of CRLSMC (Tran et al., 2015), NNTSMC and NNAOTSMC

Sl. No	Total Variance (TV)	CRLSMC	NNTSMC	NNAOTSMC
1	link 1	6.1354	2.6311	2.0468
2	link 2	4.8902	3.6610	3.5803
3	link 3	20.8775	6.9904	5.3970

by using the 2-Norm method. The control energy is expected to be as small as possible. The output and input performances are calculated for the period from 0 to 30 sec with a sampling time of 0.0001 sec. From Table 5.5.2 and 5.5.3, it clear that the values of

Table 5.5.3 : 2-Norm of input examination of CRLSMC (Tran et al., 2015), NNTSMC and NNAOTSMC

Sl. No	2-Norm of Input	CRLSMC	NNTSMC	NNAOTSMC
1	link 1	2.4778×10^3	2.2653×10^3	2.2263×10^3
2	link 2	3.4905×10^3	3.4582×10^3	3.4547×10^3
3	link 3	1.3727×10^4	1.3570×10^4	1.3552×10^4

TV and 2-Norm of input for proposed methods are very small as compared to existing method CRLSMC (Tran et al., 2015). Figure 5.15, Figure 5.16 and Figure 5.17 show the box plot of control torque for link 1, link 2 and link 3 with the mean, median, $\pm 25\%$ quartiles (notch boundaries), $\pm 75\%$ quartiles (box ends), $\pm 95\%$ bounds and the outliers. From the size of the boxes shown, it is clear that the NNAOTSMC control strategy experiences minimum variation than others. Comparing the box plot of NNTSMC and NNAOTSMC, it observed that NNAOTSMC has less variation in control input torque for link 1, link 2 and link 3 of the OTDIRM.

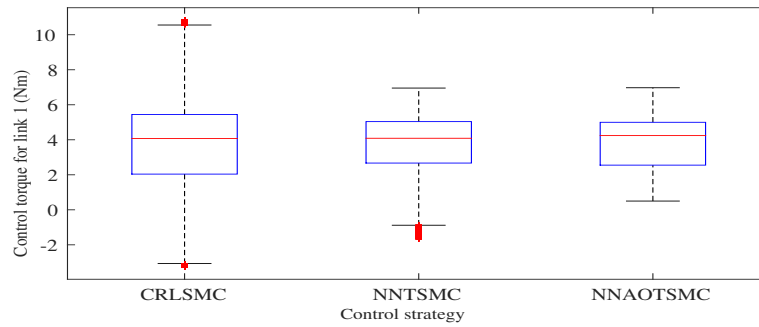


Figure 5.15 : Box plot representation of control torque for link 1.

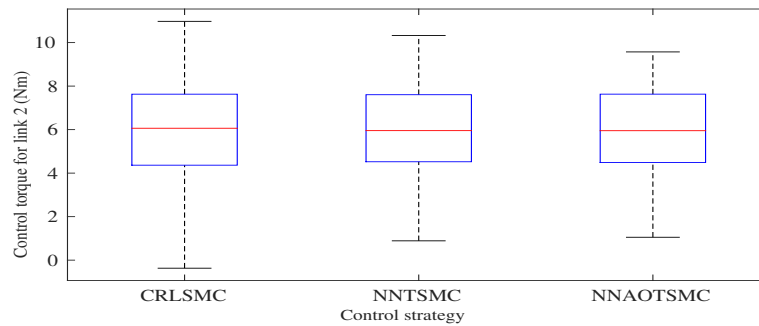


Figure 5.16 : Box plot representation of control torque for link 2.

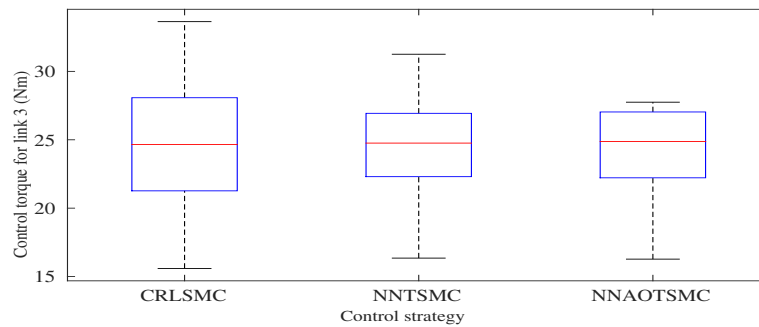


Figure 5.17 : Box plot representation of control torque for link 3.

5.6 DESIGN AND STABILITY OF BTSMC

The backstepping methodology is a nonlinear scheme generally utilized as a part of controller design. The mathematical model of the robot manipulator is expressed in (5.54), (5.55) and (5.56) as:

$$\dot{x}_1 = x_2 \tag{5.54}$$

$$\dot{x}_2 = \ddot{q} = D^{-1}(q)[\tau - (C(q, \dot{q})\dot{q} + G(q) + F(q, \dot{q}) + \tau_d)] \quad (5.55)$$

$$y = x_1 \quad (5.56)$$

where x_1 and x_2 are the position and velocity vectors of the robot manipulator. The tracking error of the position is given as:

$$e_1 = q_d - q \quad (5.57)$$

The stabilizing function is characterized as

$$\alpha_1 = \lambda_1 e_1 + \frac{1}{\lambda_2} e_1^{\frac{\Omega_1}{\Omega_2}} \quad (5.58)$$

where λ_1 , λ_2 and Ω_1 , Ω_2 ($1 < \frac{\Omega_1}{\Omega_2} < 2$) are positive odd numbers. The tracking error of the velocity has upgraded with stability function. It is characterized in Eq. (5.59) and appeared as:

$$e_2 = \dot{e}_1 + \alpha_1 \quad (5.59)$$

The primary Lyapunov stability function is characterized as:

$$V_1 = \frac{1}{2} e_1^2 \quad (5.60)$$

$$\dot{V}_1 = e_1 e_2 - \lambda_1 e_1^2 - \frac{1}{\lambda_2} e_1^{\left(\frac{\Omega_1 + \Omega_2}{\Omega_2}\right)} \quad (5.61)$$

From (1.2) and (5.59), we get

$$\begin{aligned} \dot{e}_2 = & \ddot{q}_d - D^{-1}(q)(\tau - (C(q, \dot{q})\dot{q} + G(q) + F(q, \dot{q}) + \tau_d)) + \lambda_1 \dot{e}_1 \\ & + \frac{\Omega_1}{\lambda_2 \Omega_2} e_1^{\left(\frac{\Omega_1 - \Omega_2}{\Omega_2}\right)} \dot{e}_1 \end{aligned} \quad (5.62)$$

The second Lyapunov stability function is described as:

$$V = V_1 + \frac{1}{2} s^T s \quad (5.63)$$

The satisfactory condition, which gives the affirmation that the tracking error will make an elucidation from achieving stage to sliding stage, is called the achieving condition and given in (5.64).

$$\dot{V} < 0, s \neq 0 \quad (5.64)$$

The sliding surface 's' is characterized as:

$$s = e_1 + e_2 \quad (5.65)$$

The derivative of the second Lyapunov stability function is given in equation (5.66).

$$\dot{V} = e_1 e_2 - \lambda_1 e_1^2 - \frac{1}{\lambda_2} e_1^{\left(\frac{\Omega_1 + \Omega_2}{\Omega_2}\right)} + s^T (\dot{e}_1 (1 + \lambda_1) + \frac{\Omega_1}{\lambda_2 \Omega_2} e_1^{\left(\frac{\Omega_1 - \Omega_2}{\Omega_2}\right)} \dot{e}_1 + \ddot{q}_d - \ddot{q}) \quad (5.66)$$

The total control torque (τ) to the robot manipulator is characterized as:

$$\tau = \tau_0 + \tau_c \quad (5.67)$$

By substituting (5.67) in (5.66), we get

$$\begin{aligned} \dot{V} = & e_1 e_2 - \lambda_1 e_1^2 - \frac{1}{\lambda_2} e_1^{\left(\frac{\Omega_1 + \Omega_2}{\Omega_2}\right)} + s^T \left[\dot{e}_1 (1 + \lambda_1) + \frac{\Omega_1}{\lambda_2 \Omega_2} e_1^{\left(\frac{\Omega_1 - \Omega_2}{\Omega_2}\right)} \dot{e}_1 \right. \\ & \left. + \ddot{q}_d - D^{-1}(q) ((\tau_0 + \tau_c) - (C(q, \dot{q})\dot{q} + G(q) + F(q, \dot{q}) + \tau_d)) \right] \end{aligned} \quad (5.68)$$

The arrangement of $\dot{s} = 0$ gives the control signal, which is known as equivalent control law and it is denoted by ' τ_0 '. This equivalent control law is essential to fulfill the execution of favored trajectory tracking without considering disturbances and uncertainties (i.e. $\tau_d = 0$).

$$\tau_0 = D(q) \left(\dot{e}_1 (1 + \lambda_1) + \frac{\Omega_1}{\lambda_2 \Omega_2} e_1^{\left(\frac{\Omega_1 - \Omega_2}{\Omega_2}\right)} \dot{e}_1 + \ddot{q}_d \right) + C(q, \dot{q})\dot{q} + G(q) + F(q, \dot{q}) \quad (5.69)$$

An extra control exertion is needed to wipe out the unpredictable disturbances and uncertainties as equivalent control torque (τ_0) is lacking to provide the favored tracking performance. Ultimately, the tracking error dies out asymptotically, which means the sliding surface becomes stable. To exhibit the stability of the created control framework for robot manipulator, the Lyapunov-like Lemma is utilized.

From (5.68) and (5.69) we arrive at an expression for \dot{V} as follows:

$$\dot{V} = e_1 e_2 - \lambda_1 e_1^2 - \frac{1}{\lambda_2} e_1^{\left(\frac{\Omega_1 + \Omega_2}{\Omega_2}\right)} + s^T (-D^{-1}(q) \tau_c) \quad (5.70)$$

To meet the Lyapunov stability condition, the corrective control law (τ_c) is defined as

$$\tau_c = D(q) \left(\frac{1}{s^T} (e_1 e_2 - \frac{1}{\lambda_2} e_1^{\left(\frac{\Omega_1 + \Omega_2}{\Omega_2}\right)}) + K_w \text{sign}(s) \right) \quad (5.71)$$

By substituting τ_c in (5.70) and yields:

$$\dot{V} = -\lambda_1 e_1^2 - K_w s^T \text{sign}(s) \quad (5.72)$$

where K_w is the sliding gain.

$$\dot{V} \leq -\lambda_1 |e_1^2| - K_w |s| \quad (5.73)$$

where $|s| = s^T \text{sign}(s)$. The chattering effect on the control input signal is introduced by the signum function ('sign'), which is utilized as a part of (5.72), so as to diminish or dispense with this impact, the signum function ('sign') is substituted by the hyperbolic tangent function ('tanh') as given in (5.74).

$$\dot{V} \leq -\lambda_1 e_1^2 - K_w s^T \tanh(s) \quad (5.74)$$

The term ' $s^T \tanh(s)$ ' in (5.74) is constantly positive so that whole condition gets to be negative (i.e. $s^T \tanh(s) > 0$ if either $s > 0$ or $s < 0$). The achieving control signal (τ_c) is modified as:

$$\tau_c = D(q) \left(\frac{1}{s^T} (e_1 e_2 - \frac{1}{\lambda_2} e_1^{\left(\frac{\Omega_1 + \Omega_2}{\Omega_2}\right)}) + K_w \tanh(s) \right) \quad (5.75)$$

Where $K_w = \text{diag}\{K_{w1}, K_{w2}, \dots, K_{wn}\}$ is control gain matrix.

The BTSMC control law is defined as:

$$\tau_c = D(q) \left(\frac{1}{s^T} (e_1 e_2 - \frac{1}{\lambda_2} e_1^{\left(\frac{\Omega_1 + \Omega_2}{\Omega_2}\right)}) \right) + K \tanh\left(\frac{s}{\phi}\right) \quad (5.76)$$

where $K = D(q)K_w$.

When $s = 0$ is reached at $t = t_r$, $e_1 = 0$ becomes terminal surface, i.e. $e_1 + e_2 = 0$. The effect of terminal surface will take the state of e_1 from $e_1(t_r) \neq 0$ to $e_1(t_r + t_s) = 0$ with finite time t_s given by

$$t_s = \frac{1}{(1 + \lambda_1) \left(\frac{\Omega_1}{\Omega_2} - 1\right)} \left(\ln((1 + \lambda_1)e_1 + \frac{1}{\lambda_2} e_1^{\frac{\Omega_1}{\Omega_2}}) - \frac{\Omega_1}{\Omega_2} \ln(e_1) \right) \quad (5.77)$$

5.7 DESIGN OF NNBTSMC

In this section, the RBFNN is utilized to build up the control plans for the robot manipulator to track the desired trajectories under unknown dynamics of the system. Figure 5.18 demonstrates the schematic representation of NNBTSMC.

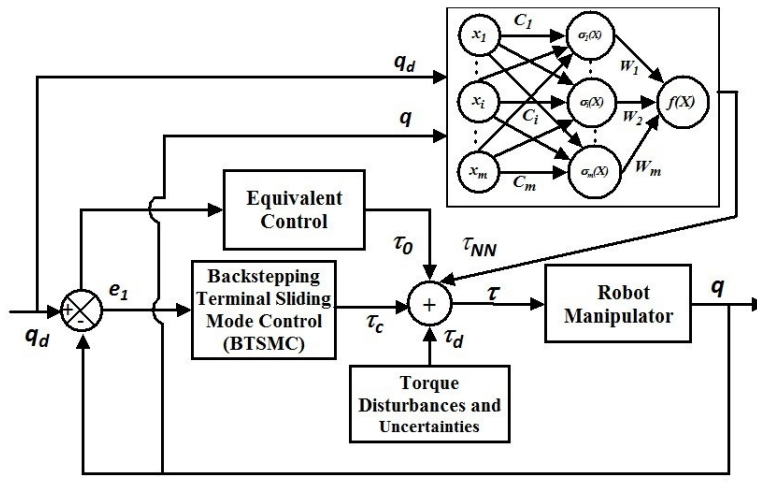


Figure 5.18 : Block diagram of NNBTSMC scheme.

Tracking error of position is defined as:

$$e_1 = q_d - q \quad (5.78)$$

$$\dot{q}_r = \dot{q}_d + (1 + \lambda_1)e_1 + \frac{1}{\lambda_2} e_1^{\frac{\Omega_1}{\Omega_2}} \quad (5.79)$$

where ‘ \dot{q}_r ’ is auxiliary signal. The modified sliding surface (s) is characterized as:

$$s = \dot{q}_r - \dot{q} = (1 + \lambda_1)e_1 + \frac{1}{\lambda_2} e_1^{\frac{\Omega_1}{\Omega_2}} + \frac{d}{dt} e_1 \quad (5.80)$$

From (1.18), (5.79) and (5.80), we get

$$D(q)\dot{s} = -C(q, \dot{q})s + f(X) + \tau_d - \tau \quad (5.81)$$

where ‘ τ_d ’ represents external torque disturbances.

$$f(X) = D(q)\ddot{q}_r + C(q, \dot{q})\dot{q}_r + F(q, \dot{q}) + G(q) \quad (5.82)$$

where $X = [\ddot{q}_d^T, \dot{q}_d^T, q_d^T, \dot{q}^T, q^T]^T$.

The approximation of $f(X)$ is defined in (5.83).

$$f(X) = \hat{W}^T \sigma(X) \quad (5.83)$$

where ‘ $\sigma(X)$ ’ is the basis function and ‘ \hat{W} ’ is the NN adjustment law. Now (5.81) can be revised as:

$$D(q)\dot{s} = -C(q, \dot{q})s + \tilde{W}^T \sigma(X) + \hat{W}^T \sigma(X) + \varepsilon^* + \tau_d - \tau \quad (5.84)$$

where $\tilde{W} = W^* - \hat{W}$, W^* and ε^* are ideal weights matrix and approximation error respectively.

Theorem 5.7.1. Consider the robot manipulator is demonstrated by (1.18), if the total control torque is expressed as $\tau = \tau_0 + \tau_c + \tau_{NN}$, in which control law of BTSMC is characterized as $\tau_c = k_1 s + K \tanh(\frac{s}{\phi})$ and $\tau_{NN} = \hat{W}^T \sigma(X)$. The evaluated adaptive law for the NN identifier is characterized as:

$$\dot{\hat{W}}^T = -\dot{\tilde{W}}^T = B \sigma(X) s^T \quad (5.85)$$

where ‘ B ’ is a positive definite matrix and the tracking errors of position and velocity (i.e. e and \dot{e}) of the system asymptotically converge to zero as $t \rightarrow \infty$.

Proof. NNBTSMC stability function is given in (5.86).

$$V = \frac{1}{2} s^T D(q) s + \frac{1}{2} \text{tr}(\tilde{W}^T B^{-1} \tilde{W}) \quad (5.86)$$

$$\dot{V} = \frac{1}{2} s^T \dot{D}(q) s + s^T D(q) \dot{s} + \text{tr}(\tilde{W}^T B^{-1} \dot{\tilde{W}}) \quad (5.87)$$

By substituting (5.84) in (5.87), we get

$$\begin{aligned} \dot{V} = & \frac{1}{2} s^T [\dot{D}(q) - 2C(q, \dot{q})] s + s^T [\tilde{W}^T \sigma(X) + \varepsilon^* + \tau_d - k_1 s \\ & - K \tanh(\frac{s}{\phi})] + \text{tr}(\tilde{W}^T B^{-1} \dot{\tilde{W}}) \end{aligned} \quad (5.88)$$

Since, $\dot{D}(q) - 2C(q, \dot{q})$ is a skew symmetric matrix, the first term in (5.88) becomes zero

(i.e. $\frac{1}{2}s^T [\dot{D}(q) - 2C(q, \dot{q})]s = 0$), from (5.74) and (5.85), \dot{V} can be rewritten as:

$$\dot{V} \leq -k_1 s^T s + \|s\| \delta_0 \quad (5.89)$$

where ‘ δ_0 ’ is the upper bound of $\|\varepsilon^* + \tau_d\|$. The term $\|s\| \delta_0$ is bounded by $\|s\| \delta_0 \leq \frac{1}{2}(\|s\|^2 + \rho \delta_0^2)$, where $\rho > 0$ is picked to such an extent that $\int_0^\infty \rho dt < \infty$ and further substituted in (5.89) to get stability criteria with finite boundedness.

$$\dot{V} \leq -k_1 \|s\|^2 + \frac{1}{2}(\|s\|^2 + \rho \delta_0^2) \quad (5.90)$$

Integrating both sides of (5.90) from $t = 0$ to T , yields

$$V(T) - V(0) \leq -(k_1 - \frac{1}{2}) \int_0^T \|s\|^2 dt + \frac{1}{2} \delta_0^2 \int_0^T \rho dt, \quad (\forall k_1 > 2) \quad (5.91)$$

Since, $V(T) \geq 0$ and $\int_0^\infty \rho dt < \infty$ holds,

$$\limsup_{T \rightarrow \infty} \frac{1}{T} \int_0^T \|s\|^2 dt \leq \frac{1}{(k_1 - \frac{1}{2})} \left[V(0) + \frac{1}{2} \delta_0^2 \int_0^\infty \rho dt \right] \limsup_{T \rightarrow \infty} \frac{1}{T} = 0 \quad (5.92)$$

From (5.91) and (5.92), we get $s \rightarrow 0$ as $t \rightarrow \infty$. Subsequently, we can conclude, from (5.80), the tracking errors of position and velocity (i.e. e and \dot{e}) asymptotically converge to zero as $t \rightarrow \infty$. Therefore, the stability criteria is fulfilled by the proposed NNBTSMC scheme. \square

Remark 5.7.2. *The addition of BTSMC and NN identifier provides the robust controller, and such errors caused by extrinsic disturbances and uncertainties. The NN identifier can be remunerated to give better trajectory tracking and intensify the disturbance rejection under different disturbance conditions.*

5.8 AN ADAPTIVE OBSERVER BASED CONTROL OF ROBOT MANIPULATOR

The neural network based adaptive observer backstepping terminal sliding mode control (NNAOBTSMC) is developed with the help of NNAO for precise desired trajectory tracking and improve the disturbance rejection under different working conditions (i.e. external disturbances and uncertainties) of the robot manipulator. Figure 5.19 demonstrates the structure of the NNAOBTSMC. The evaluated error of the link position is characterized as:

$$\hat{e}_1 = q_d - \hat{q} \quad (5.93)$$

The estimated sliding surface ‘ \hat{s} ’ is designed as:

$$\hat{s} = \frac{(1 + \lambda_1) \hat{e}_1 + \frac{1}{\lambda_2} \hat{e}_1^{\frac{\Omega_1}{2}} + \frac{d}{dt} \hat{e}_1}{\phi} \quad (5.94)$$

Theorem 5.8.1. *Considered robot manipulator described by (1.18). Let the NNAO estimates q and p as \hat{q} and \hat{p} , estimation errors are $\tilde{q} = q - \hat{q}$ and $\tilde{p} = p - \hat{p}$. Then, the approximation function of $f(X)$ described in (5.82) is conveyed as:*

$$\hat{f}(\hat{X}) = \hat{W}_c^T \sigma(\hat{X}), \quad \hat{X} = [\ddot{q}_d^T, \dot{q}_d^T, \dot{q}_d^T, \hat{p}^T, \hat{q}^T]^T \quad (5.95)$$

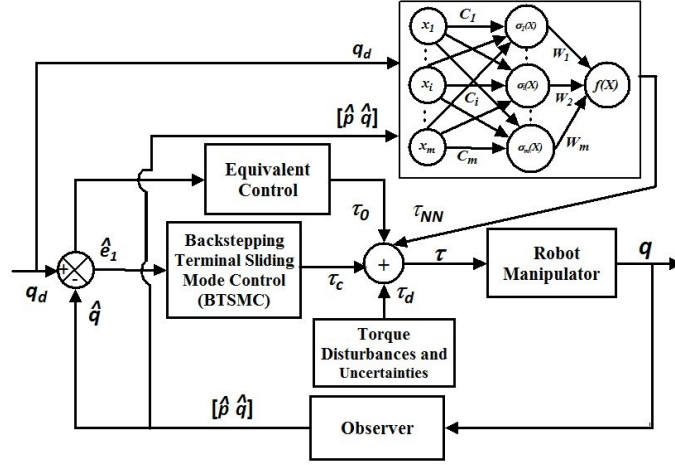


Figure 5.19 : Block diagram of the NNAOBTSMC scheme.

where ' \hat{W}_c ' is estimated adaptation matrix.
The adaptation law is defined as:

$$\dot{\hat{W}}_c = -\dot{\tilde{W}}_c = B_c \sigma(\hat{X}) s^T \quad (5.96)$$

The NNAOBTSMC law is characterized as:

$$\tau = \Lambda_3 \hat{s} + K \tanh\left(\frac{\hat{s}}{\phi}\right) + \hat{W}_c^T \sigma(\hat{X}) \quad (5.97)$$

where ' $\Lambda_3 \hat{s} + K \tanh(\frac{\hat{s}}{\phi})$ ' is the boundary sliding mode control law and ' $\hat{W}_c^T \sigma(\hat{X})$ ' is the approximation function to robot manipulator, then the estimation errors \tilde{q} and \tilde{p} are asymptotically converge to zero.

Proof. The Lyapunov stability candidate function for NNAOBTSMC is characterized as:

$$V = V_o + V_c \quad (5.98)$$

where ' V_o ' and ' V_c ' are the observer stability and controller stability candidate functions respectively.

$$V_o = \tilde{p}^T \tilde{p} + \frac{1}{2} \text{tr}(\tilde{W}_o^T B_o^{-1} \tilde{W}_o) \quad (5.99)$$

$$V_c = \frac{1}{2} s^T D(q) s + \frac{1}{2} \text{tr}(\tilde{W}_c^T B_c^{-1} \tilde{W}_c) \quad (5.100)$$

The derivative of (5.100) becomes

$$\dot{V}_c = \frac{1}{2} s^T \dot{D}(q) s + s^T D(q) \dot{s} + \text{tr}(\tilde{W}_c^T B_c^{-1} \dot{\tilde{W}}_c) \quad (5.101)$$

Since, $\dot{D}(q) - 2C(q, p)$ is a skew symmetric matrix and $s = \hat{s} + \tilde{q} + \Lambda_1 \tilde{q} = \hat{s} + \tilde{p}$, then we get

$$\begin{aligned} \dot{V}_c = & \hat{s}^T \{ \hat{W}_c^T \tilde{\sigma}(\hat{X}) + \varepsilon^* + \tau_d \} + \tilde{p}^T \{ \tilde{W}_c^T \sigma(\hat{X}) + \hat{W}_c^T \tilde{\sigma}(\hat{X}) + \varepsilon^* - \tau_d \} \\ & - \Lambda_3 \hat{s}^T \hat{s} - \Lambda_3 \tilde{p}^T \hat{s} - K \hat{s}^T \tanh\left(\frac{\hat{s}}{\phi}\right) + \text{tr}\{ \tilde{W}_c^T (B_c^{-1} \dot{\tilde{W}}_c + \sigma(\hat{X}) \hat{s}^T) \} \end{aligned} \quad (5.102)$$

where ' γ_0 ' is maximum limit of $\| \hat{W}_c^T \tilde{\sigma}(\hat{X}) + \varepsilon^* + \tau_d \|$ and $\zeta = \{ \tilde{W}_c^T \sigma(\hat{X}) + \hat{W}_c^T \tilde{\sigma}(\hat{X}) + \varepsilon^* + \tau_d \}$, corresponding to this ' ζ ', there exists a positive constant ' ζ_0 ' such that $\| \zeta \| \leq \zeta_0$.

$$\dot{V}_c \leq \| \hat{s} \| \gamma_0 + \| \tilde{p} \| \zeta_0 - \Lambda_3 \hat{s}^T \hat{s} - \Lambda_3 \tilde{p}^T \hat{s} \quad (5.103)$$

The terms $\|\hat{s}\|\gamma_0$, $\|\tilde{p}\|\zeta_0$ and $-\Lambda_3\tilde{p}^T\hat{s}$ are bounded by $\|\hat{s}\|\gamma_0 \leq \frac{1}{2}(\|\hat{s}\|^2 + \rho\gamma_0^2)$, $\|\tilde{p}\|\zeta_0 \leq \frac{1}{2}(\|\tilde{p}\|^2 + \rho\zeta_0^2)$ and $-\Lambda_3\tilde{p}^T\hat{s} \leq \frac{\Lambda_3}{2}(\|\tilde{p}\|^2 + \|\hat{s}\|^2)$ respectively. To induce stability criteria with finite boundedness, the constrained terms are substituted in (5.103). The expression for \dot{V}_c gets to be:

$$\dot{V}_c \leq -\left(\frac{\Lambda_3}{2} - \frac{1}{2}\right)\|\hat{s}\|^2 + \left(\frac{\Lambda_3}{2} + \frac{1}{2}\right)\|\tilde{p}\|^2 + \frac{1}{2}\rho(\gamma_0^2 + \zeta_0^2), \quad \forall (\Lambda_3 > 2) \quad (5.104)$$

The derivative of (5.99) and from (4.33), we will get

$$\begin{aligned} \dot{V}_o &= \tilde{p}^T \{W_o^{*T} \tilde{\sigma}_o(q, p) - D^{-1}(q)\tau_d + \varepsilon_o^*\} - \Lambda_3\tilde{p}^T\tilde{p} + tr\{\tilde{W}_o^T (B_o^{-1}\dot{W}_o \\ &\quad + \sigma_o(\hat{q}, \hat{p})\tilde{p}^T)\} \end{aligned} \quad (5.105)$$

Since, $\|W_o^{*T} \tilde{\sigma}_o(q, p) - D^{-1}(q)\tau_d + \varepsilon_o^*\| \leq \beta_0$ and $\|\tilde{p}\|\beta_0$ is bounded by $\|\tilde{p}\|\beta_0 \leq \frac{1}{2}(\|\tilde{p}\|^2 + \rho\beta_0^2)$, then

$$\dot{V}_o \leq -\Lambda_3\tilde{p}^T\tilde{p} + \frac{1}{2}(\|\tilde{p}\|^2 + \rho\beta_0^2) \quad (5.106)$$

$$\dot{V} = \dot{V}_o + \dot{V}_c \quad (5.107)$$

$$\begin{aligned} \dot{V} &\leq -\frac{1}{2}(\Lambda_3 - 2)\|\tilde{p}\|^2 - \frac{1}{2}(\Lambda_3 - 1)\|\hat{s}\|^2 + \frac{1}{2}\rho(\gamma_0^2 + \zeta_0^2 \\ &\quad + \beta_0^2), \quad \forall (\Lambda_3 > 2) \end{aligned} \quad (5.108)$$

Integrating both sides from $t = 0$ to T , yields

$$\begin{aligned} V(T) - V(0) &\leq -\frac{1}{2}(\Lambda_3 - 1) \int_0^T \|\hat{s}\|^2 dt - \frac{1}{2}(\Lambda_3 - 2) \int_0^T \|\tilde{p}\|^2 dt \\ &\quad + \frac{1}{2}(\gamma_0^2 + \zeta_0^2 + \beta_0^2) \int_0^T \rho dt \end{aligned} \quad (5.109)$$

Since, $V(T) \geq 0$ and $\int_0^\infty \rho dt < \infty$ holds,

$$\begin{aligned} \limsup_{T \rightarrow \infty} \frac{1}{T} \left[(\Lambda_3 - 1) \int_0^T \|\hat{s}\|^2 dt + (\Lambda_3 - 2) \int_0^T \|\tilde{p}\|^2 dt \right] &\leq 2 \left[V(0) \right. \\ &\quad \left. + \frac{1}{2}(\gamma_0^2 + \zeta_0^2 + \beta_0^2) \int_0^\infty \rho dt \right] \limsup_{T \rightarrow \infty} \frac{1}{T} = 0 \end{aligned} \quad (5.110)$$

From (5.109) and (5.110), it is clear that $\tilde{p} \rightarrow 0$, $\hat{s} \rightarrow 0$ as $t \rightarrow \infty$. That concludes $\tilde{q} \rightarrow 0$ and $\tilde{p} \rightarrow 0$. Thus, the proposed NNAOBTSMC fulfills the stability criteria. \square

5.9 RESULTS AND DISCUSSIONS FOR BTSMC

The desired reference trajectories for de-icing robot manipulator and essential parameters that influence the control activity of the robotic systems (i.e., uncertainties and external disturbances) are considered according to literature (Tran et al., 2015). The physical parameters of the OTDIRM are listed in Table 4.8.1. BTSMC parameters are $\lambda_1 = 980$, $\lambda_2 = 100$, $\Omega_1=5$, $\Omega_2=3$, $K_{w1} = 440$, $K_{w2} = 440$, $K_{w3} = 440$ and $\phi = 0.1$. The finite times (t_s) for proposed method (i.e., NNAOBTSMC) are calculated as 0.0422 sec,

0.0405 sec and 0.0438 sec for link 1, link 2 and link 3 respectively. The simulated responses of the OTDIRM are compared with those presented in (Tran et al., 2015) are shown in figures from 5.20 to 5.31.

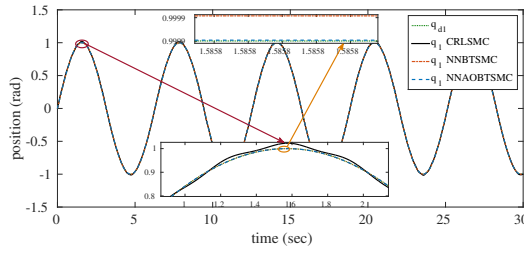


Figure 5.20 : Position tracking of link 1.

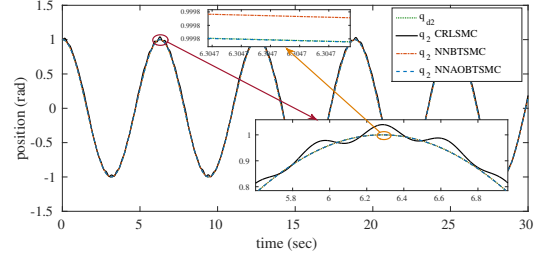


Figure 5.21 : Position tracking of link 2.

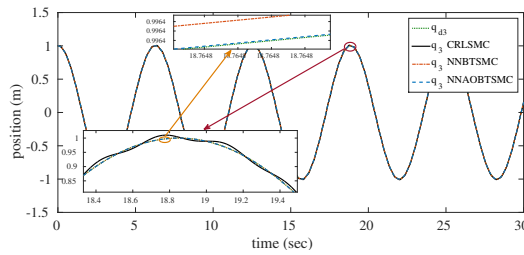


Figure 5.22 : Position tracking of link 3.

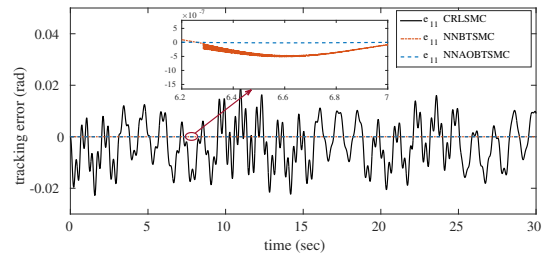


Figure 5.23 : Tracking error of link 1.

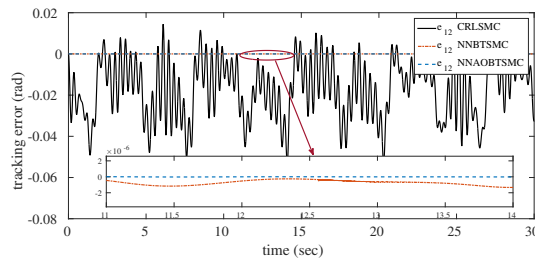


Figure 5.24 : Tracking error of link 2.

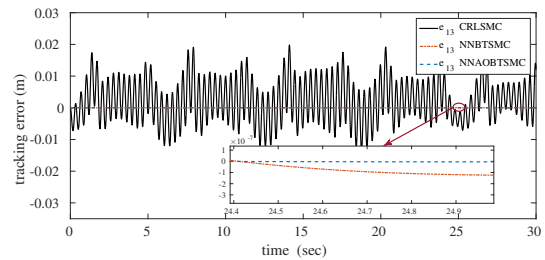


Figure 5.25 : Tracking error of link 3.

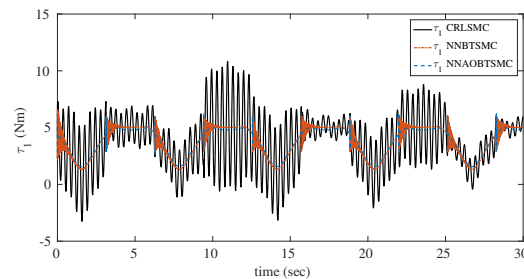


Figure 5.26 : Control input for link 1.

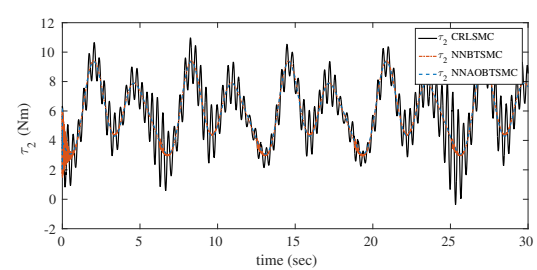


Figure 5.27 : Control input for link 2.

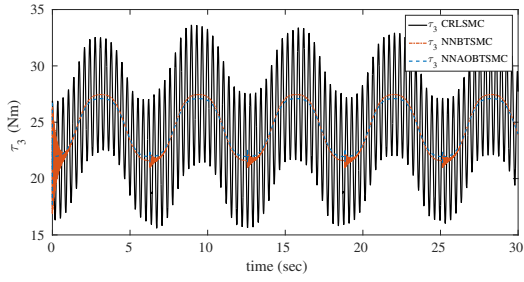


Figure 5.28 : Control input for link 3.

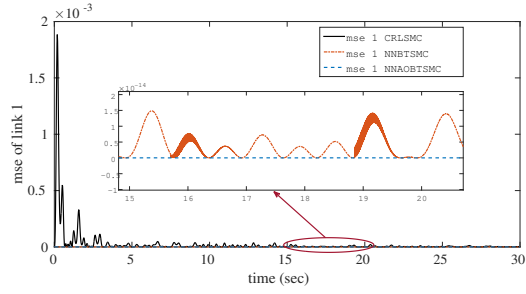


Figure 5.29 : MSE of link 1.

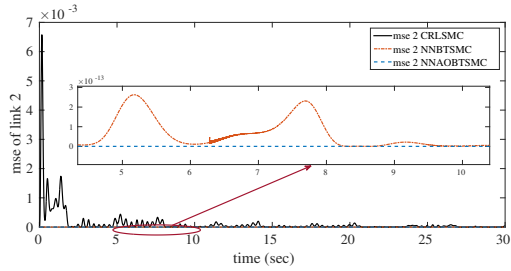


Figure 5.30 : MSE of link 2.

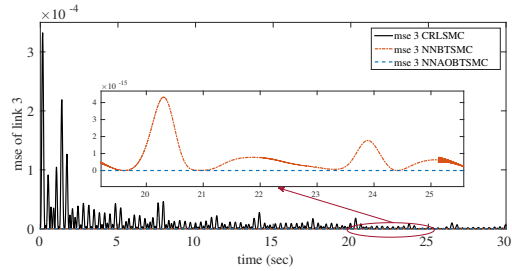


Figure 5.31 : MSE of link 3.

Table 5.9.1 : MSE examination of CRLSMC (Tran et al., 2015), NNBTSMC and NNAOBTSMC

Sl. No	MSE	CRLSMC	NNBTSMC	NNAOBTSMC
1	link 1	2.732×10^{-6}	2.451×10^{-15}	4.118×10^{-17}
2	link 2	3.526×10^{-5}	2.007×10^{-14}	3.924×10^{-20}
3	link 3	4.864×10^{-6}	9.321×10^{-16}	1.44×10^{-20}

The MSE values of the 3-DOF OTDIRM trajectories under different control methodologies, such as CRLSMC in (Tran et al., 2015), NNBTSMC and NNAOBTSMC are presented in Table 5.9.1. From the table, it is ascertained that NNAOBTSMC provides least MSE values in comparison with other methods (i.e., NNAOBTSMC system has better tracking trajectory performance). Figure 5.20 to Figure 5.22 indicate tracking positions, Figure 5.23 to Figure 5.25 indicate tracking errors and Figure 5.26 to Figure 5.28 show control torque. From the Figure 5.26 to Figure 5.28, it is clear that the control torque is smoother for NNAOBTSMC compared with existing CRLSMC (Tran et al., 2015). This indicates that the proposed method requires less control effort for same trajectory tracking. The MSE response plots of the OTDIRM link trajectories exhibited from Figure 5.29 to Figure 5.31. The energy of the input signal is calculated by

Table 5.9.2 : Total variance examination of CRLSMC (Tran et al., 2015), NNBTSMC and NNAOBTSMC

Sl. No	Total Variance (TV)	CRLSMC	NNBTSMC	NNAOBTSMC
1	link 1	6.1354	1.8337	1.4024
2	link 2	4.8902	3.5510	3.4074
3	link 3	20.8775	5.1885	4.0198

using the 2-Norm method. The control energy is expected to be as small as possible. The output and input performances are calculated for the period from 0 to 30 sec with a sampling time of 0.0001 sec. From Table 5.9.2 and 5.9.3, it clear that the values of

Table 5.9.3 : 2-Norm of input examination of CRLSMC (Tran et al., 2015), NNBTSMC and NNAOBTSMC

Sl. No	2-Norm of Input	CRLSMC	NNBTSMC	NNAOBTSMC
1	link 1	2.4778×10^3	2.2119×10^3	2.1856×10^3
2	link 2	3.4905×10^3	3.4535×10^3	3.4452×10^3
3	link 3	1.3727×10^4	1.3550×10^4	1.3530×10^4

TV and 2-Norm of input for proposed methods are very small as compared to existing method CRLSMC (Tran et al., 2015). Figure 5.32, Figure 5.33 and Figure 5.34

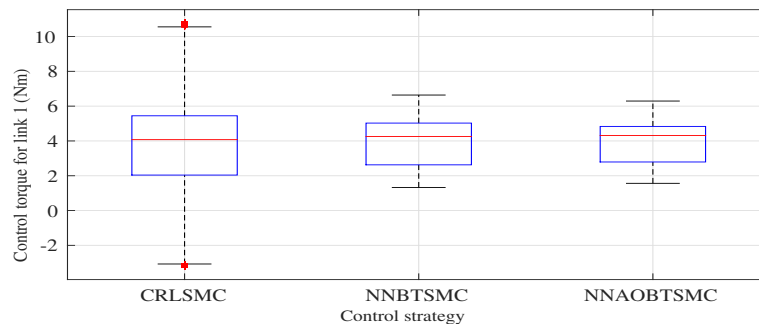


Figure 5.32 : Box plot representation of control torque for link 1.

show the box plot of control torque for link 1, link 2 and link 3 with the mean, median, $\pm 25\%$ quartiles (notch boundaries), $\pm 75\%$ quartiles (box ends), $\pm 95\%$ bounds and the outliers. From the size of the boxes shown, it is clear that the NNAOBTSMC

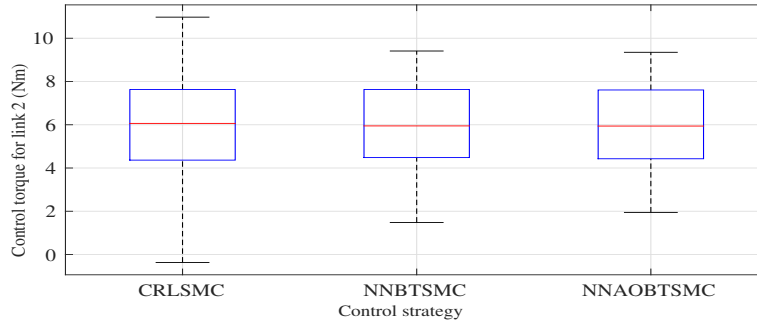


Figure 5.33 : Box plot representation of control torque for link 2.

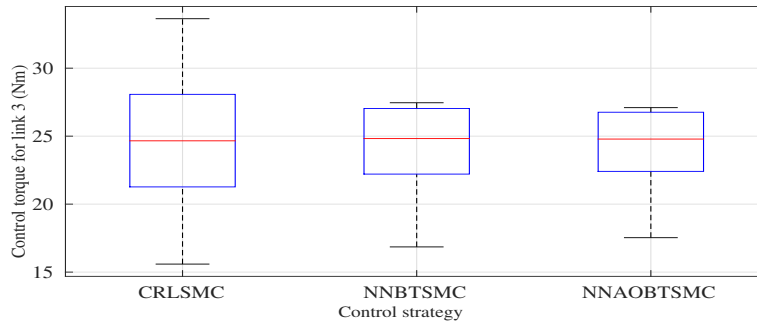


Figure 5.34 : Box plot representation of control torque for link 3.

control strategy experiences minimum variation than others. Comparing the box plot of NNBTSMC and NNAOBTSMC, it observed that NNAOBTSMC has less variation in control input torque for link 1, link 2 and link 3 of the OTDIRM.

5.10 DESIGN OF IBTSMC

The backstepping methodology is a nonlinear scheme generally utilized as a part of controller design. The mathematical model of robot manipulator is expressed in (5.111), (5.112) and (5.113) as:

$$\dot{x}_1 = x_2 \quad (5.111)$$

$$\dot{x}_2 = \ddot{q} = D^{-1}(q)[\tau - (C(q, \dot{q})\dot{q} + G(q) + F(q, \dot{q}) + \tau_d)] \quad (5.112)$$

$$y = x_1 \quad (5.113)$$

where x_1 and x_2 are the position and velocity vectors of the robot manipulator. The position tracking error of the system is given as:

$$e_1 = q_d - q \quad (5.114)$$

The stabilizing function is characterized as

$$\alpha_1 = \lambda_1 e_1 + \frac{1}{\lambda_2} e_1^{\frac{\Omega_1}{\Omega_2}} \quad (5.115)$$

The integral action of the tracking error of position is characterized as:

$$\alpha_2 = \lambda_3 \int_0^t e_1 dt \quad (5.116)$$

where $\lambda_1, \lambda_2, \lambda_3 > 0$ and Ω_1, Ω_2 ($1 < \frac{\Omega_1}{\Omega_2} < 2$) are positive odd numbers. The tracking error of the velocity has upgraded with stability function and integral action of tracking error of position of the robot manipulator. It is characterized in Eq. (5.117) and appeared as:

$$e_2 = \dot{e}_1 + \alpha_1 + \alpha_2 \quad (5.117)$$

The primary Lyapunov stability function is characterized as:

$$V_1 = \frac{1}{2} e_1^2 \quad (5.118)$$

$$\dot{V}_1 = e_1 e_2 - \lambda_1 e_1^2 - \frac{1}{\lambda_2} e_1^{\left(\frac{\Omega_1 + \Omega_2}{\Omega_2}\right)} - \lambda_3 e_1 \int_0^t e_1 dt \quad (5.119)$$

From (1.2) and (5.117), we get

$$\begin{aligned} \dot{e}_2 = & \ddot{q}_d - D^{-1}(q)(\tau - (C(q, \dot{q})\dot{q} + G(q) + F(q, \dot{q}) + \tau_d)) + \lambda_1 \dot{e}_1 \\ & + \frac{\Omega_1}{\lambda_2 \Omega_2} e_1^{\left(\frac{\Omega_1 - \Omega_2}{\Omega_2}\right)} \dot{e}_1 + \lambda_3 e_1 \end{aligned} \quad (5.120)$$

The second Lyapunov stability function is described as:

$$V = V_1 + \frac{1}{2} s^T s \quad (5.121)$$

The satisfactory condition, which gives the affirmation that the tracking error will make an elucidation from achieving stage to sliding stage, is generally called the achieving condition and given in (5.122).

$$\dot{V} < 0, s \neq 0 \quad (5.122)$$

Where 's' is the sliding surface. It is characterized as:

$$s = e_1 + e_2 \quad (5.123)$$

The derivative of the second Lyapunov stability function is given in equation (5.124).

$$\begin{aligned} \dot{V} = & e_1 e_2 - \lambda_1 e_1^2 - \frac{1}{\lambda_2} e_1^{\left(\frac{\Omega_1 + \Omega_2}{\Omega_2}\right)} - \lambda_3 e_1 \int_0^t e_1 dt + s^T (\dot{e}_1 (1 + \lambda_1)) \\ & + \frac{\Omega_1}{\lambda_2 \Omega_2} e_1^{\left(\frac{\Omega_1 - \Omega_2}{\Omega_2}\right)} \dot{e}_1 + \lambda_3 e_1 + \ddot{q}_d - \ddot{q} \end{aligned} \quad (5.124)$$

The total input control torque (τ) to the robot manipulator is characterized as:

$$\tau = \tau_0 + \tau_c \quad (5.125)$$

By substituting (5.125) in (5.124), we get

$$\begin{aligned} \dot{V} = & e_1 e_2 - \lambda_1 e_1^2 - \frac{1}{\lambda_2} e_1^{\left(\frac{\Omega_1 + \Omega_2}{\Omega_2}\right)} - \lambda_3 e_1 \int_0^t e_1 dt + s^T [\dot{e}_1 (1 + \lambda_1) \\ & + \frac{\Omega_1}{\lambda_2 \Omega_2} e_1^{\left(\frac{\Omega_1 - \Omega_2}{\Omega_2}\right)} \dot{e}_1 + \lambda_3 e_1 + \ddot{q}_d - D^{-1}(q)((\tau_0 + \tau_c) - (C(q, \dot{q})\dot{q} + G(q) \\ & + F(q, \dot{q}) + \tau_d))] \end{aligned} \quad (5.126)$$

The arrangement of $\dot{s} = 0$ gives the control signal, which is known as equivalent control law and it is denoted by ' τ_0 '. This equivalent control law is essential to fulfill the execution of favored trajectory tracking without considering disturbances and uncertainties (i.e. $\tau_d = 0$).

$$\begin{aligned} \tau_0 = & D(q) (\dot{e}_1 (1 + \lambda_1) + \frac{\Omega_1}{\lambda_2 \Omega_2} e_1^{\left(\frac{\Omega_1 - \Omega_2}{\Omega_2}\right)} \dot{e}_1 + \lambda_3 e_1 + \ddot{q}_d) + C(q, \dot{q}) \dot{q} \\ & + G(q) + F(q, \dot{q}) \end{aligned} \quad (5.127)$$

An extra control exertion is needed to wipe out the unpredictable disturbances and uncertainties as equivalent control torque (τ_0) is lacking to provide the favored tracking performance. Ultimately, the tracking error dies out asymptotically, which means the sliding surface becomes stable. To exhibit the stability of the created control framework for the robot manipulator, the Lyapunov-like Lemma is utilized.

From (5.126) and (5.127) we arrive at an expression for \dot{V} as follows:

$$\dot{V} = e_1 e_2 - \lambda_1 e_1^2 - \frac{1}{\lambda_2} e_1^{\left(\frac{\Omega_1 + \Omega_2}{\Omega_2}\right)} - \lambda_3 e_1 \int_0^t e_1 dt + s^T (-D^{-1}(q) \tau_c) \quad (5.128)$$

To meet the Lyapunov stability condition, the corrective control law (τ_c) is defined as

$$\tau_c = D(q) \left(\frac{1}{s^T} (e_1 e_2 - \frac{1}{\lambda_2} e_1^{\left(\frac{\Omega_1 + \Omega_2}{\Omega_2}\right)} - \lambda_3 e_1 \int_0^t e_1 dt) + K_w \text{sign}(s) \right) \quad (5.129)$$

by substituting τ_c in (5.128) and yields,

$$\dot{V} = -\lambda_1 e_1^2 - K_w s^T \text{sign}(s) \quad (5.130)$$

where K_w is the sliding gain.

$$\dot{V} \leq -\lambda_1 |e_1^2| - K_w |s| \quad (5.131)$$

where $|s| = s^T \text{sign}(s)$. The chattering effect on the control input signal is introduced by the signum function ('sign'), which is utilized as a part of (5.130), so as to diminish or dispense with this impact, the signum function ('sign') is substituted by the hyperbolic tangent function ('tanh') as given in (5.132).

$$\dot{V} \leq -\lambda_1 e_1^2 - K_w s^T \tanh(s) \quad (5.132)$$

The term ' $s^T \tanh(s)$ ' in (5.132) is constantly positive so that whole condition gets to be negative (i.e. $s^T \tanh(s) > 0$ if either $s > 0$ or $s < 0$). The achieving control signal (τ_c) is modified as:

$$\tau_c = D(q) \left(\frac{1}{s^T} (e_1 e_2 - \frac{1}{\lambda_2} e_1^{\left(\frac{\Omega_1 + \Omega_2}{\Omega_2}\right)} - \lambda_3 e_1 \int_0^t e_1 dt) + K_w \tanh(s) \right) \quad (5.133)$$

Where $K_w = \text{diag}\{K_{w1}, K_{w2}, \dots, K_{wn}\}$ is control gain matrix. The IBTSMC control law is defined as:

$$\tau_c = D(q) \left(\frac{1}{s^T} (e_1 e_2 - \frac{1}{\lambda_2} e_1^{\left(\frac{\Omega_1 + \Omega_2}{\Omega_2}\right)} - \lambda_3 e_1 \int_0^t e_1 dt) + K \tanh\left(\frac{s}{\phi}\right) \right) \quad (5.134)$$

where $K = D(q)K_w$.

When $s = 0$ is reached at $t = t_r$, $e_1 = 0$ becomes terminal surface, i.e. $e_1 + e_2 = 0$. The effect of terminal surface will take the state of e_1 from $e_1(t_r) \neq 0$ to $e_1(t_r + t_s) = 0$ with finite time t_s given by

$$t_s = \frac{1}{(1 + \lambda_1) \left(\frac{\Omega_1}{\Omega_2} - 1\right) + \frac{\lambda_3}{2} \left(\frac{\Omega_1}{\Omega_2} - 2\right) e_1} \left(\ln(\lambda_2) - \left(\frac{\Omega_1}{\Omega_2} - 1\right) \ln(1 + \lambda_1) e_1 \right) + \left(\frac{\Omega_1}{\Omega_2} - 2\right) \ln\left(\frac{\lambda_3 e_1}{2}\right) \quad (5.135)$$

5.11 DESIGN OF NEURAL NETWORK BASED INTEGRAL BACKSTEPPING TERMINAL SLIDING MODE CONTROL (NNIBTSMC)

In this section, the RBFNN is utilized to build up the control plans for the robot manipulator to track the desired trajectories under unknown dynamics of the system. Figure 5.35 demonstrates the schematic representation of NNIBTSMC.

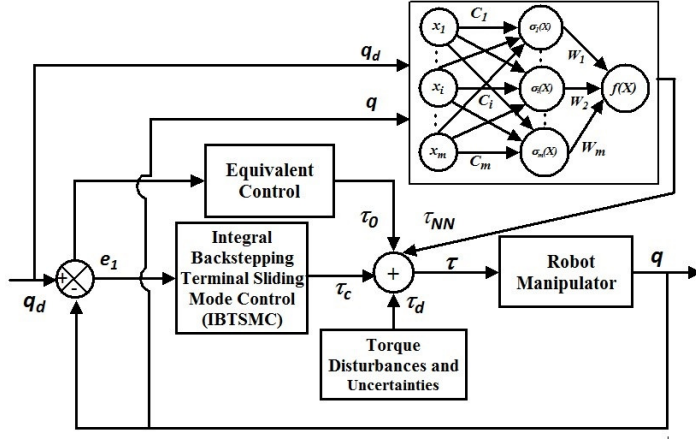


Figure 5.35 : Block diagram of NNIBTSMC scheme.

$$\dot{q}_r = \dot{q}_d + (1 + \lambda_1)e_1 + \frac{1}{\lambda_2}e_1^{\frac{\Omega_1}{\Omega_2}} + \lambda_3 \int_0^t e_1 dt \quad (5.136)$$

where ‘ \dot{q}_r ’ is auxiliary signal. The modified sliding surface (s) is characterized as:

$$s = \dot{q}_r - \dot{q} = (1 + \lambda_1)e_1 + \frac{1}{\lambda_2}e_1^{\frac{\Omega_1}{\Omega_2}} + \lambda_3 \int_0^t e_1 dt + \frac{d}{dt}e_1 \quad (5.137)$$

From (1.18), (5.136) and (5.137), we get

$$D(q)\dot{s} = -C(q, \dot{q})s + f(X) + \tau_d - \tau \quad (5.138)$$

where ‘ τ_d ’ represents external torque disturbances.

$$f(X) = D(q)\ddot{q}_r + C(q, \dot{q})\dot{q}_r + F(q, \dot{q}) + G(q) \quad (5.139)$$

where $X = [\ddot{q}_d^T, \dot{q}_d^T, q_d^T, \dot{q}^T, q^T]^T$.

The approximation of $f(X)$ is defined in (5.140).

$$f(X) = \hat{W}^T \sigma(X) \quad (5.140)$$

where ‘ \hat{W} ’ is the NN adjustment law, $\sigma(X)$ is the basis function. Now (5.138) can be revised as:

$$D(q)\dot{s} = -C(q, \dot{q})s + \tilde{W}^T \sigma(X) + \hat{W}^T \sigma(X) + \varepsilon^* + \tau_d - \tau \quad (5.141)$$

where $\tilde{W} = W^* - \hat{W}$, W^* and ε^* are ideal weights matrix and approximation error respectively.

Theorem 5.11.1. Consider the robot manipulator modeled by (1.18), if the total control torque is expressed as $\tau = \tau_0 + \tau_c + \tau_{NN}$, in which control law of IBTSMC is defined as $\tau_c = k_1 s + K \tanh(\frac{s}{\phi})$ and $\tau_{NN} = \hat{W}^T \sigma(X)$. The evaluated adaptive law for the NN identifier is characterized as:

$$\dot{\hat{W}}^T = -\dot{\tilde{W}}^T = B\sigma(X)s^T \quad (5.142)$$

where ‘ B ’ is a positive definite matrix and the tracking errors of position and velocity (i.e. e and \dot{e}) of the system asymptotically converge to zero as $t \rightarrow \infty$.

Proof. NNIBTSMC stability function is given in (5.143).

$$V = \frac{1}{2}s^T D(q)s + \frac{1}{2}tr(\tilde{W}^T B^{-1}\tilde{W}) \quad (5.143)$$

$$\dot{V} = \frac{1}{2}s^T \dot{D}(q)s + s^T D(q)\dot{s} + tr(\tilde{W}^T B^{-1}\dot{\tilde{W}}) \quad (5.144)$$

By substituting (5.141) in (5.144), we get

$$\dot{V} = \frac{1}{2}s^T [\dot{D}(q) - 2C(q, \dot{q})]s + s^T [\tilde{W}^T \sigma(X) + \varepsilon^* + \tau_d - k_1 s - K \tanh(\frac{s}{\phi})] + tr(\tilde{W}^T B^{-1}\dot{\tilde{W}}) \quad (5.145)$$

Since, $\dot{D}(q) - 2C(q, \dot{q})$ is a skew symmetric matrix, the first term in (5.145) becomes zero (i.e. $\frac{1}{2}s^T [\dot{D}(q) - 2C(q, \dot{q})]s = 0$), from (5.132) and (5.142), \dot{V} can be rewritten as:

$$\dot{V} \leq -k_1 s^T s + \|s\| \delta_0 \quad (5.146)$$

where ‘ δ_0 ’ is upper bound of $\|\varepsilon^* + \tau_d\|$. The term $\|s\| \delta_0$ is bounded by $\|s\| \delta_0 \leq \frac{1}{2}(\|s\|^2 + \rho \delta_0^2)$, where $\rho > 0$ is picked to such an extent that $\int_0^\infty \rho dt < \infty$ and further substituted in (5.146) to get stability criteria with finite boundedness.

$$\dot{V} \leq -k_1 \|s\|^2 + \frac{1}{2}(\|s\|^2 + \rho \delta_0^2) \quad (5.147)$$

Integrating both sides of (5.147) from $t = 0$ to T , yields

$$V(T) - V(0) \leq -(k_1 - \frac{1}{2}) \int_0^T \|s\|^2 dt + \frac{1}{2} \delta_0^2 \int_0^T \rho dt, \quad (\forall k_1 > 2) \quad (5.148)$$

Since, $V(T) \geq 0$ and $\int_0^\infty \rho dt < \infty$ holds,

$$\limsup_{T \rightarrow \infty} \frac{1}{T} \int_0^T \|s\|^2 dt \leq \frac{1}{(k_1 - \frac{1}{2})} \left[V(0) + \frac{1}{2} \delta_0^2 \int_0^\infty \rho dt \right] \limsup_{T \rightarrow \infty} \frac{1}{T} = 0 \quad (5.149)$$

From (5.148) and (5.149), we get $s \rightarrow 0$ as $t \rightarrow \infty$. Subsequently, we can conclude, from (5.137), the tracking errors of position and velocity (i.e. e and \dot{e}) asymptotically converge to zero as $t \rightarrow \infty$. Therefore, the stability criteria is fulfilled by the proposed NNIBTSMC scheme. \square

Remark 5.11.2. *The combination of IBTSMC and NN approximation makes the controller more robust, and errors caused by uncertainties of parameters and external disturbances. The developed NN identifiers can be compensated to provide better tracking behavior and enhance the rejection of disturbances under various disturbance conditions and parameter uncertainties.*

5.12 AN ADAPTIVE OBSERVER BASED CONTROL OF ROBOT MANIPULATOR

The neural network based adaptive observer integral backstepping terminal sliding mode control (NNAOIBTSMC) is developed with help of NNAO for precise desired trajectory tracking and improve the disturbance rejection under different working conditions (i.e. external disturbances and uncertainties) of robot manipulator. Figure 5.36 demonstrates structure of the NNAOIBTSMC.

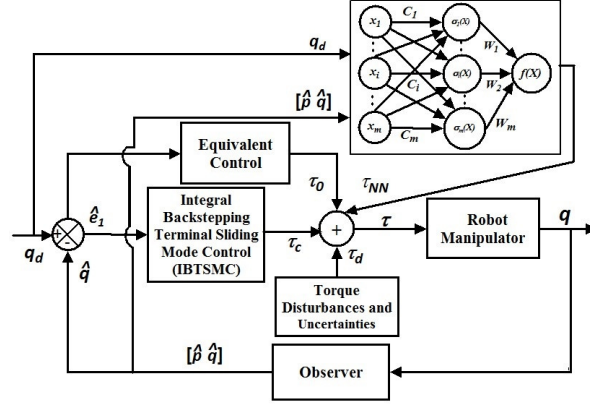


Figure 5.36 : Block diagram of the NNAOIBTSMC scheme.

The evaluated error of the link position is characterized as:

$$\hat{e}_1 = q_d - \hat{q} \quad (5.150)$$

The estimated sliding surface ‘ \hat{s} ’ is designed as:

$$\hat{s} = \frac{(1 + \lambda_1)\hat{e}_1 + \frac{1}{\lambda_2}\hat{e}_1^{\Omega_1} + \lambda_3 \int_0^t \hat{e}_1 dt + \frac{d}{dt}\hat{e}_1}{\phi} \quad (5.151)$$

Theorem 5.12.1. Considered robot manipulator described by (1.18). Let the NNAO estimates q and p as \hat{q} and \hat{p} , estimation errors are $\tilde{q} = q - \hat{q}$ and $\tilde{p} = p - \hat{p}$. Then, the approximation function of $f(X)$ described in (5.139) is conveyed as:

$$\hat{f}(\hat{X}) = \hat{W}_c^T \sigma(\hat{X}), \quad \hat{X} = [\hat{q}_d^T, \hat{q}_d^T, \hat{q}_d^T, \hat{p}^T, \hat{q}^T]^T \quad (5.152)$$

where ‘ \hat{W}_c ’ is estimated adaptation matrix.
The adaptation law is defined as:

$$\dot{\hat{W}}_c = -\dot{\tilde{W}}_c = B_c \sigma(\hat{X}) \hat{s}^T \quad (5.153)$$

The NNAOIBTSMC law is characterized as:

$$\tau = \Lambda_3 \hat{s} + K \tanh\left(\frac{\hat{s}}{\phi}\right) + \hat{W}_c^T \sigma(\hat{X}) \quad (5.154)$$

where ‘ $\Lambda_3 \hat{s} + K \tanh(\frac{\hat{s}}{\phi})$ ’ is the boundary sliding mode control law and ‘ $\hat{W}_c^T \sigma(\hat{X})$ ’ is the approximation function to robot manipulator, then the estimation errors \tilde{q} and \tilde{p} are asymptotically converge to zero.

Proof. The Lyapunov stability candidate function for NNAOIBTSMC is characterized as:

$$V = V_o + V_c \quad (5.155)$$

where ‘ V_o ’ and ‘ V_c ’ are the observer stability and controller stability candidate functions respectively.

$$V_o = \tilde{p}^T \tilde{p} + \frac{1}{2} \text{tr}(\tilde{W}_o^T B_o^{-1} \tilde{W}_o) \quad (5.156)$$

$$V_c = \frac{1}{2} s^T D(q) s + \frac{1}{2} \text{tr}(\tilde{W}_c^T B_c^{-1} \tilde{W}_c) \quad (5.157)$$

The derivative of (5.157) becomes

$$\dot{V}_c = \frac{1}{2} s^T \dot{D}(q) s + s^T D(q) \dot{s} + \text{tr}(\tilde{W}_c^T B_c^{-1} \dot{\tilde{W}}_c) \quad (5.158)$$

Since, $\dot{D}(q) - 2C(q, p)$ is a skew symmetric matrix and $s = \hat{s} + \dot{q} + \Lambda_1 \tilde{q} = \hat{s} + \tilde{p}$, then we get

$$\begin{aligned} \dot{V}_c = & \hat{s}^T \{ \hat{W}_c^T \tilde{\sigma}(\hat{X}) + \varepsilon^* + \tau_d \} + \tilde{p}^T \{ \tilde{W}_c^T \sigma(\hat{X}) + \hat{W}_c^T \tilde{\sigma}(\hat{X}) + \varepsilon^* + \tau_d \} \\ & - \Lambda_3 \hat{s}^T \hat{s} - \Lambda_3 \tilde{p}^T \hat{s} - K \hat{s}^T \tanh\left(\frac{\hat{s}}{\phi}\right) + \text{tr}\{ \tilde{W}_c^T (B_c^{-1} \dot{W}_c + \sigma(\hat{X}) \hat{s}^T) \} \end{aligned} \quad (5.159)$$

where ‘ γ_0 ’ is maximum limit of $\| \hat{W}_c^T \tilde{\sigma}(\hat{X}) + \varepsilon^* + \tau_d \|$ and $\zeta = \{ \tilde{W}_c^T \sigma(\hat{X}) + \hat{W}_c^T \tilde{\sigma}(\hat{X}) + \varepsilon^* + \tau_d \}$, corresponding to this ‘ ζ ’, there exists a positive constant ‘ ζ_0 ’ such that $\| \zeta \| \leq \zeta_0$.

$$\dot{V}_c \leq \| \hat{s} \| \gamma_0 + \| \tilde{p} \| \zeta_0 - \Lambda_3 \hat{s}^T \hat{s} - \Lambda_3 \tilde{p}^T \hat{s} \quad (5.160)$$

The terms $\| \hat{s} \| \gamma_0$, $\| \tilde{p} \| \zeta_0$ and $-\Lambda_3 \tilde{p}^T \hat{s}$ are bounded by $\| \hat{s} \| \gamma_0 \leq \frac{1}{2} (\| \hat{s} \|^2 + \rho \gamma_0^2)$, $\| \tilde{p} \| \zeta_0 \leq \frac{1}{2} (\| \tilde{p} \|^2 + \rho \zeta_0^2)$ and $-\Lambda_3 \tilde{p}^T \hat{s} \leq \frac{\Lambda_3}{2} (\| \tilde{p} \|^2 + \| \hat{s} \|^2)$ respectively. To induce stability criteria with finite boundedness, the constrained terms are substituted in (5.160). The expression for \dot{V}_c gets to be:

$$\dot{V}_c \leq -\left(\frac{\Lambda_3}{2} - \frac{1}{2}\right) \| \hat{s} \|^2 + \left(\frac{\Lambda_3}{2} + \frac{1}{2}\right) \| \tilde{p} \|^2 + \frac{1}{2} \rho (\gamma_0^2 + \zeta_0^2), \quad \forall (\Lambda_3 > 2) \quad (5.161)$$

The derivative of (5.156) and from (4.33), we will get

$$\dot{V}_o = \tilde{p}^T \{ W_o^{*T} \tilde{\sigma}_o(q, p) - D^{-1}(q) \tau_d + \varepsilon_o^* \} - \Lambda_3 \tilde{p}^T \tilde{p} + \text{tr}\{ \tilde{W}_o^T (B_o^{-1} \dot{W}_o + \sigma_o(\hat{q}, \hat{p}) \tilde{p}^T) \} \quad (5.162)$$

Since, $\| W_o^{*T} \tilde{\sigma}_o(q, p) - D^{-1}(q) \tau_d + \varepsilon_o^* \| \leq \beta_0$ and $\| \tilde{p} \| \beta_0$ is bounded by $\| \tilde{p} \| \beta_0 \leq \frac{1}{2} (\| \tilde{p} \|^2 + \rho \beta_0^2)$, then

$$\dot{V}_o \leq -\Lambda_3 \tilde{p}^T \tilde{p} + \frac{1}{2} (\| \tilde{p} \|^2 + \rho \beta_0^2) \quad (5.163)$$

$$\dot{V} = \dot{V}_o + \dot{V}_c \quad (5.164)$$

$$\dot{V} \leq -\frac{1}{2} (\Lambda_3 - 2) \| \tilde{p} \|^2 - \frac{1}{2} (\Lambda_3 - 1) \| \hat{s} \|^2 + \frac{1}{2} \rho (\gamma_0^2 + \zeta_0^2 + \beta_0^2), \quad \forall (\Lambda_3 > 2) \quad (5.165)$$

Integrating both sides from $t = 0$ to T , yields

$$\begin{aligned} V(T) - V(0) \leq & -\frac{1}{2} (\Lambda_3 - 1) \int_0^T \| \hat{s} \|^2 dt - \frac{1}{2} (\Lambda_3 - 2) \int_0^T \| \tilde{p} \|^2 dt \\ & + \frac{1}{2} (\gamma_0^2 + \zeta_0^2 + \beta_0^2) \int_0^T \rho dt \end{aligned} \quad (5.166)$$

Since, $V(T) \geq 0$ and $\int_0^\infty \rho dt < \infty$ holds,

$$\begin{aligned} \limsup_{T \rightarrow \infty} \frac{1}{T} \left[(\Lambda_3 - 1) \int_0^T \| \hat{s} \|^2 dt + (\Lambda_3 - 2) \int_0^T \| \tilde{p} \|^2 dt \right] \leq & 2 \left[V(0) \right. \\ & \left. + \frac{1}{2} (\gamma_0^2 + \zeta_0^2 + \beta_0^2) \int_0^\infty \rho dt \right] \limsup_{T \rightarrow \infty} \frac{1}{T} = 0 \end{aligned} \quad (5.167)$$

From (5.166) and (5.167), it is clear that $\tilde{p} \rightarrow 0$, $\hat{s} \rightarrow 0$ as $t \rightarrow \infty$. That concludes $\tilde{q} \rightarrow 0$ and $\tilde{p} \rightarrow 0$. Thus, the proposed NNAOIBTSMC fulfills the stability criteria. \square

5.13 RESULTS AND DISCUSSIONS FOR IBTSMC

The desired reference trajectories for de-icing robot manipulator and important parameters that affect the control performance of the robotic systems (i.e. uncertainties and ex-

ternal disturbances) are considered according to literature (Tran et al., 2015). IBTSMC parameters are $\lambda_1 = 980$, $\lambda_2 = 100$, $\lambda_3 = 540$, $\Omega_1=5$, $\Omega_2=3$, $K_{w1} = 440$, $K_{w2} = 440$, $K_{w3} = 440$ and $\phi = 0.01$. The finite times (t_s) for proposed method (i.e. NNAOIBTSMC) are calculated as 0.0327 sec, 0.031 sec and 0.0343 sec for link 1, link 2 and link 3 respectively.

The MSE values of the 3-DOF OTDIRM trajectories under different control method-

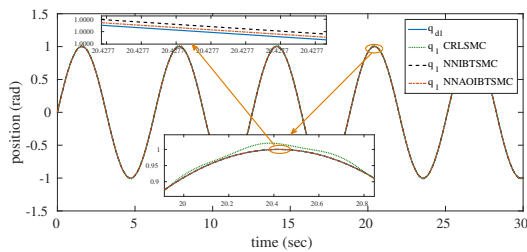


Figure 5.37 : Position tracking of link 1.

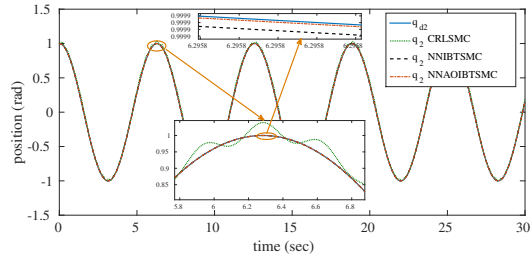


Figure 5.38 : Position tracking of link 2.

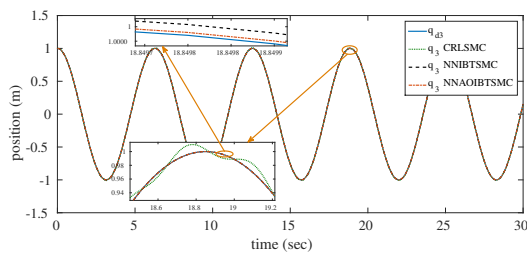


Figure 5.39 : Position tracking of link 3.

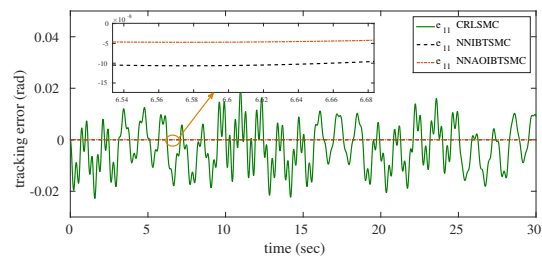


Figure 5.40 : Tracking error of link 1.

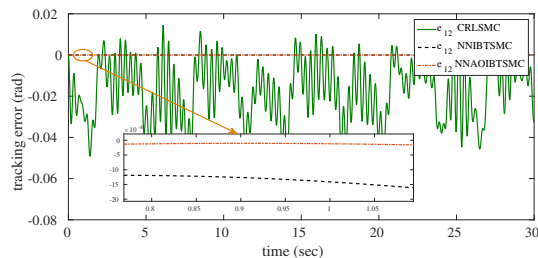


Figure 5.41 : Tracking error of link 2.

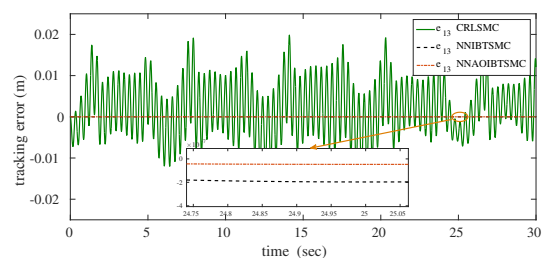


Figure 5.42 : Tracking error of link 3.

ologies, such as CRLSMC in (Tran et al., 2015), NNIBTSMC and NNAOIBTSMC are presented in Table 5.13.1. From the table, it is ascertained that NNAOIBTSMC provides least MSE values in comparison with other methods (i.e., NNAOIBTSMC system

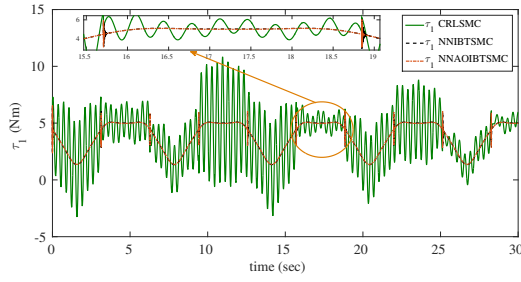


Figure 5.43 : Control input for link 1.

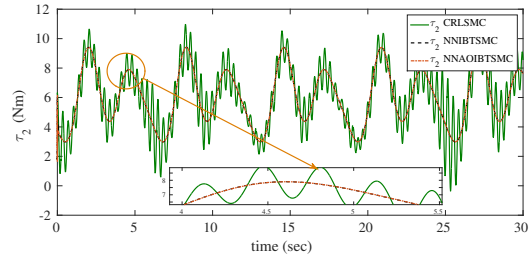


Figure 5.44 : Control input for link 2.

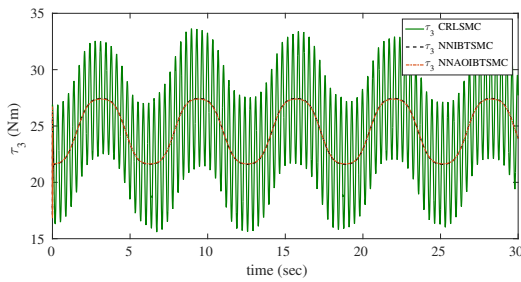


Figure 5.45 : Control input for link 3.

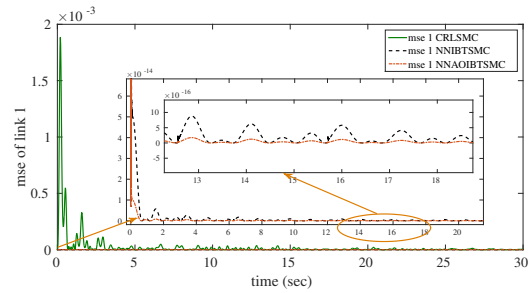


Figure 5.46 : MSE of link 1.

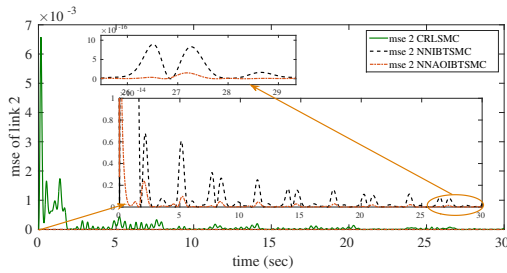


Figure 5.47 : MSE of link 2.

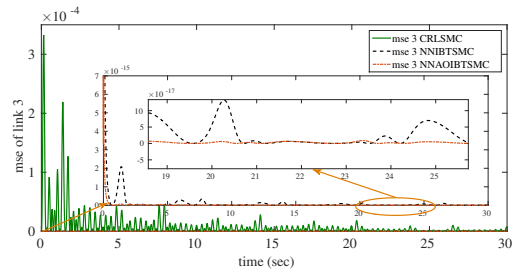


Figure 5.48 : MSE of link 3.

Table 5.13.1 : MSE examination of CRLSMC (Tran et al., 2015), NNIBTSMC and NNAOIBTSMC

Sl. No	MSE	CRLSMC	NNIBTSMC	NNAOIBTSMC
1	MSE_1	2.732×10^{-6}	1.224×10^{-16}	2.52×10^{-17}
2	MSE_2	3.526×10^{-5}	3.291×10^{-16}	1.595×10^{-17}
3	MSE_3	4.864×10^{-6}	1.004×10^{-17}	6.667×10^{-22}

has better tracking trajectory performance). Figure 5.37 to Figure 5.39 indicate tracking positions, Figure 5.40 to Figure 5.42 indicate tracking errors and Figure 5.43 to Figure 5.45 show control torque. From the Figure 5.43 to Figure 5.45, it is clear that the control torque is smoother for NNAOIBTSMC compared with existing CRLSMC

(Tran et al., 2015). This indicates that the proposed method requires less control effort for same trajectory tracking. The MSE response plots of the OTDIRM link trajectories exhibited from Figure 5.46 to Figure 5.48. The energy of the input signal is calculated

Table 5.13.2 : Total variance examination of CRLSMC (Tran et al., 2015), NNIBTSMC and NNAOIBTSMC

Sl. No	Total variance (TV)	CRLSMC	NNIBTSMC	NNAOIBTSMC
1	link 1	6.1354	1.7592	1.7059
2	link 2	4.8902	3.5363	3.5200
3	link 3	20.8775	5.0991	4.9425

by using the 2-Norm method. The control energy is expected to be as small as possible. The output and input performances are calculated for the period from 0 to 30 sec with a sampling time of 0.0001 sec. From Table 5.13.2 and 5.13.3, it clear that the values of

Table 5.13.3 : 2-Norm of input examination of CRLSMC (Tran et al., 2015), NNIBTSMC and NNAOIBTSMC

Sl. No	2-Norm of Input	CRLSMC	NNIBTSMC	NNAOIBTSMC
1	link 1	2.4778×10^3	2.2068×10^3	2.2031×10^3
2	link 2	3.4905×10^3	3.4526×10^3	3.4512×10^3
3	link 3	1.3727×10^4	1.3548×10^4	1.3544×10^4

TV and 2-Norm of input for proposed methods are very small as compared to existing method CRLSMC (Tran et al., 2015).

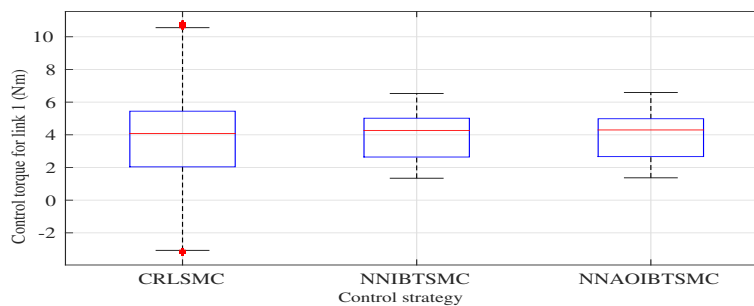


Figure 5.49 : Box plot representation of control torque for link 1.

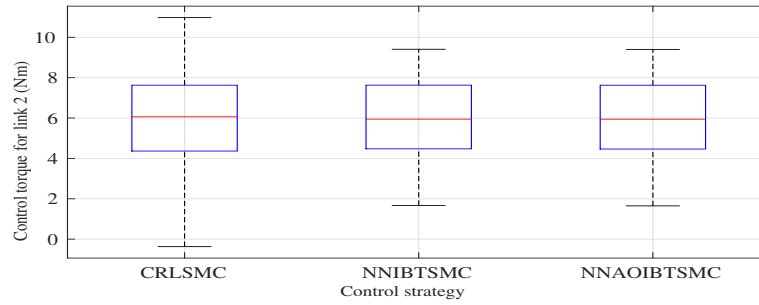


Figure 5.50 : Box plot representation of control torque for link 2.

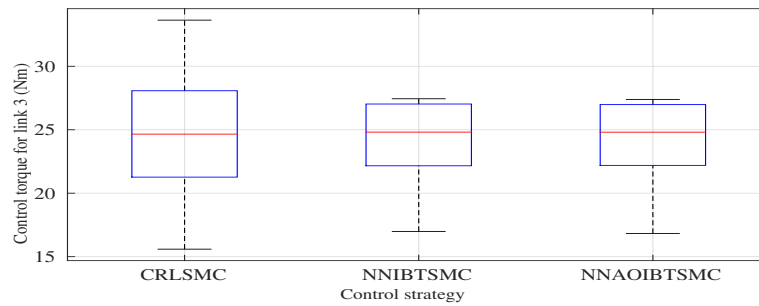


Figure 5.51 : Box plot representation of control torque for link 3.

Figure 5.49, Figure 5.50 and Figure 5.51 show the box plot of control torque for link 1, link 2 and link 3 with the mean, median, $\pm 25\%$ quartiles (notch boundaries), $\pm 75\%$ quartiles (box ends), $\pm 95\%$ bounds and the outliers. From the size of the boxes shown, it is clear that the NNAOIBTSMC control strategy experiences minimum variation than others. Comparing the box plot of NNIBTSMC and NNAOIBTSMC, it observed that NNAOIBTSMC has less variation in control input torque for link 1, link 2 and link 3 of the OTDIRM.

5.14 SUMMARY

In this chapter, the distinctive control techniques of the 3-DOF OTDIRM are addressed. The different types of neural network-based non-linear control methodologies (i.e., NNTSMC, NNBTSMC and NNIBTSMC) are developed to track the desired trajectory of the robot manipulator in presence of uncertainties and external disturbances. For the precise trajectory tracking performance and to enhance disturbance rejection under var-

ious disturbance conditions, neural network-based adaptive observer terminal sliding mode control methodologies are designed. Lyapunov stability theorem guaranteed the stability of the proposed control systems. Simulation responses depict the effectiveness of the terminal sliding mode control based proposed schemes.

Chapter 6

CONCLUSION

6.1 CONCLUSION

Among the existing controllers, there is a need to investigate, understand the properties and propose suitable modifications thereby making them more adaptable depending on the applications. For robotic applications, especially in 2-DOF and 3-DOF, the use of classical controllers often does not fulfill the desired performance criteria. In such cases, use of hybrid controllers is more logical. With this thought, the main contributions of this thesis are the proposal and verification of the variety of fused controller for the robotic manipulator. It involves in designing/modifying adaptive non-linear control methods for robot manipulators under different disturbance conditions. The developed predictive modeling methods are to estimate the position and velocity vectors for precise trajectory tracking performance and enhance disturbance rejection under various operating conditions for robot manipulators.

Two-mass single-link robot with the gearbox is developed, and the control parameters are tuned using Fminsearch and Genetic Algorithm. The variation of the SMC controller where the PID sliding surface is taken into consideration and controlling parameters are obtained by using PSO for control of 2-DOF robot manipulator. The different tracking control strategies for 3-DOF robot manipulator are discussed. The compositions of an observer-based different modified sliding mode controllers are developed for 3-DOF OTDIRM. Lyapunov stability theorem guaranteed the stability of the proposed control systems. In general, the results illustrate that the proposed observer-based con-

troller offers a superior tracking performance and smoother control input compared to other existing methods. The derivation of the control law guarantees the convergence of the tracking error. Several performance methods are examined to support the strength of the proposed and existing control approaches.

6.2 FUTURE WORK

In the future work, it will be a new and challenging task to develop a control algorithm for robot manipulator with model parameter uncertainties and various disturbances in torque. Further, research work will be continued with separate input signals such as step, triangular waves and high-frequency signals for desired trajectories. Future work might also include the fault disturbance observer-based tolerant control and an integrated fault diagnosis system for robot manipulator at various operating conditions. In addition, experimental evaluation of the 3-DOF robot manipulator with the proposed control strategies will be attempted.

Bibliography

- Abdel, B., Othaman, M., and Khalis, A. (2011). “A robust fuzzy tracking control scheme for robot manipulators with experimental verification”. *Journal of Intelligent Control and Automation*, 2, 100–111.
- Agrawal, S., Panigrahi, B., and Tiwari, M. K. (2008). “Multiobjective particle swarm algorithm with fuzzy clustering for electrical power dispatch”. *IEEE Transactions on Evolutionary Computation*, 12(5), 529–541.
- Aloui, S., Pagès, O., El Hajjaji, A., Chaari, A., and Koubaa, Y. (2011). “Improved fuzzy sliding mode control for a class of mimo nonlinear uncertain and perturbed systems”. *Applied soft computing*, 11(1), 820–826.
- Amer, A. F., Sallam, E. A., and Elawady, W. M. (2011). “Adaptive fuzzy sliding mode control using supervisory fuzzy control for 3 dof planar robot manipulators”. *Applied Soft Computing*, 11(8), 4943–4953.
- Ang, K. H., Chong, G., and Li, Y. (2005). “Pid control system analysis, design, and technology”. *IEEE transactions on control systems technology*, 13(4), 559–576.
- Arimoto, S. (1996). “*Control theory of nonlinear mechanical systems*”. Oxford University Press, Inc.
- Asif, M., Khan, M. J., and Memon, A. Y. (2017). “Integral terminal sliding mode formation control of non-holonomic robots using leader follower approach”. *Robotica*, 35(7), 1473–1487.
- Barrero, F., Gonzalez, A., Torralba, A., Galvan, E., and Franquelo, L. G. (2002). “Speed

- control of induction motors using a novel fuzzy sliding-mode structure”. *IEEE Transactions on Fuzzy Systems*, 10(3), 375–383.
- Benosman, M. and Le Vey, G. (2004). “Control of flexible manipulators: A survey”. *Robotica*, 22(5), 533–545.
- Branicky, M. S. (1998). “Multiple lyapunov functions and other analysis tools for switched and hybrid systems”. *IEEE Transactions on automatic control*, 43(4), 475–482.
- Caldwell, D. G. (2012). *Robotics and automation in the food industry: Current and future technologies*. Elsevier.
- Cannon Jr, R. H. and Schmitz, E. (1984). “Initial experiments on the end-point control of a flexible one-link robot”. *The International Journal of Robotics Research*, 3(3), 62–75.
- Castillo, O. and Melin, P. (2014). “A review on interval type-2 fuzzy logic applications in intelligent control”. *Information Sciences*, 279, 615–631.
- Chang, J. L. (2013). “Sliding mode control design for mismatched uncertain systems using output feedback”. In *Automatic Control Conference (CACs), 2013 CACS International*, 462–467. IEEE.
- Chang, J.-L. (2016). “Sliding mode control design for mismatched uncertain systems using output feedback”. *International Journal of Control, Automation and Systems*, 14(2), 579–586.
- Chaoui, H., Gueaieb, W., Biglarbegian, M., and Yagoub, M. C. (2013). “Computationally efficient adaptive type-2 fuzzy control of flexible-joint manipulators”. *Robotics*, 2(2), 66–91.
- Chaoui, H., Khayamy, M., and Aljarboua, A. A. (2017). “Adaptive interval type-2 fuzzy logic control for pmsm drives with a modified reference frame”. *IEEE Transactions on Industrial Electronics*, 64(5), 3786–3797.

- Chaoui, H., Sicard, P., and Gueaieb, W. (2009). “Ann-based adaptive control of robotic manipulators with friction and joint elasticity.”. *IEEE Trans. Industrial Electronics*, 56(8), 3174–3187.
- Chaudhary, H., Panwar, V., Sukavanam, N., and Prasad, R. (2014). “Anfis pd+ i based hybrid force/position control of an industrial robot manipulator”. *International Journal of Materials, Mechanics and Manufacturing*, 2(2).
- Chen, F.-S. and Lin, J.-S. (2005). “Nonlinear control design of robotic manipulators with velocity observers”. *IFAC Proceedings Volumes*, 38(1), 193–198.
- Chen, M. and Jiang, B. (2013). “Adaptive control and constrained control allocation for overactuated ocean surface vessels”. *International Journal of Systems Science*, 44(12), 2295–2309.
- Chen, S., Hong, X., Luk, B. L., and Harris, C. J. (2009). “Non-linear system identification using particle swarm optimisation tuned radial basis function models”. *International Journal of Bio-Inspired Computation*, 1(4), 246–258.
- Chen, W.-H. (2004). “Disturbance observer based control for nonlinear systems”. *IEEE/ASME transactions on mechatronics*, 9(4), 706–710.
- Chen, W.-H., Ballance, D. J., Gawthrop, P. J., and O’Reilly, J. (2000). “A nonlinear disturbance observer for robotic manipulators”. *IEEE Transactions on industrial Electronics*, 47(4), 932–938.
- Craig, J. J. (1989). “Introduction to robotics. mechanics and control. series in electrical and computer engineering: Control engineering”. ed: *Addison-Wesley, Reading, MA, USA*.
- Curk, B. and Jezernik, K. (2001). “Sliding mode control with perturbation estimation: application on dd robot mechanism”. *Robotica*, 19(6), 641–648.
- De Filippis, L. (2012). “*Advanced Path Planning and Collision Avoidance Algorithms for UAVs*”. PhD thesis, Politecnico di Torino.

- Dinh, H. T. (2012). “*Dynamic neural network-based robust control methods for uncertain nonlinear systems*”. University of Florida.
- Dong, F., Ieng, S.-H., Savatier, X., Etienne-Cummings, R., and Benosman, R. (2013). “Plenoptic cameras in real-time robotics”. *The International Journal of Robotics Research*, 32(2), 206–217.
- Firdaus, A. R. and Rahman, A. S. (2012). “Genetic algorithm of sliding mode control design for manipulator robot”. *TELKOMNIKA (Telecommunication Computing Electronics and Control)*, 10(4), 645–654.
- Fu, K. S., Gonzalez, R., and Lee, C. G. (1988). “*Robotics: Control Sensing. Vis.*”. Tata McGraw-Hill Education.
- Gao, Y.-F., Sun, X.-M., Wen, C., and Wang, W. (2017). “Observer-based adaptive nn control for a class of uncertain nonlinear systems with nonsymmetric input saturation”. *IEEE transactions on neural networks and learning systems*.
- Ge, H.-W., Liang, Y.-C., and Marchese, M. (2007). “A modified particle swarm optimization-based dynamic recurrent neural network for identifying and controlling nonlinear systems”. *Computers & Structures*, 85(21), 1611–1622.
- Ginoya, D., Shendge, P., and Phadke, S. (2014). “Sliding mode control for mismatched uncertain systems using an extended disturbance observer”. *IEEE Transactions on Industrial Electronics*, 61(4), 1983–1992.
- Gopinathan, L., Datta, K. B., and Ray, G. (2012). “Design of a set of controllers for an n-link robot manipulator”. *International Journal of Automation and Control*, 6(3-4), 277–290.
- Gracia, L., Sala, A., and Garelli, F. (2012). “A path conditioning method with trap avoidance”. *Robotics and Autonomous Systems*, 60(6), 862–873.
- Ho, H., Wong, Y.-K., and Rad, A. B. (2009). “Adaptive fuzzy sliding mode control with chattering elimination for nonlinear siso systems”. *Simulation Modelling Practice and Theory*, 17(7), 1199–1210.

- Houpis, C. H. and Sheldon, S. N. (2013). “*Linear Control System Analysis and Design with MATLAB*”. CRC Press.
- Hu, Q., Xu, L., and Zhang, A. (2012). “Adaptive backstepping trajectory tracking control of robot manipulator”. *Journal of the Franklin Institute*, 349(3), 1087–1105.
- Hu, W., Xiao, G., and Li, X. (2011). “An analytical method for pid controller tuning with specified gain and phase margins for integral plus time delay processes”. *ISA transactions*, 50(2), 268–276.
- Huang, J.-Q. and Lewis, F. L. (2003). “Neural-network predictive control for nonlinear dynamic systems with time-delay”. *IEEE Transactions on Neural Networks*, 14(2), 377–389.
- Huang, J.-W. and Lin, J.-S. (2008). “Backstepping control design of a single-link flexible robotic manipulator”. *IFAC Proceedings Volumes*, 41(2), 11775–11780.
- Iordanou, H. N. and Surgenor, B. W. (1997). “Experimental evaluation of the robustness of discrete sliding mode control versus linear quadratic control”. *IEEE Transactions on control systems technology*, 5(2), 254–260.
- Jafarnejadsani, H., Pieper, J., and Ehlers, J. (2013). “Adaptive control of a variable-speed variable-pitch wind turbine using radial-basis function neural network”. *IEEE transactions on control systems technology*, 21(6), 2264–2272.
- Jang, J.-S. (1993). “Anfis: adaptive-network-based fuzzy inference system”. *IEEE transactions on systems, man, and cybernetics*, 23(3), 665–685.
- Kelly, R. (1997). “Pd control with desired gravity compensation of robotic manipulators: a review”. *The International Journal of Robotics Research*, 16(5), 660–672.
- Khalil, H. K. (2002). “Nonlinear systems”. *Prentice-Hall, New Jersey*, 2(5), 5–1.
- Kim, M. K. and Kang, H. J. (2003). “An optimal control approach to robust control of robot manipulators”. In *Science and Technology, 2003. Proceedings KORUS 2003. The 7th Korea-Russia International Symposium on*, 2, 440–446. IEEE.

- Kohrt, C., Stamp, R., Pipe, A., Kiely, J., and Schiedermeier, G. (2013). “An online robot trajectory planning and programming support system for industrial use”. *Robotics and Computer-Integrated Manufacturing*, 29(1), 71–79.
- Lagarias, J. C., Reeds, J. A., Wright, M. H., and Wright, P. E. (1998). “Convergence properties of the nelder–mead simplex method in low dimensions”. *SIAM Journal on optimization*, 9(1), 112–147.
- Lai, X.-Z., Pan, C.-Z., Wu, M., Yang, S. X., and Cao, W.-H. (2015). “Control of an underactuated three-link passive–active–active manipulator based on three stages and stability analysis”. *Journal of Dynamic Systems, Measurement, and Control*, 137(2), 021007.
- Lewis, F. L., Abdallah, C. T., and Dawson, D. M. (1993). “*Control of robot manipulators*”, 236. Macmillan New York.
- Lin, F. and Brandt, R. D. (1998). “An optimal control approach to robust control of robot manipulators”. *IEEE Transactions on Robotics and Automation*, 14(1), 69–77.
- Liu, R. and Li, S. (2014). “Optimal integral sliding mode control scheme based on pseudospectral method for robotic manipulators”. *International Journal of Control*, 87(6), 1131–1140.
- Liu, Y.-J., Li, S., Tong, S., and Chen, C. P. (2017). “Neural approximation-based adaptive control for a class of nonlinear nonstrict feedback discrete-time systems”. *IEEE transactions on neural networks and learning systems*, 28(7), 1531–1541.
- Liu, Z.-G. and Wu, Y.-Q. (2014). “Modelling and adaptive tracking control for flexible joint robots with random noises”. *International Journal of Control*, 87(12), 2499–2510.
- Ma, X., Xu, B., and Cao, Y. (2008). “Guaranteed cost h infinity robust control for uncertain multiple time-varying delays systems with nonlinear perturbation”. In *Intelligent Computation Technology and Automation (ICICTA), 2008 International Conference on*, 1, 364–369. IEEE.

- Merchán-Cruz, E. A. and Morris, A. S. (2006). “Fuzzy-ga-based trajectory planner for robot manipulators sharing a common workspace”. *IEEE Transactions on Robotics*, 22(4), 613–624.
- Mittal, R. and Nagrath, I. (2003). “*Robotics and control*”. Tata McGraw-Hill.
- Mondal, S. and Mahanta, C. (2014). “Adaptive second order terminal sliding mode controller for robotic manipulators”. *Journal of the Franklin Institute*, 351(4), 2356–2377.
- Nagrath, I. and Gopal, M. “Control systems engineering, (2007), isbn: 81-224-2008-7”. *New Age International Publishers*, 193–268.
- Naidu, D. S. (2002). “*Optimal control systems*”. CRC press.
- Noshadi, A., Shi, J., Lee, W. S., Shi, P., and Kalam, A. (2017). “Robust control of an active magnetic bearing system using h and disturbance observer-based control”. *Journal of Vibration and Control*, 23(11), 1857–1870.
- Park, S., Deyst, J., and How, J. P. (2007). “Performance and lyapunov stability of a nonlinear path-following guidance method”. *Journal of Guidance Control and Dynamics*, 30(6), 1718–1728.
- Pereira, J. N., Silva, P., Lima, P. U., and Martinoli, A. (2014). “Formalization, implementation, and modeling of institutional controllers for distributed robotic systems”. *Artificial life*, 20(1), 127–141.
- Perez, J., Perez, J. P., Soto, R., Flores, A., Rodriguez, F., and Meza, J. L. (2012). “Trajectory tracking error using pid control law for two-link robot manipulator via adaptive neural networks”. *Procedia Technology*, 3, 139–146.
- Piltan, F. and Sulaiman, N. B. (2012). “Review of sliding mode control of robotic manipulator”. *World Applied Sciences Journal*, 18(12), 1855–1869.
- Pradhan, S. K. (2013). “*Development of New Adaptive Control Strategies for a Two-Link Flexible Manipulator*”. PhD thesis.

- Pradhan, S. K. and Subudhi, B. (2012). “Real-time adaptive control of a flexible manipulator using reinforcement learning”. *IEEE Transactions on Automation Science and Engineering*, 9(2), 237–249.
- Prieto, P. J., Cazarez-Castro, N. R., Aguilar, L. T., and Cardenas-Maciel, S. L. (2017). “Chattering existence and attenuation in fuzzy-based sliding mode control”. *Engineering Applications of Artificial Intelligence*, 61, 152–160.
- Rehiara, A. B. and Smit, W. (2010). “Controller design of a modeled adeptthree robot arm”. In *Modelling, Identification and Control (ICMIC), The 2010 International Conference on*, 854–858. IEEE.
- Romdhane, N. M. B. and Damak, T. (2010). “Terminal sliding mode feedback linearization control”. *International Journal of Sciences and Techniques of Automatic control & computer engineering, IJ-STA*, 4(1), 1174–1187.
- Rossomando, F. G., Soria, C., and Carelli, R. (2014). “Sliding mode neuro adaptive control in trajectory tracking for mobile robots”. *Journal of Intelligent & Robotic Systems*, 74(3-4), 931.
- Sage, H., De Mathelin, M., and Ostertag, E. (1999). “Robust control of robot manipulators: a survey”. *International Journal of control*, 72(16), 1498–1522.
- Santhakumar, M. and Asokan, T. (2010). “Investigations on the hybrid tracking control of an underactuated autonomous underwater robot”. *Advanced Robotics*, 24(11), 1529–1556.
- Sharkawy, A. B., Othman, M. M., and Khalil, A. M. A. (2011). “A robust fuzzy tracking control scheme for robotic manipulators with experimental verification”. *Intelligent Control and Automation*, 2(2), 100–111.
- Sharma, N., Bhasin, S., Wang, Q., and Dixon, W. E. (2011). “Predictor-based control for an uncertain euler–lagrange system with input delay”. *Automatica*, 47(11), 2332–2342.
- Siciliano, B. and Khatib, O. (2016). *Springer handbook of robotics*. Springer.

- Song, Z. and Sun, K. (2014). “Adaptive backstepping sliding mode control with fuzzy monitoring strategy for a kind of mechanical system”. *ISA transactions*, 53(1), 125–133.
- Spong, M. W. and Vidyasagar, M. (2008). “*Robot dynamics and control*”. John Wiley & Sons.
- Sun, G., Li, D., and Ren, X. (2015). “Modified neural dynamic surface approach to output feedback of mimo nonlinear systems”. *IEEE transactions on neural networks and learning systems*, 26(2), 224–236.
- Sun, H. and Guo, L. (2017). “Neural network-based dobc for a class of nonlinear systems with unmatched disturbances”. *IEEE transactions on neural networks and learning systems*, 28(2), 482–489.
- Sun, T., Pei, H., Pan, Y., Zhou, H., and Zhang, C. (2011). “Neural network-based sliding mode adaptive control for robot manipulators”. *Neurocomputing*, 74(14), 2377–2384.
- Tan, K. K., Wang, Q.-G., and Hang, C. C. (2012). “*Advances in PID control*”. Springer Science & Business Media.
- Tarokh, M. and Zhang, X. (2014). “Real-time motion tracking of robot manipulators using adaptive genetic algorithms”. *Journal of Intelligent & Robotic Systems*, 74(3-4), 697.
- Thomas, S., Pillai, G., Pal, K., and Jagtap, P. (2016). “Prediction of ground motion parameters using randomized anfis (ranfis)”. *Applied Soft Computing*, 40, 624–634.
- Tran, T., Wang, Y., Ao, H., and Truong, T. K. (2015). “Sliding mode control based on chemical reaction optimization and radial basis functional link net for de-icing robot manipulator”. *Journal of Dynamic Systems, Measurement, and Control*, 137(5), 051009.
- Utkin, V. I. (1993). “Sliding mode control design principles and applications to electric drives”. *IEEE transactions on industrial electronics*, 40(1), 23–36.

- Vijay, M. and Jena, D. (2016). “Intelligent adaptive observer-based optimal control of overhead transmission line de-icing robot manipulator”. *Advanced Robotics*, 30(17-18), 1215–1227.
- Wai, R.-J., Chen, M.-W., and Yao, J.-X. (2016). “Observer-based adaptive fuzzy-neural-network control for hybrid maglev transportation system”. *Neurocomputing*, 175, 10–24.
- Wai, R.-J. and Muthusamy, R. (2013). “Fuzzy-neural-network inherited sliding-mode control for robot manipulator including actuator dynamics”. *IEEE Transactions on Neural Networks and learning systems*, 24(2), 274–287.
- Wai, R.-J., Yao, J.-X., and Lee, J.-D. (2015). “Backstepping fuzzy-neural-network control design for hybrid maglev transportation system”. *IEEE transactions on neural networks and learning systems*, 26(2), 302–317.
- Wei, S., Wang, Y., and Zuo, Y. (2012). “Wavelet neural networks robust control of farm transmission line deicing robot manipulators”. *Computer Standards & Interfaces*, 34(3), 327–333.
- Wen, S., Chen, M. Z., Zeng, Z., Yu, X., and Huang, T. (2017). “Fuzzy control for uncertain vehicle active suspension systems via dynamic sliding-mode approach”. *IEEE Transactions on Systems, Man, and Cybernetics: Systems*, 47(1), 24–32.
- Xie, Q. and Li, J. (2006). “Current situation of natural disaster in electric power system and countermeasures”. *Journal of Natural Disasters*, 15(4), 126.
- Yang, J., Li, S., and Yu, X. (2013). “Sliding-mode control for systems with mismatched uncertainties via a disturbance observer”. *IEEE Transactions on Industrial Electronics*, 60(1), 160–169.
- Zeinali, M. and Notash, L. (2010). “Adaptive sliding mode control with uncertainty estimator for robot manipulators”. *Mechanism and Machine Theory*, 45(1), 80–90.

- Zhang, L., Li, Z., and Yang, C. (2017). “Adaptive neural network based variable stiffness control of uncertain robotic systems using disturbance observer”. *IEEE Transactions on Industrial Electronics*, 64(3), 2236–2245.
- Zhao, G., Zhao, C., and Cheng, J. (2014). “Decoupled terminal sliding-mode control for a class of under-actuated mechanical systems with hybrid sliding surfaces”. *International Journal of Innovative Computing, Information and Control*, 10(6), 2011–2023.
- Zheng, X., Jian, X., Wenzheng, D., and Hongjie, C. (2015). “Nonlinear integral sliding mode control for a second order nonlinear system”. *Journal of Control Science and Engineering*, 2015, 2.

DISSEMINATION OF THE RESEARCH WORK

International Journals

- [1] Vijay, M., & Jena, D. (2018). Backstepping terminal sliding mode control of robot manipulator using radial basis functional neural networks. *Computers & Electrical Engineering*, 67, 690-707, (Elsevier).
- [2] Vijay, M., & Jena, D. (2017). PSO based neuro fuzzy sliding mode control for a robot manipulator. *Journal of Electrical Systems and Information Technology*, 4(1), 243-256, (Elsevier).
- [3] Vijay, M., & Jena, D. (2016). Intelligent adaptive observer-based optimal control of overhead transmission line de-icing robot manipulator. *Advanced Robotics*, 30(17-18), 1215-1227. (Taylor & Francis).

International Conferences

- [1] Vijay, M., & Jena, D. (2018, January). PSO based backstepping sliding mode controller and observer for robot manipulators. In 2018 International Conference on Power, Instrumentation, Control and Computing (PICC) (pp. 1-6). IEEE.
- [2] Vijay, M., & Jena, D. (2015, February). Optimal backstepping sliding mode control for robot manipulator. In *Signal Processing, Informatics, Communication and Energy Systems (SPICES)*, 2015 IEEE International Conference on (pp. 1-5). IEEE.
- [3] Vijay, M., & Jena, D. (2014, December). Optimal GA based SMC with adaptive PID sliding surface for robot manipulator. In *Industrial and Information Systems (ICIIS)*, 2014 9th International Conference on (pp. 1-6). IEEE.
- [4] Vijay, M., & Jena, D. (2014, March). GA based adaptive optimal controller for 2 DOF robot manipulator. In *Advances in Control and Optimization of Dynamical Systems*, 3(1), 670-675 (Elsevier Proceedings).

BIO-DATA

Name : M VIJAY

Email Id : mokenapalli.vijay@gmail.com

Mobile : +91-9844667126

Date of Birth : June 10, 1988

Address :

M VIJAY,

S/o YELLAIAH,

H.No. 7-19,

Kothapally Village, Gambhiraopet Mandal,

Rajanna Siricilla Dist-505304

Telangana-India

Educational Qualifications:

Degree	Year of Passing	University
B.E.	2009	Osmania University, Hyderabad
M.Tech.	2012	NITK, Surathkal, India